ADAPTIVE MR-GUIDED RADIOTHERAPY: FROM CONCEPT TO ROUTINE PRACTICE

Bohoudi, Omar

2022

ADAPTIVE MR-GUIDED RADIOTHERAPY

FROM CONCEPT TO ROUTINE PRACTICE

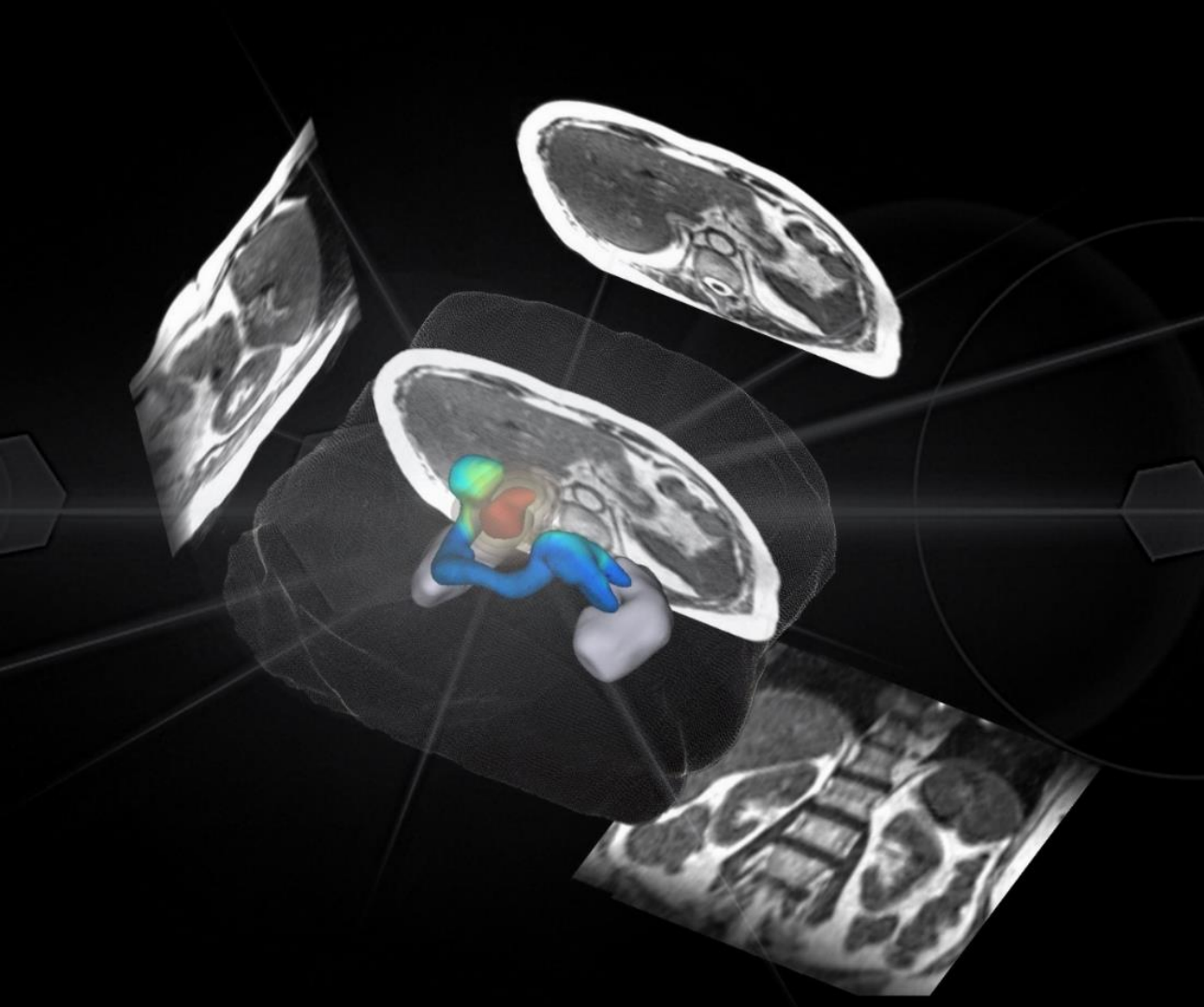

OMAR BOHOUDI

ADAPTIVE MR-GUIDED RADIOTHERAPY: FROM CONCEPT TO ROUTINE PRACTICE

Omar Bohoudi

Cover design by: Omar Bohoudi
Lay-out: Omar Bohoudi
Financial support by ViewRay Inc., Mountain View, USA

VRIJE UNIVERSITEIT

ADAPTIVE MR-GUIDED RADIOTHERAPY: FROM CONCEPT TO ROUTINE PRACTICE

ACADEMISCH PROEFSCHRIFT

ter verkrijging van de graad Doctor aan
de Vrije Universiteit Amsterdam,
op gezag van de rector magnificus
prof.dr. J.J.G. Geurts,
in het openbaar te verdedigen
ten overstaan van de promotiecommissie
van de Faculteit der Geneeskunde
op vrijdag 20 mei 2022 om 13.45 uur
in een bijeenkomst van de universiteit,
De Boelelaan 1105

door

Omar Bohoudi

geboren te Meknès, Marokko

promotor:	prof.dr. S. Senan
copromotoren:	dr. F.J. Lagerwaard dr. M.A. Palacios
promotiecommissie:	prof.dr. M.R. Meijerink prof.dr. U.A. van der Heide prof.dr. E. Özyar prof.dr. M.S. Hoogeman dr. D. Cusumano dr. L.G.W. Kerkmeijer

Bismillahirrahmanirrahim, voor Salah mijn "gharbous",

Table of contents

Chapter 1

General introduction

Cancer is the second leading cause of death worldwide, with over 9.6 million deaths in 2018[1]. In the Netherlands alone, more than 110,000 people are newly diagnosed with cancer each year[2]. However, due to better treatment options available and earlier diagnosis, the five-year overall survival rates for all tumors has increased from 48% for patients diagnosed in the 1990s, to 66% in the last decade[2]. Radiotherapy is one of the main treatment options for cancer, in addition to surgery and chemotherapy. Approximately half of all new patients with cancer will undergo radiotherapy as part of their treatment[3]. Radiotherapy can be delivered using radiation-emitting sources inserted into the tumor (known as brachytherapy), or by using high-energy megavoltage radiation beam directed towards the tumor from an external source. The absorbed radiation damages the genetic material of cells, and without repair it leads to cell death. However, damage to healthy cells can also occur when normal organs surrounding the target tumor area are also irradiated[4]. Therefore, the main goal of radiation therapy is to damage the cancer cells while sparing the surrounding healthy tissues as much as possible[4]. Tumor cells are less efficient than healthy tissue cells for repairing the accumulated damage. Therefore, traditionally radiation therapy has been delivered in small fractions in order to allow enough healthy tissue recovery and limit toxicity.

Before radiotherapy commences, a treatment plan is created based on a pre-treatment planning CT scan, on which the visible tumor (GTV; gross tumor volume), the volumes suspected for containing tumor cells (CTV; clinical target volume), a margin for daily set up variation, organ motion and change in organ shape and size (PTV; planning target volume), and the surrounding organs-at-risk (OAR) are contoured. Delivery of intensity modulated radiation therapy (IMRT) allows the radiation dose distribution to conform more precisely to the shape of the tumor, by means of modulation of the shape and intensity of the radiation beams[5]. IMRT

enables higher radiation doses to be focused on the tumor while minimizing the dose to OARs, by using computerized dose calculations to determine the dose intensity pattern needed for a more conformal high-dose region. Furthermore, a steep-dose gradient outside the target is also achieved to avoid high doses in the OARs adjacent to the target volume[5]. The baseline treatment plan specifies the direction, multileaf collimator (MLC) settings, and the fluence intensity of radiation beams from the linear accelerator (LINAC) used to deliver the planned radiation dose.

A baseline treatment plan is typically based on the patient anatomy at the time of the initial planning-CT scan. This plan is typically delivered for all treatment fractions after patient alignment and registration. However, the patient internal anatomy undergoes daily variations and frequent displacements and changes in target volumes and OARs have been reported[6]. Advances in the use of image guided radiation therapy (IGRT) have resulted in traditional setups on the bony anatomy being replaced by soft-tissues registrations on the target volume using cone-beam CT scans (CBCT). In prostate cancer, it is common to use implanted gold markers as organ surrogate for daily patient setup in conventional radiotherapy[7]. However, inter- and intra-fractional changes in the patient anatomy may remain unnoticed, leading to significant differences between the planned and actual delivered doses to both the target and adjacent OARs[8].

In conventional radiotherapy, the dose is delivered in 25 to 35 daily fractions of 1.8 to 2.0 Gy over up to 7 weeks. Technological advances in radiation oncology have led to the implementation of stereotactic ablative radiotherapy (SABR) or stereotactic body radiation therapy (SBRT). SABR aims to deliver high radiation doses to the tumor in 8 or fewer fractions with the aim to increase the biologically effective dose (BED) to the tumor. This increase in the BED has been shown to improve tumor

control rates without causing higher toxicities[9]. SBRT delivery requires hence high precision in order to minimize damage to healthy tissues[9].

Adaptive radiation therapy (ART) aims to adapt the baseline treatment plans in response to anatomical changes or functional changes occurring on the target and/or the OARs during treatment[6,8]. ART is not yet widely adopted in routine clinical practice, but clinical workflows have been described using an off-line ART protocol based on CBCT imaging[10,11]. Another ART involves use of a library of treatment plans that are created before treatment to account for expected anatomical changes, such as variations in bladder volume[12]. Ideally, inter-fractional changes are accounted for daily by adapting the treatment plan according to the "anatomy of the day". Because the patient lies in treatment position, this process should be performed as efficient and quick as possible. Several studies have suggested a dosimetric benefit of online treatment plan adaptation for tumors of the prostate, bladder and pancreas[13–15]. However, the clinical use of online ART has been limited by two main factors: 1) the need of daily high-quality images with enough contrast for target and OAR definition; 2) the slow calculation speed for the newly adapted plans in combination with absence of robust planning methods to account for anatomical changes.

Magnetic resonance guided radiation therapy

Magnetic-resonance imaging (MRI) offers superior anatomical imaging for delineating the target volume and critical structures[16,17] (Figure 1). In addition, the use of MRI does not result in additional radiation dose to the patient[10]. However, MRI acquisitions lack the electron density information required to perform dose calculation and treatment plan optimization and they usually require longer times than CT. Because of the superior contrast of MRI with respect to CT, hybrid MR-linac systems have recently been developed which allow to combine MRI and

radiation therapy delivery. This has led to the clinical introduction of Magnetic Resonance Guided Radiation Therapy (MRgRT), replacing traditional CBCT setup. Two MRgRT systems are now in clinical use; the MRIdian system[18] (ViewRay Inc., Mountain View, USA) and the Elekta Unity (Elekta AB, Stockholm, Sweden)[19].

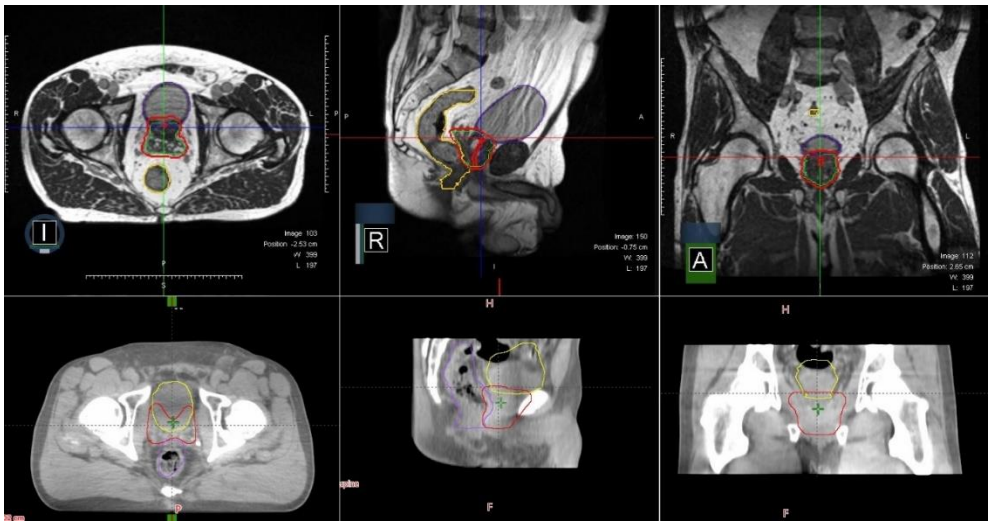

Figure 1: *An example of setup imaging for prostate cancer using MRI (upper panel; MRIdian, ViewRay, high-resolution scan, 0.35 Tesla) and CBCT (lower panel; OBI, TrueBeam, Varian medical systems). Bladder = purple, rectum = yellow and prostate = green.*

In 2016, MRgRT was clinically introduced at the Amsterdam UMC using the MRIdian system from ViewRay (Figure 2). The first system combined a split-bore 0.35T MRI with a radiation therapy delivery system consisting of a ring gantry with three multileaf collimator-equipped 60Co heads. The MRIdian Linac is a second generation device which integrates a split-bore 0.35T MRI (double-donut) with a 6 MV flattening-filter-free (FFF) linear accelerator. The double focused MLC consisting of two layers are used to create a sharp penumbra to shape the beam and to achieve an effective leaf width of 4.15 mm at 90 cm SAD[20]. The superior soft tissue imaging capability of MRgRT improves the visualization of the tumor and surrounding OARs, and allows precise soft tissue setup, real-time planar imaging and gated delivery without the need of inserted fiducials. An integrated Monte

Carlo-based treatment planning system allows online adaptive planning for optimal dose delivery, based on the actual daily anatomy of the patient[18]. Several studies have shown the feasibility and clinical implementation of MRgRT at various tumor sites[21–25].

***Figure 2**: The MRIdian system at Amsterdam UMC (left panel) and an overview of hardware (right panel www.viewray.com).*

Despite the state-of-the-art capabilities of these MRgRT systems, considerable logistic challenges exist in the overall workflow and efficiency of the treatment process[26]. MRgRT with daily plan adaptation is both cost- and resource intensive, among other reasons because daily plan adaptation relies heavily on the presence of the physician and/or physicist at the treatment console. Therefore, fast and reliable workflows are required in MRgRT to streamline the treatment process. Defining the optimal use of MRgRT requires the study of dosimetric and clinical benefits, and to identify the patients who are most likely to benefit from this approach.

Dose accumulation

The availability of improved imaging before and during each fraction, in combination with dose accumulation strategies, provide an unique opportunity to measure the actual doses delivered during the entire MRgRT treatment[27]. Assessing the cumulative doses over the full course of radiotherapy may improve the accuracy

of outcome models for studying tumor control probability (TCP) and normal tissue complication probability (NTCP). Current models are mainly based on a 'snapshot' of dose distributions calculated on a single pre-treatment planning CT scan[27]. Deformable image registration (DIR) allows for a voxel-to-voxel mapping between a baseline reference image (MRI or CT) and subsequent images of deformed tissues, allowing for doses to be accumulated over multiple fractions[28]. Reliable dose accumulation for all delivered fractions faces many challenges[29] and a validation of DIR-based dose accumulation methods are lacking. Therefore, a thorough evaluation before its clinical implementation is needed.

Outline of this thesis

We developed a novel, in-house clinical strategy for robust and fast online adaptation which is described in **Chapter 2**. This approach relies on DIR, a physician's review of only the OARs within a distance of 2 – 3 cm from the PTV, and robust prediction of optimization objectives. This strategy also involves partitioning OAR contours in separate areas around the target in order to allow for spatial control of the dose distribution.

MR-guided soft tissue imaging capability improves the visualization of the prostate, the base of seminal vesicles and surrounding organs at risk, allowing for precise soft tissue setup, real-time planar imaging and gated delivery with minimal safety margins. **Chapter 3** describes our clinical experience with a daily online adaptive MRgRT workflow for prostate SBRT. We studied the time needed for our clinical MRgRT workflow, and the frequency of online corrections due to intrafractional variations in prostate position. Patient-reported outcomes of MRgRT and results from patient-specific QA are presented. Finally, potential pitfalls of MRgRT are highlighted.

MRgRT with daily plan adaptation is also a time- and resource-intensive treatment. In **chapter 4**, we analyzed the benefits for target coverage and OAR sparing when daily plan adaptation was applied to 36 consecutive patients with locally advanced pancreatic cancer. A decision-tree analysis was performed to identify subgroups most, or least, likely to benefit from routine plan adaptation.

Chapter 5 describes the inter-fractional changes in GTV and OARs during MRgRT for metastases in the adrenal glands. The role of online plan re-optimization in ensuring both adequate target coverage for the adrenal lesions and OAR sparing were studied.

MRgRT with plan adaptation can improve target coverage and normal tissue sparing, which in turn can result in improved local control and/or decreased toxicity. In **chapter 6**, we evaluated the clinical impact of stereotactic MRgRT and routine plan re-optimization in 36 patients with a primary renal cell carcinoma.

Following the clinical implementation of MRgRT, inter-fraction plan adaptation has become a clinical reality. The extent of intra-fractional changes in relevant OARs and the need for intrafractional plan adaptation, is unknown. **Chapter 7** describes a first attempt to quantify the relative importance of inter- and intra-fractional plan adaptation. Fixed fraction partitioning was used to perform intrafractional plan adaptation, which in this patient case, was at 50% of delivery of the planned MRgRT fraction for a locally advanced pancreatic cancer. Between successive deliveries, the patient remained in the treatment position and all steps of the initial plan adaptation were repeated. The second re-optimization served as an intrafractional plan adaptation at 50% of the total delivery.

There is a growing interest in DIR-based dose accumulation for adaptive radiation therapy. **Chapter 8** evaluates our DIR-based dose accumulation strategy to ensure

an accurate reconstruction of the total delivered dose. An anthropomorphic phantom of the human pelvic region was used to simulate a SBRT prostate cancer treatment course.

Data on the relationship between delivered SBRT doses and toxicity are currently limited. In **Chapter 9**, we identified dose parameters that correlated with acute urinary toxicity based on the total accumulated delivered bladder dose. For this purpose, we deployed a DIR-based dose accumulation strategy described in chapter 8 to reconstruct the actual delivered dose in 101 prostate cancer patients treated with stereotactic adaptive MRgRT. To facilitate future ART strategies, we also studied whether prospective bladder dose accumulation (approximately halfway during treatment) could be used as an early predictor of urinary toxicity. If validated, the approach described here could be used to further optimize MRgRT for the remaining fractions.

In **Chapter 10**, we discussed the context of the work presented in this thesis, and explored future perspectives for MRgRT delivery.

References

1. Bray, F. *et al.* Global cancer statistics 2018: GLOBOCAN estimates of incidence and mortality worldwide for 36 cancers in 185 countries. *CA. Cancer J. Clin.* **68**, 394–424 (2018).
2. cijfersoverkanker. *The Netherlands Cancer Registry* http://www.cijfersoverkanker.nl http://www.cijfersoverkanker.nl (2020).
3. Borras, J. M. *et al.* The optimal utilization proportion of external beam radiotherapy in European countries: An ESTRO-HERO analysis. *Radiother. Oncol.* **116**, 38–44 (2015).
4. Baskar, R., Lee, K. A., Yeo, R. & Yeoh, K. W. Cancer and radiation therapy: Current advances and future directions. *International Journal of Medical Sciences* vol. 9 193–199 (2012).
5. Bortfeld, T., Schmidt-Ullrich, R., De Neve, W. & Wazer, D. E. *Image-guided IMRT. Image-Guided IMRT* (Springer Berlin Heidelberg, 2006). doi:10.1007/3-540-30356-1.
6. Sonke, J. J., Aznar, M. & Rasch, C. Adaptive Radiotherapy for Anatomical Changes. *Seminars in Radiation Oncology* vol. 29 245–257 (2019).
7. Dang, A., Kupelian, P. A., Cao, M., Agazaryan, N. & Kishan, A. U. Image-guided radiotherapy for prostate cancer. *Translational Andrology and Urology* vol. 7 308–320 (2018).
8. Ahunbay, E. E. *et al.* An on-line replanning scheme for interfractional variations. *Med. Phys.* **35**, 3607–3615 (2008).
9. Benedict, S. H. *et al.* Stereotactic body radiation therapy: The report of AAPM Task Group 101. *Med. Phys.* **37**, 4078–4101 (2010).
10. Nijkamp, J. *et al.* Adaptive Radiotherapy for Prostate Cancer Using Kilovoltage Cone-Beam Computed Tomography: First Clinical Results. *Int. J. Radiat. Oncol. Biol. Phys.* **70**, 75–82 (2008).
11. Park, S. S. *et al.* Adaptive image-guided radiotherapy (IGRT) eliminates the risk of biochemical failure caused by the bias of rectal distension in prostate cancer treatment planning: Clinical evidence. *Int. J. Radiat. Oncol. Biol. Phys.* **83**, 947–952 (2012).
12. Heijkoop, S. T. *et al.* Clinical implementation of an online adaptive plan-of-the-day protocol for nonrigid motion management in locally advanced cervical cancer IMRT. *Int. J. Radiat. Oncol. Biol. Phys.* **90**, 673–679 (2014).
13. Ahunbay, E. E. *et al.* Online adaptive replanning method for prostate radiotherapy. *Int. J. Radiat. Oncol. Biol. Phys.* **77**, 1561–1572 (2010).
14. Liu, F., Erickson, B., Peng, C. & Li, X. A. Characterization and management of interfractional anatomic changes for pancreatic cancer radiotherapy. *Int. J. Radiat.*

Oncol. Biol. Phys. **83**, e423–e429 (2012).

15. Vestergaard, A. *et al.* Adaptive plan selection vs. re-optimisation in radiotherapy for bladder cancer: a dose accumulation comparison. *Radiother. Oncol.* **109**, 457–62 (2013).
16. Kupelian, P. & Sonke, J. J. Magnetic Resonance-Guided Adaptive Radiotherapy: A Solution to the Future. *Semin. Radiat. Oncol.* **24**, 227–232 (2014).
17. Noel, C. E. *et al.* Comparison of onboard low-field magnetic resonance imaging versus onboard computed tomography for anatomy visualization in radiotherapy. *Acta Oncol. (Madr).* **54**, 1474–1482 (2015).
18. Mutic, S. & Dempsey, J. F. The ViewRay System: Magnetic Resonance-Guided and Controlled Radiotherapy. *Semin. Radiat. Oncol.* **24**, 196–199 (2014).
19. Lagendijk, J. J. W., Raaymakers, B. W. & van Vulpen, M. The Magnetic Resonance Imaging-Linac System. *Semin. Radiat. Oncol.* **24**, 207–209 (2014).
20. Klüter, S. Technical design and concept of a 0.35 T MR-Linac. *Clin. Transl. Radiat. Oncol.* **18**, 98–101 (2019).
21. Acharya, S. *et al.* Online Magnetic Resonance Image Guided Adaptive Radiation Therapy: First Clinical Applications. *Int. J. Radiat. Oncol.* **94**, 394–403 (2016).
22. Werensteijn-Honingh, A. M. *et al.* Feasibility of stereotactic radiotherapy using a 1.5 T MR-linac: Multi-fraction treatment of pelvic lymph node oligometastases. *Radiother. Oncol.* **134**, 50–54 (2019).
23. Cai, B. *et al.* Feasibility of Stereotactic Body Radiation Therapy for Non–small Cell Lung Cancer Using a Linear Accelerator-Based Magnetic Resonance Image Guided Radiation Therapy System. *Int. J. Radiat. Oncol.* **99**, E643–E644 (2017).
24. Henke, L. E. *et al.* Online Adaptive MR Guided Stereotactic Body Radiation Therapy for the Treatment of Oligometastatic Disease of the Abdomen and Central Thorax: Characterization of Potential Advantages. *Int. J. Radiat. Oncol.* **93**, S20–S21 (2015).
25. Dunlop, A. *et al.* Daily adaptive radiotherapy for patients with prostate cancer using a high field MR-linac: Initial clinical experiences and assessment of delivered doses compared to a C-arm linac. *Clin. Transl. Radiat. Oncol.* **23**, 35–42 (2020).
26. Kashani, R. & Olsen, J. R. Magnetic Resonance Imaging for Target Delineation and Daily Treatment Modification. *Semin. Radiat. Oncol.* **28**, 178–184 (2018).
27. Jaffray, D. A., Lindsay, P. E., Brock, K. K., Deasy, J. O. & Tomé, W. A. Accurate Accumulation of Dose for Improved Understanding of Radiation Effects in Normal Tissue. *Int. J. Radiat. Oncol. Biol. Phys.* **76**, 135–139 (2010).
28. Chetty, I. J. & Rosu-Bubulac, M. Deformable Registration for Dose Accumulation. *Seminars in Radiation Oncology* vol. 29 198–208 (2019).
29. Janssens, G. *et al.* Evaluation of nonrigid registration models for interfraction dose accumulation in radiotherapy. *Med. Phys.* **36**, 4268–4276 (2009).

Chapter 2

Fast and robust online adaptive planning in stereotactic MR-guided adaptive radiation therapy (SMART) for pancreatic cancer

Omar Bohoudi
Anna M.E Bruynzeel
Suresh Senan
Johan P. Cuijpers
Ben J. Slotman
Frank J. Lagerwaard
Miguel A. Palacios

Radiotherapy and Oncology. 2017; 125 : 439–44.

Abstract

Background and Purpose: To implement a robust and fast stereotactic MR-guided adaptive radiation therapy (SMART) online strategy in locally advanced pancreatic cancer (LAPC).

Material and Methods: SMART strategy for plan adaptation was implemented with the MRIdian system (ViewRay Inc.). At each fraction, OAR (re-)contouring is done within a distance of 3 cm from the PTV surface. Online plan re-optimization is based on robust prediction of OAR dose and optimization objectives, obtained by building an artificial neural network (ANN). Proposed limited re-contouring strategy for plan adaptation ($SMART_{3CM}$) is evaluated by comparing 50 previously delivered fractions against a standard (re-)planning method using full-scale OAR (re-)contouring (FULLOAR). Plan quality was assessed using PTV coverage ($V_{95\%}$, D_{mean}, D_{1cc}) and institutional OAR constraints (e.g. V_{33Gy}).

Results: $SMART_{3CM}$ required a significant lower number of optimizations than FULLOAR (4 vs 18 on average) to generate a plan meeting all objectives and institutional OAR constraints. PTV coverage with both strategies was identical (mean $V_{95\%}$ =89%). Adaptive plans with $SMART_{3CM}$ exhibited significant lower intermediate and high doses to all OARs than FULLOAR, which also failed in 36% of the cases to adhere to the V_{33Gy} dose constraint.

Conclusions: $SMART_{3CM}$ approach for LAPC allows good OAR sparing and adequate target coverage while requiring only limited online (re-)contouring from clinicians.

Introduction

Adaptive radiotherapy (ART) entails adjusting treatment plans in response to specific anatomic and/or biological changes which may occur during the course of the treatment. The ideal method to account for inter-fractional changes is to adapt treatment plans based on the anatomy of the day, which can be performed either offline or online[1,2]. Online plan adaptation needs to be performed fast with the patient in treatment position[3–5]. In recent years, several studies have shown the dosimetric benefit of treatment plan adaptation for tumor sites such as the cervix, prostate, bladder and pancreas[3,4,6–8]. However, often using a library of plans and not based on the exact anatomy.

Upper abdominal tumors such as pancreatic cancer are particularly suitable for performing ART because of the proximity of several critical normal organs such as the duodenum, stomach and bowel. Daily variations in the position of the pancreas can be as large as 20 mm in all directions[9–12] and for the stomach even up to 35 mm[13]. In addition, mean displacements of the pancreas of 23, 11 and 7 mm in cranio-caudal, antero-posterior and lateral directions, respectively, due to breathing (intra-fraction motion) have been reported as well[14,15]. In recent years there has been growing interest in using hypofractionated radiation therapy, in particular stereotactic body radiotherapy (SBRT), for treatment of locally advanced pancreatic cancer (LAPC) (14–23). IMRT techniques have been shown to reduce the dose to organs at risk (OAR) in pancreatic cancer[22,23], which is especially important for the duodenum, for which a significant correlation between the actuarial rates of grade ≥2 toxicity and dose has been reported[24,25].

The soft tissue contrast of available cone-beam CT scans is insufficient for ART in abdominal tumors. Magnetic-resonance imaging (MRI) offers superior anatomical

imaging during the course of radiation therapy with the potential for improved delineation of the target volume and critical structures[26]. We recently implemented stereotactic MR-guided adaptive radiotherapy (SMART) for LAPC using IMRT with the MRIdian system (ViewRay Inc., Mountain View). This dedicated device combines a split-bore 0.35T MR scanner with ^{60}Co radiation therapy (for a detailed description of the system see, for instance[27]). The system allows the acquisition of high-resolution volumetric MR images of the patient immediately prior to treatment, and deformable image registration with automatic contour propagation to account for inter-fractional changes and plan adaptation based on the volumetric image of the day[28].

For a robust and fast online plan adaptation, we introduced an ART online strategy which can be performed within minutes, and which only requires limited (re-)contouring by the physician. The same beam parameters are used for plan (re-)optimization and optimization objectives rely on a model which predicts OAR dose as a function of distance from the target. To evaluate our online SMART strategy with limited (re-)contouring, we compared 50 completed ART fractions against a simulated standard (re-)planning method using full-scale OAR (re-)contouring, where optimization objectives were used for the entire OAR.

Material and Methods

General SMART workflow for LAPC

The online SMART procedure for LAPC consists of three steps: 1) MR simulation during breath-hold, 2) deformation and adjustment of OAR contours and 3) online plan re-optimisation. MR acquisition is performed during a 17 second breath-hold in shallow inspiration, using a FOV of 45 cm and 1.6mm x 1.6mm x 3mm resolution.

MR protocol for delineation is based on a true FISP sequence (Siemens) with a TR/TE of 3.83/1.62 ms and Flip Angle of 60°. The contours of the OAR, i.e. the duodenum, stomach, bowel and kidney are propagated from a pre-treatment MR simulation on the MRIdian to the MR of the day using deformable image registration and manually adjusted. ViewRay deformable registration uses an intensity-based algorithm which minimizes a cost function that measures the similarity between the images and it also uses a regularization term in order to obtain smoother deformation fields and prevent sharp discontinuities. The target volume is rigidly registered to the anatomy of the day and only edited when needed (for instance, in the case of rotations). The target volume (PTV) is generated from the GTV plus an isotropic 3 mm margin, excluding any possible overlap with OARs. In SBRT for LAPC in our institution which is performed under breath-hold conditions, CTV is considered to be equal to the GTV. Prescription dose is 40 Gy (95% isodose line) in 5 fractions and the plan is re-optimised for each fraction, allowing a D1% of PTV up to 50 Gy (125% of prescribed dose).

Treatment plans for LAPC are based on IMRT step-and-shoot and consist of 6 beam groups, with each beam group consisting of three equidistant beams at 60° separation in correspondence with the geometry of the three ^{60}Co sources on the gantry. During optimization, the optimizer can assign no fluence to a particular beam in case it turns out to be an unfavourable direction, according to the internal anatomy. Dose calculation is performed with a Monte-Carlo algorithm implemented in the MRIdian system with a statistical uncertainty of 1% and grid size of 0.3cm x 0.3cm x 0.3cm by using the electron density map of the CT of the patient. At each fraction, the electron density map of the CT is deformed to the primary MR image representing the anatomy of the day, and it can be edited online before plan (re-)optimization if a discrepancy in air pockets or filling of OARs is detected. Before

treatment delivery, patient-specific QA is performed with an independent Monte-Carlo dose calculation algorithm and gamma analysis.

Institutional OAR constraints for SMART for LAPC are: V_{33Gy} and V_{25Gy} less than 1 cc and 20 cc, respectively for duodenum, stomach and bowel. For the kidney and liver, the V_{12Gy} should be less than 25% and 50%, respectively. PTV coverage at 95% of prescription dose usually ranges from 85% to 95% depending on the vicinity of OARs and their geometry around the PTV, because OAR constraints have a higher priority than PTV coverage.

SMART strategy for daily plan re-optimisation

The SMART strategy for online plan adaptation is based on the following components: 1) A robust baseline IMRT plan for online (re-)optimization is produced with the MRIdian planning system (see below, *Generating robust baseline plans*); 2) After deformation of contours at each fraction, OARs are reviewed and adjusted by the physician within a distance of 3 cm from the PTV; 3) OAR contours are subsequently spatially partitioned and combined in OAR portions located at 1, 2 and 3 cm from the PTV surface with the aid of a script for auto-contouring. Figure 1 shows an example of this OAR partitioning and the cumulative OAR volume around the PTV at 1 (OAR_{1cm}), 2 (OAR_{2cm}) and 3 (OAR_{3cm}) cm distance from the PTV; 4) The plan is re-optimized with the same MRIdian planning software available at the treatment console, keeping the same beam parameters and optimization objectives (see below, *Generating robust baseline plans*). In summary, for each fraction, plan parameters and optimization objectives are kept unchanged and OAR_{1cm}, OAR_{2cm} and OAR_{3cm} structures used in the optimization are generated for each fraction according to the anatomy of that particular day.

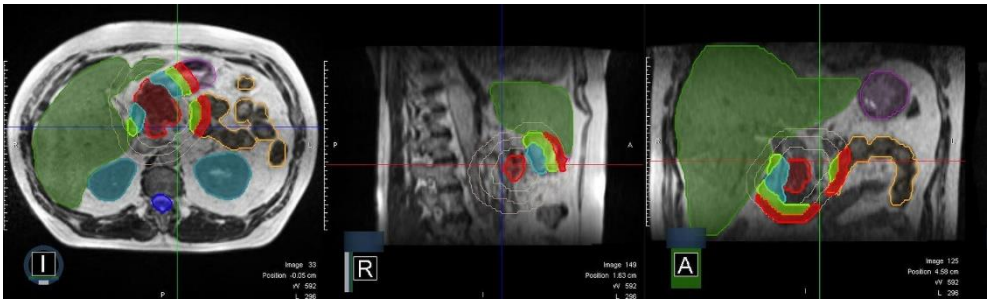

Figure 1. *Example of OAR partitioning within a distance of 3 cm from PTV for a random patient with LAPC. OAR_{1cm} is highlighted in light blue, OAR_{2cm} in yellow and OAR_{3cm} in red. OAR_{1-3cm} are structures which are generated for each fraction. PTV is indicated in red, duodenum in cyan, stomach in purple, bowel in orange, liver in green and spinal cord in dark blue.*

Generating robust baseline plans

Robust and high quality baseline plans are generated using an in-house developed artificial neural network (ANN) approach (IBM SPSS Modeler v18, IBM®). To build this ANN (see also Supplementary material at the end of the chapter), a total of 66 SBRT treatment plans for LAPC produced with the MRIdian treatment planning system were used as training plans, resulting in a model which predicts doses in OARs based on patient-specific geometric parameters. The following input parameters were used to build the ANN: PTV (cc), OAR_{1cm} (cc), OAR_{2cm} (cc), OAR_{3cm} (cc) and total patient-specific effective depth (cm) to the isocenter for all beams. Estimates of the median dose (D_{median}) at discretized portions of the OARs from 1 mm up to 50 mm distance from the PTV were generated as output parameters. These were also used as optimization objectives for OAR_{1cm}, OAR_{2cm} and OAR_{3cm} structures for plan (re-)optimization with the $SMART_{3CM}$ strategy to generate the SBRT plans (see supplementary material). To generate all plans and achieve best dose gradients at the OARs, weights for optimization were manually obtained for each iteration by using the definition of the penalty function for OARs as implemented in the MRIdian TPS. ANN provided thus robust individualized optimization objectives according to patient-specific geometric parameters. All plans used to build the ANN were generated using our institutional constraints. This ANN model for dose

prediction was validated on a total of 42 new SBRT treatment plans. Additional details about how the ANN for SMART$_{3CM}$ strategy was built are provided with the Supplementary material at the end of the chapter.

Evaluation of SMART strategy for plan adaptation and statistical analysis

The developed SMART online strategy (SMART$_{3CM}$) for LAPC was evaluated against a standard (re-)optimisation method using entire OARs for plan optimization (FULLOAR). As in the case of SMART$_{3CM}$, the definition of the penalty function for OARs as defined in the MRIdian TPS was used to achieve the best dose fall-off outside of the target. The only difference between SMART$_{3CM}$ and FULLOAR for plan generation is the use of OAR partitioning and of an ANN for dose prediction in SMART$_{3CM}$. Comparable baseline plans using both methodologies, fulfilling all institutional medical constraints were generated. For the adapted plans, full OARs were manually edited from the contour propagation, so also outside the 3cm, in order to have a realistic comparison. For baseline planning, the number of optimizations to achieve a high quality plan was not restrained, whereas for online plan re-optimization both strategies are performed with only one optimization iteration, with time constraints during treatment delivery in mind. Simulated plan adaptations with both strategies were performed using the MR volumetric image sets from 50 adaptive fractions for 10 LAPC patients treated with the MRIdian system at our institute. As summary, the following plans were generated to compare both adaptive strategies: 1) FULLOAR–baseline plans with no restriction on the number of iterations; 2) SMART$_{3CM}$–baseline plans with no restrictions on the number of iterations and which require only the 3 cm of the OARs closest to the PTV using an ANN to derive optimization objectives ; 3) FULLOAR–adaptive plans with only 1 iteration allowed using the same beam and optimization settings as for the baseline plan, but with daily contours as input; 4) SMART$_{3CM}$–adaptive plans with

only 1 iteration allowed using the same beam and optimization settings as for the baseline plan using the ANN, but with daily OAR contours (only the closest 3 cm) as input.

Dosimetric evaluation of both methods is carried out by comparing $V_{95\%}$ (%), D_{mean} (Gy) and D_{1cc} (Gy) in the PTV for the baseline plans as well as for the adaptive plans. The Conformity Index (CI) and Homogeneity Index (HI) [29] were used as additional quality metrics for the plans. For the duodenum, stomach and bowel, quality of plans was measured according to the volumes of OAR receiving doses in the range between 6 and 35 Gy, and more specifically, to the institutional dose constraints at 33 Gy and 25 Gy, i.e. V_{33Gy} (cc) and V_{25Gy} (cc). For kidneys and liver, the dosimetric parameter that was used for evaluation was the V_{12Gy}(%). Baseline plan optimization efficiency for both strategies, $SMART_{3CM}$ and FULLOAR was evaluated by the number of optimization iterations needed to generate a high quality plan which complied with the institutional medical constraints.

Statistical analysis of dosimetric parameters was performed using paired *t*-tests (IBM® SPSS Statistics v20, Armonk, NY, USA). A p-value < 0.05 was considered to be statistically significant.

Results

An overview of PTV and OAR volumes up to a distance of 3 cm from the PTV of the 10 patients included in the study is shown in Table 1. PTV size at baseline ranged from 16 to 99 cc and, because of non-adapting the GTV, there was little inter-fraction variation in PTV size. The small inter-fraction variations in PTV size that were seen were caused by the variation in OAR volumes at the proximity of the GTV that are

excluded during the generation of PTV's from the GTV's. Inter-fractional changes in duodenum, stomach and bowel were larger than for PTV and generally of random nature.

Table 1. *Overview of PTV and OAR volumes within a distance of 3 cm from PTV for the baseline plan and for the adaptive fractions. Contours were deformed and manually adjusted before every fraction on the basis of a high-resolution breath-hold MR scan.*

Pt. No.	PTV (cc)		Duodenum (cc)		Stomach (cc)		Bowel (cc)	
	Baseline	(range-fx)*	Baseline	(range-fx)	Baseline	(range-fx)	Baseline	(range-fx)
1	31.6	(30.7 – 31.8)	14.1	(12.4 - 26.6)	45.7	(21.7 – 33.7)	34.2	(0 – 49.8)
2	89.3	(82.1 – 89.3)	58.9	(55.2 – 77.3)	66.9	(49.9 – 77.2)	32.9	(25.4 – 52.0)
3	33.2	(33.1– 33.9)	45.2	(45.0 – 49.6)	54.6	(41.7 – 62.4)	0.0	(0.0 – 55.2)
4	26.7	(26.7 – 26.9)	46.4	(48.2 – 57.3)	27.1	(0.0 – 50.9)	28.5	(16.4 – 55.4)
5	36.8	(34.8 – 37.3)	64.9	(57.4 – 72.1)	33.0	(30.3 – 47.7)	6.2	(0.1 – 25.9)
6	19.6	(19.0 – 21.7)	38.9	(35.7 – 64.8)	7.5	(1.1 – 14.9)	37.7	(1.8 – 57.1)
7	99.3	(96.3 – 100)	33.2	(24.3 – 36.8)	71.8	(64.7 – 98.4)	32.6	(16.0 – 43.3)
8	33.1	(32.5 – 33.1)	65.4	(47.0 - 68.6)	20.3	(31.9 – 54.7)	20.5	(18.3 – 30.5)
9	15.7	(15.6 – 16.5)	54.5	(28.4 – 63.0)	6.3	(4.2 – 36.2)	48.8	(24.3 – 43.6)
10	43.4	(43.1 – 43.8)	40.9	(31.5 – 48.4)	43.0	(34.0 – 47.3)	11.3	(0.2 -14.9)

* Inter-fractional changes in PTV size were caused by variations of OAR volumes at the proximity of GTV and the exclusion of these volumes when generating the PTV from the GTV.

Comparable baseline plans were obtained with both $SMART_{3CM}$-baseline and FULLOAR-baseline, meeting all OAR constraints of our clinical protocol. Table 2 shows an overview of the baseline and re-optimized plan quality parameters for both strategies. The only significant differences for baseline plans were a slightly higher D_{mean} ($p = 0.01$) and a lesser number of optimizations to achieve a plan meeting all criteria for $SMART_{3CM}$-baseline (4 vs 18 on average, $p < 0.001$). Both strategies resulted in identical PTV coverage for all adaptive fractions (mean V95% = 89.6%), albeit a mean increase of 1 Gy for D_{mean} and D_{1cc} in the PTV for $SMART_{3CM}$-adaptive was observed ($p < 0.001$). It is worth noting that $SMART_{3CM}$-adaptive resulted in a

significantly higher number of IMRT segments for the daily adaptive fractions than FULLOAR-adaptive (mean of 51 vs 45 segments, see Table 2). However, this did not result in a considerable increase in the beam-on time, as $SMART_{3CM}$-adaptive produced on average plans which were only 0.4 min longer than FULLOAR-adaptive.

Table 2. *Overview of plan quality parameters for baseline and (re-)optimized plans for both adaptive strategies, $SMART_{3CM}$ and FULLOAR.*

	Baseline plans				**Plans Fx**			
	$SMART_{3CM}$-baseline		FULLOAR-baseline		$SMART_{3CM}$-adaptive		FULLOAR-adaptive	
	mean	(range)	mean	(range)	mean	(range)	mean	(range)
PTV $V_{95\%}$ (Gy)	89.4	(74.0 – 95.1)	89.4	(74.0 – 95.1)	89.6	(66.5 – 99.0)	89.6	(66.5 – 99.0)
PTV D_{mean} (Gy)	43.7	(42.4 – 44.8)	43.1	(41.7 – 43.9)	44.0	(40.9 – 45.9)	43.0	(40.4 – 44.6)
PTV D_{1cc} (Gy)	50.6	(49.4 – 53.2)	50.0	(48.6 – 51.3)	50.9	(46.7 – 53.6)	49.9	(46.0 – 53.4)
HI	1.28	(1.24 – 1.34)	1.26	(1.22 – 1.31)	1.28	(1.17 – 1.34)	1.26	(1.16 – 1.35)
CI	1.18	(0.91 – 1.34)	1.17	(0.91 – 1.32)	1.19	(0.81 – 1.41)	1.17	(0.75 – 1.40)
Beam-on time*	9.16	(7.85 – 11.3)	9.20	(8.48 – 10.5)	9.24	(7.11 – 12.9)	8.89	(7.07 – 11.1)
Segments	52	(36 – 79)	50	(31 – 80)	51	(33 – 76)	45	(30 – 73)
Optimizations**	4	(2-6)	18	(12 – 22)	1	(1 – 1)	1	(1 – 1)

*Beam-on time refers to the radiation time from the Co-60 sources needed to deposit prescription dose to the PTV and is similar to the number of monitor units for a conventional linac.
**For (re-)optimized plans only one single optimization is allowed simulating adaptive workflow while the patient is in treatment position.

$SMART_{3CM}$-adaptive consistently resulted in plans which complied with the V_{33Gy} dose constraint for OARs, whereas $SMART_{FULLOAR}$-adaptive failed overall in 36% of the fractions. Figure 2 shows box-and-whisker plots of the volume of OAR receiving a specific dose (or more) across the relevant dose range (6 Gy up to 35 Gy) for duodenum, stomach and bowel for both strategies. FULLOAR-adaptive led to significantly larger volumes of OARs at all dose values for the daily adaptive fractions with the exception of doses below 9 Gy for bowel. The close-ups for the

high dose range between 30 and 35 Gy clearly show a significant better sparing of all OARs following the SMART3CM-adaptive strategy (combined *p*-values of <0.001, <0.001 and 0.007 for duodenum, stomach and bowel, respectively). At 33 Gy for instance, SMART3CM-adaptive resulted on average in 0.37 cc, 0.36 cc and 0.50 cc lower volumes for duodenum, stomach and bowel, respectively than FULLOAR-adaptive. For kidney and liver, there was no significant difference found between both strategies for the adaptive plan (re-) optimization, meeting all plans the institutional clinical constraints (results not shown).

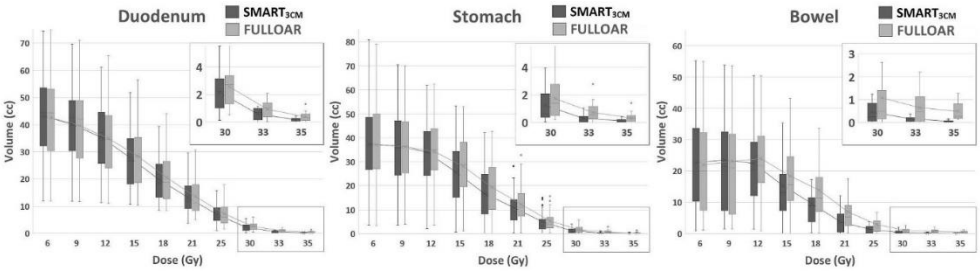

Figure 2. *Box-and-whisker plots of volumes of OAR receiving a specific dose across the 6 – 35 Gy dose range for SMART3CM-adaptive and FULLOAR-adaptive strategies. Continuous lines connect all mean values for the OARs. Close-ups show the volumes of OARs receiving high doses (between 30 and 35 Gy).*

Discussion

We describe an ART strategy for daily online plan (re-)optimization that is currently in clinical use at our institution. The strategy consistently resulted in high quality plans, which complied with all institutional OAR constraints for LAPC. The methodology used relies on robust prediction of optimization objectives, deformation and physician's review of OARs within a distance of 3 cm from the PTV, and partitioning OAR contours in separate portions to allow for spatial control of the dose distribution. Proposed ART methodology produced similar plans at baseline to a standard planning approach using entire OARs for dose optimization.

However, at online (re-)optimization and with time constraints in mind allowing only a single optimization, SMART3CM (re-)optimized plans always fulfilled clinical constraints from the institutional protocol and resulted in lower doses to OARs than the standard planning approach (FULLOAR-adaptive). This is attributed to a better control of dose gradients and spatial dose distribution around the PTV by OAR partitioning, certainly for the high-dose areas.

Online ART for LAPC is challenging, because of substantial daily variations in the relation between the PTV and surrounding critical OAR. An example of these variations is illustrated in Figure 3, in a patient who showed a large shift in bowel position relative to the baseline MRI, causing a substantial increase in OAR volumes in the vicinity of the PTV. Even with these extreme shifts of anatomy, the SMART3CM-adaptive approach performed much better than re-optimization on full organs, sparing OAR from high doses.

An obvious important advantage of the SMART3CM approach in comparison to FULLOAR is that it is a faster methodology, with a lower number of optimizations needed to derive optimal plans meeting all constraints from clinical protocol. In addition, much less time is needed for re-contouring OAR's. Although not described in this paper, the same ART methodology can easily be adopted for less challenging tumour sites, e.g. prostate cancer.

This SMART3CM strategy for the MRIdian system can also be applied in conventional linacs using CBCT for plan adaptation, as long as there is good visualization of the target volume and surrounding OAR. Due to the requirement of delivery precision and higher doses per fraction with steep-dose gradients, our strategy is especially relevant for hypofractionated treatments. From MR acquisition to dose plan calculation, it took on average 12 minutes (SD 4.5 min) per patient to deform, review

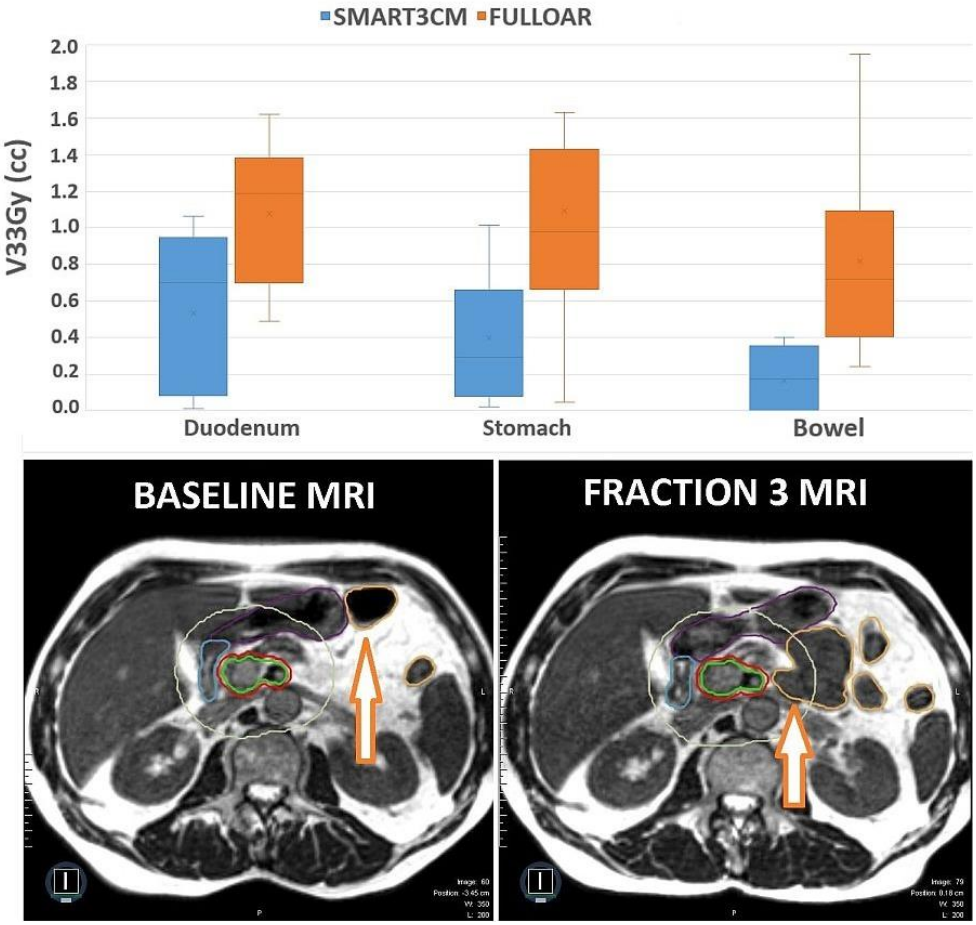

Figure 3. *Box-and-whisker plot showing V_{33Gy} (cc) values for $SMART_{3CM}$-adaptive (blue) and FULLOAR-adaptive (orange) for duodenum, stomach and bowel for those adaptive fractions where there is an increase of volume in OAR_{1cm} with respect to baseline (top row). Example of inter-fractional changes in the anatomy of patient 3 (bottom row). Target structures GTV (green) and PTV (red) are shown together with OAR structures of duodenum (light blue), stomach (purple) and bowel (orange). Big arrow indicates an extreme inter-fractional change for bowel.*

and manually adjust contours within 3 cm from the PTV and perform plan (re-)optimization with dose calculation, which is an acceptable time frame. Reviewing of contours and optimization objectives for the partitioned OARs was restricted to 3 cm from the PTV. This distance was chosen as beyond 3 cm all doses are well below 35% of the prescribed dose for all OARs, as extracted from the 66 plans used to build the model (Supplementary Figure 1, end of this chapter). Most complications and

toxicity in LAPC arise from high doses to OARs[19,21,22,25,30–34]. Murphy et al.[25] established a dosimetric model of duodenal toxicity after SBRT for pancreatic cancer, in which a good correlation was found between the actuarial rates of toxicity and the volumes of duodenum delineated within 3 cm from PTV receiving high doses.

Our $SMART_{3CM}$ approach relies on a model which is able to predict dose in OAR and provides optimization objectives for robust planning based on anatomical information. The OAR_{1cm}, OAR_{2cm} and OAR_{3cm} structures used in the optimization are variable and adapted at each fraction according to the anatomy of the day. Therefore, the dose gradient from PTV to OARs is also adapted at plan re-optimization according to the anatomy of the day.

Our strategy shares some similarities with the gradient maintenance method proposed by Ahunbay et al.[5]. However, there are also differences. By using ANN in our ART strategy for dose prediction and generation of robust baseline plans, information about the dose in different volumes of each OAR is provided, allowing for robust plans which are less dependent on the dosimetrist skills. Furthermore, if an OAR comes closer to the PTV at treatment in comparison to baseline, the proposed method by Ahunbay et al[5] is not able to produce a new dose gradient, whereas that situation is accounted for with our $SMART_{3CM}$ strategy.

Conclusion

In this manuscript a new adaptive strategy is proposed for plan (re-)optimization which produces robust and fast treatment plans meeting all clinical constraints and achieving good OAR sparing. This approach requires clinicians to only review and adjust OARs located within 3 cm from the PTV. This methodology has been analysed

for pancreatic tumours but it can also be implemented for other treatment sites which benefit from daily plan adaptation, such as prostate or adrenal gland.

Acknowledgments

We thank A. Bohoudi and G. Ybeles Smit from FUTURE FACTS Amsterdam for their advice and knowledge regarding the ANN model.

References

1. Wu, Q. J., Li, T., Wu, Q. & Yin, F. F. Adaptive radiation therapy: Technical components and clinical applications. *Cancer Journal* **17**, 182–189 (2011).
2. McVicar, N., Popescu, I. A. & Heath, E. Techniques for adaptive prostate radiotherapy. *Physica Medica* **32**, 492–498 (2016).
3. Li, Y. *et al.* Dosimetric benefit of adaptive re-planning in pancreatic cancer stereotactic body radiotherapy. *Med. Dosim.* **40**, 318–324 (2015).
4. Ahunbay, E. E. *et al.* Online adaptive replanning method for prostate radiotherapy. *Int. J. Radiat. Oncol. Biol. Phys.* **77**, 1561–1572 (2010).
5. Ahunbay, E. E. & Li, X. A. Gradient maintenance: A new algorithm for fast online replanning. *Med. Phys.* **42**, 2863–2876 (2015).
6. Oh, S. *et al.* Hybrid adaptive radiotherapy with on-line MRI in cervix cancer IMRT. *Radiother. Oncol.* **110**, 323–328 (2014).
7. Vestergaard, A. *et al.* Adaptive plan selection vs. re-optimisation in radiotherapy for bladder cancer: a dose accumulation comparison. *Radiother. Oncol.* **109**, 457–62 (2013).
8. Liu, F., Erickson, B., Peng, C. & Li, X. A. Characterization and management of interfractional anatomic changes for pancreatic cancer radiotherapy. *Int. J. Radiat. Oncol. Biol. Phys.* **83**, e423–e429 (2012).
9. Wysocka, B. *et al.* Interfraction and Respiratory Organ Motion During Conformal Radiotherapy in Gastric Cancer. *Int. J. Radiat. Oncol. Biol. Phys.* **77**, 53–59 (2010).
10. Li, X. A. *et al.* Interfractional Variations in Patient Setup and Anatomic Change Assessed by Daily Computed Tomography. *Int. J. Radiat. Oncol. Biol. Phys.* **68**, 581–591 (2007).
11. Shiinoki, T. *et al.* Interfractional reproducibility in pancreatic position based on four-dimensional computed tomography. *Int. J. Radiat. Oncol. Biol. Phys.* **80**, 1567–1572 (2011).
12. Jayachandran, P. *et al.* Interfractional Uncertainty in the Treatment of Pancreatic Cancer With Radiation. *Int. J. Radiat. Oncol. Biol. Phys.* **76**, 603–607 (2010).
13. Isobe, K. *et al.* A case of gastric lymphoma with marked interfractional gastric movement during radiation therapy. *Int. J. Clin. Oncol.* **11**, 159–161 (2006).
14. Knybel, L. *et al.* The analysis of respiration-induced pancreatic tumor motion based on reference measurement. *Radiat. Oncol.* **9**, 192 (2014).
15. Heerkens, H. D. *et al.* MRI-based tumor motion characterization and gating schemes for radiation therapy of pancreatic cancer. *Radiother. Oncol.* **111**, 252–257 (2014).
16. Lin, J. C., Jen, Y. M., Li, M. H., Chao, H. L. & Tsai, J. T. Comparing outcomes of stereotactic body radiotherapy with intensity-modulated radiotherapy for patients

with locally advanced unresectable pancreatic cancer. *Eur. J. Gastroenterol. Hepatol.* **27**, 259–264 (2015).

17. Chang, D. T. *et al.* Stereotactic radiotherapy for unresectable adenocarcinoma of the pancreas. *Cancer* **115**, 665–672 (2009).
18. Kim, S. K., Wu, C. C. & Horowitz, D. P. Stereotactic body radiotherapy for the pancreas: A critical review for the medical oncologist. *Journal of Gastrointestinal Oncology* **7**, 479–486 (2016).
19. Trakul, N., Koong, A. C. & Chang, D. T. Stereotactic Body Radiotherapy in the Treatment of Pancreatic Cancer. *Semin. Radiat. Oncol.* **24**, 140–147 (2014).
20. Mahadevan, A. *et al.* Stereotactic body radiotherapy and gemcitabine for locally advanced pancreatic cancer. *Int. J. Radiat. Oncol. Biol. Phys.* **78**, 735–742 (2010).
21. Schellenberg, D. *et al.* Gemcitabine Chemotherapy and Single-Fraction Stereotactic Body Radiotherapy for Locally Advanced Pancreatic Cancer. *Int. J. Radiat. Oncol. Biol. Phys.* **72**, 678–686 (2008).
22. Bittner, M.-I., Grosu, A.-L. & Brunner, T. B. Comparison of toxicity after IMRT and 3D-conformal radiotherapy for patients with pancreatic cancer – A systematic review. *Radiother. Oncol.* **114**, 117–121 (2015).
23. Yovino, S. *et al.* Intensity-modulated radiation therapy significantly improves acute gastrointestinal toxicity in pancreatic and ampullary cancers. *Int. J. Radiat. Oncol. Biol. Phys.* **79**, 158–162 (2011).
24. Goldsmith, C. *et al.* Dose-Volume Histogram Analysis of Stereotactic Body Radiotherapy Treatment of Pancreatic Cancer: A Focus on Duodenal Dose Constraints. *Seminars in Radiation Oncology* **26**, 149–156 (2016).
25. Murphy, J. D. *et al.* A dosimetric model of duodenal toxicity after stereotactic body radiotherapy for pancreatic cancer. *Int. J. Radiat. Oncol. Biol. Phys.* **78**, 1420–1426 (2010).
26. Kupelian, P. & Sonke, J. J. Magnetic Resonance-Guided Adaptive Radiotherapy: A Solution to the Future. *Semin. Radiat. Oncol.* **24**, 227–232 (2014).
27. Mutic, S. & Dempsey, J. F. The ViewRay System: Magnetic Resonance-Guided and Controlled Radiotherapy. *Semin. Radiat. Oncol.* **24**, 196–199 (2014).
28. Acharya, S. *et al.* Online Magnetic Resonance Image Guided Adaptive Radiation Therapy: First Clinical Applications. *Int. J. Radiat. Oncol.* **94**, 394–403 (2016).
29. Shaw, E. *et al.* Single dose radiosurgical treatment of recurrent previously irradiated primary brain tumors and brain metastases: final report of RTOG protocol 90-95. **47**, 291–298 (2000).
30. Moningi, S. *et al.* Stereotactic body radiation therapy in pancreatic cancer: The new frontier. *Expert Review of Anticancer Therapy* **14**, 1461–1475 (2014).
31. Brunner, T. B., Nestle, U., Grosu, A.-L. & Partridge, M. SBRT in pancreatic cancer: what is the therapeutic window? *Radiother. Oncol.* **114**, 109–16 (2015).

32. De Bari, B. *et al.* Hypofractionated radiotherapy in pancreatic cancer: Lessons from the past in the era of stereotactic body radiation therapy. *Crit. Rev. Oncol. Hematol.* **103**, 49–61 (2016).

33. Koong, A. C. *et al.* Phase I study of stereotactic radiosurgery in patients with locally advanced pancreatic cancer. *Int. J. Radiat. Oncol. Biol. Phys.* **58**, 1017–1021 (2004).

34. Elhammali, A. *et al.* Late gastrointestinal tissue effects after hypofractionated radiation therapy of the pancreas. *Radiat. Oncol.* **10**, 186 (2015).

Supplementary materials

Data preparation for ANN training

A total of 66 high quality SBRT treatment plans produced with the MRIdian TPS fulfilling constraints of clinical protocol for LAPC were used as training plans. A database was assembled from patient-specific anatomical information (PTV (cc), GTV (cc), Duodenum (cc), Bowel (cc), Stomach (cc), Kidneys (cc), Liver (cc), OAR_{1cm} (cc), OAR_{2cm} (cc), OAR_{3cm} (cc) and average patient effective depth to isocenter (cm)), plan quality parameters (CI, HI and GI) and dosimetric information ($D_{prescription}$ and the D_{median} at discretized portions of the OARs from 1 mm up to 50 mm distance from the PTV). Figure 1 shows a jitter graph of the most relevant parameters for dose prediction extracted from the 66 SBRT treatment plans. Database was subsequently imported into a dedicated machine learning software platform (IBM SPSS Modeler v18, IBM®). As an additional analysis, which is outside the scope of this manuscript, other algorithms were also evaluated, but none showed to be superior to the Artificial Neural Networks (ANN)[1]. A feature selection tool was used to select the most relevant input variables for dose prediction by measuring the predictive power of input variables through a sensitivity analysis[2].

ANN training

The architecture including input layers, hidden layers and output layer of the feed-forward multilayer ANN model is shown in figure 2. A hyperbolic tangent was used as activation function for the hidden layer consisting of 4 neurons and a linear activation function for the output layer. In general this algorithm consists of the following steps: 1) estimation of the initial weights by applying an alternated simulated annealing and training procedure on a random sample; 2) computation of

the derivative of the error function via the error back propagation algorithm; 3) update of the estimated weights via the gradient scaled conjugate gradient method.

ANN validation

The ANN model for dose prediction was validated on a total of 42 new SBRT treatment plans. The SBRT plans are based on IMRT step-and-shoot and consist of 6 beam groups, with each beam group consisting of three equidistant beams at 60° separation in correspondence with the geometry of the three ^{60}Co sources on the gantry. The inverse optimization in the MRIdian TPS is realized with a convex-nonlinear optimization algorithm where instead of dose-volume objectives, dose limiting parameters of the penalty function are directly modified, including minimum-, maximum -dose thresholds, relative weights and powers for each organ or target[3]. Standard dose thresholds were chosen for the PTV (min = 100% of $D_{prescription}$, max = 125% of $D_{prescription}$). The maximum dose thresholds (i.e. optimization objectives) for OAR_{1cm}, OAR_{2cm} and OAR_{3cm} were predicted by the ANN according to patient-specific anatomical input parameters resulting in robust individualized optimization parameters. The same relative linear weights and powers for each $OAR_{1–3cm}$ were used for (re-)optimization. Figure 3 shows the agreement between the predicted and extracted D_{median} for the partitioned OARs from 1 mm up to 50 mm distance from PTV for the 42 SBRT plans used to validate the ANN (Spearman's correlation coefficient = 0.98).

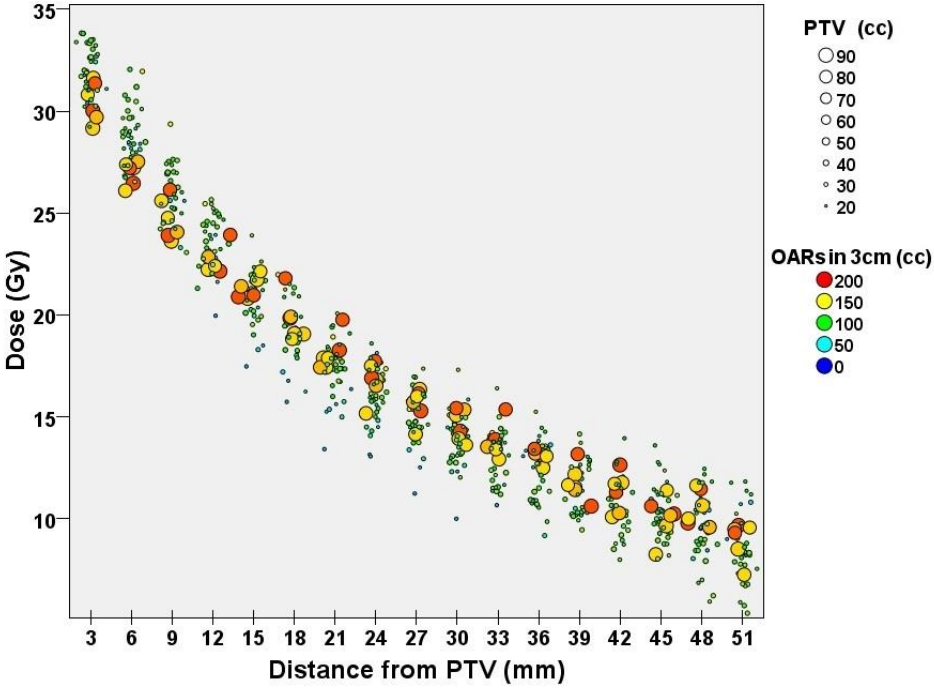

Supplementary Figure 1. *Jitter-graph of the most relevant parameters for dose prediction extracted from the 66 SBRT treatment plans. Symbol size represent PTV size (cc) and the different colours the volume of OARs around the PTV in the first 3 cm.*

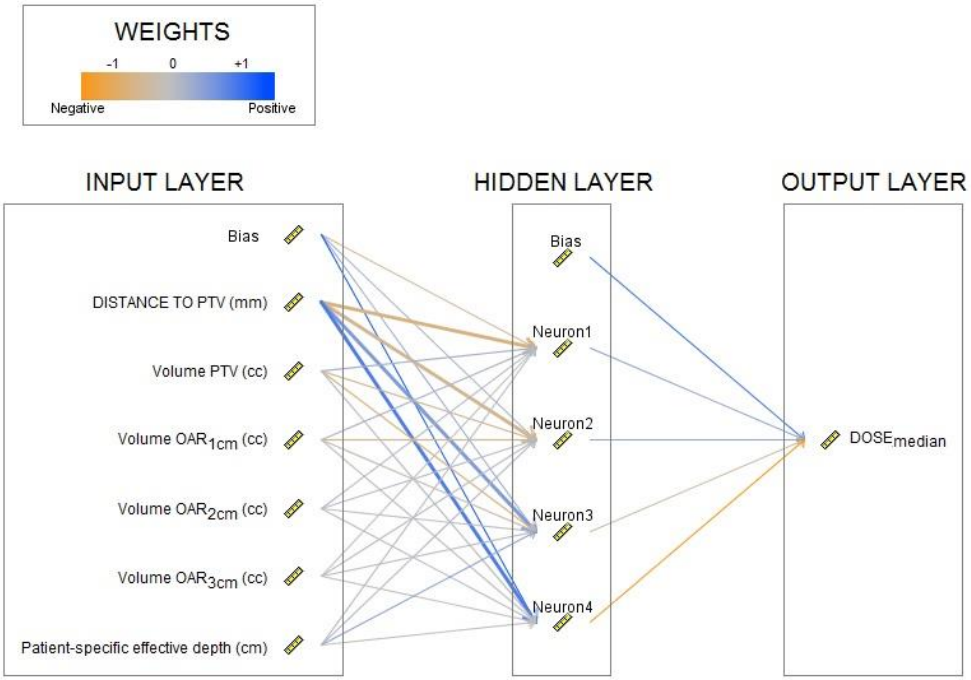

Supplementary Figure 2. *ANN architecture for dose prediction in OAR in online stereotactic MR-guided adaptive radiation therapy (SMART). Input parameters used to build the ANN were: PTV size (cc), volume of* OAR_{1cm} *(cc),* OAR_{2cm} *(cc) and* OAR_{3cm} *(cc), distance from PTV (mm) and patient-specific effective depth to isocenter (cm). Estimates of the median dose (*D_{median}*) at discretized portions of OARs from 1 mm up to 50 mm from the PTV were generated as output parameters.*

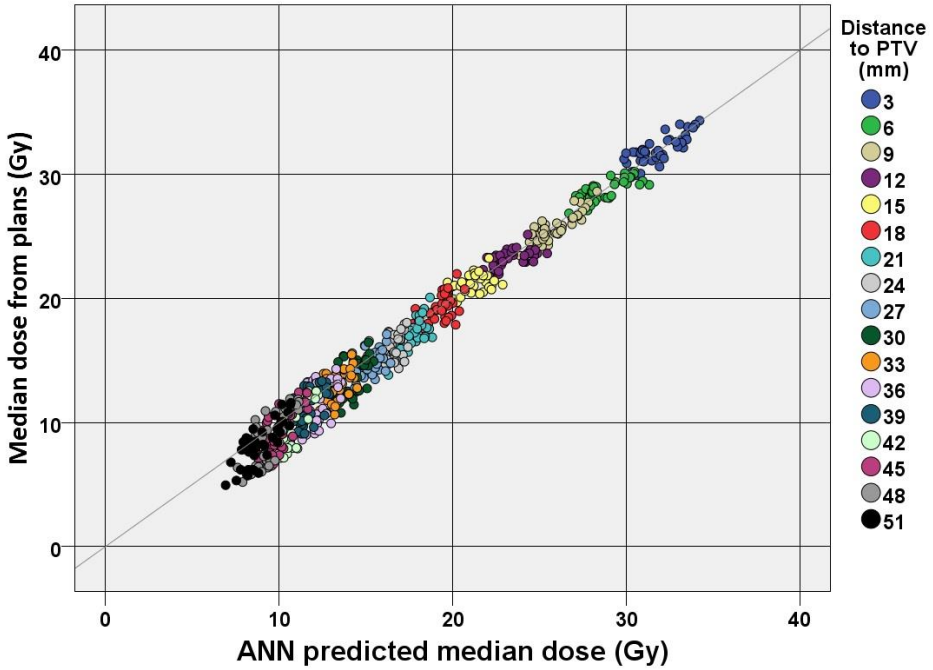

Supplementary Figure 3. *Agreement between the predicted and extracted* D_{median} *for the partitioned OARs from 1 mm up to 50 mm distance from PTV for the 42 SBRT plans used to validate the ANN (Spearman's correlation coefficient = 0.98).*

References Supplementary Materials

1. Bishop, C. M. Neural networks: a pattern recognition perspective. *Neural Networks* 1–23 (1996). doi:10.1.1.46.8742
2. A. Saltelli, Stefano Tarantola, Francesca Campolongo, M. R. *Sensitivity analysis in practice*. *Journal of Chemical Information and Modeling* **53**, (1989).
3. Wooten, H. O. *et al.* Quality of Intensity Modulated Radiation Therapy Treatment Plans Using a (60)Co Magnetic Resonance Image Guidance Radiation Therapy System. *Int. J. Radiat. Oncol. Biol. Phys.* **92**, 771–8 (2015).

Chapter 3

Clinical implementation of magnetic resonance imaging guided adaptive radiotherapy for localized prostate cancer

Shyama U. Tetar
Anna M.E Bruynzeel
Frank J. Lagerwaard
Ben J. Slotman
Omar Bohoudi
Miguel A. Palacios

Physics and Imaging in Radiation Oncology. 2019; 9: 69-76.

Abstract

Background and Purpose: Magnetic resonance-guided radiation therapy (MRgRT) has recently become available in clinical practice and is expected to expand significantly in coming years. MRgRT offers marker-less continuous imaging during treatment delivery, use of small clinical target volume (CTV) to planning target volume (PTV) margins, and finally the option to perform daily plan re-optimization.

Material and Methods: A total of 140 patients (700 fractions) have been treated with MRgRT and online plan adaptation for localized prostate cancer since early 2016. Clinical workflow for MRgRT of prostate cancer consisted of patient selection, simulation on both MR- and computed tomography (CT) scan, inverse intensity-modulated radiotherapy (IMRT) treatment planning and daily plan re-optimization prior to treatment delivery with partial organs at risk (OAR) recontouring within the first 2 cm outside the PTV. For each adapted plan online patient-specific quality assurance (QA) was performed by means of a secondary Monte Carlo 3D dose calculation and gamma analysis comparison. Patient experiences with MRgRT were assessed using a patient-reported outcome questionnaire (PRO-Q) after the last fraction.

Results: In 97% of fractions, MRgRT was delivered using the online adapted plan. Intrafractional prostate drifts necessitated 2D-corrections during treatment in approximately 20% of fractions. The average duration of an uneventful fraction of MRgRT was 45 minutes. PRO-Q's (N=89) showed that MRgRT was generally well tolerated, with disturbing noise sensations being most commonly reported.

Conclusions: MRgRT with daily online plan adaptation constitutes an innovative approach for delivering SBRT for prostate cancer and appears to be feasible, although necessitating extended timeslots and logistical challenges.

Introduction

External beam radiotherapy (EBRT) is the treatment of choice in approximately one third of patients with localized prostate cancer (cT1c-T3N0M0) and this proportion increases with higher age. When EBRT is selected as the treatment of choice, the guideline-recommended total radiation dose for localized prostate cancer is 78–80 Gy. However, delivering this total dose in small daily fractions (e.g. 1.8–2 Gy/fraction) requires up to eight weeks of fractionated EBRT. Prostate cancer appears to be characterized by a low α/β value and consequently, large radiation doses per fraction (hypofractionation) can be expected to increase tumour kill for prostate cancer while minimizing late toxicity to critical structures[1–3]. Based on this concept, many radiation oncology centers have adopted the concept of moderate hypofractionation (fraction sizes of 2.5–4 Gy) or extreme hypofractionation (fraction size >4 Gy), also known as stereotactic body radiotherapy (SBRT) for routine treatment of localized prostate cancer.

Inter- and intra-fractional organ changes entail major problems for the safe delivery of intended doses in EBRT for tumours located in the abdominal and pelvic region, especially for hypofractionated schemes. Substantial variability in rectum and bladder filling has been observed in the past for patients treated for prostate cancer[4–6] and lower biochemical tumour control was reported for patients with larger rectum volumes at the time of the CT simulation[7], presumably because of geographic misses. Several studies have investigated inter-fractional prostate variability by means of repeated CT, kV or online CBCT (for a review on this topic, see [8]). Mean prostate displacements of up to 9 mm between fractions have been reported, with the largest deviation found in the anterior-posterior (AP) direction[8,9]. Seminal vesicles, which are included in the target volume for intermediate and high risk

disease patients, are subjected to even larger inter-fractional shifts than the prostate[10]. In addition, intra-fractional rotations and deformations of prostate and seminal vesicles because of variable rectal filling have been reported[11]. Proper management of such inter- and intra-fractional variations during radiotherapy delivery may allow treatment margin reduction to 3 mm[12].

Daily image-guided radiotherapy (IGRT) improves the precision and accuracy of treatment delivery for prostate cancer[10]. Standard IGRT repositioning protocols based on patient registration on the prostate are able to adequately correct for the dosimetric effects of inter-fractional variations in approximately two-thirds of the treatment fractions[13]. Current employed IGRT techniques, such as kV radiographs or cone-beam computed tomography (CBCT) are usually combined with implanted fiducial markers; however these lack detailed target and organ at risk (OARs) visualization. MR-guided radiation therapy (MRgRT) allows for superior visualization of the prostate, base of the seminal vesicles and adjacent OARs such as the rectum and bladder prior to- and during treatment delivery. This allows for treatment with small uncertainty margins and in combination with daily plan re-optimization may result in relevant reductions of doses to normal tissues[14,15]. In addition, in-room MR imaging renders implanted gold markers redundant, thereby avoiding an invasive procedure.

Several published papers have described the use of MRgRT[16–19] in the upper abdominal region, but reports on the use of MRgRT for prostate cancer have been rather of theoretical nature[8,20]. In this study we describe the first clinical implementation of a daily online adaptive MRgRT workflow for SBRT in prostate cancer. Superior soft-tissue visualization in combination with intra-fraction motion management allowed us to reduce PTV margins to 3 mm and deliver doses of 7.25 Gy per fraction. We report on the time needed for our MRgRT clinical workflow

and the frequency of online corrections due to intra-fractional variations in the prostate position. Patient reported outcomes of MRgRT and results from patient-specific QA are also presented. Finally, we aim to illustrate potential pitfalls of MRgRT for prostate cancer.

Material and Methods

At the Amsterdam University medical center, location VUmc, clinical MRgRT has been performed since early 2016 using the MRIdian® system (ViewRay, Inc., Mountain View, CA). For localized prostate cancer, MRgRT has been delivered in 140 patients in 700 fractions between May 2016 and June 2018, initially with the tri-^{60}Co system (n = 130), currently with the MR-Linac (n = 10). The majority (n = 100) of patients have been treated within the context of a prospective phase II trial. The clinical results of this trial will become available in mid-2019.

First consultation

All patients treated with MRgRT for prostate cancer were previously discussed in a multidisciplinary tumor board. Clinical stage of patients with localized prostate cancer treated with MRgRT was T1-3b without severe urinary symptoms as measured by International Prostate Symptom Scoring (IPSS). Patients with prior local treatment, e.g. high intensity focused ultrasound (HIFU), brachytherapy, or cryotherapy were not considered candidates for SBRT with the exception of a transurethral resection of prostate (TURP) if performed more than two months prior to radiation. All patients were routinely checked for contra-indications for MRgRT, similar as for diagnostic MR scans.

Simulation

Every patient underwent a CT simulation scan with a slice thickness of 2mm for dose calculation purposes, and a high-resolution (HR) MR scan (TR/TE: 3.37 ms/1.45 ms, FA: 60°) acquired at the MRIdian with 1.5 mm x 1.5 mm x 1.5 mm resolution prior to treatment. The maximum time span between both examinations was 30 min. MR scan acquisition is based on a balanced steady-state free precession technique (True FISP) providing T2/T1-weighted contrast. The anatomy around the prostate exhibits similar contrast as in T2-weighted sequences, which is recommended for target volume delineation for primary radiation therapy of localized prostate cancer[21]. MR acquisition in the pelvic region for treatment planning at the MRIdian took between 65 and 172 seconds, depending on the scan range and field of view (FOV). Flexible coils were used which were placed around the patient in the pelvic region.

Simulation and delivery was executed in supine position with the use of (dummy) coils and head phones for noise reduction. Patient positioning was performed on an MR-compatible positioning board (Macromedics, Waddinxveen, The Netherlands), including foot, knee and arm support. The acquired CT was non-rigidly co-registered with the simulation MR, with the fusion centered on the area of interest, i.e. the prostate. When gas in rectum was variable between the CT and MR simulation, special care was taken to obtain a good agreement between the anatomies reflected in both scans after non-rigid registration, especially in the area of the CTV (prostate). Patients were instructed to empty their bladder two hours before treatment, followed by intake of 500 ml of water. No specific rectal preparations such as endorectal balloons or pre-treatment enemas were required.

Target definition and radiation dose fractionation

For MRgRT of prostate cancer, target definition was basically identical to other techniques delivering SBRT. Briefly, the clinical target volume (CTV) was delineated on the simulation MR-scan. For 'low risk' patients (cT1c-T2a, Gleason <7 and PSA <10 μg/L), the CTV consisted of the prostate gland. For 'high' and 'intermediate risk' patients[22], the base of the seminal vesicles was also included in the CTV. As a result of daily MR-based setup, low spatial distortion, online plan adaptation and real-time prostate monitoring during treatment, only a 3 mm CTV to PTV uniform margin was used for MRgRT. For baseline planning, relevant OAR, i.e. the bladder, rectum, urethra and femora were contoured on the MR-scan. A good discrimination between the posterior border of the prostate and the anterior rectal wall was obtained with current MR True FISP sequence. Although not standard in SBRT for prostate cancer, in an attempt to decrease acute and late urinary toxicity, integrated urethral sparing was used by generating an urethral $PTV_{urethra}$ with a margin of 2-3 mm around the delineated urethra (Figure 1). Most patients were treated with 5 fractions of 7.25 Gy per fraction delivered on the prostate with a simultaneous integrated sparing (SIS) of the urethra with a dose of 32.5 Gy in 5 fractions (6.5 Gy per fraction).

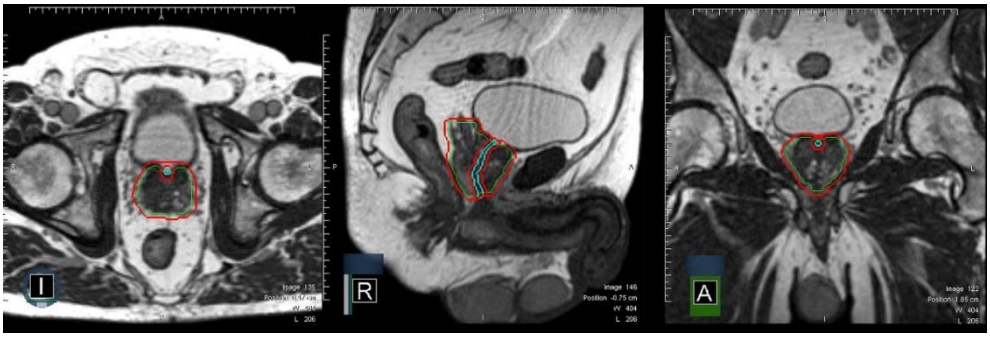

Figure 1. *Contouring for MRgRT: CTV consisting of prostate and base of vesicles (green contour), PTV (CTV + 3 mm; red contour) visualized in an axial, sagittal and coronal plane. The urethral contour (cyan contour) and urethral PRV (urethra + 2 mm) can be best seen in the sagittal plane.*

In some cases (n=10) with tumour near the urethra, the SBRT was delivered in fractions of 7 Gy up to a total dose of 35 Gy without urethral sparing. The majority of OAR constraints were expressed in absolute volume (cc), which allows partial contour delineation during the adaptive workflow (see also below).

Online contour generation

At each fraction, online new contours were generated for prostate, OARs and structures needed for treatment planning. Firstly, the CTV was rigidly copied from the pre-treatment MR scan to the MR volumetric scan of the day and both scans were rigidly registered on the target. The CTV is then edited by the physician when needed, accounting for rotations and deformations of the prostate and/or seminal vesicles. After that, a new PTV (CTV + 3 mm) was automatically generated to account for delineation uncertainties, intra-fraction motion and random spatial distortions on the MR-scan (less than 1 mm in a 20 cm DSV). A second non-rigid registration of both MR-scans was thereafter performed and the deformation field map was also applied to the OAR contours to generate structures reflecting the anatomy-of-the-day. The deformable registration algorithm implemented on the MRIdian and employed for online adaptive minimizes a cost function that measures the similarity between the images. It also uses a regularization term to obtain smoother deformation fields and prevents sharp discontinuities. The optimization method relies on a simple gradient descend performing the registration firstly on a down sampled version of the image serving the results as initial guesses for each upper level.

The electron density map generated from the CT for dose calculation underwent the same deformation applied to the OAR contours. The newly generated electron density map for that particular fraction was briefly checked by the radiation technologist and physicist for the presence of missing tissue densities and mismatch

for air pockets in rectum. In case of mismatch, structure densities were overridden and corrected online before dose calculation and plan adaptation.

Treatment planning

Treatment planning and delivery was performed with static field intensity modulated radiotherapy (IMRT). A relatively high number of beams were used (15) which provided enough degrees of freedom and flexibility to re-adapt the plan and account for anatomical changes. Typically around 45 segments were generated which in combination with the different beam angle incidence produced treatment plans achieving the modulation needed for selective urethral sparing. The MRIdian Linac version uses a double focused, double-stacked multileaf collimation (MLC) in combination with 6MV FFF photons, allowing for highly conformal dose distributions and steep dose gradients at the borders with adjacent OARs. The obtained dosimetry for treatment planning in MRgRT is comparable to VMAT techniques[23]. Our treatment planning approach for MRgRT has been developed with daily plan adaptation in mind[24], and will be presented below.

Dose calculation was performed with a Monte-Carlo algorithm implemented in the MRIdian system based on VMC and EGSnrc codes[25,26]. The algorithm can complete an IMRT plan calculation subject to a magnetic field in 2 min. For clinical plans, a statistical uncertainty of 1% was used with a dose grid resolution of 0.2 cm × 0.2 cm × 0.2 cm.

MR-guided online adaptive workflow

A summary of the treatment workflow for MRgRT with daily plan adaptation implemented at our center is visualized in Figure 2. After MR acquisition and patient registration, CTV and OAR contours always needed to be online adjusted by the attending radiation oncologist to correct for variations in the position of the upper

part of the prostate and base of the seminal vesicles. For the daily plan adaptation whilst the patient is in treatment position, only OARs in the first 2 cm outside the PTV were corrected to allow for a fast online workflow.

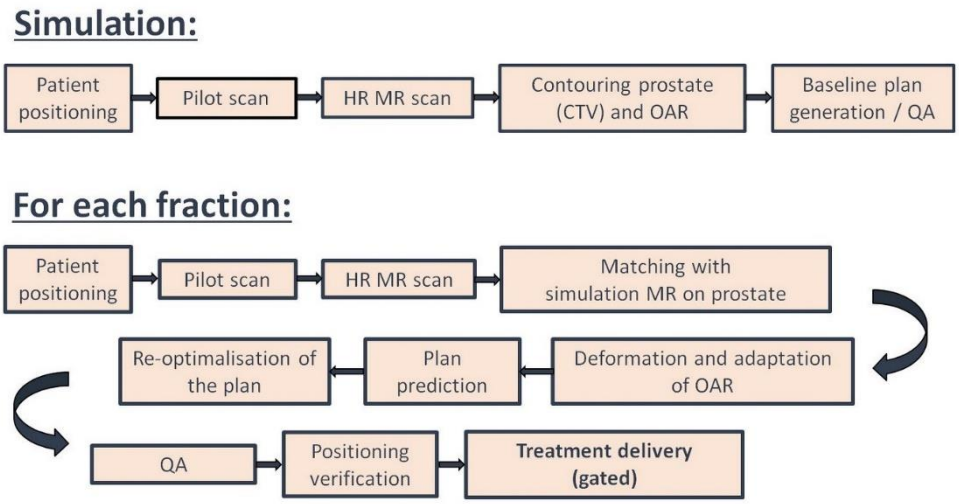

Figure 2. *Workflow for MRgRT with online plan adaptation for prostate cancer. HR = high resolution, MR = magnetic resonance, CTV = clinical target volume, OAR = organs at risk, QA = quality assurance.*

At each fraction a new electron density map for dose calculation was generated after applying deformable image registration. Subsequently, two plans were generated: the baseline plan re-calculated on the anatomy-of-the-day (predicted plan) and the re-optimized plan. The re-optimized plan was generated by OAR partitioning within the first 2 cm from the PTV surface and updating all necessary structures for treatment planning by means of an automated script. Both plans were reviewed by the radiation oncologist and physicist whether they met the preset plan objectives. An example of the potential of plan adaptation in one patient undergoing an MRgRT treatment can be seen in Figure 3, where the baseline plan, predicted plan and re-optimized plan for a particular fraction can be observed.

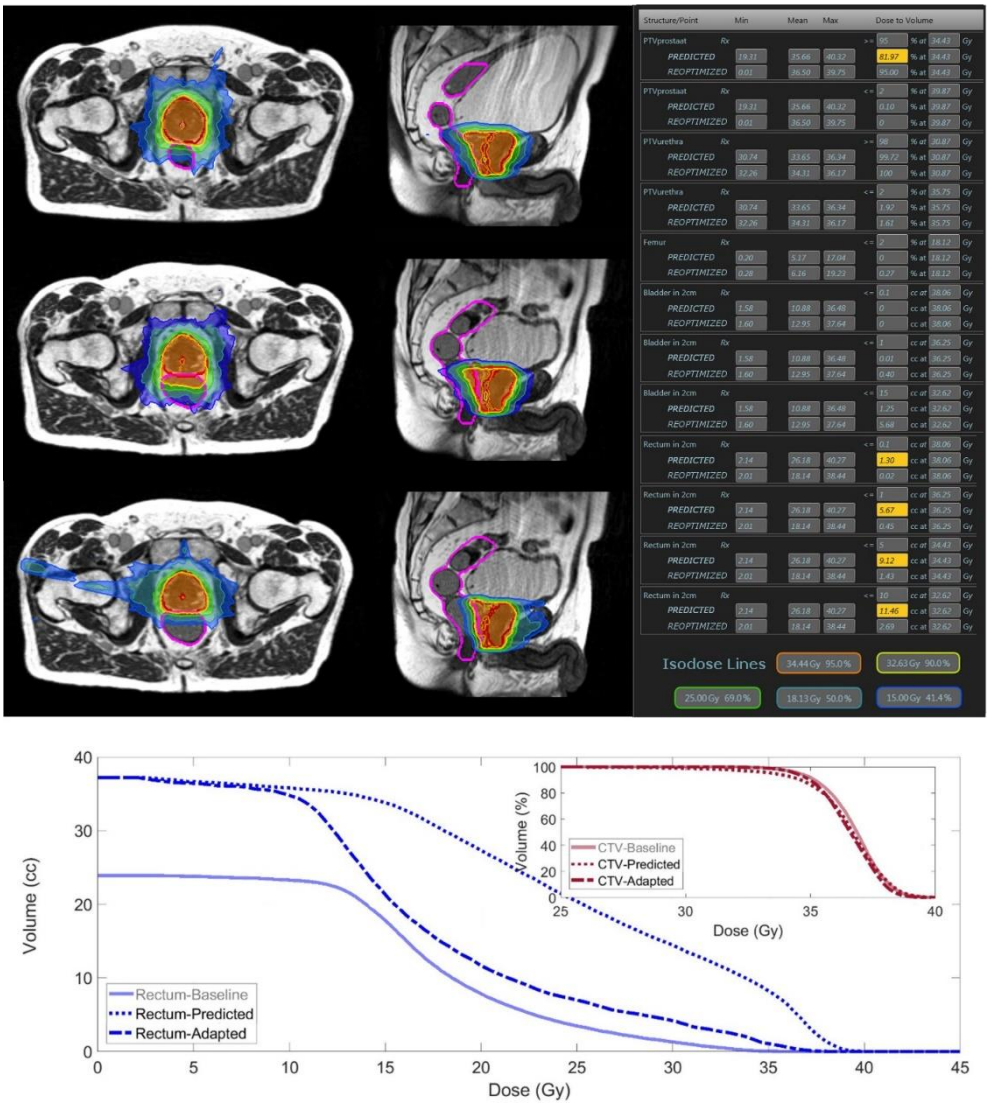

Figure 3. *Treatment plan at baseline (top row), predicted plan (middle row) and adapted plan (bottom row) at one particular fraction. Objectives and clinical constraints according to the institutional protocol for SBRT in prostate cancer can be seen on the right of the figure, where a comparison of the values achieved by the predicted and adapted plan is shown. Values which do not meet the preset values are highlighted in yellow. At the bottom of the figure, a DVH comparison of the three plans is shown.*

Initial anatomy at baseline showed some distance between the prostate and rectum allowing for adequate coverage of CTV and sparing of rectum. However, rectum distension brought forth a pitch and deformation on the prostate at one particular fraction, resulting in suboptimal CTV coverage and an increased dose to the rectum. Online plan re-optimization following proposed strategy resulted in adequate rectum sparing and recovery of CTV coverage.

Patient-specific QA

Prior to plan approval at the treatment console, patient-specific quality assurance (QA) of the adapted plan was performed using an independent Monte-Carlo dose calculation algorithm and gamma analysis (3%/3 mm)[27–30]. The Monte-Carlo engine for QA purposes uses phase space data recorded in a plane just above the MLC and the transport in the patient is loosely based on the DPM Monte-Carlo code[31]. It used the same beam parameters, segments shapes and electron density map as the treatment plan made with the MRIdian, resulting in a second 3D dose distribution. At each fraction a pdf-report was generated including gamma pass-rates and gamma mean values for the comparison of both dose distributions. In addition, other plan parameters related to the IMRT modulation in the plan were also reported[27].

Patient Reported Questionnaires

From the start of clinical MRgRT, patient experiences were assessed using an in-house developed patient-reported outcome questionnaire (PRO-Q)[32]. From July 2016 till December 2017 we collected 89 questionnaires in prostate cancer patients. This PRO-Q included questions on potential MR-related complaints and experiences, such as anxiety, temperature, and noise. These items could be scored on a 4-point scale as: “not at all”, “a little”, “moderate”, and “very much”. PRO-Qs were collected

once, immediately following the last MRgRT fraction, taking the completion of the PRO-Q on average 5 min.

Results

Target coverage and patient-specific QA

Due to common manual adjustment of the CTV and the 3 mm PTV margin used, the predicted plan is generally suboptimal particularly for target coverage. In 97% (N = 677/700 fractions) of all fractions for prostate MRgRT the plan has been re-optimized. All adapted treatment plans have passed the patient-specific QA and the obtained average γ-pass rate for all 700 adapted fractions is $99.8 \pm 0.1\%$, with $\gamma_{mean} = 0.38 \pm 0.01$.

Treatment delivery

Beam-on delivery treatment time was on average 10 min and constituted approximately one quarter of the total treatment duration. At the onset of treatment delivery a brief cine movie of 10 s duration was performed at a single sagittal plane (4 frames-per-second, slice thickness 5 mm) previously selected by the physician in order to check the tracking accuracy (Figure 4). At the same time, it was verified that the position of the CTV had not changed from the first 3D MR-scan at the beginning of the fraction. Gated IMRT delivery was performed using a 3 mm gating boundary around the CTV. The system automatically shut off radiation delivery when the system detected that more than 7% (institute specific setting) of the CTV area is outside of the gating boundary (PTV) during MR-planar acquisition for intra-fraction monitoring. Prostate drifts and intra-fraction prostate rotation/deformation led to application of 2D shifts during treatment delivery in more than 20% of all

delivered fractions (149/700 fractions). Larger prostate shifts requiring repeat 3D imaging were observed in approximately 6% of fractions (39/700 fractions).

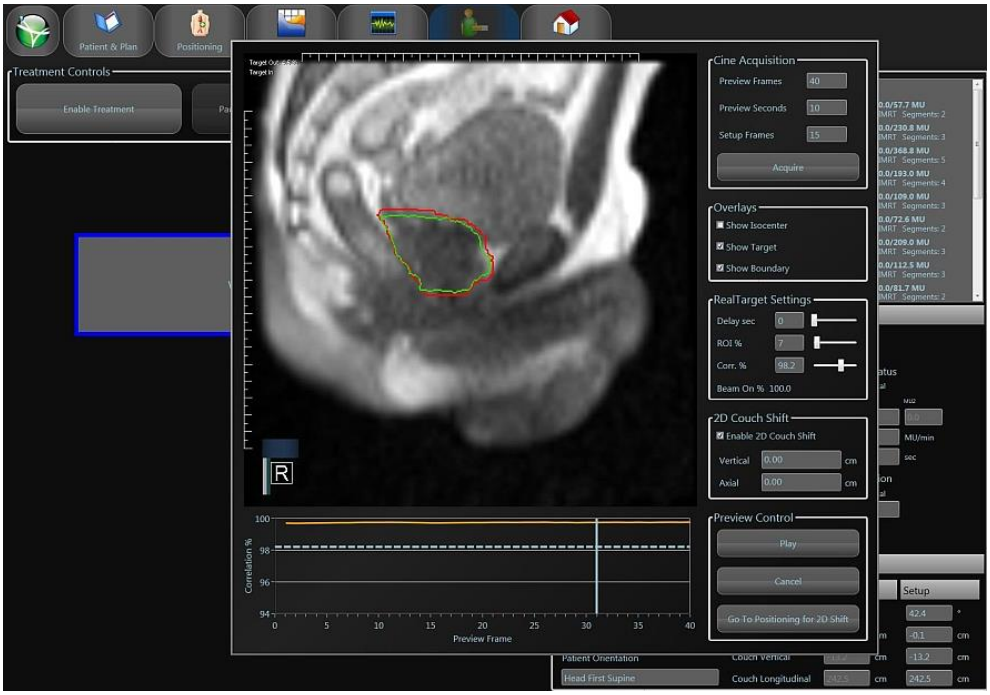

Figure 4. *Gated MRgRT delivery for prostate cancer. The gating target (CTV; green contour) and the gating boundary (red contour) are visualized on-screen. The geometric coverage ("Target out") is continuously displayed in the left upper corner.*

On average, the duration of an uneventful MRgRT fraction is approximately 45 min (range for all patients, 40–70 min). An overview of the relative duration of all the steps in our MRgRT workflow is shown in Table 1, being recontouring the step which took the longest.

Table 1. *Distribution of the measured absolute and relative duration of all steps in daily adapted MRgRT for prostate cancer. The contribution of every discipline to each of the steps is also highlighted on the last three columns (physician, physicist and radiation technologists, from left to right).*

SMART step	Time (min)	Physician	Physicist	Therapist
Patient setup	7.6			√
Registration	6.1	√		√
Delineation	10.7	√		√
Re-optimization	2.9	√	√	√
Plan QA	1.5		√	√
Beam-on Tx	15.9	√	√	√
Total	44.7			

Patient experiences

The majority of the patients tolerated MRgRT very well, and an overview of most commonly reported complaints is illustrated in Figure 5. Only a moderate proportion of patients reported light complaints of noise, paresthesia and cold because of the balanced steady-state free precession acquisition during beam-on for intra-fraction monitoring and the relatively long duration of the treatment.

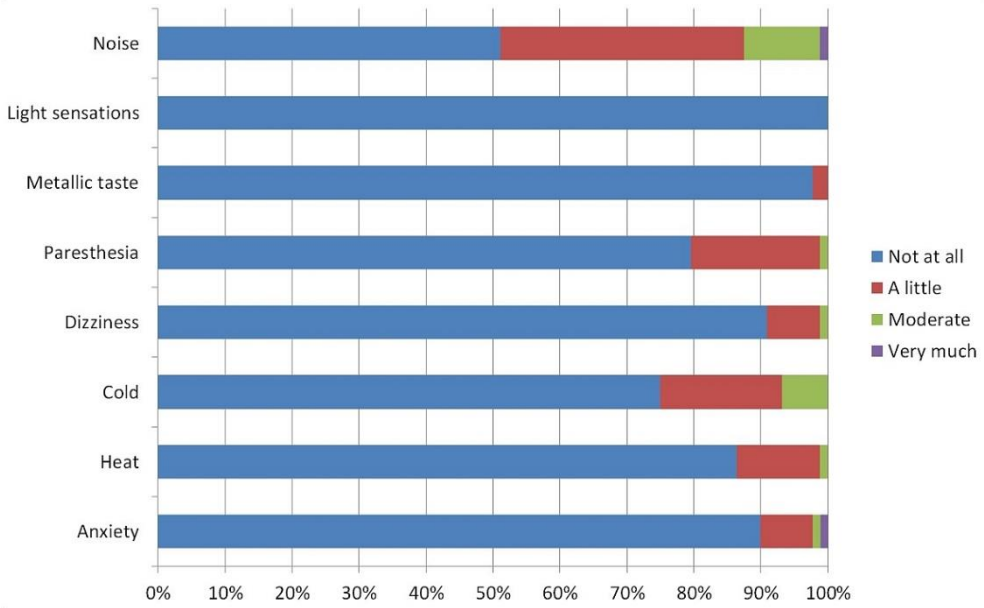

Figure 5. *Patient-reported complaints during MRgRT for prostate cancer (N = 89).*

Discussion

We have reported on our first clinical experience with MR-guided radiotherapy for prostate cancer patients. While it is customary for prostate cancer radiation therapy to instruct patients to have a full bladder prior to simulation and treatment, this appeared not to be practically for MRgRT. Initiating the MRgRT workflow with full bladder, regularly led to treatment interruptions because of the lengthy delivery time, particularly for later fractions when the first signs of radiation-induced cystitis occur. At present, patients are instructed to empty their bladder two hours before treatment, followed by intake of 500 ml of water. In clinical practice, this usually results in treatment with half full bladder, and variations in bladder and rectal filling can be corrected for by daily plan adaptation. Preselection of patients, based on IPSS scoring is recommended, not only for SBRT in general but certainly also for lengthy MRgRT[32]. Similar as for diagnostic MR scanning, severely claustrophobic patients do not tolerate MRgRT. These patients can be identified at an early stage on the basis of MR safety questionnaires, but in addition, simulation on the MR Linac aids in de-selecting these patients. Once MRgRT was started, no patient discontinued treatment for this reason, although occasional supportive anxiolytic medication was needed[32]. The presence of a hip prosthesis was no absolute contra-indication for MRgRT, as most modern implant materials are MR-compatible, the distortion caused by the metal has proven to be minimal at 0.35 T and, in addition, it has not borne additional difficulties for the delineation of the CTV.

The clinical implementation of (daily adapted) MRgRT constitutes a major logistic challenge for radiotherapy departments[20,24]. Our MR Linac is used for both simulation and treatment delivery, because using the same MR sequence facilitates subsequent co-registration and delineation. Time slots for treatment are necessarily

long (i.e. 45 min up to one hour), which indicates that daily adapted MRgRT is best tailored with (extreme) hypofractionation. We have tried to optimize our workflow by restricting recontouring of relevant OARs to the first 2 cm outside the PTV, which corresponds with the most relevant dose area for clinical toxicity and in which approximately ≥40% of the prescribed dose will be distributed[24,33]. Recontouring full OARs would take an unacceptable long time with the patient in treatment position. Similarly, OAR partitioning and adaptation steps are automatized as much as possible. Importantly, for the recontouring, quality assurance and plan approval steps, a radiation oncologist and physicist need to be physically present at the treatment console for each fraction to avoid further delays. However, even with all this preconditions, an uneventful MRgRT fraction still takes up to 45 min. A significant shorter time for each fraction is possible if further improvement in the deformable registration step of the original contours is achieved. However, other alternatives are also possible for the generation of new contours for both tumor and OARs at each fraction, such as the use of atlas based methods[34] or convolutional neural networks[35,36]. The time spent in recontouring and generating a new treatment plan could also be used to acquire additional MR sequences for offline evaluation of treatment response (for instance, diffusion weighted MRI[37]).

The ability to perform daily plan adaptation is one key advantage of MRgRT, which appeared to be required in the vast majority of patients. Both residual patient positioning errors and variations in bladder and rectal filling result in the necessity to adjust the contours of the CTV for each fraction, certainly with small 3 mm PTV margins. In actual practice, 97% of plans were delivered after plan re-optimization, mainly for this reason. For an accurate assessment of the predicted dose, i.e. recalculation of the baseline plan on the anatomy of the day, recontouring needs to be performed anyway. The plan adaptation step, including fast independent QA of

the generated plan, adds in general just a few minutes to the total treatment duration, as can been seen in Table 1. The dose calculation is performed using the electron density map from the CT-simulation after non-rigid registration to the anatomy of the day. Generation of an electron density map from the MR-scan for that particular fraction is also feasible[38], although this step would not shorten the total treatment session time. Image quality is directly related to a proper placement of the MR coils on the surface of the patient at the region of interest. Accurate patient positioning with the MR coils is also essential because the treatment couch can only be minimally moved in lateral and vertical direction.

The relatively high number of beams being used allows for a conformal dose distribution and offers the necessary degrees of freedom to the optimizer to generate a new fluence map to account for the anatomical changes. In our workflow, a full scope online re-optimization of the fluence and weights for each beam is performed, which usually produces the best results in terms of target coverage and OAR sparing[39]. However, other alternatives have been proposed when optimization and dose calculation time take too long. These include for instance, segment aperture morphing to create new apertures in combination with segment weight optimization[39] and adjustment of MLC leaf position for each subfield based on the inter-fractional target motion and deformation[40].

An innovative feature of MRgRT is the real-time imaging of a sagittal plane through the prostate, bladder and rectum, while visualizing the gating boundary. Prostate drifts have been described previously, one of the reasons why for instance 'triggered imaging' has been introduced into image-guided radiotherapy for prostate cancer. At this moment, real-time guidance with the MRIdian linac is restricted to this single plane. However, it is anticipated that multiplanar MR imaging will be available in the near future, which would result in real 3D tracking of the target volume and

improved accuracy. Intra-fractional changes in the prostate position occur relatively frequent, mostly due to air in the rectum or increasing bladder filling (see also figure in Supplementary material). One relatively simple option to correct for these positional changes is to temporarily interrupt treatment and perform a 2D shift in the table position. This 2D shift, which relies on the anatomical information provided by the MR cine in the sagittal plane, is restricted to the cranio-caudal and/or antero-posterior direction. The system can mechanically perform a shift of several cm, though as an institutional standard we restrict performing 2D shifts to a maximum of 3 mm, which is the PTV margin and also the gating boundary used for tracking. For larger changes in prostate position or suspicions of a lateral movement, treatment is interrupted and 3D positioning scans are repeated, followed by a couch shift correction, recontouring and a new dose prediction when needed. The occurrence of prostate drifts appears not to be uncommon and as a result of 3 mm margins as gating boundary, 2D shifts were needed in more than 20% of all delivered fractions (149/700 fractions). Larger prostate shifts requiring repeat 3D imaging were observed in approximately 6% of fractions (39/700 fractions). In the past it was reported that proper management of intrafractional uncertainty during radiotherapy delivery may allow treatment margin reduction to 3 mm[12]. However, such a small margin makes necessary to introduce refinements to the gated delivery using table adjustments, which has been the major reason for fractions exceeding a total duration of 45 min. At this moment, multiplanar real-time imaging, which would obviously be of benefit, is not yet clinically available on the MRIdian system.

Conclusion

In conclusion, MRgRT as a method to deliver SBRT for prostate cancer has been introduced clinically. This approach is promising but time consuming and logistically challenging requiring a multidisciplinary approach. Because of the advantages of soft-tissue setup without the need for implanted gold markers, online plan adaptation and real-time MR imaging during gated delivery, this technique is expected to expand in the coming years.

References

1. Kal, H. B. & Van Gellekom, M. P. . How low is the α/β ratio for prostate cancer? *Int. J. Radiat. Oncol.* **57**, 1116–1121 (2003).
2. Miralbell, R., Roberts, S. A., Zubizarreta, E. & Hendry, J. H. Dose-Fractionation Sensitivity of Prostate Cancer Deduced From Radiotherapy Outcomes of 5,969 Patients in Seven International Institutional Datasets: α/β = 1.4 (0.9–2.2) Gy. *Int. J. Radiat. Oncol.* **82**, e17–e24 (2012).
3. Proust-Lima, C. *et al.* Confirmation of a Low α/β Ratio for Prostate Cancer Treated by External Beam Radiation Therapy Alone Using a Post-Treatment Repeated-Measures Model for PSA Dynamics. *Int. J. Radiat. Oncol.* **79**, 195–201 (2011).
4. Pinkawa, M. *et al.* Influence of the initial rectal distension on posterior margins in primary and postoperative radiotherapy for prostate cancer. *Radiother. Oncol.* **81**, 284–290 (2006).
5. Pinkawa, M. *et al.* Bladder extension variability during pelvic external beam radiotherapy with a full or empty bladder. *Radiother. Oncol.* **83**, 163–167 (2007).
6. Landoni, V. *et al.* A study of the effect of setup errors and organ motion on prostate cancer treatment with IMRT. *Int. J. Radiat. Oncol.* **65**, 587–594 (2006).
7. de Crevoisier, R. *et al.* Increased risk of biochemical and local failure in patients with distended rectum on the planning CT for prostate cancer radiotherapy. *Int. J. Radiat. Oncol.* **62**, 965–973 (2005).
8. McPartlin, A. J. *et al.* MRI-guided prostate adaptive radiotherapy – A systematic reviewMRI-linac and prostate motion review. *Radiother. Oncol.* **119**, 371–380 (2016).
9. Moteabbed, M. *et al.* Impact of interfractional motion on hypofractionated pencil beam scanning proton therapy and VMAT delivery for prostate cancer. *Med. Phys.* **45**, 4011–4019 (2018).
10. Sheng, Y., Li, T., Lee, W. R., Yin, F.-F. & Wu, Q. J. Exploring the Margin Recipe for Online Adaptive Radiation Therapy for Intermediate-Risk Prostate Cancer: An Intrafractional Seminal Vesicles Motion Analysis. *Int. J. Radiat. Oncol.* **98**, 473–480 (2017).
11. Tanyi, J. A. *et al.* Assessment of Planning Target Volume Margins for Intensity-Modulated Radiotherapy of the Prostate Gland: Role of Daily Inter- and Intrafraction Motion. *Int. J. Radiat. Oncol.* **78**, 1579–1585 (2010).
12. Deutschmann, H. *et al.* First Clinical Release of an Online, Adaptive, Aperture-Based Image-Guided Radiotherapy Strategy in Intensity-Modulated Radiotherapy to Correct for Inter- and Intrafractional Rotations of the Prostate. *Int. J. Radiat. Oncol.* **83**, 1624–1632 (2012).
13. Peng, C. *et al.* Characterizing Interfraction Variations and Their Dosimetric Effects in Prostate Cancer Radiotherapy. *Int. J. Radiat. Oncol.* **79**, 909–914 (2011).

14. Ahunbay, E. E. & Li, X. A. Gradient maintenance: A new algorithm for fast online replanning a). *Med. Phys.* **42**, 2863–2876 (2015).

15. McVicar, N., Popescu, I. A. & Heath, E. Techniques for adaptive prostate radiotherapy. *Phys. Medica* **32**, 492–498 (2016).

16. Kashani, R. & Olsen, J. R. Magnetic Resonance Imaging for Target Delineation and Daily Treatment Modification. *Semin. Radiat. Oncol.* **28**, 178–184 (2018).

17. Palacios, M. A. *et al.* Role of daily plan adaptation in MR-guided stereotactic ablative radiotherapy for adrenal metastases. *Int. J. Radiat. Oncol.* (2018). doi:10.1016/j.ijrobp.2018.06.002

18. Henke, L. *et al.* Simulated Online Adaptive Magnetic Resonance–Guided Stereotactic Body Radiation Therapy for the Treatment of Oligometastatic Disease of the Abdomen and Central Thorax: Characterization of Potential Advantages. *Int. J. Radiat. Oncol.* **96**, 1078–1086 (2016).

19. Raaymakers, B. W. *et al.* First patients treated with a 1.5 T MRI-Linac: Clinical proof of concept of a high-precision, high-field MRI guided radiotherapy treatment. *Phys. Med. Biol.* **62**, L41–L50 (2017).

20. Pathmanathan, A. U. *et al.* Magnetic Resonance Imaging-Guided Adaptive Radiation Therapy: A "Game Changer" for Prostate Treatment? *Int. J. Radiat. Oncol. Biol. Phys.* **100**, 361–373 (2018).

21. Salembier, C. *et al.* ESTRO ACROP consensus guideline on CT- and MRI-based target volume delineation for primary radiation therapy of localized prostate cancer. *Radiother. Oncol.* **127**, 49–61 (2018).

22. Heidenreich, A. *et al.* EAU Guidelines on Prostate Cancer. Part 1: Screening, Diagnosis, and Local Treatment with Curative Intent—Update 2013. *Eur. Urol.* **65**, 124–137 (2014).

23. Bohoudi, O. *et al.* OC-0519: Radiotherapy plan quality using a double focused, double stacked multi-leaf collimator. *Radiother. Oncol.* **127**, S273 (2018).

24. Bohoudi, O. *et al.* Fast and robust online adaptive planning in stereotactic MR-guided adaptive radiation therapy (SMART) for pancreatic cancer. *Radiother. Oncol.* **125**, 439–444 (2017).

25. Kawrakow, I. & Fippel, M. Investigation of variance reduction techniques for Monte Carlo photon dose calculation using XVMC. *Phys. Med. Biol.* **45**, 2163–2183 (2000).

26. Kawrakow, I. Accurate condensed history Monte Carlo simulation of electron transport. I. EGSnrc, the new EGS4 version. *Med. Phys.* **27**, 485–498 (2000).

27. Palacios, M. A. *et al.* OC-0262: Implementation of patient specific QA for daily adaptive MR-guided radiation therapy. *Radiother. Oncol.* **123**, S134–S135 (2017).

28. Li, H. H. *et al.* Patient-specific quality assurance for the delivery of 60 Co intensity modulated radiation therapy subject to a 0.35-T lateral magnetic field. *Int. J. Radiat. Oncol. Biol. Phys.* **91**, 65–72 (2015).

29. Low, D. A. & Dempsey, J. F. Evaluation of the gamma dose distribution comparison method. *Med. Phys.* **30**, 2455–2464 (2003).

30. Low, D. A., Harms, W. B., Mutic, S. & Purdy, J. A. A technique for the quantitative evaluation of dose distributions. *Med. Phys.* **25**, 656–661 (1998).

31. Sempau, J., Wilderman, S. J. & Bielajew, A. F. DPM, a fast, accurate Monte Carlo code optimized for photon and electron radiotherapy treatment planning dose calculations. *Phys. Med. Biol.* **45**, 2263–2291 (2000).

32. Tetar, S. *et al.* Patient-reported Outcome Measurements on the Tolerance of Magnetic Resonance Imaging-guided Radiation Therapy. *Cureus* **10**, (2018).

33. Lamb, J. *et al.* Online Adaptive Radiation Therapy: Implementation of a New Process of Care. *Cureus* **9**, e1618 (2017).

34. Lustberg, T. *et al.* Clinical evaluation of atlas and deep learning based automatic contouring for lung cancer. *Radiother. Oncol.* **126**, 312–317 (2018).

35. Men, K. *et al.* Fully automatic and robust segmentation of the clinical target volume for radiotherapy of breast cancer using big data and deep learning. *Phys. Medica* **50**, 13–19 (2018).

36. Feng, M., Valdes, G., Dixit, N. & Solberg, T. D. Machine Learning in Radiation Oncology: Opportunities, Requirements, and Needs. *Front. Oncol.* **8**, (2018).

37. Liu, F., Erickson, B., Peng, C. & Li, X. A. Characterization and management of interfractional anatomic changes for pancreatic cancer radiotherapy. *Int. J. Radiat. Oncol. Biol. Phys.* **83**, e423–e429 (2012).

38. Owrangi, A. M., Greer, P. B. & Glide-Hurst, C. K. MRI-only treatment planning: Benefits and challenges. *Phys. Med. Biol.* **63**, (2018).

39. Ahunbay, E. E. *et al.* An on-line replanning scheme for interfractional variationsa). *Med. Phys.* **35**, 3607–3615 (2008).

40. Fu, W., Yang, Y., Yue, N., Heron, D. & Huq, M. SU-FF-J-02: A Cone Beam CT-guided Online Plan Modification Technique to Correct Interfractional Anatomic Changes for Prostate Cancer IMRT Treatment. *Med. Phys.* **34**, 2368–2368 (2007).

Supplementary materials

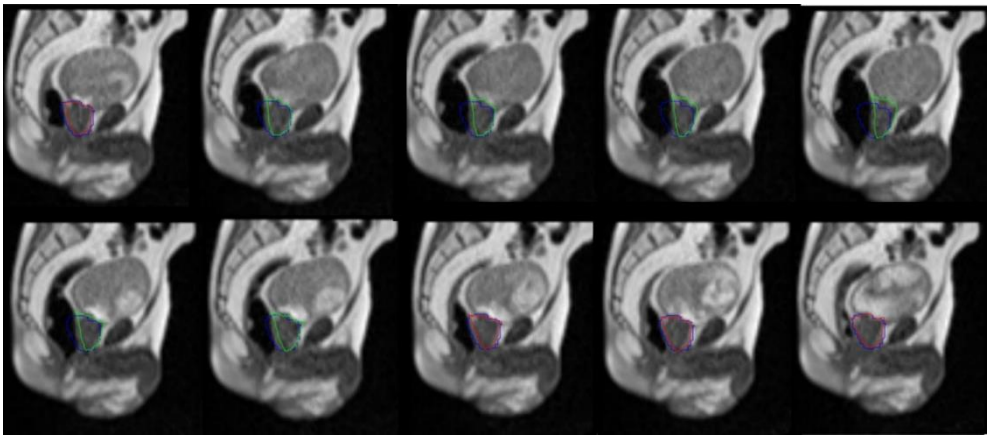

Supplementary Figure S1. *Real-time variability of position in CTV and rectal filling during MRgRT for a prostate cancer patient. CTV contour is shown in green when more than 7% is outside of the gating boundary (PTV in blue) triggering thereby a beam-hold. CTV contour in red means the target is inside the boundary within the preset value (>93%) and beam is on. Frame rate during acquisition is 4fps.*

Chapter 4

Identification of patients with locally advanced pancreatic cancer benefitting from plan adaptation in MR-guided Radiation Therapy

Omar Bohoudi
Anna M.E Bruynzeel
Martijn R. Meijerink
Suresh Senan
Ben J. Slotman
Miguel A. Palacios
Frank J. Lagerwaard

Radiotherapy and Oncology. 2019; 125: 439–44.

Abstract

Background and Purpose: MR-guided radiation therapy (MRgRT) with daily plan adaptation is a novel but time- and resource-intensive treatment for locally-advanced pancreatic cancer (LAPC). We analyzed the benefit in target coverage and organ-at-risk (OAR) sparing of daily plan adaptation in 36 consecutive LAPC patients treated with MRgRT to 40 Gy in 5 fractions.

Material and Methods: Adaptive planning was assessed for 180 fractions by comparing non-adapted plans with re-optimized plans using a) GTV coverage and OAR high-doses, and b) compliance with institutional objectives for GTV coverage and high-dose OAR constraints. Using these criteria, plan adaptation for each fraction was characterized as "not needed", "beneficial", or "no benefit". Decision-tree analysis was performed to identify subgroups most likely or not to benefit from routine plan adaptation.

Results: The percentage of plans fulfilling institutional constraints increased from 43.9% (non-adapted plans) to 83.3% after online plan adaptation, with significant improvements in GTV coverage and lower V33Gy OAR doses. Adaptive re-optimization was found to be "not needed" in 80 fractions (44.4%), "beneficial" in 95 fractions (52.8%) and of "no benefit" in 5 fractions (2.8%). Decision-tree analysis identified a grouping based on distance from tumor to OAR of ≤3mm and GTV size, respectively, to be the major determinants for the benefit of daily plan adaptation.

Conclusions: MRgRT with daily plan adaptation for LAPC was of benefit in approximately half of fractions, improving target coverage and OAR sparing. Plan adaptation appeared to be relevant mainly in cases where the GTV to adjacent OAR distance was ≤3mm.

Introduction

Despite the use of chemotherapy, either alone or combined with conventionally fractionated radiotherapy, patients with locally advanced pancreatic cancer (LAPC) have a poor prognosis. In the recently published randomized LAP07 study, chemoradiation (CRT) increased local control, but the addition of fractionated radiation therapy was not associated with a survival benefit[1]. In contrast, a systematic review including more than 8500 LAPC patients, reported that CRT was associated with a modest improved median survival (13.5 vs. 10.6 months) with multi-agent chemotherapy being an independent predictor of survival[2]. This relatively small survival benefit of CRT has to be weighed against the cost of the prolonged duration and toxicity associated with treatment. Although the use of intensity-modulated radiotherapy (IMRT) appears to have decreased both early and late toxicity[3], further advancements in precise radiation delivery, tumor motion management, and shortening overall treatment duration using e.g. stereotactic body radiation therapy (SBRT) remain warranted. The combination of SBRT with modern multi-agent chemotherapy such as FOLFIRINOX (5-FU, leucovorin, irinotecan, oxaliplatin) merits investigation. However, a key concern with SBRT applied for LAPC remains the risk for gastrointestinal toxicity[4].

MR-guided radiation therapy (MRgRT) allows for a combination of precise soft tissue setup, real-time planar imaging during treatment and gated delivery with only minimal GTV to PTV margins, and radiation plan adaptation for each fraction[5–8]. MRgRT with plan adaptation can improve target coverage and normal tissue sparing, which may result in improved local control and/or decreased toxicity[9]. However, MRgRT with daily plan adaptation is both cost- and resource intensive, among others because daily plan adaptation requires the presence of the physician

and/or physicist at the treatment console for re-contouring, plan review and approval[10]. It is therefore essential to quantify not just average dosimetric benefits of daily plan adaptation, but also to identify LAPC patients who are likely to benefit or not from this approach. In order to achieve the latter, we used decision-tree analysis to explore predictive characteristics to identify subgroups of patients with LAPC who are likely to benefit or not from routine daily adaptive planning.

Materials and Methods

Data from 36 consecutive patients (180 fractions) with LAPC or locally recurrent pancreatic cancer who underwent MRgRT on the MRIdian system (ViewRay, Cleveland, USA) between May 2016 and June 2018, were prospectively collected and analyzed after treatment. The study population included 18 females (50%) and 18 males (50%) with an age ranging from 36 to 88 years. Thirty-two patients had primary LAPC, four patients were treated for locally recurrent disease after surgery. The vast majority of patients had been treated with initial chemotherapy, usually FOLFIRINOX. The MRgRT prescription dose in all patients was 40 Gy in 5 fractions. The mean (range) value of the baseline gross tumor volume (GTV) was 30.4 cc (7.0-117.2 cc).

A simulation MR scan and CT scan were performed in supine position, with one or both arms up, during shallow inspiration breath-hold. The GTV was delineated on the simulation MR aided by diagnostic imaging, in collaboration with a gastro-intestinal intervention radiologist. The True Fast Imaging with Steady State Free Precession (True FISP) sequence is currently the only clinically available sequence on the MRIdian, on which the pancreatic tumor can usually be clearly identified as a hypodense lesion, albeit with the difficulty of evaluating the exact local extension

as is the case with all diagnostic imaging for pancreatic cancer. During contouring, on an adjacent screen the diagnostic CT scan with intravenous contrast (both 40-50 sec delayed (pancreas) and 60-70 sec delayed CT scan (portal phase)) were displayed to assist in contouring. The planning target volume for daily re-optimization (PTV_{OPT}) was generated using an isotropic margin of 3 mm around the GTV, excluding any overlap with OARs. The latter was performed in order to avoid undue high doses to surrounding critical OARs. Baseline treatment plans ($PLAN_{BASELINE}$) were generated using IMRT step-and-shoot with 5-7 beam groups where each beam group had three equidistant beams corresponding with the three ^{60}Co sources on the gantry[5]. Dose calculation was performed with a Monte-Carlo algorithm (statistical uncertainty of 1% and a grid size of 0.3cm x 0.3cm x 0.3cm) using the deformed electron density map from the simulation CT scan. Planning aimed for the maximum achievable coverage of the PTV_{OPT}, with a priority assigned to adhering to the following high-dose OAR constraints: V_{33Gy} and V_{25Gy} equal or less than 1 cc and 20 cc, respectively, for duodenum, stomach and bowel loops. The objectives for target coverage were a $V_{95\%}$ of the GTV ≥90% and a $D_{1\%}$ up to 125% of the prescribed dose.

At our center, we have opted to perform daily plan re-optimization or adaptation for each fraction for each patient as a routine strategy. In order to allow for robust and fast online adaptation, we developed an in-house strategy which can be performed within several minutes and which requires checking (and where necessary) manually adjusting the GTV and relevant OAR contours within the first 3 cm of the PTV_{OPT}[5]. Briefly, our workflow for daily plan adaptation consists of the following steps: 1) A repeat MR scan in shallow breath-hold at each fraction, followed by 3D alignment of the baseline and repeat MR-scan based on the GTV; 2) Automatic deformation of OAR contours followed by manual adjustment within a distance of 3 cm from the PTV_{OPT}; 3) Recalculation of $PLAN_{BASELINE}$ on the current

anatomy using the deformed simulation CT ($PLAN_{PREDICT}$); and 4) Routine adaptation of the $PLAN_{PREDICT}$ to derive a $PLAN_{REOPTIMIZED}$. This plan re-optimization uses the same beam numbers, beam directions and optimization objectives as $PLAN_{BASELINE}$.. The variation in OAR structures within the first 3 cm of the PTV_{OPT} guides the daily plan re-optimization (5). Patient-specific QA is performed with an independent Monte-Carlo dose calculation algorithm and gamma analysis prior to each treatment delivery while the patient remains on the table in treatment position[11]. From the start of MRgRT with routine plan adaptation in our center, we have timed the different steps in our procedure. On average, the time needed for OAR re-contouring (within 3 cm from the PTV_{OPT}), plan re-optimization and patient-specific QA using our MRgRT workflow was 15 minutes per fraction. We have found that this average of 15 minutes is also valid for other indications for MRgRT with plan adaptation, such as adrenal metastases, renal cell cancer and prostate cancer. Real-time planar cine MR images (4 frames per second) during treatment allow for respiratory-gated MRgRT. The MRIdian system automatically shuts-off delivery when the target (GTV) is outside pre-specified safety margins (PTV_{OPT}). An in-house developed visual video feedback system uses real-time projection of the target volume and safety margins from the cine MR onto a monitor. Radiation was delivered in sequential breath-holds spells, while patients observed the monitor to determine the appropriate phase for breath-hold[12]. With treatment delivery time and patient comfort in mind, this treatment generally was delivered in shallow inspiration.

As a result of the described workflow, in addition to a $PLAN_{BASELINE}$, also a $PLAN_{PREDICT}$ and $PLAN_{REOPTIMIZED}$ were available for analysis from each fraction. The dosimetric benefit of plan adaptation was assessed offline, i.e. actual treatment had been delivered on the adapted plans. All 396 plans (36 $PLAN_{BASELINE}$, 180 $PLAN_{PREDICT}$

and 180 PLAN$_{REOPTIMIZED}$) were evaluated for adherence with institutional planning objectives and constraints; i.e. a $V_{95\%}$ of the GTV ≥90%, a V_{33Gy} ≤1 cc and a V_{25Gy} ≤20 cc, respectively for duodenum, stomach as well as bowel. Statistical analysis used for plan comparisons was performed using the Wilcoxon Signed-Rank test (IBM® SPSS Statistics v20, Armonk, NY, USA). A p-value <0.05 was considered to be statistically significant.

The benefit of online plan re-optimization was qualitatively analyzed for each fraction using the following definitions:

1) "*not needed*" if the PLAN$_{PREDICT}$ already complied with all constraints.

2) *"beneficial"* if the PLAN$_{PREDICT}$ violated institutional constraints, while the PLAN$_{REOPTIMIZED}$ corrected this completely ***or*** achieved a GTV $V_{95\%}$ improvement of at least 10% and/or an OAR $V_{33\ Gy}$ dose reduction of at least 0.5 cc.

3) *"no benefit"* in case of a PLAN$_{REOPTIMIZED}$, which failed to achieve the earlier mentioned dosimetric benefit for GTV coverage and/or OARs high-doses.

A decision tree analysis (Exhaustive CHAID, IBM® SPSS® Modeler 18) was used to explore predictive characteristics, in order to identify patients where routine daily adaptive planning may or may not be beneficial[13]. A database was assembled from baseline patient-specific characteristics, geometric-, volumetric- and dosimetric information extracted from the PLAN$_{PREDICT}$ and PLAN$_{REOPTMIZED}$ (Table 1). The qualitative adaptive benefit variable (*"not needed"*, *"beneficial"*, "*no benefit*") was selected as the target variable for decision tree analysis, all other variables mentioned in Table 1 were selected as input variables. The significance level for node splitting was set at p< 0.05. Stopping parameters to prevent overfitting were applied by setting the minimum number of records in a leaf to be at least 10% of the full training data set.

Table 1: Overview and description of predictive "input" variables used in decision tree analysis.

Predictive variables	Description	mean	(range)
BMI	Patients Body Mass Index	22.1	(17.9-29.9)
GTV (cc)	Volume of GTV	30.4	(7.0-117.2)
PTV_{OPT} (cc)	Volume of (PTV minus overlap with OAR)	48.2	(14.1-152.8)
GTV to OAR (cm)	Shortest distance between GTV and OAR	0.1	(0.0-0.6)
Duodenum (cc)	Volume duodenum within 3 cm of PTV_{OPT}	43.7	(3.5-93.2)
Stomach (cc)	Volume stomach within 3 cm of PTV_{OPT}	54.2	(1.9-452.1)
Bowel loops (cc)	Volume bowel within 3 cm of PTV_{OPT}	32.1	(0-75.6)
Volume OARs (cc)	Volume all OARs within 3 cm of PTV_{OPT}	91.8	(12.42-218.4)
Beam depth (cm)	Mean beam depth (skin to isocenter)	13.9	(11.6-16.7)

Finally, this decision tree was evaluated in five patients with LAPC (25 fractions) treated more recently (Supplementary table 1, end of the chapter). Based on patient-specific baseline characteristics, the decision tree predicts if a patient (and thus for all 5 fractions) would benefit from plan adaptation. Several performance metrics (Table 3) were calculated to assess the accuracy of the configured decision tree.

Results

The baseline plan quality for all 36 patients, represented by the $V_{95\%}$ of the GTV (vertical axis) and the V_{33Gy} of the duodenum and stomach (horizontal axes) is shown in the left panel of Figure 1. The high-dose OAR constraints were met for all patients in the baseline plan, which was the primary objective of planning, although in 8 patients this necessitated a suboptimal GTV coverage of less than 90% (GTV $V_{95\%}$ range 71.9%-88.4%).

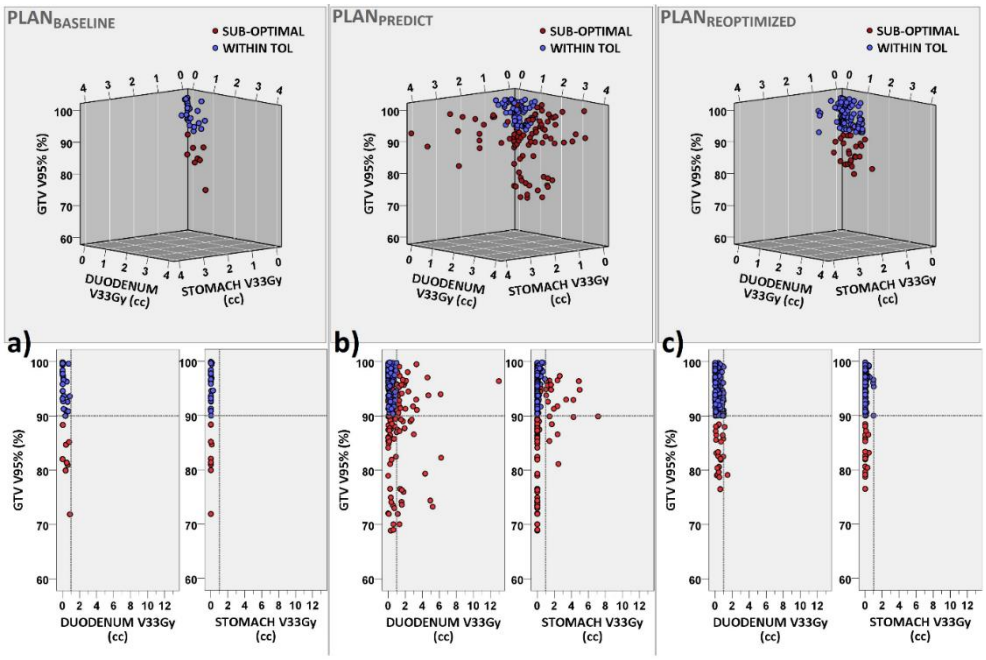

Figure 1. 3D graph illustrating (a; left panel) the baseline GTV $V_{95\%}$ and the V_{33Gy} of the stomach and duodenum in 36 patients; (b; middle panel) the same parameters for the 180 (non-adapted) PLANPREDICT; and (c; right panel) for the 180 PLANREOPTIMIZED. Lower panels showing 2D graph projections from the upper 3D graph. Blue and red dots represent fractions fulfilling and not fulfilling institutional constraints, respectively. Note: red dots projected into the box did not fulfill OAR constraints. Dashed gray lines illustrate the institutional constraints.

Figure 1b shows the same plan parameters for the (non-adapted) PLANPREDICT in 180 fractions; i.e. the baseline plan recalculated on the anatomy of the day. The PLANPREDICT complied with institutional constraints in only 79 fractions (43.9%).

Constraints were violated for GTV coverage ($V_{95\%}$ <90%) in 57 fractions (31.7%), for duodenum doses (V_{33Gy} ≤1 cc; V_{25Gy} ≤20 cc) in 53 fractions (29.4%) and 7 fractions (3.9%), respectively. Violations in the V_{33Gy} constraints for the stomach and bowel were observed in 24 fractions (13.3%) and 3 fractions (1.7%) of the PLANPREDICT, respectively, whereas the V_{25Gy} was not exceeded for the latter OARs.

Daily re-optimization resulted in significant gains, particularly for the GTV- and PTVOPT $V_{95\%}$ coverage and the duodenal V_{33Gy} parameters (Table 2).

Table 2: *Comparison of the median and interquartile range (IQR) for the GTV $V_{95\%}$ and PTV_{OPT} $V_{95\%}$, as well as OARs high-dose constraints in $PLAN_{BASELINE}$ (N=36), $PLAN_{PREDICT}$ (N=180) and $PLAN_{REOPTIMIZED}$ (N=180); p-values for comparison of the predicted and adapted plans.*

	$PLAN_{BASELINE}$ median (IQR)	**$PLAN_{PREDICT}$** median (IQR)	**$PLAN_{REOPTIMIZED}$** median (IQR)	p-value
GTV $V_{95\%}$ (%)	94.1 (90.1 – 98.1)	93.8 (88.3 – 96.8)	94.9 (90.7 – 98.1)	<0.001
PTV_{OPT} $V_{95\%}$ (%)	91.3 (83.0 – 95.9)	84.3 (78.4 – 89.6)	88.4 (83.4 – 92.8)	<0.001
Duodenum V_{33Gy} (cc)	0.1 (0.0 – 0.5)	0.4 (0.0 – 1.2)	0.1 (0.0 – 0.5)	<0.001
Duodenum V_{25Gy} (cc)	4.7 (2.6 – 8.4)	6.1 (3.3 – 9.5)	5.8 (3.2– 9.4)	0.003
Stomach V_{33Gy} (cc)	0.0 (0.0 – 0.1)	0.0 (0 – 0.2)	0.0 (0.0 – 0.0)	n.p*
Stomach V_{25Gy} (cc)	0.6 (0.1 – 3.4)	1.8 (0.1 – 5.2)	2.3 (0.4 – 4.5)	0.496
Bowel V_{33Gy} (cc)	0.0 (0.0 – 0.0)	0.0 (0.0 – 0.0)	0.0 (0.0 – 0.0)	n.p*
Bowel V_{25Gy} (cc)	0.1 (0.0 – 0.6)	0.2 (0.0 – 1.5)	0.2 (0.0 – 1.3)	0.007

**n.p : not performed*

Plan adaptation increased the percentage of plans that complied with institutional high-dose constraints from 43.9% to 83.3% (150 plans) (Figure 1c). Suboptimal re-optimized plans were due to modest exceeding of duodenal V_{33Gy} in two fractions (1.1 and 1.5 cc), and insufficient GTV coverage in 28 fractions (GTV $V_{95\%}$ 77.5%-88.5%).

Both patients with excessive duodenal V_{33Gy} also had insufficient GTV coverage. Based on the criteria defined in the Materials and Methods, adaptive re-optimization was found to be *"not needed"* in 80 fractions (44.4%), of *"benefit"* in 95 fractions (52.8%) and *"no benefit"* in 5 fractions (2.8%), respectively (Figure 2).

The CHAID decision tree analysis resulted in the generation of three terminal nodes, representing subgroups with respect to benefit of adaptive re-planning (Figure 3, left panel). The distance between the GTV and (any) OAR was the most significant predictor variable (p<0.001). If the shortest distance between the GTV and the OAR

Figure 2. Overview of qualitative analysis showing the impact of the interfractional anatomical variations and the benefit online re-optimization of the baseline plan in all fractions per patient.

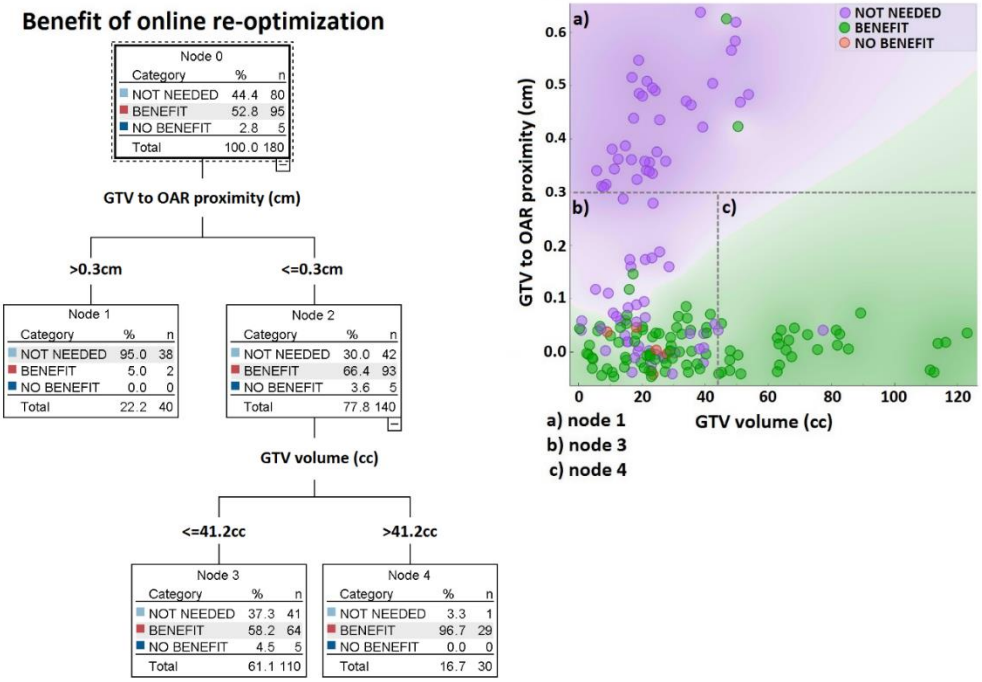

Figure 3. CHAID decision tree analysis with a total of 4 nodes, including 3 terminal nodes which represent a class with respect to benefit of adaptive re-planning. In addition to the actual tree in the left panel, the distribution of all fractions as a function of GTV size and distance between tumor and (any) OAR is shown in the right panel (jittering is used to prevents dots overlapping and class density is used to color the graph background by class).

was more than 3 mm, plan adaptation was hardly ever needed (5%; terminal node 1). In patients in which the shortest distance between the GTV and the OAR was <3mm, a second split occurred on the basis of GTV size at the level of 41 cc (p=0.018). Plan adaptation with such distance of <3mm was beneficial in more than half of patients with smaller GTV's (terminal node 3), however, adaptation was of benefit in 97% of patients with larger GTV's (terminal node 4). A graphical illustration of the branches of the decision tree is shown in the right panel of Figure 3.

The correct classification rate of the decision tree in the training set was 82.2% with a sensitivity of 98.2% and specificity of 55.9%, respectively (Table 3). In the smaller evaluation set, the corresponding rates were 92.0%, 100% and 83.3% for the correct classification rate, sensitivity and specificity, respectively.

Table 3: *Decision tree performance measures calculated from the number of True Positives (TP), True Negatives (TN), False Positives (FP) and False Negatives (FN) observations in relation to the total number (n) of observations. Performance measures were calculated for both the training (36 patients) and evaluation (5 patients) data set.*

Performance measures	**Description**	**Training** (n=180)	**Evaluation** (n= 25)
Correct classification rate, *C (%)*	*C = (TP+TN) / n*	82.2	92.0
Sensitivity, *Sn (%)*	*Sn = TP/(TP + FN)*	98.2	100
Specificity, *Sp (%)*	*Sp = TN/(TN + FP)*	55.9	83.3
Positive Predictive Value, *PPV (%)*	*PPV = TP/(TP + FP)*	78.6	86.7
Negative Predictive Value, *NPV (%)*	*NPV = TN/(TN + FN)*	95.0	100
Area under the ROC curve, *AUC*	ROC curve depicts *TP* rate versus *FP* rate at various discrimination thresholds	0.81	0.91

In this patient cohort, only acute and subacute toxicity data are available. Grade 3 or worse gastrointestinal toxicity within three months was only observed in a single patient (2.8%) in the form of hemorrhage at three weeks following treatment. It is

uncertain whether this was due to local tumor progression or radiation induced toxicity.

Discussion

The superior soft tissue imaging capabilities of MRgRT allow for daily plan adaptation in order to optimize treatment plans in response to interfractional changes in both target volumes and adjacent OARs. Due to the short overall treatment time with the five fraction MRgRT scheme used, changes in the GTV were only minimal (median variation in GTV's 0.0 cc ± 1.6 cc), however, interfractional changes relative to the simulation scan can be substantial for OARs, underscoring the importance of daily imaging and plan re-optimization. At our center, a dedicated radiation oncologist (ABR) has contoured the simulation MR-scans generated on the MRIdian of all LAPC and recurrent pancreatic cancer patients in close co-operation with a dedicated gastro-intestinal radiologist (MME). Prior to each fraction, a repeated breath-hold high-resolution MR scan was generated using the same acquisition protocol as the simulation MR, and deformable OAR contours are available for adjustment. The majority of all treatment fractions (>90%) have been either performed or supervised by the aforementioned radiation oncologist, thereby minimizing contouring errors.

The specific goal of our routine plan adaptation with MRgRT was to avoid exceeding OARs high dose constraints, even when this would result in less optimal target coverage. The dose-toxicity relationship is clear from earlier reports, and this approach with the aim to restrict severe treatment-related gastro-intestinal toxicity, which is correlated to high OAR doses, has also been used by other authors[9,14–16]. The used high-dose institutional OAR constraints in this study, i.e. a $V_{33\ Gy}$ of ≤1 cc for

the duodenum, stomach and bowel in five fractions, are commonly used in the recent literature addressing SBRT for LAPC[14,15,17]. There is less consensus in the literature for the intermediate dose constraints (e.g. $V_{25\ Gy}$). Although late toxicity results remain to be awaited in our patient group with LAPC, we have observed only a single case of grade 3 or worse gastrointestinal toxicity within three months. Whether our adaptive MRgRT approach contributes to this relatively low complication rate remains to be confirmed with longer follow-up and in a larger group of patients.

Using the above approach, our study confirms the dosimetric benefit of daily plan adaptation for LAPC, as has recently been reported for other abdominal targets[9]. Although the median benefit in target coverage and OAR sparing proved to be relatively limited over the total population, the main achievement of daily plan adaptation was prevention of undue high fraction doses to OAR. This was clearly visualized in the PLAN$_{PREDICT}$ in Figure 1, where e.g. duodenum and stomach V_{33Gy} constraints were exceeded in 29.4% and 13.3%, respectively, and were corrected after plan adaptation.

Because plan adaptation constitutes a trade-off between target coverage and OAR sparing, we chose plan compliance to institutional constraints and objectives as the endpoint for the evaluation of the benefit of daily adaptation. We have found that plan adaptation increased the percentage of plans complying with these high-dose OARs constraints and GTV coverage from 43.9% to 83.3%, which may be of clinical relevance. We have characterized a "benefit" of plan adaptation as follows: fractions in which the institutional constraints were violated in the PLAN$_{PREDICT}$ and corrected after plan adaptation and also fractions in which a GTV $V_{95\%}$ improvement of at least 10% and/or an OAR $V_{33\ Gy}$ dose reduction of at least 0.5 cc was achieved. We have additionally looked at stricter cut-off values for OAR dose sparing benefit, such as a

reduction in V_{33Gy} ranging from 0.75-2 cc. The percentage of patients defined as having "benefit" of plan adaptation decreased marginally from 52.8% (0.5 cc) to 46.7% (2 cc). The decision trees of stricter criteria for OAR are shown in Supplementary Figure 1.

We have used decision tree analysis of pretreatment characteristics in order to determine for which patients online plan adaptation would not have been necessary. A recent paper by Tyran et al.[18] describes a different clinical workflow for plan adaptation in 7 patients (35 fractions) with pancreatic cancer. Initially a daily-image visual review of superimposed original OAR contours on the MRI of the day was used to determine whether a predicted plan (re-contouring of OARs and recalculation) should be generated, after which the results of this predicted plan are used to determine the necessity of plan adaptation. The authors conclude that generation of a predicted plan, and thus including re-contouring of OAR, is mandatory for this indication in order to decide the need for plan adaptation. Our paper goes a step beyond this conclusion and proposes a model to predict upfront which patients "benefit" from online plan adaptation in a larger cohort of patients/fractions. At our center, a predicted plan is always generated, followed by routine plan adaptation. Because the re-contouring is the most time consuming step, this final plan adaptation costs only a few minutes of extra time. Our specific aim was to identify patients in whom plan adaptation was deemed to be beneficial (or alternatively not necessary) based on derived predicted and adapted plans. From this analysis, it appeared that the distance between the GTV and adjacent OARs and to a lesser extent the size of the GTV were the most relevant factors. Our specific results for distance and GTV size, however, are directly related to our adaptive planning approach and IMRT delivery with a tri-cobalt machine, and may be slightly different for sharper beam penumbra such as with MR-linacs.

Prior to this study, our hypothesis was that online plan adaptation for each fraction in LAPC would be beneficial for the majority of the patients. Given our criteria for "benefit" of plan adaptation, we found that slightly less than half of patients would not have required daily plan adaptation, particularly those with a distance from tumor to relevant OAR of >3 mm. In addition to the described decision tree evaluation, we are currently validating these results prospectively, and until then our workflow still includes routine plan adaptation for each fraction in LAPC.

Some limitations of our study have to be acknowledged. Our analysis was performed in 180 fractions, however it was restricted to patients with LAPC including two patients with recurrent disease following surgery. The accuracy of the CHAID decision-tree analysis with this number of fractions was 82%. It is our intention to repeat the analysis at the time a larger number of patients treated will be available for analysis. Our plan adaptation focuses on restricting the dose to OAR in the 25 Gy-33 Gy, which is considered to be most relevant for clinical toxicity, however the results may be slightly different when also lower doses are taken into account. Finally, other methods of plan adaptation are possible, such as manual re-normalization in order to further increase target coverage until one of the high-dose OAR constraints is reached. This approach is not performed in clinical practice with MRgRT at our center, mainly because of uncertainty of intrafractional changes in OARs, in combination with the steep dose gradients obtained in SBRT.

Conclusion

In conclusion, daily plan adaptation was overall beneficial in approximately half of patients with LAPC, and appeared less important in cases where there was ≥3 mm distance between the tumor and relevant OARs. This finding allows for pre-

treatment selection of LAPC patients for adaptive treatment, and this information can be used in the logistical challenges associated with MRgRT, including daily re-contouring, plan review and approval.

References

1. Hammel, P. *et al.* Effect of Chemoradiotherapy vs Chemotherapy on Survival in Patients With Locally Advanced Pancreatic Cancer Controlled After 4 Months of Gemcitabine With or Without Erlotinib. *JAMA* **315**, 1844 (2016).
2. Torgeson, A. *et al.* Multiagent induction chemotherapy followed by chemoradiation is associated with improved survival in locally advanced pancreatic cancer. *Cancer* **123**, 3816–3824 (2017).
3. Bittner, M.-I., Grosu, A.-L. & Brunner, T. B. Comparison of toxicity after IMRT and 3D-conformal radiotherapy for patients with pancreatic cancer – A systematic review. *Radiother. Oncol.* **114**, 117–121 (2015).
4. De Bari, B. *et al.* Hypofractionated radiotherapy in pancreatic cancer: Lessons from the past in the era of stereotactic body radiation therapy. *Crit. Rev. Oncol. Hematol.* **103**, 49–61 (2016).
5. Bohoudi, O. *et al.* Fast and robust online adaptive planning in stereotactic MR-guided adaptive radiation therapy (SMART) for pancreatic cancer. *Radiother. Oncol.* **125**, 439–444 (2017).
6. Bruynzeel, A. *et al.* OC-0425: Clinical experience with stereotactic MR-guided adaptive radiation therapy for pancreatic tumors. *Radiother. Oncol.* **123**, S224–S225 (2017).
7. Lamb, J. *et al.* Online Adaptive Radiation Therapy: Implementation of a New Process of Care. *Cureus* **9**, e1618 (2017).
8. Acharya, S. *et al.* Online Magnetic Resonance Image Guided Adaptive Radiation Therapy: First Clinical Applications. *Int. J. Radiat. Oncol.* **94**, 394–403 (2016).
9. Henke, L. *et al.* Phase I trial of stereotactic MR-guided online adaptive radiation therapy (SMART) for the treatment of oligometastatic or unresectable primary malignancies of the abdomen. *Radiother. Oncol.* **126**, 519–526 (2018).
10. Kashani, R. & Olsen, J. R. Magnetic Resonance Imaging for Target Delineation and Daily Treatment Modification. *Semin. Radiat. Oncol.* **28**, 178–184 (2018).
11. Palacios, M. A. *et al.* OC-0262: Implementation of patient specific QA for daily adaptive MR-guided radiation therapy. *Radiother. Oncol.* **123**, S134–S135 (2017).
12. van Sörnsen de Koste, J. R. *et al.* MR-guided gated stereotactic radiotherapy delivery for lung, adrenal and pancreatic tumors: a geometric analysis. *Int. J. Radiat. Oncol.* **0**, (2018).
13. IBM Software Group. IBM SPSS Modeler 18.0 Algorithms Guide. (2016).
14. Herman, J. M. *et al.* Phase 2 multi-institutional trial evaluating gemcitabine and stereotactic body radiotherapy for patients with locally advanced unresectable pancreatic adenocarcinoma. *Cancer* **121**, 1128–1137 (2015).

15. Pollom, E. L. *et al.* Single- versus multifraction stereotactic body radiation therapy for pancreatic adenocarcinoma: outcomes and toxicity. *Int. J. Radiat. Oncol. Biol. Phys.* **90**, 918–25 (2014).

16. Brunner, T. B., Nestle, U., Grosu, A.-L. & Partridge, M. SBRT in pancreatic cancer: what is the therapeutic window? *Radiother. Oncol.* **114**, 109–16 (2015).

17. Dholakia, A. S. *et al.* Mapping Patterns of Local Recurrence After Pancreaticoduodenectomy for Pancreatic Adenocarcinoma: A New Approach to Adjuvant Radiation Field Design. *Int. J. Radiat. Oncol.* **87**, 1007–1015 (2013).

18. Tyran, M. *et al.* Retrospective evaluation of decision-making for pancreatic stereotactic MR-guided adaptive radiotherapy. *Radiother. Oncol.* (2018). doi:10.1016/j.radonc.2018.08.009

Supplementary materials

Supplementary Table 1: *Baseline patient-specific characteristics, decision tree classification results and actual adaptive benefit results for the 5 patients used for decision tree evaluation.*

Patient	GTV to OAR distance (cm)	GTV volume (cc)	Decision tree classification	Adaptive beneficial (Yes or No)				
				Fx1	Fx2	Fx3	Fx4	Fx5
1	0.0	21.9	Benefit	No	Yes	Yes	Yes	No
2	0.0	64.9	Benefit	Yes	Yes	Yes	Yes	Yes
3	0.3	41.5	Not needed	No	No	No	No	No
4	0.4	12.1	Not needed	No	No	No	No	No
5	0.0	42.2	Benefit	Yes	Yes	Yes	Yes	Yes

* *Gray cells illustrate a failed classification.*

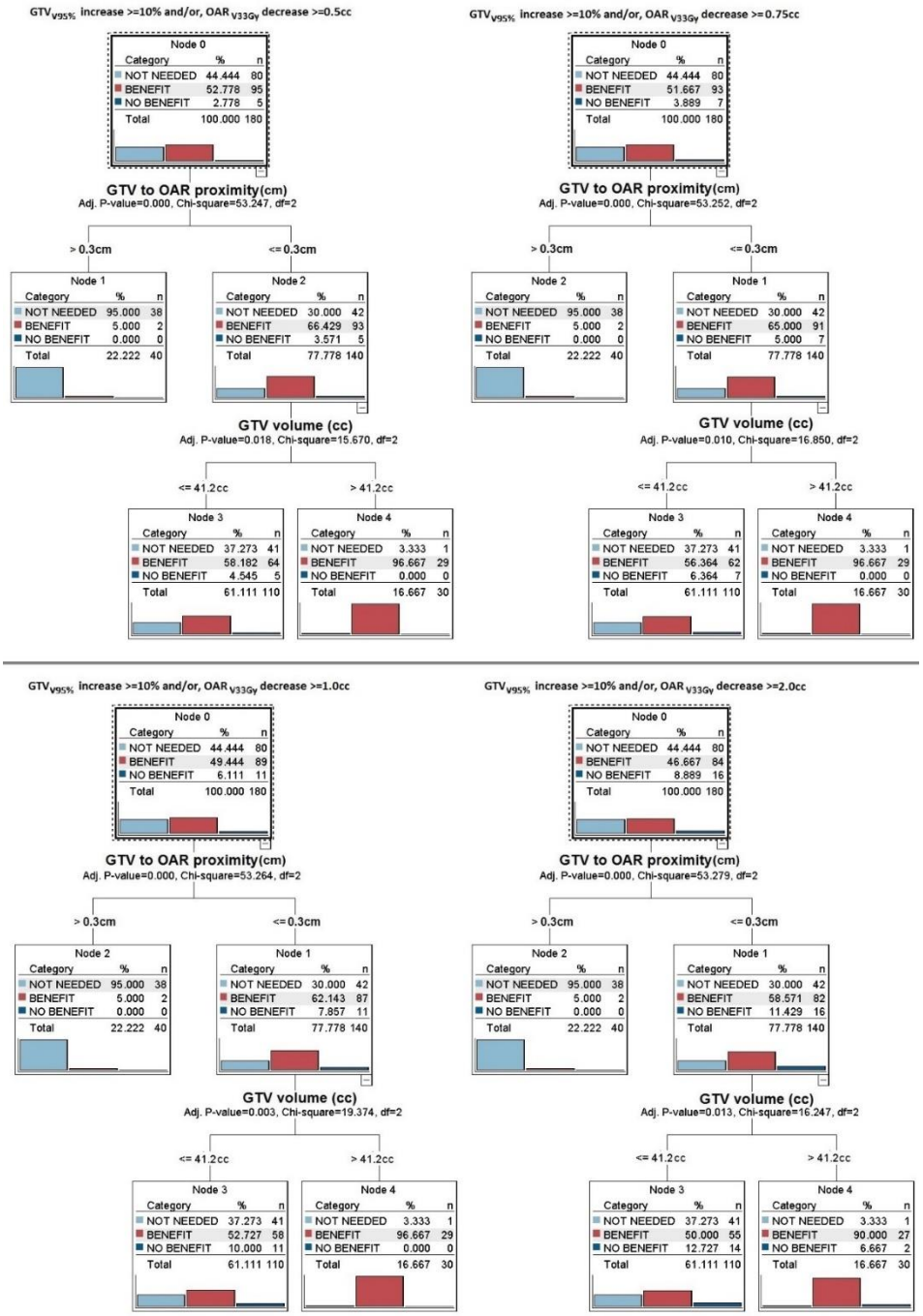

Supplementary Figure 1: *The decision trees at stricter cut-off values for OAR dose sparing benefit usinga reduction in V_{33Gy} ranging from 0.75-2 cc.*

Chapter 5

Role of Daily Plan Adaptation in MR-Guided Stereotactic Ablative Radiation Therapy for Adrenal Metastases

Miguel A. Palacios
Omar Bohoudi
Anna M.E Bruynzeel
John R. van Sörsen de Koste
Paul Cobussen
Ben J. Slotman
Frank J. Lagerwaard
Suresh Senan

International Journal of Radiation Oncology, Biology, Physics. 2018; 102: 426–433.

Abstract

Purpose: To study interfractional organ changes during magnetic resonance (MR)-guided stereotactic ablative radiation therapy for adrenal metastases and to evaluate the dosimetric advantages of online plan adaptation.

Material and Methods: Seventeen patients underwent a total of 84 fractions of video-assisted, respiration-gated, MR-guided adaptive radiation therapy to deliver either 50 Gy (5 fractions), 60 Gy (8 fractions), or 24 Gy (3 fractions). An MR scan was repeated before each fraction, followed by rigid coregistration to the gross tumor volume (GTV) on the pretreatment MR scan. Contour deformation, planning target volume (PTV) (GTV + 3 mm) expansion, and online plan reoptimization were then performed. Reoptimized plans were compared with baseline treatment plans recalculated on the anatomy-of-the-day ("predicted plans"). Interfractional changes in organs at risk (OARs) were quantified according to OAR volume changes within a 3 cm distance from the PTV surface, center of mass displacements, and the Dice similarity coefficient. Plan quality evaluation was based on target coverage (GTV and PTV) and high dose sparing of all OARs (V_{36Gy}, V_{33Gy}, and V_{25Gy}).

Results: Substantial center of mass displacements were observed for stomach, bowel, and duodenum, 17, 27 and 36 mm, respectively. Maximum volume changes for the stomach, bowel, and duodenum within 3 cm of PTV were 23.8, 20.5, and 20.9 cm^3, respectively. Dice similarity coefficient values for OARs ranged from 0.0 to 0.9 for all fractions. Baseline plans recalculated on anatomy-of-the-day revealed underdosage of target volumes and variable OAR sparing, leading to a failure to meet institutional constraints in a third of fractions. Online reoptimization improved target coverage in 63% of fractions and reduced the number of fractions not meeting the $V_{95\%}$ objective for GTV and PTV. Reoptimized plans exhibited significantly better sparing of OARs.

Conclusions: Significant interfractional changes in OAR positions were observed despite breath-hold stereotactic ablative radiation therapy delivery under MR-guidance. Online reoptimization of treatment plans led to significant improvements in target coverage and OAR sparing.

Introduction

The adrenal glands are a common site of metastases from different malignancies, with a multi-institutional review reporting that the most common primary tumors undergoing resection are non-small cell lung cancer, colorectal cancer, and renal carcinoma[1]. In patients presenting with non-small cell lung cancer and isolated adrenal metastasis, current guidelines recommend radical treatment for both the primary tumor and adrenal metastasis, especially if no lymph node metastases are present[2]. Similarly, in patients whose primary tumor is controlled, a metachronous adrenal metastasis can be considered as an oligometastasis, which is amenable to either surgery or high-dose radiation therapy.

Although surgery is generally considered the preferred treatment in fit patients, an analysis of 317 patients reported poorer results in patients with synchronous tumors; a radical resection was only achieved in 86% of patients, and the mean hospital stay was 7 days[1]. Adrenal oligometastases can be treated using stereotactic ablative radiation therapy (SABR)[3–12]. However, a systematic review reported a weighted 2-year local control of only 63% after SABR, as opposed to 84% for adrenalectomy[13]. Because of both respiratory-induced motion[14] and the proximity of mobile organs at risk (OARs)[15–17], SABR for adrenal tumors is technically challenging. A recent study reported that no local failures occurred in adrenal metastases lesions treated with biologically equivalent doses of >100 Gy, with no patients experiencing grade 3s to 5 toxicity[5].

Several groups have recently reported on the delivery of hypofractionated magnetic resonance (MR)-guided radiation therapy using the MRIdian system (ViewRay Inc., Mountain View, CA)[18–24]. The MRIdian system provides superior soft-tissue

resolution[25] and permits online plan adaptation based on the volumetric image of the day[18–20], with the real-time gated treatment delivery based on visualization of soft-tissue structures[26,27].

We introduced MR-guided adaptive radiation therapy to deliver SABR for adrenal metastases in combination with breath-hold gated delivery using the MRIdian system. Online plan adaptation was performed on a routine basis for each patient at each fraction, and we assessed interfractional changes and the importance of plan adaptation for this patient group.

Material and Methods

General MR-guided workflow for adrenal gland metastasis

The online adaptive procedure under MR-guidance for adrenal gland metastasis has previously been described for locally advanced pancreatic cancer[20]. Briefly, the process consists of 3 steps: (1) 3-dimensional (3D) MR simulation during shallow-inspiration breath-hold for pretreatment delineation and for generation of a treatment plan to be used for online plan adaptation, (2) daily 3D MR scan acquisition at each fraction, (3) deformation and adjustment of OAR contours within 3 cm of the surface of the planning target volume (PTV), and (4) online plan reoptimization. MR acquisition is performed during a 17-second breath-hold with 1.6 mm x 1.6 mm x 3.0 mm resolution. An example of an MR scan for a patient with an adrenal gland metastasis is shown in Figure 1.

All patients are instructed to fast for at least 2 hours before each treatment. At each fraction, the breath-hold MR scan representing the anatomy of the day is first rigidly

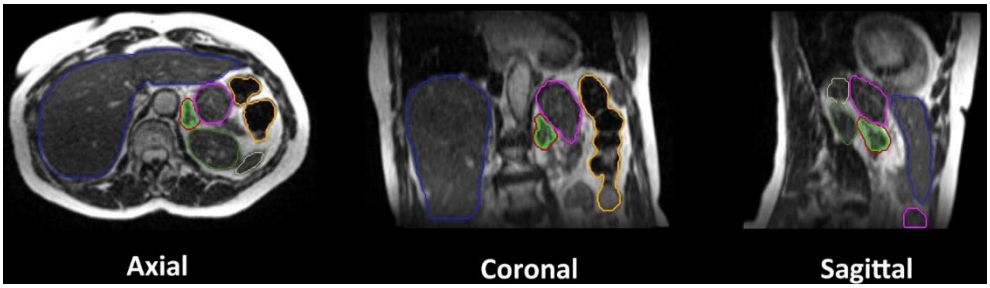

Figure 1. *Magnetic resonance scan at 0.35 T showing axial, coronal, and sagittal views of a patient with adrenal gland metastasis. Gross tumor volume is contoured in light green, planning target volume in red, liver in dark blue, stomach in purple, kidney in dark green, bowel in orange, and spleen in light yellow.*

registered to the gross tumor volume (GTV) of the pretreatment breath-hold MR, and an online couch shift is performed. Subsequently, OAR contours are propagated from the pretreatment MR simulation to the breath-hold MR of the day, using deformable image registration. Next, a clinician reviews contours and edits OAR contours, together with the GTV when deemed necessary. The online plan reoptimization approach is specifically tailored to spare high doses to the OARs[20]. The PTV is generated from the GTV plus an isotropic 3 mm margin, but regions of overlap with OARs are excluded. SABR for adrenal metastases is only performed under breath-hold conditions, and the clinical target volume is considered to be equal to the GTV.

Before delivery, patient-specific quality assurance of the treatment plan is carried out with the patient remaining in treatment position[28]. A secondary MC engine providing a 3D dose calculation is run within 2 minutes, followed immediately by a gamma analysis (3%/3 mm) comparison with the dose distribution from the MRIdian treatment planning system. Treatment delivery proceeds after plan approval by means of real-time gating of the GTV in a 2-dimensional (2D) MR planar image[18,27] with a gating window boundary representing the PTV during repeated breath-holds. To increase treatment duty-cycles, visual feedback is provided to the

patient by an MR-compatible monitor projecting the 2D cine MR image from the MRIdian console.

Treatment planning and dose fractionation

Treatment plans were produced with the MRIdian treatment planning system based on an intensity modulated radiation therapy (IMRT) step-and-shoot technique, consisting of 5 to 7 beam groups. Each beam group consists of 3 equidistant beams at 120° separation in correspondence with the geometry of the 3 ^{60}Co sources on the gantry. Depending on the location of the adrenal metastasis, contralateral beams were assigned 0 fluence and did not contribute to the treatment plan. Dose calculation was performed with an Monte Carlo (MC) algorithm and statistical uncertainty of 1% using a grid size of 0.3 cm x 0.3 cm x 0.3 cm. To assess the role of online plan adaptation in MR-guided radiation therapy for adrenal gland metastasis, we studied the plans of 17 patients. Thirteen patients presented with a left-sided adrenal lesion and 4 with a lesion on the right side. Three fractionation schemes were used: 3 fractions of 8 Gy (NCT02492568, 2 patients), 8 fractions of 7.5 Gy (NCT01446744, 1 patient) and 5 fractions of 10 Gy (our current departmental protocol, 14 patients), resulting in a $BED_{\alpha/\beta = 10Gy}$ of 60 Gy, 105 Gy and 100 Gy, respectively. Patients generally received 3 fractions of SABR per week, but deviations from this were permitted (e.g., for logistical reasons or clinician preference). Relevant OARs used during treatment planning optimization were stomach, bowel, duodenum, and, in some cases, kidney. Median GTV and PTV sizes at baseline were 19.9 cm^3 (range 3.0-48.3 cm^3) and 34.8 cm^3 (range 6.5-69.8 cm^3). $V_{95\%}$ objectives for PTV and GTV in the baseline plans were achieved for 8 (47%) and 12 (71%) patients, respectively.

Analysis of interfractional changes and online plan adaptation

Interfractional changes in breath-hold MR-guided radiation therapy for adrenal gland metastasis were assessed by analyzing (1) the 3D vector of center of mass (COM) displacements, (2) the volume changes, and (3) the Dice similarity coefficient (DSC) at each fraction by taking the pretreatment MR as reference. All interfractional changes were quantified within a 3 cm region from the surface of the PTV after rigid registration of both scans on the GTV, according to the online adaptive workflow. Online GTV adjustments resulting from rotations or small deformations were analyzed whenever a difference of at least 0.2 cm^3 from baseline values was observed. However, we excluded from this GTV analysis 2 patients in whom the treating clinician introduced a deliberate gap for at least 1 week to allow for tumor regression. All interfractional analyses were performed in 3DSlicer 4.6.2 (https://www.slicer.org/).

Online plan adaptation was assessed by a dosimetric comparison of the GTV and PTV together with OARs in predicted and reoptimized plans. Predicted plans are defined as the baseline IMRT plan derived from a pretreatment MR scan before the delivery of any fraction, recalculated on the anatomy-of-the-day after registration on the GTV, which is then adjusted when needed with partial recontouring of the OARs. For the 2 patients in whom tumor regression was observed, a new baseline IMRT plan was generated after the first 2 fractions to better account for the observed anatomic changes. Reoptimized plans are defined as the new IMRT plans obtained after reoptimization of beam fluences, taking into account the adapted GTV and OARs at each fraction. Target coverage was evaluated by quantifying the D_{mean} and $V_{95\%}$ of GTV and PTV and by the number of fractions fulfilling V95% ≥95%. Doses to the stomach, bowel, and duodenum were evaluated in those patients treated with the 5 x 10 Gy fractionation scheme using institutional OAR constraints V_{36Gy}, V_{33Gy},

and V_{25Gy}, which should be lower than 0.1, 1.0, and 5 cm^3, respectively. In total, 84 and 70 fractions, respectively, were used to evaluate the role of online plan adaptation regarding target coverage and sparing of OARs. All dosimetric analyses were performed using MATLAB and Statics Toolbox Release 2012b (The MathWorks, Inc, Natick, MA) after importing the dose volume histograms (DVHs) and structure volumes present in each treatment plan.

Statistical analysis

Statistical analysis of dosimetric parameters was performed using either paired *t* tests or the Wilcoxon signed-rank test (IBM SPSS Statistics v20, Armonk, NY) after testing for normality of the corresponding variable. A P value < .05 was considered to be statistically significant.

Logistic regression was employed to assess the most relevant variables determining target coverage improvement in the reoptimized plans. Improved target coverage was defined as a dichotomous variable assigned a value of 1 if $V_{95\%}$ of PTV in reoptimized plans was higher than $V_{95\%}$ in predicted plans. Otherwise, a value of 0 was assigned. Variables selected to build the logistic regression model and tested for statistical significance were the change in GTV size; the cumulative change in OAR volume at 1 cm, 2 cm, and 3 cm from the PTV; DSC of GTV, stomach, bowel, and duodenum; and total effective-depth to the isocenter. Logistic regression was carried out in IBM SPSS Statistics v20 (Armonk, NY), and a P value < .05 was considered to be statistically significant.

Results

Interfractional changes in breath-hold MR-guided radiation therapy adrenal gland metastasis

Substantial interfractional changes were observed across all fractions for the 17 patients studied. Figure 2 (top) shows box-and-whisker plots of the 3D vectors associated to the COM displacements at each fraction with respect to the pretreatment situation after online rigid registration on the GTV. Maximum COM displacements of several centimeters were observed for all OARs. The median COM displacement for GTV, stomach, bowel, and duodenum was 0.6, 5.2, 6.3, and 6.2 mm, respectively. Volume changes with respect to the pretreatment situation were random, as indicated by median values close to 0 of the box-whisker-plots shown in Figure 2 (middle). Maximum volume changes of 23.8, 20.5, and 20.9 cm^3 were observed for stomach, bowel, and duodenum, respectively. Online adjustments of GTV contours were performed in 71% of the fractions, resulting in volume changes of less than 1 cm^3 in the majority of cases (80%). For 2 patients, the treating physician decided to introduce a treatment gap between fractions 2 and 3, in an attempt to allow improved OAR sparing by tumor shrinkage. This gap led to a 15% reduction in GTV size in these patients (4.9 cm^3 and 9.3 cm^3), a reduction that continued during delivery of the subsequent 3 fractions. Figure 2 (bottom) shows the DSC values for GTV, stomach, bowel, and duodenum. The DSC for the GTV was high (median 0.85), but that for OARs ranged from 0.0 to 0.9.

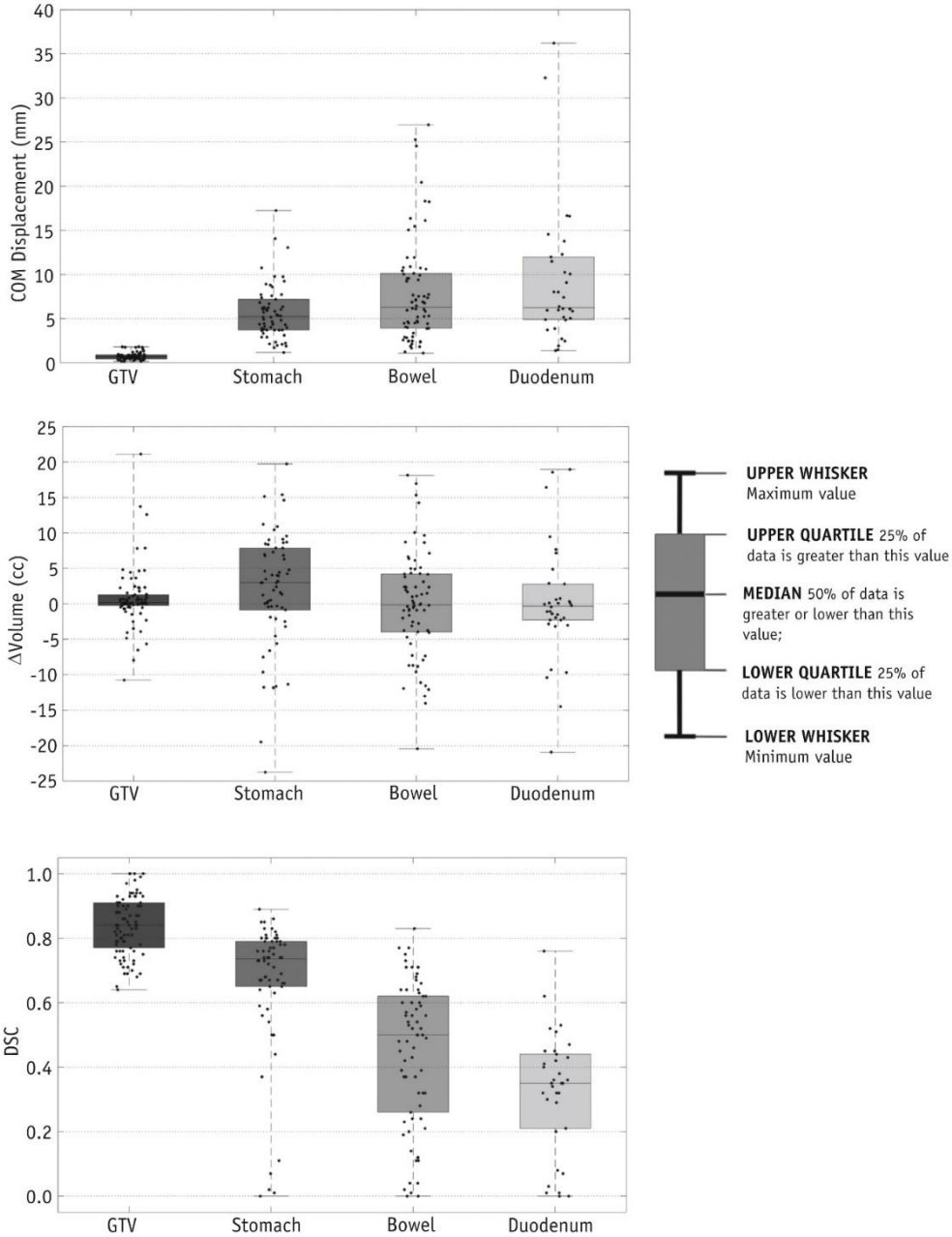

Figure 2. *Interfractional changes for gross tumor volume, stomach, bowel, and duodenum in breath-hold stereotactic ablative radiation therapy for adrenal gland metastases, after performing online rigid registration on the gross tumor volume. Interfractional changes in position of organs at risk were assessed in a region up to 3 cm from the planning target volume surface. Displacement of center of mass (top), difference in volume (middle), and Dice similarity coefficient (bottom) at each fraction are reported with respect to the baseline situation.*

Online plan adaptation in breath-hold MR-guided radiation therapy for adrenal gland metastasis

Online plan reoptimization improved target coverage in 63% of the fractions in all patients by achieving both a higher $V_{95\%}$ value and a higher D_{mean} in PTV. The reoptimized plan was chosen for treatment for all fractions because it was judged superior to the predicted plan in all but 1 fraction. Figure 3 shows the proportion of fractions fulfilling $V_{95\%} \geq 95\%$ of prescription dose for the adrenal PTV in both the predicted and reoptimized plans. Reoptimization improved by 31% the number of fractions in which more than 95% of the PTV was covered by 95% of the prescription dose. For the GTV, a corresponding increase in coverage of 16% was observed (results not shown).

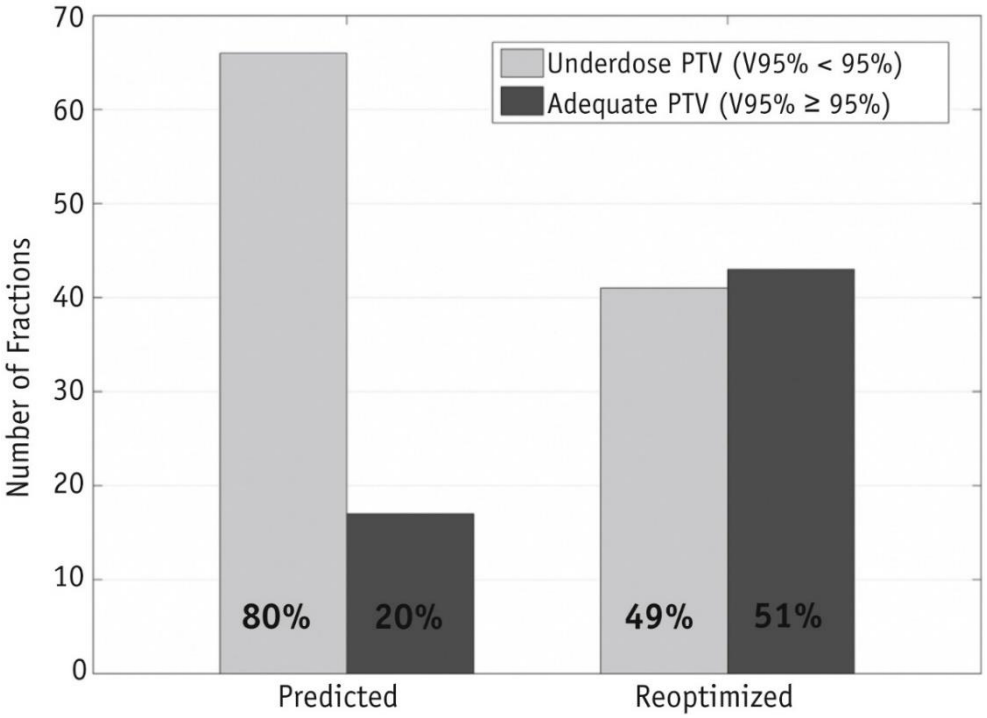

Figure 3. *Number of fractions in the predicted and reoptimized plans exhibiting underdose ($V_{95\%}$<95%) or adequate ($V_{95\%}$≥95%) planning target volume coverage.*

Figure 4 summarizes the overall improvements in target coverage in the reoptimized plans. The box-and-whisker plots show the distribution of $V_{95\%}$ values for GTV and PTV in the predicted and reoptimized plans. The difference in D_{mean} per fraction of GTV in the reoptimized plans with respect to the predicted plans ranged from -0.3 to 0.7 Gy (5th to 95th interval), which resulted in cumulative $BED_{\alpha/\beta = 10Gy}$ changes over the course of the treatment of -2.1 to 8.7 Gy (5th to 95th interval).

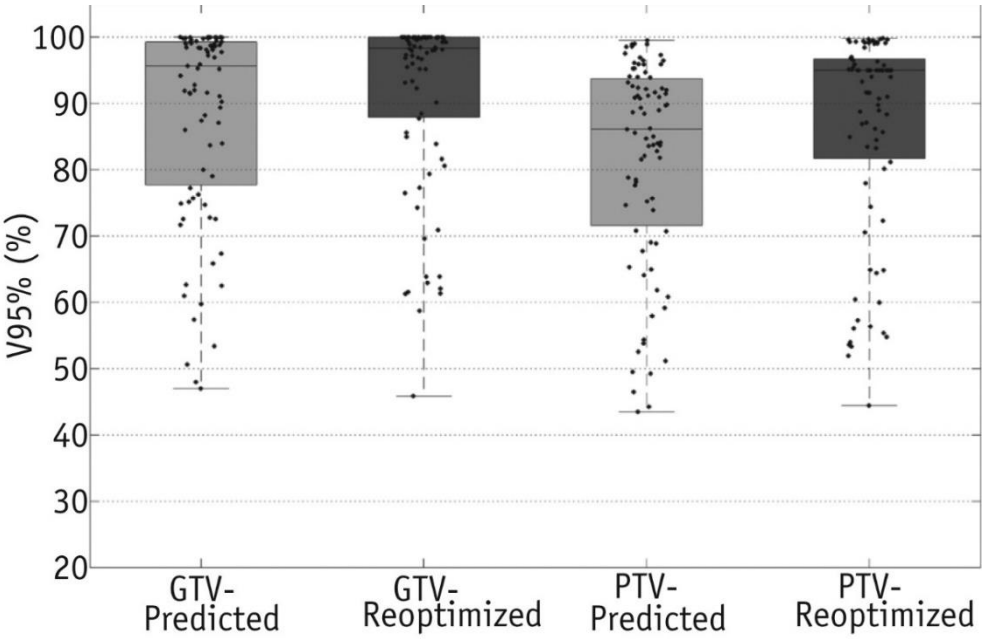

***Figure 4**. Box-and-whisker plots of gross tumor volume and planning target volume coverage (percentage of volume receiving $V_{95\%}$) in predicted and reoptimized plans.*

Reoptimized plans did not lead to improved target coverage in 21 fractions in which protocol violations of OAR dose had been observed in their predicted plans. The average DVHs of PTV and the combined OARs for those 21 fractions are shown in Figure 5. Although the average DVH of the PTV in the reoptimized plans is close to that of predicted plans, the average DVH of the combined OARs exhibited

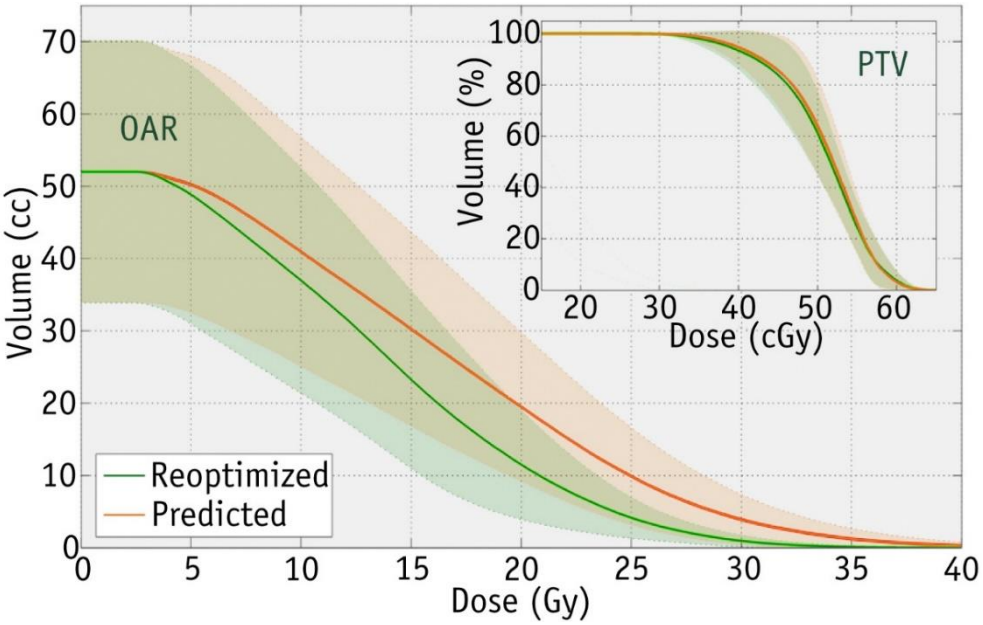

Figure 5. *Average of dose volume histograms for planning target volume and organs at risk for those fractions (21) in which the reoptimized plans (green) showed similar or lower coverage compared with the predicted plans (orange). Shaded areas represent the standard deviation of the dose volume histograms.*

significantly lower doses in the reoptimized plans, especially in regions treated to more than 25 Gy. The standard deviation, shown as the shaded area, of the DVH of the combined OARs is also considerably narrower above 25 Gy for the reoptimized plans than for predicted plans. Reoptimized plans also resulted in more limited protocol violations of OAR doses for 3 fractions (Table 1), violations that just exceeded institutional dose constraints. In all 3 cases, reoptimized plans were superior to the initial plan calculated on the anatomy-of-the-day. For all but 1 treatment fraction, the online reoptimized plan was chosen by the clinician for treatment delivery, either because of OAR sparing or beam-on times. The differences in the volume of the OARs receiving 36 Gy, 33 Gy, and 25 Gy (V_{36Gy}, V_{33Gy}, and V_{25Gy}, reoptimized minus predicted) are summarized in Table 1. However, the improvements in OAR sparing in the reoptimized plans were statistically significant only for the bowel and stomach, not for the duodenum.

Table 1. *Percentage of fractions not complying with institutional dose constraints for organs at risk (reoptimized vs predicted) and 5th to 95th percentile of difference in volume of organs at risk (reoptimized minus predicted) receiving 36, 33, and 25 Gy.*

	Stomach	Bowel	Duodenum
Protocol violation (reoptimized. vs predicted)	4% vs 27%	0% vs 13%	0% vs 3%
Δ Volume (cm^3) at 36 Gy	[0.0, –2.8]∗	[0.0, –2.1]∗	[0.0, –0.3]
Δ Volume (cm^3) at 33 Gy	[0.1, –4.1]∗	[0.1, –2.8]∗	[0.0, –0.6]
Δ Volume (cm^3) at 25 Gy	[2.8, –12.8]∗	[3.1, –4.6]	[0.2, –2.4]

∗ Statistically significant difference between reoptimized and predicted plans (P < .05).

Predictors for improved target coverage in online plan adaptation

A logistic regression model resulted in a change of volume in GTV (ΔV_{GTV}) and a cumulative volume change of OAR within 1 cm from the PTV surface (ΔV_{OAR1cm}) at every fraction as the best predictors for improved target coverage in online plan adaptation:

$$\mathbf{ODDS_{plan\text{ - }adapt} = 1.3 + 0.3 \cdot \Delta V_{GTV} - 0.4 \cdot \Delta V_{OAR1cm}}$$

The logistic regression model explained all (100%) fractions, leading to improved target coverage, and 29% of the fractions in which the reoptimized plans did not improve PTV coverage, resulting in an overall 82% correct percentage. The obtained *P* values for ΔV_{GTV} and ΔV_{OAR1cm} were < .01, and .04, respectively.

Discussion

We implemented breath-hold SABR delivery for adrenal gland metastases under MR guidance and describe here both interfractional changes and the effect of online plan adaptation in this patient group.

Our main findings were that the OARs in the vicinity of the GTV exhibit significant interfractional changes. Consequently, online plan reoptimization led to significant

improvements in target coverage and OAR sparing. Changes in the GTV size at each fraction can be ascribed to factors such as rotations, which cannot be corrected in an MR-guided radiation therapy unit; deformations; for 2 of our patients, changes were attributed to either tumor progression or regression. For OARs, volumetric changes and DSC scores in the 3 cm region surrounding the PTV indicate a range of different anatomic changes with respect to the pretreatment situation in a region most relevant for online adaptive radiation therapy. Because changes outside the 3 cm region were not considered in this study, our results may not reflect the variability in the entire OAR. As such, the reported DSC value of 0 is highly unlikely to occur for the entire OAR.

Our routine protocol mandates delivery of a $BED_{\alpha/\beta = 10Gy}$ of at least 100 Gy because this dose has been reported to be an important predictor of long-term tumor control[5,11]. The low-dose scheme of 3 fractions of 8 Gy was only used in patients included in an ongoing study of immune-radiation therapy (NCT02492568). Online plan adaptation resulted in improved target coverage and adequate sparing of the OARs. Predicted plans for left-sided adrenal lesions failed more frequently to fulfill clinical constraints than those for the right-sided lesions, a finding attributed to the proximity of more OARs to left-sided tumors. In general, higher D_{mean} values for GTV were observed in the reoptimized plans. A recent phase 1 trial of online adaptive MR-guided radiation therapy in the treatment of oligometastatic malignancies in the abdomen included 2 patients with adrenal metastases[24] and concluded that online adaptive MR-guided radiation therapy enabled safer delivery of SABR and, in some cases, could permit dose escalation when the anatomy-of-the-day was favorable.

A retrospective study reported that 90% of failures after delivery of SABR to adrenal metastases occurred within the high-dose regions, but no local failures were

observed in patients treated with a biological equivalent dose of ≥100 Gy[5]. Grade 2 toxicity was limited to patients with a stomach and small bowel D_{max} <50 Gy delivered in 10 fractions[5], thereby emphasizing that efforts at dose escalation must ensure restriction of OAR doses. Our data indicate that PTV doses in the reoptimized plans were compromised whenever OAR doses exceeded the tolerance limits in the predicted plans. In those situations, online plan reoptimization significantly reduced the dose to the OARs and ensured safe delivery, as shown in Figure 5. Because tumor shrinkage was observed in 2 patients, use of their baseline treatment plan could lead to an overestimate of the need for plan adaption. Therefore, we generated a new baseline plan after delivery of the first 2 fractions in these patients. Plan comparisons for subsequent fractions were based on the second plan.

Overall, reoptimized plans resulted in improved target coverage and reduced dose to the OARs. Because our PTV definition was the GTV + 3 mm but excluded any overlap with OARs, the daily PTV is subject to some variations resulting from the interfractional OAR changes. Treatment delivery was accomplished with repeated breath-hold gated delivery based on the visualization of the GTV on a 2D cine planar image[26], ensuring that the dose was correctly delivered to the target.

One limitation of our study is the lack of analysis on dose accumulation in both the target and OAR, and this is a necessary step in future studies evaluating the clinical impact of online plan adaptation. Another limitation of this study is that tumor control rates are unavailable because a majority of our patients underwent treatment within the last year.

Changes in the GTV size (ΔV_{GTV}) and the cumulative volume change of OAR within 1 cm from the PTV surface (ΔV_{OAR1cm}) at every fraction were identified as the best predictors for improved target coverage. Other variables did not lead to improvement of the model and were not statistically significant. Any increment in

GTV size with respect to the pretreatment situation ($\Delta V_{GTV} > 0$) increases the odds that reoptimized plans will improve target coverage. On the other hand, larger amounts of OAR within 1 cm from the PTV ($\Delta V_{OAR1cm} > 0$) with respect to the baseline situation decrease the odds of improving target coverage. It is not surprising that a change in GTV size is a predictor for improved target coverage. However, it should be noted that in 80% of the fractions in which an adjustment of GTV contours took place, volume changes were less than 1 cm^3. Furthermore, an ongoing analysis of interobserver variations in delineation of the stomach in our study patients found this to be limited (results not shown). Nevertheless, further research on the intra- and interobserver variability in delineations during online MR-guided adaptive radiation therapy is warranted.

Our strategy for online plan adaptation for adrenal metastasis relies on the geometric and volumetric configuration of the OARs contained in a region up to 3 cm from the PTV surface (20). Recently, Lamb et al[21] proposed a similar approach, limiting the online recontouring to a region within 1 cm from the PTV. This appears sufficient to ensure sparing of the OARs in the upper abdominal region, where most complications and toxicity have been reported to stem from the high-dose regions[29–31]. Others have reported a dosimetric model of duodenal toxicity after pancreatic SABR that relies exclusively on the volumes of duodenum located within 3 cm from the PTV[32]. Recontouring only in a limited region surrounding the PTV ensures a fast and efficient online adaptive process. In our patients with adrenal tumors, it took on average 16.5 ± 6.2(SD) minutes to recontour and reoptimize the plan.

Conclusion

In breath-hold gated SABR delivery under MR-guidance, significant volumetric changes and displacements were observed for OARs in the region surrounding the GTV. Because reoptimization of treatment plans significantly improved target coverage and OAR sparing, our results indicate that online plan adaptation will be beneficial in adrenal SABR.

References

1. Moreno, P. *et al.* Adrenalectomy for solid tumor metastases: Results of a multicenter European study. *Surgery* **154**, 1215–1223 (2013).
2. Novello, S. *et al.* Metastatic non-small-cell lung cancer: ESMO Clinical Practice Guidelines for diagnosis, treatment and follow-up. *Ann. Oncol.* **27**, V1–V27 (2016).
3. Holy, R., Piroth, M., Pinkawa, M. & Eble, M. J. Stereotactic Body Radiation Therapy (SBRT) for treatment of adrenal gland metastases from non-small cell lung cancer. *Strahlentherapie und Onkol.* **187**, 245–251 (2011).
4. Scorsetti, M. *et al.* Long-term local control achieved after hypofractionated stereotactic body radiotherapy for adrenal gland metastases: A retrospective analysis of 34 patients. *Acta Oncol. (Madr).* **51**, 618–623 (2012).
5. Chance, W. W. *et al.* Stereotactic ablative radiotherapy for adrenal gland metastases: Factors influencing outcomes, patterns of failure, and dosimetric thresholds for toxicity. *Pract. Radiat. Oncol.* **7**, e195–e203 (2017).
6. Zhou, L.-Y. *et al.* Radiotherapy treatment of adrenal gland metastases from hepatocellular carcinoma: clinical features and prognostic factors. *BMC Cancer* **14**, 878 (2014).
7. Franzese, C. *et al.* Minimally Invasive Stereotactical Radio-ablation of Adrenal Metastases as an Alternative to Surgery. *Cancer Res. Treat.* **49**, 20–28 (2017).
8. Jung, J. *et al.* Radiotherapy for Adrenal Metastasis from Hepatocellular Carcinoma: A Multi-Institutional Retrospective Study (KROG 13-05). *PLoS One* **11**, e0152642 (2016).
9. Gamsiz, H. *et al.* Evaluation of Stereotactic Body Radiation Therapy in the Management of Adrenal Metastases from Non-Small Cell Lung Cancer. *Tumori J.* **101**, 98–103 (2015).
10. Rudra, S. *et al.* Stereotactic Body Radiation Therapy for Curative Treatment of Adrenal Metastases. *Technol. Cancer Res. Treat.* **12**, 217–224 (2013).
11. Desai, A. *et al.* A Retrospective Review of CyberKnife Stereotactic Body Radiotherapy for Adrenal Tumors (Primary and Metastatic): Winthrop University Hospital Experience. *Front. Oncol.* **5**, (2015).
12. Chawla, S. *et al.* Stereotactic Body Radiotherapy for Treatment of Adrenal Metastases. *Int. J. Radiat. Oncol.* **75**, 71–75 (2009).
13. Gunjur, A., Duong, C., Ball, D. & Siva, S. Surgical and ablative therapies for the management of adrenal 'oligometastases' – A systematic review. *Cancer Treat. Rev.* **40**, 838–846 (2014).
14. Chen, B. *et al.* Respiratory motion of adrenal gland metastases: Analyses using four-dimensional computed tomography images. *Phys. Medica* **38**, 54–58 (2017).
15. Isobe, K. *et al.* A case of gastric lymphoma with marked interfractional gastric

movement during radiation therapy. *Int. J. Clin. Oncol.* **11**, 159–161 (2006).

16. Wysocka, B. *et al.* Interfraction and Respiratory Organ Motion During Conformal Radiotherapy in Gastric Cancer. *Int. J. Radiat. Oncol.* **77**, 53–59 (2010).
17. Knybel, L. *et al.* The analysis of respiration-induced pancreatic tumor motion based on reference measurement. *Radiat. Oncol.* **9**, 192 (2014).
18. Acharya, S. *et al.* Online Magnetic Resonance Image Guided Adaptive Radiation Therapy: First Clinical Applications. *Int. J. Radiat. Oncol.* **94**, 394–403 (2016).
19. Fischer-Valuck, B. W. *et al.* Two-and-a-half-year clinical experience with the world's first magnetic resonance image guided radiation therapy system. *Adv. Radiat. Oncol.* **2**, 485–493 (2017).
20. Bohoudi, O. *et al.* Fast and robust online adaptive planning in stereotactic MR-guided adaptive radiation therapy (SMART) for pancreatic cancer. *Radiother. Oncol.* (2017). doi:10.1016/j.radonc.2017.07.028
21. Lamb, J. *et al.* Online Adaptive Radiation Therapy: Implementation of a New Process of Care. *Cureus* **9**, e1618 (2017).
22. Bruynzeel, A. *et al.* OC-0425: Clinical experience with stereotactic MR-guided adaptive radiation therapy for pancreatic tumors. *Radiother. Oncol.* **123**, S224–S225 (2017).
23. Henke, L. *et al.* Simulated Online Adaptive Magnetic Resonance–Guided Stereotactic Body Radiation Therapy for the Treatment of Oligometastatic Disease of the Abdomen and Central Thorax: Characterization of Potential Advantages. *Int. J. Radiat. Oncol.* **96**, 1078–1086 (2016).
24. Henke, L. *et al.* Phase I trial of stereotactic MR-guided online adaptive radiation therapy (SMART) for the treatment of oligometastatic or unresectable primary malignancies of the abdomen. *Radiother. Oncol.* **126**, 519–526 (2018).
25. Noel, C. E. *et al.* Comparison of onboard low-field magnetic resonance imaging versus onboard computed tomography for anatomy visualization in radiotherapy. *Acta Oncol. (Madr).* **54**, 1474–1482 (2015).
26. Mutic, S. & Dempsey, J. F. The ViewRay System: Magnetic Resonance-Guided and Controlled Radiotherapy. *Semin. Radiat. Oncol.* **24**, 196–199 (2014).
27. Mazur, T. R. *et al.* SIFT-based dense pixel tracking on 0.35 T cine-MR images acquired during image-guided radiation therapy with application to gating optimization. *Med. Phys.* **43**, 279–293 (2015).
28. Palacios, M. A. *et al.* OC-0262: Implementation of patient specific QA for daily adaptive MR-guided radiation therapy. *Radiother. Oncol.* **123**, S134–S135 (2017).
29. Moningi, S. *et al.* Stereotactic body radiation therapy in pancreatic cancer: the new frontier. *Expert Rev. Anticancer Ther.* **14**, 1461–1475 (2014).
30. De Bari, B. *et al.* Hypofractionated radiotherapy in pancreatic cancer: Lessons from the past in the era of stereotactic body radiation therapy. *Crit. Rev. Oncol. Hematol.*

103, 49–61 (2016).

31. Brunner, T. B., Nestle, U., Grosu, A.-L. & Partridge, M. SBRT in pancreatic cancer: What is the therapeutic window? *Radiother. Oncol.* **114**, 109–116 (2015).

32. Murphy, J. D. *et al.* A Dosimetric Model of Duodenal Toxicity After Stereotactic Body Radiotherapy for Pancreatic Cancer. *Int. J. Radiat. Oncol.* **78**, 1420–1426 (2010).

Chapter 6

The Role of Daily Adaptive Stereotactic MR-guided Radiotherapy for Renal Cell Cancer

Shyama Tetar*
Omar Bohoudi*
Suresh Senan
Miguel A. Palacios
Swie S. Oei
Antoinet M. van der Wel
Ben J. Slotman
Jeroen A. van Moorselaar
Frank J. Lagerwaard and Anna M.E Bruynzeel

**Both authors contributed equally to this paper*

Cancers (Basel). 2020; 12(10), 2763

Abstract

Novel magnetic-resonance-guided radiotherapy (MRgRT) permits real-time soft-tissue visualization, respiratory-gated delivery with minimal safety margins, and time-consuming daily plan re-optimisation. We report on early clinical outcomes of MRgRT and routine plan re-optimization for large primary renal cell cancer (RCC). Thirty-six patients were treated with MRgRT in 40 Gy / 5 fractions. Prior to each fraction, re-contouring of tumor and normal organs on a pretreatment MR-scan allowed daily plan re-optimization. Treatment-induced toxicity and radiological responses were scored, which was followed by an offline analysis to evaluate the need for such daily re-optimization in 180 fractions. Mean age and tumor diameter were 78.1 years and 5.6 cm, respectively. All patients completed MRgRT with an average fraction duration of 45 min. Local control (LC) and overall survival rates at one year were 95.2% and 91.2%. No grade ≥3 toxicity was reported. Plans without re-optimization met institutional radiotherapy constraints in 83.9% of 180 fractions. Thus, daily plan re-optimization was required for only a minority of patients, who can be identified upfront by a higher volume of normal organs receiving 25 Gy in baseline plans. In conclusion, stereotactic MRgRT for large primary RCC showed low toxicity and high LC, while daily plan re-optimization was required only in a minority of patients.

Introduction

A radical or partial nephrectomy is the preferred standard curative treatment for localized renal cell carcinoma (RCC)[1–4]. Ablative local treatment, such as radiofrequency ablation (RFA), cryoablation (CA), or microwave ablation (MWA), is an alternative in elderly patients who present with a high surgical risk due to several comorbidities[3]. Radiotherapy does not have a prominent role in current international and national guidelines in treating primary RCC[1–4]. In recent years, stereotactic ablative radiation therapy (SABR) has been evaluated in several smaller retrospective and prospective studies[5–14], usually in RCC patients unsuitable for surgery. Outcomes of a multi-institutional pool from nine institutions, utilizing either single or multi-fractionated treatment in 223 patients, have been reported by the International Radiosurgery Oncology Consortium for Kidney (IROCK)[15]. SABR for RCC was found to be well tolerated, achieved local control (LC) rates exceeding 95% at four years of follow-up and grade ≥3 toxicity rates of 1.3%, and had an average decrease in glomerular filtration rate of 5.5 mL per minute. The majority of the tumors in this pooled analysis was ≤4 cm and clinical data for larger tumors is limited. A retrospective analysis of a subgroup of 95 patients with tumors >4 cm was recently published[16], but with the exception of these data, clinical outcomes on cT1b-T2 RCC SABR are scarce. Due to the inherent limitations to a pooled analyses, the Trans-Tasman Radiation Oncology Group (TROG) and the Australian and New Zealand Urogenital and Prostate Cancer Trials Group (ANZUP) have initiated a prospective, multi-institutional phase II study in 70 patients with biopsy-confirmed medical inoperable RCC patients[17]. Full accrual has recently been completed, and the data of this trial are eagerly awaited.

Technical challenges in renal SABR include the management of intra-fractional motion, and potential solutions using an internal target volume-approach, fiducial-assisted robotic SABR or abdominal compression[18] have been described. Magnetic-resonance (MR)-guided radiotherapy (MRgRT) has been considered a promising option because of its improved visualization of kidney tumors in relation to critical adjacent organs such as a small bowel, duodenum, and stomach and the opportunity of real-time tumor tracking and automated gated delivery[18,19]. MRgRT also facilitates daily plan re-optimization as a means to reduce organs at risk (OAR) doses when abdominal organs are near the primary tumor. Furthermore, MRgRT is an outpatient treatment for which no invasive procedures or anesthesia is required. However, to the best of our knowledge, clinical data on MR-guided SABR for localized RCC have not been reported.

Stereotactic MRgRT with routine daily plan adaptation was clinically implemented at our center in 2016 for a variety of clinical indications. The aim of the current paper is to describe our technique, early clinical outcomes, and the role of daily plan adaptation in MRgRT for patients with primary large RCC.

Material and Methods

Data from all patients treated with MRgRT on the MRIdian-system (ViewRay Inc., Mountain View, USA) at the Amsterdam University Medical Centers are collected within a prospective institutional review board approved database. Between May 2016 and February 2020, a total of 51 patients were treated for a primary RCC (n = 36), local recurrences (n = 5), renal metastases from other primary tumors (n = 3), or a diagnosis of urothelial carcinoma (n = 7). This analysis is restricted to the remaining 36 patients who were treated for primary RCC.

All patients underwent stereotactic adaptive MRgRT delivered to a dose of 40 Gy in five fractions in a two-week period. Implanted fiducials were not required, and the adaptive workflow was similar to that which had been described previously for pancreatic tumors [20]. Briefly, for simulation, both a MR-scan (0.35T True-FISP, TR/TE: 3.37 ms/1.45 ms, FA: 60°, 17-s with 1.6 mm × 1.6 mm × 3.0 mm resolution) and computed tomography (CT)-scan (slice thickness of 2 mm) are acquired during a shallow-inspiration breath-hold. Geometric accuracy of the MRIdian system is < 0.1 cm in a sphere of 10 cm radius around the isocenter, and <0.15 cm in a sphere of 17.5 cm radius. Every patient was brought as close to the isocenter as possible for each fraction, and the maximum distance from the tumor or any other critical structure to the isocenter was always below 10 cm. Geometric accuracy was assessed with two different dedicated phantoms for spatial integrity measurements. Contouring of the primary tumor (also called gross tumor volume; GTV) and OAR is performed on breath-hold MR-images with the aid of diagnostic imaging, generally contrast-enhanced CT scans. The PTV (planning target volume) is derived from the GTV plus an isotropic 3-mm margin. A co-planar baseline plan consisting of between 30 and 42 intensity modulated radiotherapy (IMRT)-segments is generated, using the MRIdian treatment planning software. Dose calculation was executed with a VMC and EGSnrc code-based Monte-Carlo algorithm (statistical uncertainty of 1% and a grid size of 0.3 cm × 0.3 cm × 0.3 cm) using the deformed electron density map from the simulation CT scan. Institutional target coverage and OAR constraints are summarized in Table 1. We perform routine plan re-optimization using the daily pre-SABR breath-hold MR-imaging acquired in the treatment position. After rigid registration on the GTV, OAR contours are propagated to the repeat MR using deformable image registration.

Table 1. *Dose prescription for institutional target coverage and normal tissue constraints. The constraints represent the cut-off doses for radiotherapy planning with the aim of dose sparing in the surrounding organs (contralateral kidney, liver, duodenum, bowel and stomach) while at the same time aiming to achieve a high dose in the tumor with margin, which is represented as planning target volume. Organs at risk are only re-contoured within 2 cm of the tumor and for adaptive setting only dose in these structured are optimized.*

Structure	Dose to Volume			
Planning Target Volume	≥50	% at	38	Gy
	≤1	cc at	50	Gy
Kidney Contralateral	≤25	% at	12	Gy
Liver	≤50	% at	12	Gy
Duodenum, Bowel, Stomach in 2 cm	≤0.1	cc at	36	Gy
	≤1	cc at	33	Gy

The ViewRay deformable image registration algorithm uses an intensity-based algorithm, which minimizes a cost function that measures the similarity between the images including a regularization term in order to obtain smoother deformation fields and prevent sharp discontinuities. The GTV and OAR contours are checked and adjusted where needed within a 2-cm distance of the PTV by the attending radiation oncologist. Next, the baseline IMRT plan is recalculated on the new anatomy ("predicted plan"), and subsequently re-optimized using the target and OAR optimization objectives of the baseline plan ("re-optimized plan"). Plan re-optimization prioritizes avoiding high doses to OARs, even when this is at the cost of decreased PTV coverage. Both the predicted and re-optimized plans are reviewed, and the re-optimized plan is selected for the actual delivery.

MRgRT delivery is performed using respiratory gating during subsequent breath-hold periods in shallow inspiration. The tracking structure for gating is either the primary tumor, or the kidney itself on a single sagittal plane (Figure 1), depending on the visibility on this sagittal plane. Gating is augmented by visual and/or auditory feedback provided to patients during

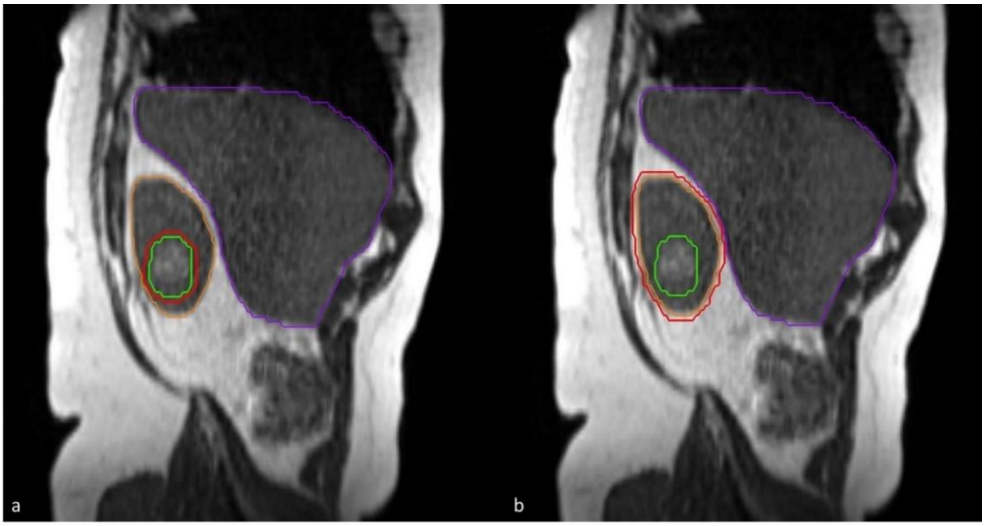

Figure 1. *Sagittal plane for tumor tracking: either (a) tracking on gross tumor volume (green) or (b) tracking on the whole kidney (orange). A boundary of 3 mm (red) for gated delivery.*

treatment[21]. Visual feedback is performed with the aid of an in-room MR compatible monitor on which both the tracking structure (GTV or kidney) and the gating boundary (3 mm), generally corresponding to the PTV, is projected in real-time. The 2D MR images during treatment were acquired with a True FISP sequence with the MRIdian (0.35 T) at a frequency of four frames-per-second (TR: 2.1 ms, TE: 0.91 ms, FA: 60°). FOV was 0.35 cm × 0.35 cm and the slice thickness was 0.7 cm. Due to the low magnetic field and low FA, "real-time" MR images of the patient were performed without interruption during the beam-on time. A previous analysis showed a treatment duty cycle efficiency between 67% and 87% for upper abdominal tumors[22].

Baseline patient and tumor characteristics and follow-up data including LC, renal function, and toxicity were collected. Acute and late toxicity was scored using the Common Terminology Criteria for Adverse Events (CTCAE) version 4.0. Follow-up imaging was assessed by a CT-scan or ultrasound, and the tumor response was classified according to RECIST 1.1. criteria.

An offline analysis was performed to evaluate the need for daily plan re-optimization in MRgRT for RCC in a total of 180 fractions. For this purpose, predicted and re-optimized plans were analyzed for adherence with planning target objectives and OAR constraints, i.e., a V_{38Gy} of the GTV ≥ 90%, and V_{33Gy} ≤ 1 cc for stomach, duodenum, and bowel. Re-optimization was defined as "needed" when the predicted plan violated the above-mentioned GTV and/or OAR constraints, which was subsequently corrected by re-optimization. In contrast, plan re-optimization was defined as "redundant" when predicted plans already complied with the planning objectives. In addition, the value of plan re-optimization was analyzed on a patient level by studying the number of fractions per patient that were considered suboptimal.

Statistical Analysis

Descriptive statistics were used for baseline patient and tumor characteristics. The change in renal function (eGFR) from baseline versus post-treatment at the latest available time point in follow-up was evaluated using the paired sampled t-test. Local, regional, distant disease control and overall survival (OS) were estimated using the Kaplan-Meier method. OS was calculated as the time between the first fraction of MRgRT and the date of the last follow-up. LC was calculated as the time between the first fraction of MRgRT and the date of last imaging. Statistical analysis used for plan comparisons was performed using the Wilcoxon Signed-Rank test. A p-value of < 0.05 was considered to be statistically significant. Decision tree analysis (CHAID, Chi-square automatic interaction detection) was used to explore predictive pretreatment characteristics and most significant cut-off values to identify patients for whom daily re-optimization was needed. Baseline volumetric, geometric, and dosimetric parameters, i.e., GTV size (cc), laterality (left, right), location (interpolar, upper or lower pole), V_{33Gy}, V_{30Gy}, V_{25Gy}, and V_{20Gy} for each OAR structure separately

or combined in one structure were used as input variables. The qualitative re-optimization benefit variable ("redundant" or "needed") was selected as the target variable for decision tree analysis. The significance level for node splitting was set at $p < 0.05$. Stopping parameters to prevent over-fitting were applied by setting the minimum number of records in a leaf to be at least 10% of the data set. The Statistical Package for the Social Sciences (SPSS) version 26 (IBM® SPSS Statistics, Armonk, NY, USA) was used to perform all statistical analyses.

Results

Clinical Outcomes

All 36 patients were referred for SABR after discussion in a multidisciplinary tumor board, and reasons for referral included a high surgical risk due to comorbidity (n = 9), which is unsuitable for other ablative therapies due to tumor size (n = 10) or location (n = 5), patient preference (n = 5), co-existing second malignancy (n = 3), use of anti-coagulants (n = 2), and chronic stage ≥IV kidney disease (n = 2). Baseline patient characteristics are summarized in Table 2. The mean age of this cohort was 78.1 years with a preponderance of men (66.7%). The mean tumor diameter was 5.6 cm (range 2.4–9.3 cm) with 86.1% of tumors measuring ≥4 cm in the largest dimension of which 23 patients have a cT1b tumor and 8 patients have a cT2a tumor. Five patients (13.9%) had metastasized RCC at the time of diagnosis. Pathologic confirmation of RCC before treatment was achieved in approximately half of patients (55.6%) of which the majority was diagnosed with Fuhrman grade 2 (n = 14). Other patients with histology included Fuhrman grade 1 (n = 1), Fuhrman grade 3 (n = 1), a RCC with sarcomatoid features (n = 1), and a chromophobe tumor (n = 1).

Table 2. *Baseline patient characteristics (n = 36) Abbreviations: RCC = renal cell carcinoma, GTV = gross tumor volume, PTV = planning target volume, CKD = chronic kidney disease.*

Mean age (Range), Years		**78.1 (58–95)**
Sex, *n* (%)		
Male		24 (66.7)
Female		12 (33.3)
WHO performance status, *n* (%)		
0		3 (7.9)
1		21 (58.3)
2		12 (33.3)
Charlson comorbidity, *n* (%)		
Mean (SD)		6.4 (2.5)
2–3		3 (8.3)
4–6		18 (50)
7–9		10 (27.8)
10–13		5 (13.9)
Histology RCC, *n* (%)		
Yes		20 (55.6)
No		16 (44.4)
Tumor Laterality, *n* (%)		
Left		13 (36.1)
Right		23 (63.9)
Tumor location, *n* (%)		
Interpolair		13 (36.1)
Lower pole		13 (36.1)
Upper pole		10 (27.8)
Tumor size largest dimension, cm		
Mean (SD)		5.6 (1.6)
Median (range)		5.5 (2.4–9.3)
T-stage, *n* (%)		
cT1a		5 (13.9)
cT1b		23 (63.9)
cT2a		8 (22.2)
GTV, cc		
Mean (range)		79.7 (7.7–350.4)
PTV, cc		
Mean (range)		108.6 (14.3–445.9)
Renal function (eGFR), ml/min/1,73 m²		
Mean (SD)		55.8 (20.1)
CKD classification, *n* (%)		
I	Normal (eGFR ≥ 90)	0 (0)
II	Mild (eGFR ≥ 60 to < 90)	15 (41.7)
IIIa	Mild-Moderate (eGFR ≥ 45 to < 60)	10 (27.8)
IIIb	Moderate-Severe (eGFR ≥ 30 to < 45)	8 (22.2)
IV	Severe (eGFR < 30)	2 (5.6)
V	Kidney failure (eGFR < 15)	1 (2.8)

In two patients, no grading was available because pathologic confirmation was obtained from systemic metastases. All patients were able to complete adaptive MRgRT with an average time per fraction of 45 min. An overview of the average duration of the different components of adaptive MRgRT for RCC is shown in Figure 2. Three patients completed treatment while tracking on the kidney instead of the tumor.

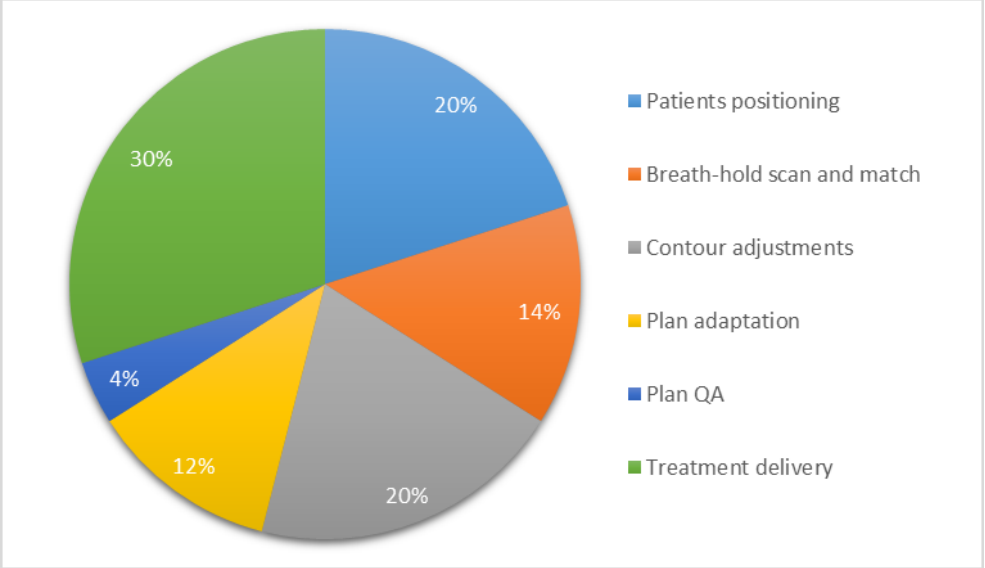

Figure 2. *Pie-chart of the average duration of the different components of breath-hold gated adaptive MR-guided radiotherapy with an average time per fraction of 45 min.*

The median follow-up was 16.4 months. Overall survival was 91.2% at one year (Figure 3), LC was 95.2% (Figure 3), and freedom from any progression was 91% at one year. Two patients had local recurrences. One patient had progressive distant disease at recurrence for which systemic therapy was delivered, and the second patient with an isolated local recurrence underwent radiofrequency ablation as salvage. Treatment-related acute toxicity grade ≥ 2 in the form of nausea was observed in a single patient, which responded to oral ondansetron. No other acute or late grade ≥2 toxicity was reported. The mean eGFR at baseline was 55.3 (SD ±19.0)

mL/min/1.73 m². With a mean interval of 16 months and mean eGFR post-MRgRT was 49.3 (SD ± 19.1) mL/min/1.73 m², which indicates a decrease of 6.0 mL/min/1.73 m². No patient in this cohort required dialysis during follow-up.

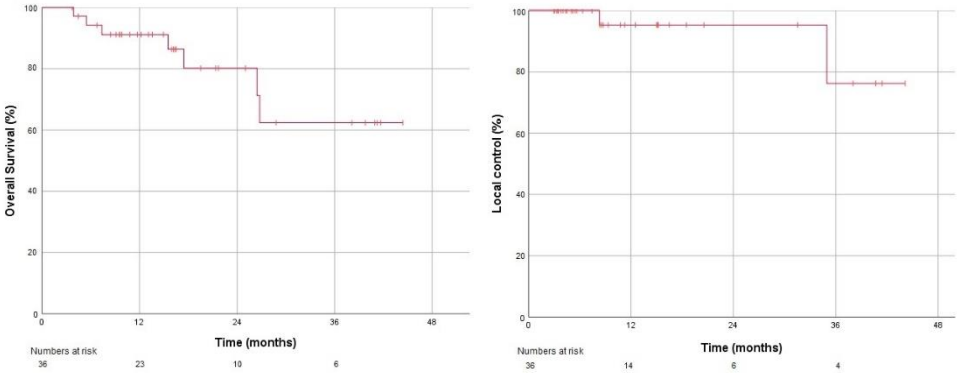

Figure 3. *Kaplan-Meier plots for overall survival (left) and local control (right).*

The Need for Daily Plan Re-Optimization

In 151 out of 180 fractions (83.9%), the predicted plans (without re-optimization) met all institutional target and OAR constraints. In these fractions, predicted and re-optimized plans were of similar quality with a mean GTV V_{38Gy} of 98.8% and 99.1%, respectively, and mean V_{33Gy} of 0 cc for both stomach, duodenum, and bowel. In the other 29 fractions, predicted plans were suboptimal with insufficient GTV coverage in two out of 180 fractions (1.1%) exceeding OAR constraints in 25 fractions (13.9%), and both insufficient GTV coverage and exceeded OAR constraints in another two fractions (1.1%). There was no significant difference in suboptimal predicted plans for left-sided or right-sided RCC ($p = 0.56$). For these suboptimal plans, on-couch re-optimization corrected the GTV V_{38Gy} from a mean of 88.7% (predicted) to 97.4% (re-optimized). Similarly, re-optimization corrected OAR $V_{33Gy} \leq 1$ cc violations from on average V_{33Gy} of 4.1 (predicted plans) to 0.3 cc (re-optimized plans). Analysis on a patient basis showed that the 29 insufficient predicted fractions were distributed

among 11 patients (11/36, 30.6%). However, three or more suboptimal fractions were seen in only five patients (13.9%).

Decision tree analysis identified the baseline OAR V_{25Gy} (combined structure of stomach, bowel, and duodenum) as the most significant predictor variable for daily adaptive planning needs with 0.5 cc as an optimal cut-off value ($p < 0.001$). In all cases with a baseline OAR V_{25Gy} of ≤ 0.5 cc, plan adaptation was redundant as the predicted plans already complied with institutional constraints. In patients with baseline OAR V_{25Gy} of more than 0.5 cc, plan re-optimization was needed in 32.2% of fractions in order to fulfill the preset target coverage and OAR constraints (Table 3).

Table 3. *Results in the Chi-square automatic interaction detection (CHAID) tree table.*

	Redundant *n* (%)	**Needed *n* (%)**	**Total *n* (%)**	**Predictive Variable**	**Split Values**	**Chi-Square**	**df**	***p-value***
Parent node: all cases	151 (83.9)	29 (16.1)	180 (100)					
Split group 1	90 (100)	0 (0)	90 (100)	OAR V_{25Gy}	≤ 0.5 cc	34.6	1	< 0.001
Split group 2	61 (67.8)	25 (32.2)	90 (100)	OAR V_{25Gy}	> 0.5 cc	34.6	1	< 0.001

The correct classification rate of the decision tree was 86.1% with a sensitivity of 100% and a specificity of 67.7%. The difference between re-optimized and predicted dose parameters for target (GTV $V_{95\%}$) and OAR (V_{33Gy}) stratified for split group 1 and 2 (Table 3) is shown in Figure 4.

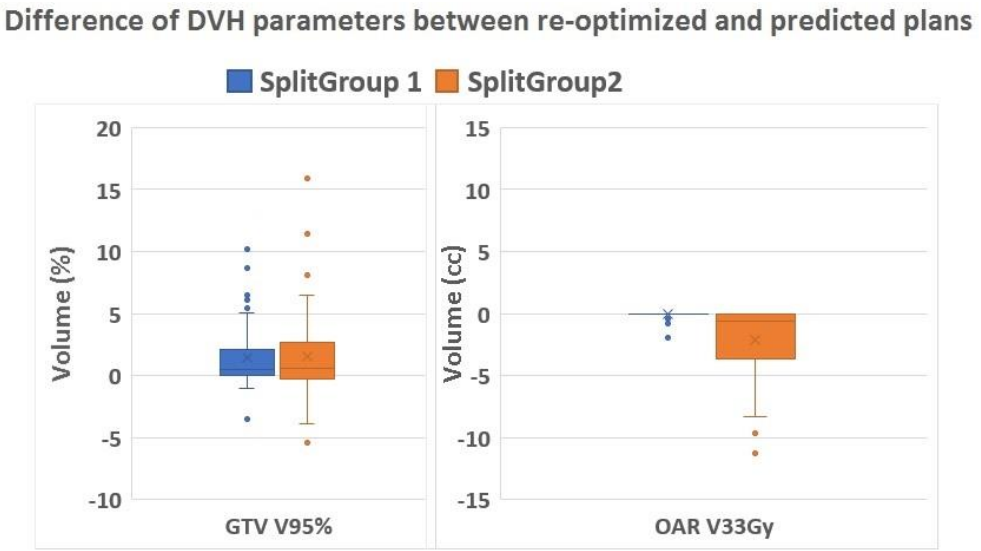

Figure 4. *Difference of DVH parameters. Boxplots showing the relative volume difference in GTV $_{V95\%}$ (%) and absolute difference in OAR V_{33Gy} (cc) of the re-optimized compared to the predicted plans stratified for Split group 1 (re-optimization not needed) and 2 (re-optimization needed). Abbreviations: DVH = dose volume histogram, GTV = gross target volume, OAR = organs at risk.*

Discussion

To the best of our knowledge, this is the first series of patients treated for primary RCC using MRgRT with routine daily plan re-optimization. We applied a commonly used fractionation scheme of 40 Gy in five fractions[18,23,24] in an overall treatment time of two weeks. Only a single patient reported nausea as acute toxicity, and no grade ≥ 2 late toxicity was observed. Despite the inclusion of large tumors, mostly T1b and T2, which had a mean tumor diameter of 5.6 cm and were generally unsuitable for other local therapies, we observed an LC rate of 95.2%. Our local response scoring has been according to the RECIST 1.1 criteria, and 83.3% had stable disease. In addition, 11.1% had partial remission, while 5.6% showed local progression. Fast tumor size regression is uncommon after SABR as previously reported by Sun and colleagues[11]. This preponderance of stable disease is in accordance with their paper. Both LC and OS are reported to be poorer for larger primary RCC than for the

smaller lesions[25,26]. Despite this observation, our LC rate is within the high range of what was reported in recent systematic reviews, meta-analyses, and pooled analyses of SABR for primary RCC[15,24,27].

MRgRT with daily plan re-optimization was feasible with an average fraction duration of 45 min, even in poorer condition patients with multiple co-existing diseases. Despite this prolonged treatment duration, all patients were able to complete treatment, which indicates good tolerability. Our fractionation scheme of 40 Gy in five fractions is commonly used and seems safe without severe toxicity. With a mean interval of well over one year, the mean decline in eGFR in our study was only 6.0 (SD ± 9.8) mL/min/1.73 m^2. This value corresponds well with the mean decline in eGFR of 5.5 (SD ± 13.3) mL/min/1.73 m^2 that was described in previous SABR studies [15,28]. This limited decline in renal function in our patients with relatively large RCC may well be the result of this gated approach with small mobility boundaries, instead of using internal target volumes incorporating full tumor motion.

MRgRT also offers the advantage of using plan re-optimization for each delivered fraction at the cost of additional time. Our offline analysis showed that daily plan re-optimization was required in only 16% of fractions in which the predicted plan failed to meet the predetermined high-dose OAR constraints or target coverage objectives. Decision tree analysis showed that patients for whom daily plan re-optimization is not required can be identified upfront on the basis of a V_{25Gy} of the combined OAR of less than 0.5 cc in the baseline plan. It is, however, unlikely that an isolated single fraction violating high OAR dose or target constraints will be clinically relevant, and three out of five insufficient predicted plans were seen in only 14% of patients. Performing MRgRT without plan re-optimization indicates that the re-contouring, plan adaptation, and plan quality assurance phases can be

omitted, which would enable respiratory-gated MRgRT fractions to be completed in 30 minutes. Furthermore, when plan adaptation is redundant, this indicates that the presence of the radiation oncologist at the MR Linac is not necessary. As a result of our analysis, we are currently introducing the found V_{25Gy} selection criterion in clinical practice.

The main limitation of our study is the relative short and unstructured patient follow-up. The limited number of RCC patients reflects the limited role of SABR in current international treatment guidelines, as only patients unsuitable for or refusing other local treatments are referred for curative radiation therapy. Another limitation includes the absence of pathology in half of our patients. Incomplete pathology confirmation is partly inherent to our patient population with generally frail elderly patients, which is unsuitable for other treatment modalities. Moreover, in a number of patients, a diagnostic biopsy was considered contra-indicated because of anticoagulant use or the anatomical location of the tumor. All patients had been discussed in a multidisciplinary tumor board with access to all available diagnostic imaging. Contrast enhanced multi-phasic CT has a high sensitivity and specificity for characterization and detection of RCC[3,29] and this specific imaging was available for all patients without pathological confirmation.

Prior to the MRgRT era, the need for radiologists to implant fiducial markers has also been an obstacle for referral for SABR. Our data show that MRgRT can be a valid alternative in patients unsuitable for the more commonly used local treatments, because of patient vitality or tumor size. The only contra-indication for MRgRT is having MR-incompatible devices. The main advantage of MRgRT is that it is an outpatient, non-invasive treatment for which not even the placement of fiducial markers is necessary. Whether MRgRT can also be considered as an alternative to partial nephrectomy or cryotherapy needs to be addressed in a

prospective randomized study, which should also evaluate quality of life and cost-effectiveness. With regard to the favorable outcome in the data on SABR literature as well as the current analysis on MRgRT, a more prominent role of SABR in the treatment guidelines for RCC appears warranted.

Conclusion

In conclusion, hypo-fractionated MRgRT for large RCC resulted in high LC and very low toxicity rates. Gated treatment without the need for anesthesia or fiducials appeared well tolerated. Even in this group with large RCCs, daily plan re-optimization was not needed for the majority of patients, who can be identified upfront by a combined OAR V_{25Gy} of ≤ 0.5 cc in the baseline plans. This is a favorable result since online MRgRT plan adaptation is a time-consuming procedure. In this group of patients, MRgRT delivery will be faster, and these patients could be candidates for further hypofractionation[30].

References

1. Escudier, B. *et al.* Renal cell carcinoma: ESMO Clinical Practice Guidelines for diagnosis, treatment and follow-up. *Ann. Oncol.* **30**, 706–720 (2019).
2. Campbell, S. *et al.* Renal Mass and Localized Renal Cancer: AUA Guideline. *J. Urol.* **198**, 520–529 (2017).
3. Ljungberg, B. *et al.* European Association of Urology Guidelines on Renal Cell Carcinoma: The 2019 Update. *Eur. Urol.* **75**, 799–810 (2019).
4. Motzer, R. J. *et al.* Kidney Cancer, Version 2.2017: Clinical practice guidelines in oncology. *JNCCN Journal of the National Comprehensive Cancer Network* **15**, 804–834 (2017).
5. Peddada, A. V. *et al.* Nephron-Sparing Robotic Radiosurgical Therapy for Primary Renal Cell Carcinoma: Single-Institution Experience and Review of the Literature. *Adv. Radiat. Oncol.* **5**, 204–211 (2020).
6. Siva, S. *et al.* Stereotactic ablative body radiotherapy for inoperable primary kidney cancer: a prospective clinical trial. *BJU Int.* **120**, 623–630 (2017).
7. Staehler, M. *et al.* Single fraction radiosurgery for the treatment of renal tumors. *J. Urol.* **193**, 771–775 (2015).
8. Ponsky, L. *et al.* Phase I dose-escalation study of stereotactic body radiotherapy (SBRT) for poor surgical candidates with localized renal cell carcinoma. *Radiother. Oncol.* **117**, 183–187 (2015).
9. Pham, D. *et al.* Stereotactic ablative body radiation therapy for primary kidney cancer: A 3-dimensional conformal technique associated with low rates of early toxicity. *Int. J. Radiat. Oncol. Biol. Phys.* **90**, 1061–1068 (2014).
10. Kaidar-Person, O., Price, A., Schreiber, E., Zagar, T. M. & Chen, R. C. Stereotactic Body Radiotherapy for Large Primary Renal Cell Carcinoma. *Clin. Genitourin. Cancer* **15**, e851–e854 (2017).
11. Sun, M. R. M. *et al.* Effect of stereotactic body radiotherapy on the growth kinetics and enhancement pattern of primary renal tumors. *Am. J. Roentgenol.* **206**, 544–553 (2016).
12. Chang, J. H. *et al.* Stereotactic Ablative Body Radiotherapy for Primary Renal Cell Carcinoma in Non-surgical Candidates: Initial Clinical Experience. *Clin. Oncol.* **28**, e109–e114 (2016).
13. Beitler, J. J., Makara, D., Silverman, P. & Lederman, G. Definitive, high-dose-per-fraction, conformal, stereotactic external radiation for renal cell carcinoma. *Am. J. Clin. Oncol. Cancer Clin. Trials* **27**, 646–648 (2004).
14. McBride, S. M., Wagner, A. A. & Kaplan, I. D. A Phase 1 Dose-Escalation Study of Robotic Radiosurgery in Inoperable Primary Renal Cell Carcinoma. *Int. J. Radiat.*

Oncol. **87**, S84 (2013).

15. Siva, S. *et al.* Pooled analysis of stereotactic ablative radiotherapy for primary renal cell carcinoma: A report from the International Radiosurgery Oncology Consortium for Kidney (IROCK). *Cancer* **124**, 934–942 (2018).
16. Siva, S. *et al.* Stereotactic Ablative Radiotherapy for ≥T1b Primary Renal Cell Carcinoma: A Report From the International Radiosurgery Oncology Consortium for Kidney (IROCK). *Int. J. Radiat. Oncol. Biol. Phys.* (2020). doi:10.1016/j.ijrobp.2020.06.014
17. Siva, S. *et al.* TROG 15.03 phase II clinical trial of Focal Ablative STereotactic Radiosurgery for Cancers of the Kidney - FASTRACK II 11 Medical and Health Sciences 1103 Clinical Sciences 11 Medical and Health Sciences 1112 Oncology and Carcinogenesis. *BMC Cancer* **18**, (2018).
18. Rühle, A., Andratschke, N., Siva, S. & Guckenberger, M. Is there a role for stereotactic radiotherapy in the treatment of renal cell carcinoma? *Clinical and Translational Radiation Oncology* **18**, 104–112 (2019).
19. Corradini, S. *et al.* MR-guidance in clinical reality: Current treatment challenges and future perspectives. *Radiation Oncology* **14**, (2019).
20. Bohoudi, O. *et al.* Fast and robust online adaptive planning in stereotactic MR-guided adaptive radiation therapy (SMART) for pancreatic cancer. *Radiother. Oncol.* **125**, 439–444 (2017).
21. Tetar, S. *et al.* Patient-reported Outcome Measurements on the Tolerance of Magnetic Resonance Imaging-guided Radiation Therapy. *Cureus* **10**, (2018).
22. van Sörnsen de Koste, J. R. *et al.* MR-guided gated stereotactic radiotherapy delivery for lung, adrenal and pancreatic tumors: a geometric analysis. *Int. J. Radiat. Oncol.* **0**, (2018).
23. Francolini, G. *et al.* Stereotactic body radiation therapy (SBRT) on renal cell carcinoma, an overview of technical aspects, biological rationale and current literature. *Critical Reviews in Oncology/Hematology* **131**, 24–29 (2018).
24. Siva, S., Pham, D., Gill, S., Corcoran, N. M. & Foroudi, F. A systematic review of stereotactic radiotherapy ablation for primary renal cell carcinoma. *BJU International* **110**, (2012).
25. Siva, S. *et al.* Stereotactic Body Radiotherapy for Large Primary Renal Cell Carcinoma: A Report from the International Radiosurgery Oncology Consortium for Kidney (IROCK). *Int. J. Radiat. Oncol.* **105**, E257–E258 (2019).
26. Wegner, R. E., Abel, S., Vemana, G., Mao, S. & Fuhrer, R. Utilization of Stereotactic Ablative Body Radiation Therapy for Intact Renal Cell Carcinoma: Trends in Treatment and Predictors of Outcome. *Adv. Radiat. Oncol.* **5**, 85–91 (2020).
27. Correa, R. J. M. *et al.* The Emerging Role of Stereotactic Ablative Radiotherapy for Primary Renal Cell Carcinoma: A Systematic Review and Meta-Analysis. *European Urology Focus* **5**, 958–969 (2019).

28. Siva, S. *et al.* Impact of stereotactic radiotherapy on kidney function in primary renal cell carcinoma: Establishing a dose-response relationship. *Radiother. Oncol.* **118**, 540–546 (2016).

29. Musaddaq, B., Musaddaq, T., Gupta, A., Ilyas, S. & von Stempel, C. Renal Cell Carcinoma: The Evolving Role of Imaging in the 21st Century. *Semin. Ultrasound, CT MRI* **41**, 344–350 (2020).

30. Grant, S. R. *et al.* Stereotactic Body Radiation Therapy for the Definitive Treatment of Early Stage Kidney Cancer: A Survival Comparison With Surgery, Tumor Ablation, and Observation. *Adv. Radiat. Oncol.* **5**, 495–502 (2020).

Chapter 7

Combined Inter- and Intrafractional Plan adaptation Using Fraction Partitioning in Magnetic Resonance-guided Radiotherapy Delivery

Frank J. Lagerwaard
Omar Bohoudi
Shyama Tetar
Marjan A. Admiraal
Tezontl S. Rosario
Anne M.E. Bruynzeel

Cureus. 2018; 10: 1–11

Abstract

Magnetic resonance-guided radiation therapy (MRgRT) not only allows for superior soft-tissue setup and online MR-guidance during delivery but also for inter-fractional plan re-optimization or adaptation. This plan adaptation involves repeat MR imaging, organs at risk (OARs) re-contouring, plan prediction (i.e., recalculating the baseline plan on the anatomy of that moment), plan re-optimization, and plan quality assurance. In contrast, intrafractional plan adaptation cannot be simply performed by pausing delivery at any given moment, adjusting contours, and re-optimization because of the complex and composite nature of deformable dose accumulation. To overcome this limitation, we applied a practical workaround by partitioning treatment fractions, each with half the original fraction dose. In between successive deliveries, the patient remained in the treatment position and all steps of the initial plan adaptation were repeated. Thus, this second re-optimization served as an intrafractional plan adaptation at 50% of the total delivery. The practical feasibility of this partitioning approach was evaluated in a patient treated with MRgRT for locally advanced pancreatic cancer (LAPC).

MRgRT was delivered in 40Gy in 10 fractions, with two fractions scheduled successively on each treatment day. The contoured gross tumor volume (GTV) was expanded by 3 mm, excluding parts of the OARs within this expansion to derive the planning target volume for daily re-optimization (PTV_{OPT}). The baseline GTV $V_{95\%}$ achieved in this patient was 80.0% to adhere to the high-dose constraints for the duodenum, stomach, and bowel (V_{33Gy} <1 cc and V_{36Gy} <0.1 cc). Treatment was performed on the MRIdian (ViewRay Inc, Mountain View, USA) using video-assisted breath-hold in shallow inspiration. The dual plan adaptation resulted, for each partitioned fraction, in the generation of $PLAN_{PREDICTED1}$, $PLAN_{RE\text{-}OPTIMIZED1}$

(interfractional adaptation), $PLAN_{PREDICTED2}$, and $PLAN_{RE\text{-}OPTIMIZED2}$ (intrafractional adaptation). An offline analysis was performed to evaluate the benefit of inter-fractional versus intrafractional plan adaptation with respect to GTV coverage and high-dose OARs sparing for all five partitioned fractions.

Interfractional changes in adjacent OARs were substantially larger than intrafractional changes. Mean GTV $V_{95\%}$ was 76.8 ± 1.8% ($PLAN_{PREDICTED1}$), 83.4 ± 5.7% ($PLANRE\text{-}OPTIMIZED1$), 82.5 ± 4.3% ($PLAN_{PREDICTED2}$), and 84.4 ± 4.4% ($PLAN_{RE\text{-}OPTIMIZED2}$). Both plan re-optimizations appeared important for correcting the inappropriately high duodenal V_{33Gy} values of 3.6 cc ($PLAN_{PREDICTED1}$) and 3.9 cc ($PLAN_{PREDICTED2}$) to 0.2 cc for both re-optimizations. To a smaller extent, this improvement was also observed for V_{25Gy} values. For the stomach, bowel, and all other OARs, high and intermediate doses were well below preset constraints, even without re-optimization. The mean delivery time of each daily treatment was 90 minutes.

This study presents the clinical application of combined inter-fractional and intrafractional plan adaptation during MRgRT for LAPC using fraction partitioning with successive re-optimization. Whereas, in this study, interfractional plan adaptation appeared to benefit both GTV coverage and OARs sparing, intrafractional adaptation was particularly useful for high-dose OARs sparing. Although all necessary steps lead to a prolonged treatment duration, this may be applied in selected cases where high doses to adjacent OARs are regarded as critical.

Introduction

Magnetic resonance-guided radiation therapy (MRgRT) has become a clinical reality with a number of centers reporting feasibility and preliminary clinical results[1–3]. In addition to superior soft-tissue setup and online MR-guidance during delivery, an attractive option with MRgRT could be to perform a daily plan re-optimization, or adaptation, prior to the delivery of each fraction. At our center, respiratory-gated MRgRT is delivered during subsequent breath-hold spells in combination with real-time MR guidance of the gross tumor volume (GTV). This approach allows for ensuring adequate target coverage, even with the use of minimal GTV to planning target volume (PTV) margins. Interfractional plan adaptation is routinely performed for each patient and each fraction at our center. Several recent publications and presentations have highlighted the relevance of interfractional plan adaptation, for instance, for prostate, adrenal, and pancreatic tumors[1,2,4,5]. In contrast, however, the extent of intrafractional changes in the position and volume of surrounding organs at risk (OARs) during radiation delivery, and thereby the relevance of intrafractional plan adaptation, is largely unknown. At our center, MRgRT is delivered in the form of intensity modulated radiotherapy (IMRT) using the MRIdian system (ViewRay Inc, Mountain View, USA), resulting in highly conformal treatment plans. Using the current software, however, intrafractional plan adaptation cannot be simply performed by pausing delivery at any given moment, adjusting contours, and Reoptimization because of the complex and composite nature of deformable dose accumulation.

To overcome this limitation, we developed and investigated a practical workaround by partitioning treatment fractions at a fixed interval, each with half of the original fraction dose. In between successive deliveries, repeat MR imaging (MRI), OAR re-

contouring, and plan re-optimization were performed with the patient remaining in the treatment position. Thus, this second re-optimization serves as an intrafractional plan adaptation at 50% of the total radiation delivery. The practical feasibility of this partitioning approach was evaluated in a patient treated with stereotactic MR-guided radiation therapy (SMART) for locally advanced pancreatic cancer (LAPC).

Case Presentation

The patient is a 66-year-old female, who was diagnosed with LAPC in March 2017 and was treated with Folfirinox. Chemotherapy was discontinued after three courses as a result of severe toxicity, at which time, diagnostic computed tomography (CT) scans showed a stable disease. She was referred by her medical oncologist for stereotactic radiotherapy in the form of MRgRT. After performing a simulation CT and MR scan on MRIdian, both in shallow inspiration breath-hold, contouring of the GTV and relevant OARs was performed in collaboration with a radiologist specialized in gastrointestinal radiology, No separate margins for the clinical target volume (CTV) were applied (GTV=CTV), and the PTV for daily re-optimization (PTV_{OPT}) was defined by adding an isotropic 3 mm margin to the GTV, excluding parts of OARs within this expansion. The standard fractionation scheme for MRgRT in LAPC at our center is 40Gy in five fractions, in three fractions per week. In this case, the 40Gy was prescribed in 10 fractions, with two fractions scheduled immediately successive on each treatment day. The generation of a robust baseline treatment plan (BL) (Figure 1), also for use in daily adaptation, was performed as previously described[1].

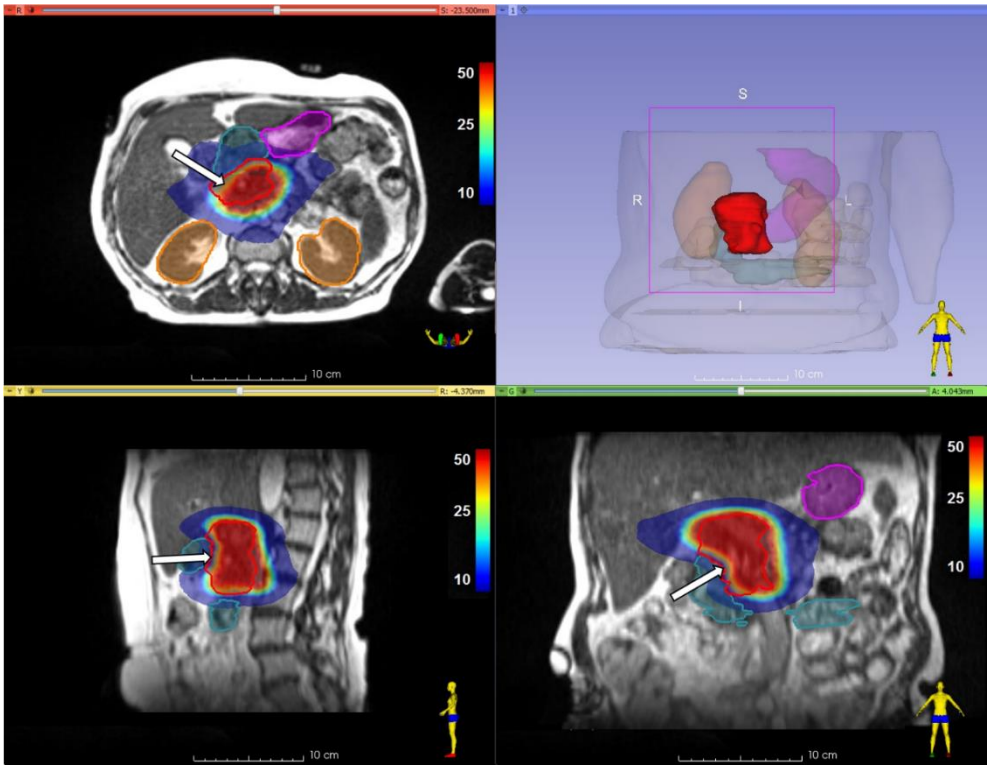

***Figure 1**. Baseline IMRT plan with dose (Gy) in color wash. Relative PTVOPT underdosing can be seen at the border between the PTVOPT and the duodenum (arrows), in order to adhere to high-dose OARs constraints. PTVOPT = red contour, Duodenum = cyan color wash, Stomach = purple color wash, Kidneys = orange color wash.*

The patient was positioned with one arm up using an MR-compatible positioning board. A new high-resolution MR scan in shallow inspiration was acquired and aligned with the simulation GTV. After deformable contour propagation of the OARs from the BL plan, the OARs contours were manually adjusted in the first 3 cm around the PTVOPT. Subsequently, the BL plan was recalculated on the anatomy of the moment (PLANPREDICTED1) and re-optimized using the same number and direction of beams (PLANRE-OPTIMIZED1; plan A). This approach of maintaining the original beam setup increases the speed of plan adaptation, facilitates patient-specific QA, and can be performed within minutes, with the patient remaining in treatment position. After patient-specific plan quality assurance (QA), radiation

delivery (4Gy) was performed under patient-controlled breath-hold conditions with video feedback.

Immediately after the completion of plan A, the high-resolution MR imaging in breath-hold was repeated, with the patient remaining in the treatment position. After re-alignment on the GTV, because of a different breath-hold, deformed OARs were again manually adjusted, if needed. This time, however, instead of the BL plan, plan A was used as a primary imaging set. This allows for faster recontouring because only intrafractional OARs changes needed to be adjusted. Calculation of plan A on the repeated MR scan ($PLAN_{PREDICTED2}$) was again followed by plan re-optimization ($PLAN_{RE\text{-}OPTIMIZED2}$; plan B) and QA, which was subsequently delivered (4Gy) using the same breath-hold conditions. The average total duration of delivering such a partitioned, twice re-optimized treatment fraction was approximately 90 minutes in comparison to 75 minutes for our standard single re-optimized treatment.

The extent of changes in the OARs surrounding the PTV between the simulation scan and the pretreatment scan (interfractional) was substantially larger than in between both partitioned fractions, shown for the sagittal planes in Figure 2 (corresponding axial and coronal planes in Figures 6-7, Appendix).

An offline analysis was performed to evaluate the benefit of interfractional ($PLAN_{PREDICTED1}$ vs. $PLAN_{RE\text{-}OPTIMIZED1}$) versus intrafractional plan adaptation ($PLAN_{PREDICTED2}$ vs. $PLAN_{RE\text{-}OPTIMIZED2}$) with respect to target coverage and high-dose

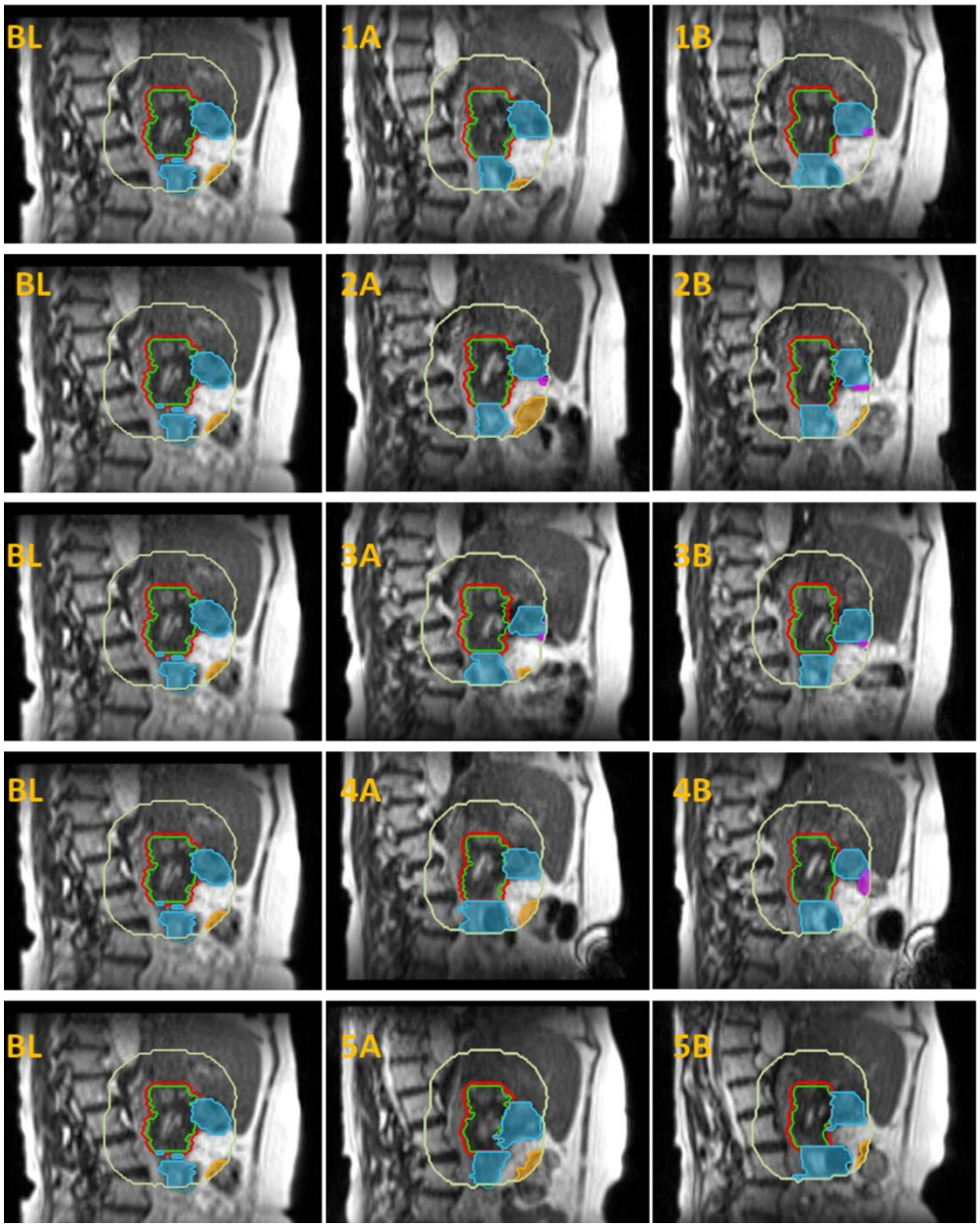

Figure 2. *Anatomical changes in the position of relevant OARs in the first 3 cm outside the* PTV_{OPT}*, shown in a sagittal plane through the center of the GTV. The simulation MR is shown in the left panels. The middle panels show the anatomy prior to the delivery of plan A (fractions 1A-5A, respectively). The right panels illustrate the OARs position after the delivery of 4Gy; prior to the delivery of plan B (fractions 1B-5B, respectively). GTV = Green contour,* PTV_{OPT} *= red contour, Duodenum = cyan color wash, Stomach = purple color wash, Bowel = orange color wash, 3 cm Ring = light yellow contour.*

OARs sparing for all five partitioned fractions. In comparison to the baseline GTV V95% of 80.0%, the average GTV V95% in the partitioned plans was 76.8 ± 1.8% ($PLAN_{PREDICTED1}$), 83.4 ± 5.7% ($PLAN_{RE\text{-}OPTIMIZED1}$), 82.5 ± 4.3% ($PLAN_{PREDICTED2}$), and 84.4 ± 4.4% ($PLAN_{RE\text{-}OPTIMIZED2}$) (Figure 3).

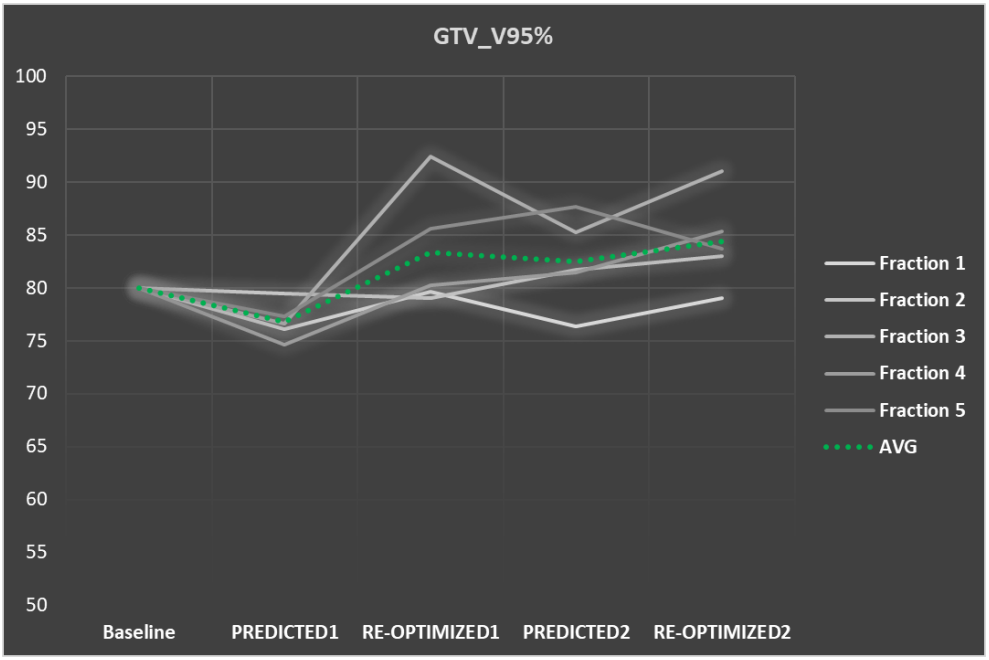

Figure 3. *GTV coverage ($V_{95\%}$) for the five fractions. Target coverage in $PLAN_{RE\text{-}OPTIMIZED1}$ is clearly improved in comparison to $PLAN_{PREDICTED1}$. After repeat setup on the GTV, the second plan adaptation had a limited effect on target coverage. Average coverage is seen as a green dotted line.*

Both plan re-optimizations appeared important for substantially restricting the duodenal high doses (V36 Gy/V33 Gy). For each fraction, duodenal V 36 Gy was <0.1 cc after the first and second re-optimizations (Figure 4, left panel). As per institutional protocol, the duodenal V33 Gy should be ≤1 cc. Inappropriately high mean V33 Gy values of 3.6 cc ($PLAN_{PREDICTED1}$) and 3.9 cc ($PLAN_{PREDICTED2}$) were corrected to a mean of 0.2 cc for both re-optimizations (Figure 4, right panel). To a lesser extent, this improvement was also observed for V25 Gy values (data not shown). For the stomach and bowel, as well as other OARs at a bigger distance

(kidneys, liver, and spinal cord), all high and intermediate doses were well below preset constraints, even without re-optimization.

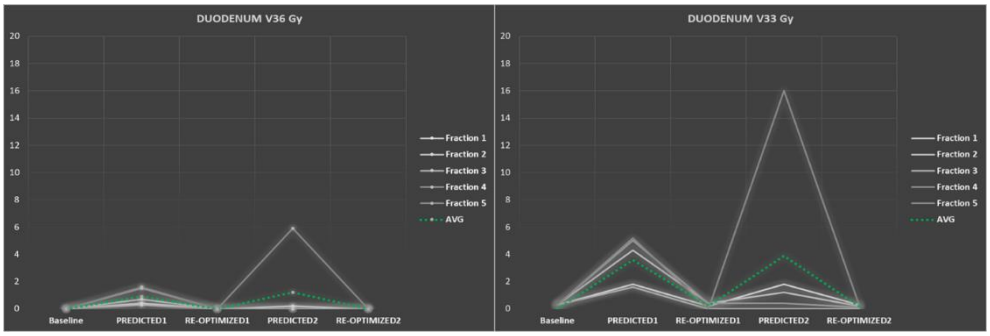

Figure 4. *Results of inter- and intrafractional plan adaptation for high doses to the duodenum. Both re-optimization steps clearly correct any high duodenal V36 Gy and V33 Gy for all fractions. Green dotted line indicates average for all fractions.*

Discussion

With the implementation of MRgRT, real-time plan adaptation has become a clinical reality, which has been reported to increase target coverage and/or OARs sparing for various indications. The extent of intrafractional changes in relevant OARs during radiation delivery and, consequently, the need for intrafractional plan adaptation, is currently unknown. This case report describes a first attempt to quantify the relative importance of inter-fractional and intrafractional plan adaptation. Because our current software version does not allow for intrafractional plan adaptation at any given moment due to the absence of dose accumulation, a workaround using fixed fraction partitioning is needed to perform intrafractional plan adaptation, in this case, at 50% of total fraction delivery. In this simplified manner, dose accumulation is feasible by prescribing an adequate GTV coverage and adhering to high-dose OARs constraints for each partitioned fraction.

Our case underscores the importance of inter-fractional plan adaptation, visualized by substantial changes in OARs between the simulation scan and the pre-fractional MR scans, as well as by the increase in GTV coverage and the decrease in high doses to OARs after the first plan re-optimization. This observed relevance of inter-fractional plan adaptation may be greater because of the use of small (3 mm) GTV to PTV margins, steep dose gradients, generating a new PTV_{OPT} for each fraction, and, certainly, the relatively lengthy delivery procedure. Our preliminary results regarding intrafractional plan adaptation are less clear-cut. Intrafractional plan adaptation had only a modest effect on target coverage, however, it did decrease high-doses to the duodenum in several fractions. This could be expected after repeat setup on the GTV with the patient remaining in the treatment position. Furthermore, the first re-optimized plan was taken as a reference for the second re-optimization, which reflects the anatomy of that day better than the BL plan. A single fraction showed an extreme benefit of the second re-optimization, which was due to expansion and displacement of the duodenum during the delivery of plan A. A 3D image of the PTV_{OPT} and the duodenum illustrates this intrafractional change better than the single slice coronal view (Figure 5). Reassuringly, such anatomical changes did not occur systematically, and the cumulative dosimetric consequences will be limited. This finding does, however, illustrate the potential danger of re-optimizing followed by re-normalizing to the limit of critical OARs constraints since such intrafractional changes may occur. Some limitations of our analysis have to be mentioned here. Because simulation, as well as all partitioned fractions, have been performed during patient-controlled shallow-inspiration breath-hold, small differences in respiratory phase may exist both in the analysis of inter-fractional and intrafractional plan adaptation. In addition, small contouring variations may influence particularly the high-dose OAR results for all parts of this analysis. We have tried to minimize the latter by having the same specialized radiation oncologist

performing the recontouring for all fractions. Finally, the results may be different for other approaches of re-optimization, for example, in cases where a new plan with different beam numbers and directions is generated for each adaptation.

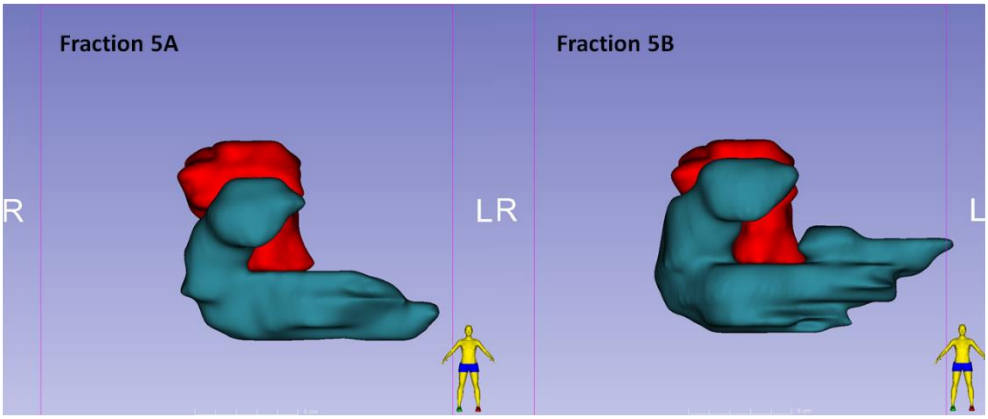

Figure 5. *3D image of the PTVOPT (red volume) and duodenum (cyan volume) for fractions A and B of fraction 5, showing a significant change in the anatomy. This intrafractional changes resulted in a high dose to the duodenum in the* $PLAN_{PREDICTED2}$*, which was subsequently corrected by the second re-optimization.*

Conclusions

To the best of our knowledge, this case presentation is the first clinical application of combined inter-fraction and intrafraction plan adaptation during MRgRT. In order to achieve this, we have used fraction partitioning with successive re-optimization. Whereas inter-fractional plan adaptation appears to benefit both GTV coverage and OARs sparing, intrafraction plan adaptation was found to be particularly useful for OARs sparing in this specific case we described. Although all necessary steps result in a prolonged treatment duration, this may be used in selected cases where the high doses to adjacent OARs are regarded to be critical. Intrafractional plan adaptation will benefit from future three-dimensional (3D) real-time MR imaging, as well as from software improvements to allow faster re-optimization and dose-accumulation.

References

1. Bohoudi, O. *et al.* Fast and robust online adaptive planning in stereotactic MR-guided adaptive radiation therapy (SMART) for pancreatic cancer. *Radiother. Oncol.* **125**, 439–444 (2017).

2. Henke, L. *et al.* Phase I trial of stereotactic MR-guided online adaptive radiation therapy (SMART) for the treatment of oligometastatic or unresectable primary malignancies of the abdomen. *Radiother. Oncol.* **126**, 519–526 (2018).

3. Lamb, J. *et al.* Online Adaptive Radiation Therapy: Implementation of a New Process of Care. *Cureus* **9**, e1618 (2017).

4. Bruynzeel, A. *et al.* Stereotactic MR-Guided Adaptive Radiation Therapy (SMART) for Locally Advanced Pancreatic Tumors. *Int. J. Radiat. Oncol.* **99**, S125 (2017).

5. Lagerwaard, F. *et al.* Stereotactic MR-Guided Adaptive Radiation Therapy (SMART) for Prostate Cancer. *Int. J. Radiat. Oncol.* **99**, E681–E682 (2017).

Supplementary materials

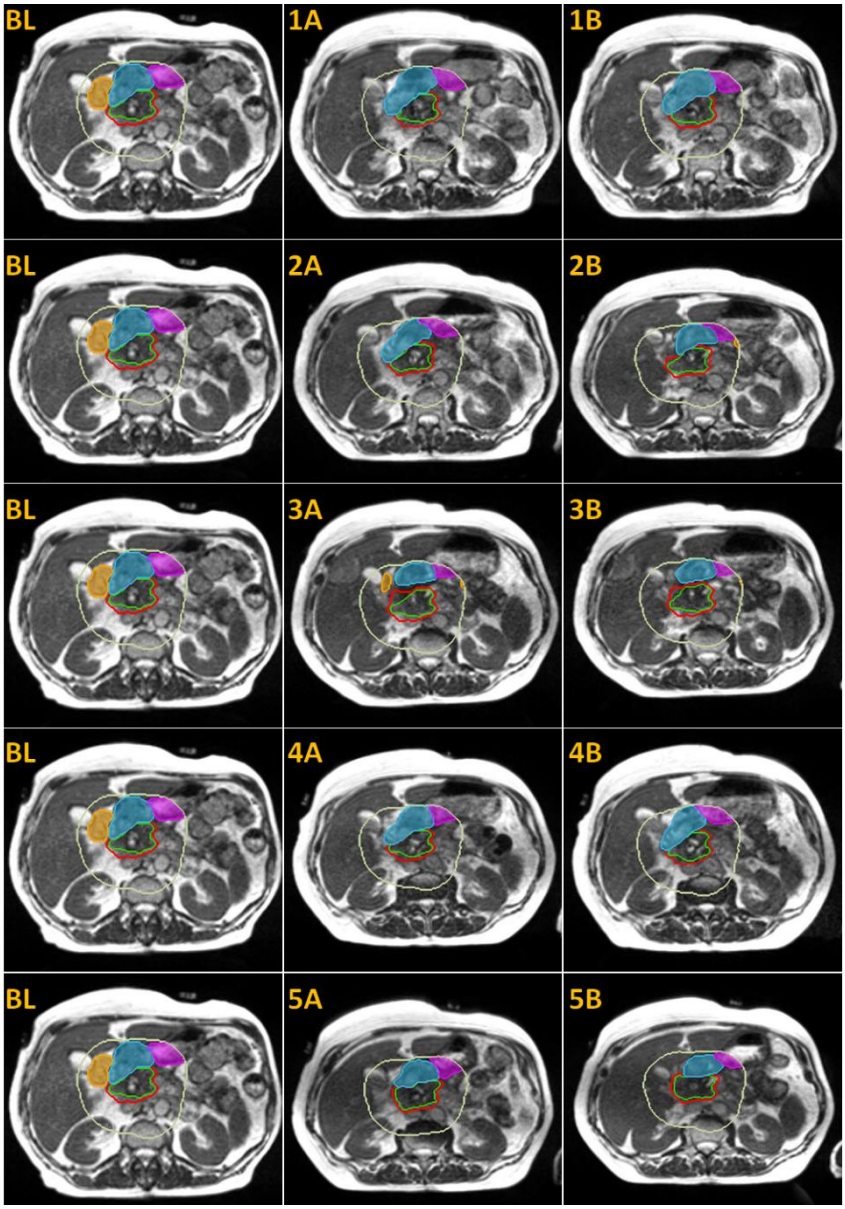

Supplementary Figure 6. *Anatomical changes in the positions of relevant OARs in the first 3cm outside PTV$_{OPT}$, shown in an axial plane through the center of the GTV. The simulation MR is shown in the left panels. The middle panels show the anatomy prior to the delivery of plan A (fractions 1A-5A, respectively). The right panels illustrate the OARs position after the delivery of 4Gy; prior to the delivery of plan B (fractions 1B-5B, respectively). GTV = green contour, PTV$_{OPT}$ = red contour, Duodenum = cyan color wash, Stomach = purple color wash, Bowel = orange color wash, 3 cm ring = light yellow contour.*

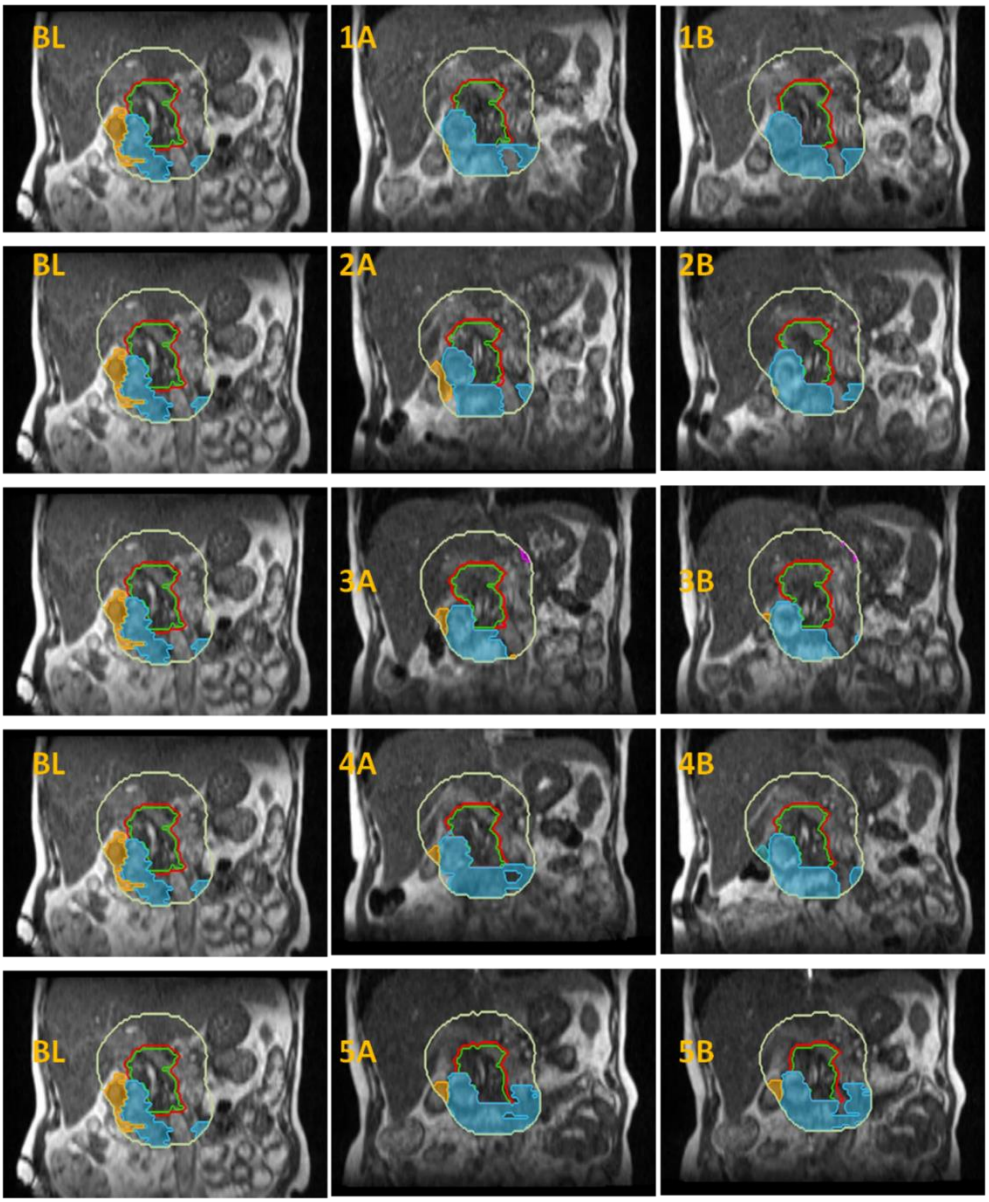

Supplementary Figure 7. *Anatomical changes in the position of relevant OARs in the first 3 cm outside the PTVOPT, shown in a coronal plane through the center of the GTV. The simulation MR is shown in the left panels. The middle panels show the anatomy before the delivery of plan A (fractions 1A-5A, respectively). The right panels illustrate the OARs position after the delivery of 4Gy; prior to the delivery of plan B (fractions 1B-5B, respectively). GTV = green contour, PTVOPT = red contour, Duodenum = cyan color wash, Stomach = purple color wash, Bowel orange color wash, 3 cm ring = light yellow contour.*

Chapter 8

End-to-end empirical validation of dose accumulation in MRI-guided adaptive radiotherapy for prostate cancer using an anthropomorphic deformable pelvis phantom

Omar Bohoudi
Frank J. Lagerwaard
Anna M.E Bruynzeel
Nina I. Niebuhr
Wibke Johnen
Suresh Senan
Ben J. Slotman
Asja Pfaffenberger
Miguel A. Palacios

Radiotherapy and Oncology. 2019; 141: 200-207.

Abstract

Background and Purpose: This work evaluates the accuracy of deformable dose accumulation for organs at risk (OAR) in MR-guided prostate SBRT using an anthropomorphic deformable phantom.

Material and Methods: Six MR-guided prostate SBRT treatment courses were simulated using volumetric OAR (bladder and rectum) information derived from actual patient data. Deformed OAR contours, geometrical landmarks and GafChromic EBT3 film strips (1.25 × 2.0 cm^2) placed at the surface of the OARs were used to validate DIR-based dose accumulation in MRgRT. Two DIR methods were applied: an intensity-based deformation (IB-D) applied to the whole image, and a contour-based deformation (CB-D), resulting in a separate deformation and dose accumulation for each OAR. Dosimetric accuracy was evaluated by quantifying the dose differences, and performing a gamma-index analysis between measured and DIR-derived accumulated dose for both OARs. Geometrical accuracy was assessed by measuring the Dice similarity coefficient (DSC), Hausdorff distance (HDD) and residual distance error (RDE) for all markers at each fraction.

Results: CB-D resulted in an average dose deviation from film measurements for rectum and bladder surfaces of 0.6% and 0.3%, respectively. IB-D led to worse results resulting in an overall average dose accumulation inaccuracy of 7.2% and 2.5% for rectum and bladder. CB-D also showed a higher geometrical accuracy than IB-D with significantly higher DSC values and lower RDE and HDD deviations.

Conclusions: Empirical validation of dose accumulation in MR-guided SBRT for prostate cancer obtained a good agreement with reference film measurements when using a contour-based DIR approach.

Introduction

In-room image-guidance has become a cornerstone in radiotherapy, both for assessing inter-fractional anatomical changes and performing adaptive radiotherapy (ART)[1,2]. The position and shape of target and critical organs may vary during the course of radiotherapy and, in the absence of online plan adaptation, can lead to differences between the planned and the actual delivered dose distribution[3,4]. Recently, the potential of MR-guided radiotherapy (MRgRT) for better visualization of inter-fractional anatomical changes and online plan adaptation in prostate cancer has been appraised[5,6]. Besides online plan adaptation, knowledge of the inter-fractional changes that have taken place has also drawn interest towards the evaluation of the accumulated dose received by the target and critical organs during the course of the treatment[7–9].

For an accurate determination of the cumulative total dose delivered to the target volume and organs at risk (OAR), dose accumulation over all fractions is required. Deformable image registration (DIR) allows voxel-to-voxel mapping between a baseline reference image (MRI or CT) and subsequent images of deformed tissues. Application of the deformation map to the dose distribution enables dose warping from all fractions to the reference image and estimation of the total received dose. For this reason, DIR-based dose accumulation methods have been developed and explored during the last years[10–13]. However, performance evaluation and estimation of the uncertainty in the accumulated dose is essential prior to clinical implementation[7,14], especially in the regions of high dose gradients, where small errors in the deformation map can result in significant changes in the accumulated dose. This might be the case, for instance, with the dose received by the rectum and bladder across all fractions in prostate radiotherapy.

Anthropomorphic phantoms are valuable tools for the performance evaluation of DIR-based dose accumulation because they can be used for evaluating the entire process, including image acquisition with possible distortion and noise, data transfer and import, image registration and dose delivery[14]. The phantom needs to represent the anatomy of a patient, be equipped with realistic organ densities visually distinguishable by the image modality being employed and finally, be able to accommodate suitable dosimeters and geometrical landmarks in clinically relevant locations. These phantoms should also offer controllable motion and deformation, be able to reproduce different clinical situations and suitable to perform reference measurements for DIR evaluation[14].

In the past, validations of dose accumulation using CBCT images of (numerical) phantoms were performed[15–21], but thus far no empirical validation of dose accumulation for online adaptive MRgRT has been reported. MRgRT introduces possible sources of error such as spatial distortion of MR images, use of deformed electron density for dose calculation and variability in intensity levels of MR images. An end-to-end test of dose accumulation performance under these conditions is essential prior to clinical use.

Several groups have reported on DIR-based dose accumulation in actual patients[16,22–25], but there is a lack of studies in the literature validating DIR-based dose accumulation over a radiotherapy treatment course involving realistic clinical situations. In this study, such a validation for dose accumulation in MRgRT is presented. For this purpose, an anthropomorphic, deformable and multimodal phantom of the male pelvis was used[26] to simulate actual clinical situations derived from previously treated patients. Six stereotactic body radiotherapy (SBRT) treatment courses for prostate cancer were simulated using all five fractions, and the

accuracy of the final accumulated dose in critical organs assessed using GafChromic EBT3 film dosimetry.

Material and Methods

Phantom specification

The ADAM-pelvis phantom, an Anthropomorphic, Deformable And Multimodal phantom developed in the German Cancer Research Center (DKFZ), was used in this study (Figure 1a). The construction and specification of this phantom is described in greater detail by Niebuhr et al.[26–28]. Briefly, in the engineering of this pelvis phantom, agarose gels loaded with sodium fluoride and a Gadolinium-based contrast agent were used for multimodal simulation of soft tissue, whereas vegetable oils were used to mimic adipose tissue. Simulation of pelvic bones was realized by applying gypsum bandage and Vaseline to a 3D printed hollow bone case, resulting in both a fatty bone marrow signal in MRI and high- and low attenuation areas in CT scans. The prostate-, bladder- and rectum surrogates were cast using 3D printed molds generated from real patient-data. These organ surrogates were manufactured of silicone to allow controllable and reproducible organ motion and deformation, enabling simulation of various realistic MR-guided adaptive radiation delivery scenarios. Imaging marker points and pockets for dosimeters were implemented into the surfaces of these organ surrogates to serve as a geometric and dosimetric reference in the evaluation of geometric DIR and dose accumulation accuracy. Dosimetric evaluation was performed using GafChromic EBT3 films, which has been reported to be suitable and shown high accuracy in the presence of a 0.35 T magnetic field[29]. Custom-fit film strips (1.25 × 2.0 cm^2) were inserted in seven bladder

and two rectum surface pockets (Figure. 1b and c) to evaluate the dose to critical structures.

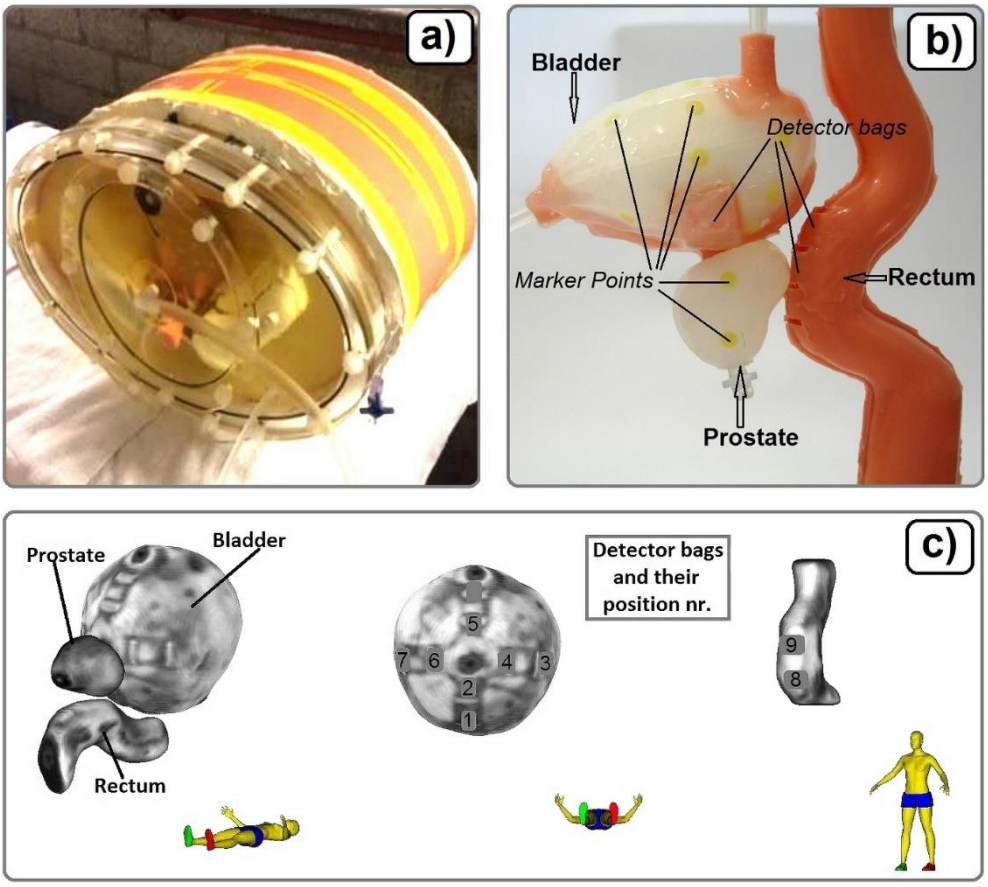

Figure 1. *Illustration of the ADAM deformable pelvic phantom (a), and corresponding image of organ surrogates including imaging marker points and pockets for dosimeters (b). The lower panel (c) shows an MRI surface plot of the bladder, prostate and rectum of the phantom. The positions of the detector bags for film strips are numbered from 1 to 9.*

MRgRT simulation

Six patients with prostate cancer who previously underwent MRgRT treatments with online plan adaption, delivered in five fractions on the MRIdian system (ViewRay Inc., Mountain View, USA), were simulated on this phantom (TX_{PAT}). The bladder volumes and consistency of the rectum filling (air or "substance", simulated

with sponge (water/dry)) were varied before each simulated fraction, based on available patient imaging data to create realistic organ deformation scenarios. At each fraction, an MR scan (TR/TE: 3.37 ms/1.45 ms; FA: 60°) with 1.5 mm × 1.5 mm × 1.5 mm resolution was performed on the phantom. Dose prescriptions delivered for the actual treatment (5 × 7.25 Gy) were rescaled to 5 × 2 Gy in order to remain in the best dose range performance of GafChromic EBT3 films (0.2–10 Gy). Baseline treatment plans were generated using IMRT step-and-shoot with 5 beam groups where each beam group had three equidistant beams corresponding with three ^{60}Co sources on the gantry. Dose calculation at each fraction was performed with a Monte-Carlo algorithm (statistical uncertainty of 1%) with a grid resolution of 0.3 cm × 0.3 cm × 0.3 cm using the deformed electron density map from the simulation CT scan.

The same procedures as in the clinical setting were followed for daily online plan adaptation for each TX_{PAT} (see also Fig. 1, Supplementary material): (1) A repeat MR scan for each fraction, followed by 3D alignment of the baseline and repeat MR-scan based on the CTV; (2) Automatic deformation of OAR contours; and (3) Plan re-optimization using the same beam numbers, beam directions and optimization objectives.

For each TX_{PAT} the EBT3 film strips remained in the same pockets indicated in Figure 1 keeping identical orientation during all 5 delivered fractions, in order to measure the cumulative delivered dose and to serve as benchmark for assessing the accuracy DIR-based dose accumulation. At the end of each TX_{PAT} (after 5 fractions) the irradiated EBT3 film strips were taken out and stored in light-shielding bags. After 24 h each filmstrip was digitized according to the procedure described by Barten et al.[29].

DIR algorithm and dose accumulation

For each TX_{PAT}, the acquired 3D MR scan, contours and dose distribution were imported into the publicly available open-source software 3DSlicer (v4.10.0)[30]. Elastix, an intensity-based DIR toolkit available through the SlicerElastix extension, was used for voxel-to-voxel mapping between the reference image (MRI fraction 1; MR_{REF}) and subsequent images (MR fraction 2–5; MR_{FR2-5})[31,32]. DIR parameters used in this study were a normalized mutual information similarity metric with a B-spline parameterized transformation. Furthermore, a three-level multiresolution registration scheme was used with image resolution and grid spacing down sampled by a factor of 2 at each multiresolution level, and final B-spline grid spacing of 10 mm. Gradient descent optimization was used with up to 500 iterations at each multiresolution level.

Two different DIR approaches were assessed for each TX_{PAT} (Figure 2): (1) full image DIR approach (IB-D), were a voxel-to-voxel mapping between the ***entire*** MR_{REF} and the ***entire*** MR_{FR2} to MR_{FR5} was established, resulting in 4 consecutive deformation vector fields for each subsequent fraction of TX_{PAT} (DVF^{FX2-5}); (2) contour–guided DIR approach (CB-D), were a separate bladder- and rectum-specific voxel-to-voxel mapping is established between MR_{REF} and MR_{FR2-5}, resulting in 4 consecutive DVF for the bladder ($DVF_{(bladder)}^{FR2-5}$) and 4 consecutive DVF for the rectum ($DVF_{(rectum)}^{FX2-5}$). With the CB-D approach the DIR is thus constrained to the volume encompassed by the respective OAR contour, i.e. bladder or rectum. MR images used as input for both IB-D and CB-D approaches were previously registered to the CTV of the pre-treatment image during the online adaptive workflow (see also, Supplementary material and[5,33]). The DVF^{FX2-5} from the IB-D approach were applied to the dose distributions of fractions 2, 3, 4 and 5 respectively, in order to map the dose distributions at each fraction to the dose distribution of fraction 1 (reference image,

MR_{REF}). Finally, the warped dose distributions were summed up to obtain the total accumulated dose for each TX_{PAT}. For the second DIR approach CB-D, a bladder- and rectum-specific accumulated dose was obtained using the $DVF_{(rectum/bladder)}^{FX2-5}$ after following the same procedure for each organ separately.

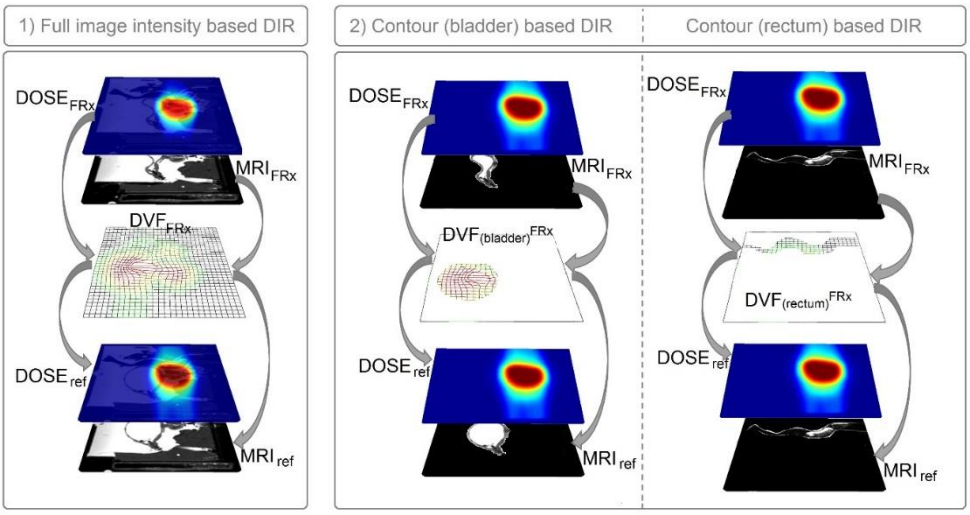

Figure 2. *Schematic illustration demonstrating the workflow for both DIR approaches.*

Dosimetric and geometric evaluation of DIR

To evaluate the DIR-based dose accumulation accuracy, the exact location of all EBT3 films strips on MR_{REF} were identified and marked with a ROI in Slicer for each treatment simulation (see also Figure 2, suppl. material). The accumulated dose distribution within these ROIs after applying both methods, IB-D and CB-D, were extracted and exported from Slicer in the same format (tiff) as the digitalized EBT3 filmstrips. A pixel-by-pixel analysis of the calibrated filmstrips (dose readout) and the extracted ROIs with the accumulated doses was performed using OmniPo-I'mRT v.1.7 software (IBA Dosimetry, Schwarzenbruck) (Figure 3, supplementary material). A correction for the dose contribution from the simulation CT carried out at baseline was performed by adding a constant absolute dose value to each pixel in

the ROIs containing the accumulated dose distribution (see also Supplementary material). Relative dose difference calculations across all pixels in the films ($\Delta DOSE_{(\%)} = 100\% * (Dose_{(EBT3)} / DOSE_{(DIR)})$) were performed to evaluate the dosimetric accuracy of both DIR strategies, IB-D and CB-D. In addition, the accumulated spatial dose distributions of TX_{PAT1-6} were further evaluated using the gamma index (3%/2 mm) for all film strips[34].

Quantitative evaluation of the geometric DIR accuracy was performed to complement the dose accumulation analysis. Two similarity metrics were used to quantify the organ deformation before and after DIR: Dice similarity coefficient (DSC)[35] and Hausdorff distance (HDD)[36]. The bladder and rectum contour volumes for all TX_{PAT1-6} PRE-DIR, and after IB-D and CB-D strategies were evaluated and compared to the reference contours (MR_{FX1}). Sixteen marker points available on the surface of the bladder and rectum were identified on each MRI to generate a reference position for each fraction. A total of 56 and 8 marker data points were generated per TXPAT over the 4 fractions for the bladder and rectum, respectively. The marker points defined on MR_{FR2-5} were propagated to MR_{REF} using the relevant DVFs. The geometric accuracy of DIR was evaluated by calculating the Euclidean distance (residual distance error, RDE) between the propagated and reference marker point locations.

Statistical analysis comparing both DIR approaches was performed using the Wilcoxon Signed-Rank test (IBM® SPSS Statistics v20, Armonk, NY, USA). A p-value <0.05 was considered to be statistically significant.

Results

Figure 3 shows a 3D representation of the simulated treatments and OAR inter-fractional changes in the anthropomorphic pelvis phantom. Variations in bladder and rectum volume were substantial reflecting different anatomical situations at each fraction. Figure 4 reports on the DSC, HDD and changes in bladder and rectum volume with respect to the MR_{REF} before applying DIR (PRE-DIR).

Figure 3. *An overview of 3D recreations of the prostate, rectum and bladder on the ADAM-pelvis phantom for all fractions of the six simulated SBRT prostate treatments (TX_{PAT1-6}). The MR anatomical scan of the ADAM-pelvis phantom is shown for the reference situation. Bladder at each fraction is depicted in green whereas the rectum is depicted in blue. Densities in rectum were variable according to the simulated clinical data. Baseline anatomy for the OAR is represented at each fraction with translucent structures to show inter-fractional anatomical changes.*

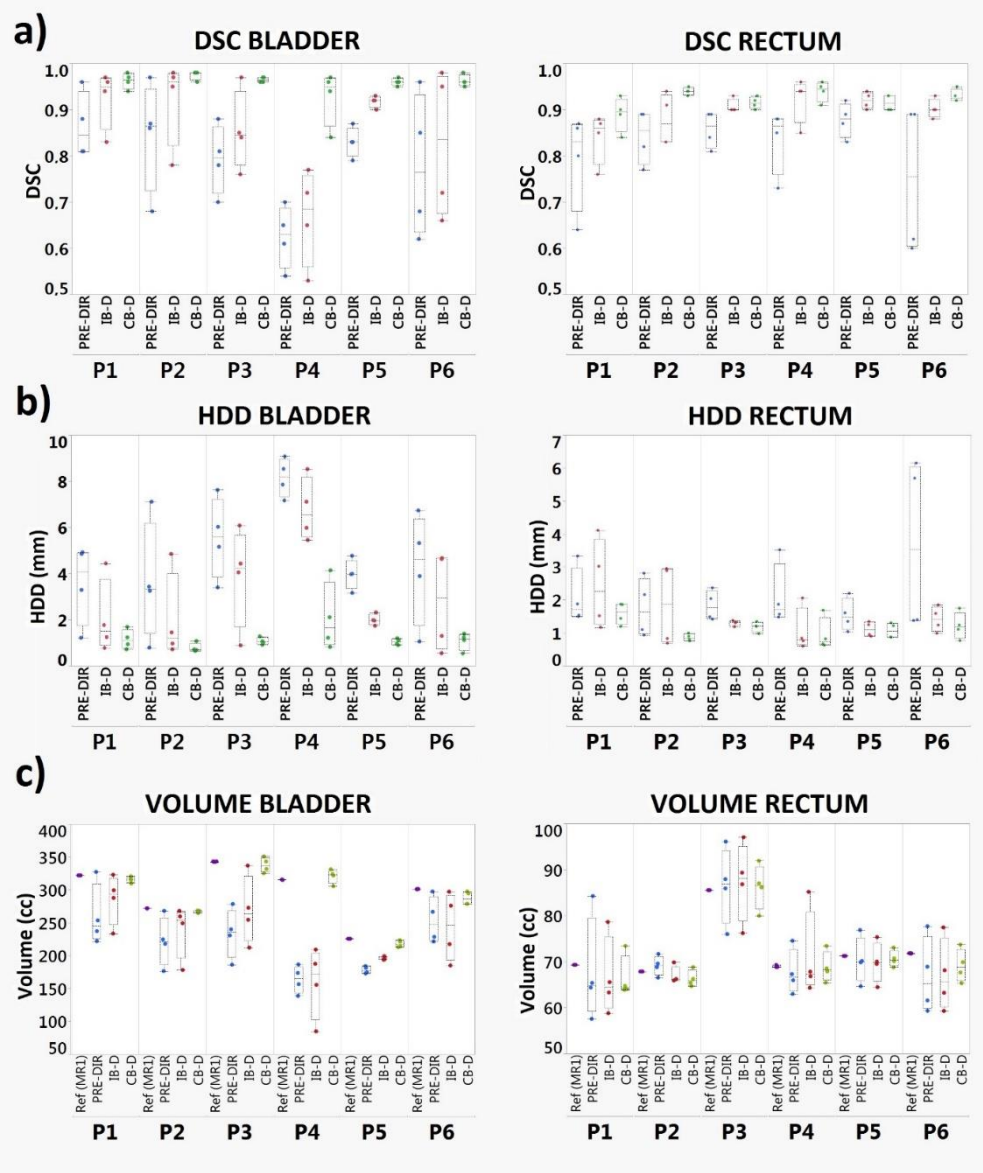

Figure 4. *The DSC, HDD and volumes of bladder and rectum changes with respect to* MR_{REF} *before (PRE-DIR) applying DIR and after IB-D and CB-D strategies.*

Dosimetric accuracy of DIR

Both IB-D and CB-D dose accumulation approaches were carried out for all TXPAT. A detailed overview of the $\Delta DOSE_{(\%)}$ for both IB-D and CB-D with respect to the

dose readout of the films located at the bladder- and rectum surfaces is shown in Table 1. An excellent agreement with the measured values was achieved by CB-D, whereas the IB-D approach resulted in large deviations for several patients. Overall the mean $\Delta DOSE_{(\%)}$ averaged over all pixels for all TXPAT showed a relative dose difference of 2.5% (SD = 8.7) and −0.6% (SD = 2.0) at the bladder surface, and 7.2% (SD = 10.9) and 0.3% (SD = 1.3) at the rectum surface for IB-D and CB-D, respectively. The higher correspondence of CB-D with the reference film measurements was significant for both bladder surface ($p = 0.024$) and rectum surface ($p = 0.033$). Analysis of gamma pass rates between the film dose readouts and the accumulated doses by IB-D and CB-D are also listed in Table 1. CB-D dose accumulation resulted in high gamma pass rates values for all TX_{PAT} whereas IB-D exhibited significant lower values and clearly underperformed for several TX_{PAT}.

Table 1: *Relative dose difference and gamma (3%/2mm) pass-rates for both dose accumulation methods with respect to the film dose readouts at the bladder- and rectum surface in TX_{PAT1} to TX_{PAT6}.*

		ΔDOSE (%)		**gamma pass rate % (γ<1) (3%/2mm)**	
		IB-DIR	CB-DIR	IB- DIR	CB-DIR
TX_{PAT1}	Bladder	1.3 ±1.2	-0.7 ±1.0	97.1	98.6
	Rectum	25.7 ±11.3	0.4 ±0.5	45.0	99.0
TX_{PAT2}	Bladder	0.9 ±5.9	-2.2 ±1.7	75.3	92.4
	Rectum	8.9 ±0.9	0.1 ±0.4	51.8	98.2
TX_{PAT3}	Bladder	-3.3 ±5.2	0.3 ±2.1	83.6	93.9
	Rectum	2.5 ±3.0	0.7 ±0.6	81.4	95.3
TX_{PAT4}	Bladder	6.7 ±6.6	-0.5 ±1.2	70.6	94.8
	Rectum	4.4 ±5.6	0.7 ±1.6	80.8	87.9
TX_{PAT5}	Bladder	2.0 ±6.4	-0.6 ±0.9	87.3	96.0
	Rectum	-3.0 ±1.1	-1.1 ±0.2	79.8	90.3
TX_{PAT6}	Bladder	7.3 ±15.1	-0.2 ±2.9	73.6	91.2
	Rectum	4.6 ±7.9	1.1 ±2.2	78.0	91.8

Geometric accuracy of DIR

Similar to the dosimetric results, CB-D turned out to be superior to IB-D and achieved a higher accuracy to represent the actual geometry at each fraction. The mean bladder DSC and HDD after IB-D registration over all $TX_{PAT1–6}$ was 0.85 (SD = 0.12) and 3.18 mm (SD = 2.27), respectively. CB-D resulted in an improved DIR registration for the bladder with DSC and HDD mean values of 0.96 (SD = 0.03) and 1.20 mm (SD = 0.70), respectively ($p < 0.001$, $p < 0.001$). Likewise, IB-D resulted in an inferior registration than CB-D for the rectum, with mean values of DSC and HDD of 0.89 (SD = 0.04) and 1.53 mm (SD = 0.86) vs 0.93 (SD = 0.03) and 1.15 mm (SD = 0.36) ($p < 0.001$, $p = 0.025$). The obtained bladder and rectum contour volumes for all $TX_{PAT1–6}$ after IB-D and CB-D registration in comparison to the reference contours (MR_{REF}) are shown in Figure 4c. The resulting contour volumes after CB-D showed a higher correspondence than IB-D with the reference contour volumes in all $TX_{PAT1–6}$ for both, bladder and rectum ($r^2 = 0.95$ vs 0.37 for bladder, $r^2 = 0.82$ vs 0.52 for rectum).

The mean RDE averaged over all bladder imaging marker points was 7.9 mm (SD = 10.6) and 3.3 mm (SD = 3.9) for IB-D and CB-D, respectively (see also Supplementary material). When using CB-D, only TX_{PAT4} led to a deviation larger than 3 mm for the markers located at the bladder surface, whereas all $TX_{PAT1–6}$ for IB-D showed a mean RDE ≥4 mm. For the rectum, the mean RDE was 5.7 mm (SD = 7.7) and 2.5 mm (SD = 2.5) for IB-D and CB-D, respectively. Only TX_{PAT1} and TX_{PAT2} exhibited a mean RDE >3 mm for the rectum imaging markers when using both, IB-D and CB-D approaches. Statistical analysis showed that CB-D exhibited a higher correspondence with the reference marker positions for the bladder ($p = 0.000$) as well as the rectum surface ($p = 0.005$) compared to IB-D.

Discussion

Parallel with the development of recent improvements for in-room image guidance, there has been a growing interest in DIR and dose accumulation for adaptive radiotherapy. Several groups have reported on DIR-based dose accumulation in actual patients[16,22–25], but there is a lack of studies in the literature validating DIR dose accumulation over a radiotherapy treatment course involving realistic clinical situations. This study provides such a validation using an anthropomorphic phantom of the human pelvic region to simulate a SBRT prostate cancer treatment course. Our results show an excellent agreement between the accumulated dose and the film measurements after delivery of 5 fractions at the surface of the OARs, i.e. bladder and rectum, especially when using the CB-D approach.

Some previous studies have reported on the accuracy of DIR algorithms for dose accumulation using different classes of deformable phantoms[19–21,37]. In contrast to the present study, none of those reports simulated an entire MRgRT treatment course using realistic deformations obtained from actual clinical patient data. The performance of such end-to-end tests is a critical component to ensure the accuracy of all steps involved in MRgRT and perform DIR-based dose accumulation. Usually, a single deformation was applied in those studies and the obtained degree of accuracy of the DIR-based dose accumulation was variable, with uncertainties ranging from 1.5 to 4.7%, but with outliers of up to 30%, and mean geometric uncertainties of 1.0–2.1 mm. Our results obtained with the CB-D strategy agreed with the measured doses, with an average deviation of −0.6% and 0.3% for bladder and rectal surfaces, respectively. In addition, the ability to verify the cumulative irradiated dose by means of film dosimetry allowed us to not only estimate the average uncertainty, but also to verify local dose distributions and dose gradients by the gamma index. High gamma pass-rates were obtained for all films

measurements with CB-D dose accumulation, whereas performance of IB-D was significantly worse. The mean geometric uncertainties assessed by the CB-D in our study were 3.3 mm and 2.5 mm for the bladder and rectum marker points. Overall, the AAPM recommends an overall DIR geometric accuracy of approximately 2–3 mm[14]. Our results point out that the CB-D method applied accurately predicts the accumulated dose in regions of high dose gradients for patients undergoing substantial deformations and tissue density changes. These results agree with those of Cazoulat et al.[17] who also found that a surface constrained DIR for bladder and rectum using numerical phantoms reduced the local difference between the reference and accumulated doses.

The agreement of the DIR-based accumulated dose with the reference measurements exhibits a correlation with the geometrical error after DIR. Figure 5 shows the average dose difference for all $TX_{PAT1–6}$ across all fractions plotted against the mean HDD and DSC after DIR. A larger HDD or lower DSC, reflecting a worse correspondence of reference and deformed contour was correlated with a larger average dose difference error. In general, we found that wen using CB-D, HDD distances <3 mm and DSC values >0.90 correlated with dosimetric errors of less than 3% for both, bladder and rectum surfaces. A similar pattern for prostate cancer patients was also found in the past[17]. The anatomical variations in a few SBRT fractions were more difficult to manage by the Elastix DIR algorithm which resulted in higher geometrical uncertainties for both approaches. TX_{PAT4} resulted in >3 mm average marker position deviation from the reference for the bladder surface, and TX_{PAT1-2} for the rectum surface. In the case of TX_{PAT4}, the reference image at baseline showed a full bladder whereas subsequent fractions exhibited a substantial bladder volume decrease, i.e. deformations larger than average were present.

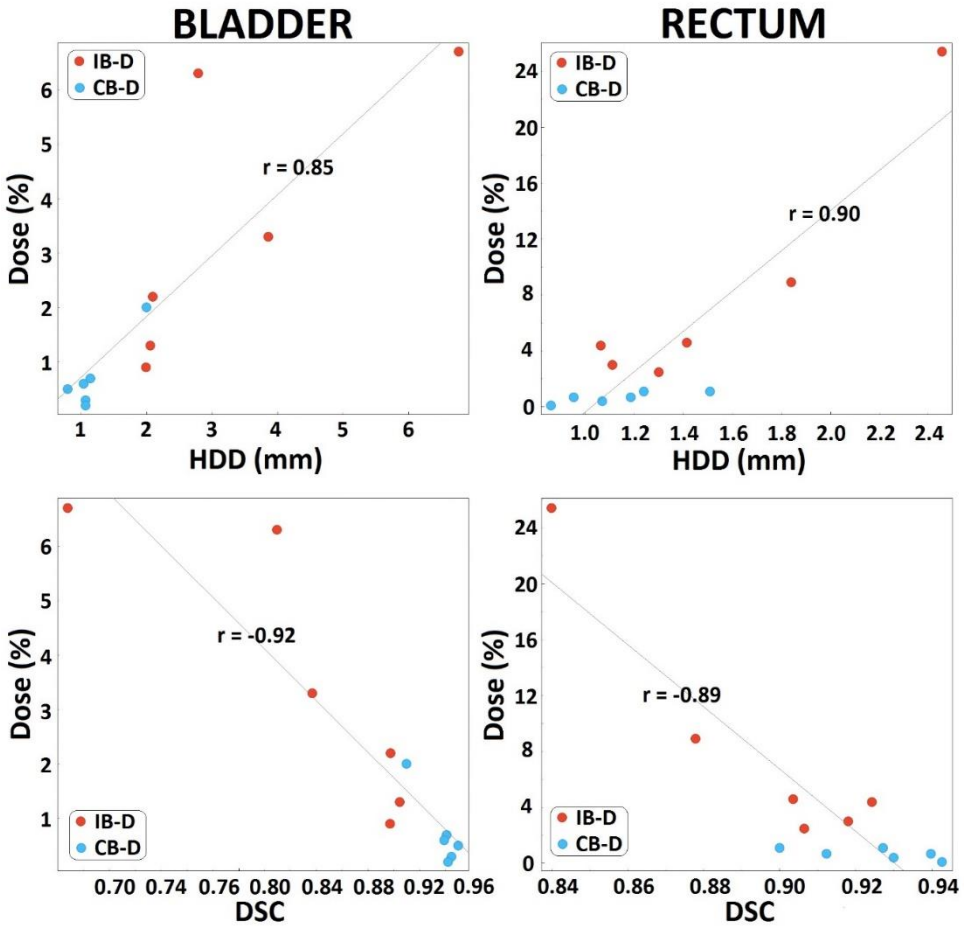

Figure 5. Mean dose difference for all TX$_{PAT1-6}$ across all fractions plotted against the mean HDD and DSC after applying DIR. Correlation coefficients are shown in the subplots.

For TX$_{PAT1-2}$, a substantial density change was observed in the voxels comprised by the rectum structure (air vs water equivalent material) in a few fractions, hampering the DIR algorithm to obtain an accurate deformation field locally around the rectum structure. Both extreme situations led to large deviations in the accumulated dose by IB-D, whereas CB-D was still able to accurately accumulate the dose and obtain a good agreement with the experimental measurements. It is worth noting that the largest geometrical deviations found for the bladder reference markers were located

cranially, whereas there were no film pockets at those locations since they are dosimetrically less relevant (low dose spill).

Conclusions

Our study simulated MR-guided SBRT treatments using actual inter-fractional changes from six prostate cancer patients previously treated in our clinic. MRgRT has shown much potential to improve radiotherapy treatment by means of target volume reduction, online plan adaptation and management of inter-fractional changes[38–43]. Validation of DIR dose accumulation in OARs enables future assessment of the received dose by the critical structures and holds much promise for radiotherapy plan adaptation based on the partially received dose at mid-treatment.

References

1. Wu, Q. J., Li, T., Wu, Q. & Yin, F. F. Adaptive radiation therapy: Technical components and clinical applications. *Cancer Journal* **17**, 182–189 (2011).
2. McVicar, N., Popescu, I. A. & Heath, E. Techniques for adaptive prostate radiotherapy. *Physica Medica* **32**, 492–498 (2016).
3. Song, W., Wong, E., Bauman, G., Battista, J. & Van Dyk, J. SU-DD-A3-01: Dosimetric Evaluation of Daily Rigid and Non-Rigid Geometric Correction Strategies During On-Line Image-Guided Radiation Therapy (IGRT) of Prostate Cancer. *Med. Phys.* **34**, 2327–2328 (2007).
4. Godley, A., Ahunbay, E., Peng, C. & Li, X. A. Automated registration of large deformations for adaptive radiation therapy of prostate cancer. *Med. Phys.* **36**, 1433–1441 (2009).
5. Tetar, S. U. *et al.* Clinical implementation of magnetic resonance imaging guided adaptive radiotherapy for localized prostate cancer. *Phys. Imaging Radiat. Oncol.* **9**, 69–76 (2019).
6. McPartlin, A. J. *et al.* MRI-guided prostate adaptive radiotherapy – A systematic reviewMRI-linac and prostate motion review. *Radiotherapy and Oncology* **119**, 371–380 (2016).
7. Jaffray, D. A., Lindsay, P. E., Brock, K. K., Deasy, J. O. & Tomé, W. A. Accurate Accumulation of Dose for Improved Understanding of Radiation Effects in Normal Tissue. *Int. J. Radiat. Oncol. Biol. Phys.* **76**, 135–139 (2010).
8. Andersen, E. S. *et al.* Bladder dose accumulation based on a biomechanical deformable image registration algorithm in volumetric modulated arc therapy for prostate cancer. *Phys. Med. Biol.* **57**, 7089–7100 (2012).
9. Takayama, Y. *et al.* Evaluation of the performance of deformable image registration between planning CT and CBCT images for the pelvic region: Comparison between hybrid and intensity-based DIR. *J. Radiat. Res.* **58**, 567–571 (2017).
10. Kashani, R. *et al.* Objective assessment of deformable image registration in radiotherapy: a multi-institution study. *Med. Phys.* **35**, 5944–53 (2008).
11. Latifi, K. *et al.* Practical quantification of image registration accuracy following the AAPM TG-132 report framework. *J. Appl. Clin. Med. Phys.* **19**, 125–133 (2018).
12. Moteabbed, M. *et al.* Validation of a deformable image registration technique for cone beam CT-based dose verification. *Med. Phys.* **42**, 196–205 (2015).
13. Motegi, K. *et al.* Usefulness of hybrid deformable image registration algorithms in prostate radiation therapy. *J. Appl. Clin. Med. Phys.* **20**, 229–236 (2019).
14. Brock, K. K., Mutic, S., McNutt, T. R., Li, H. & Kessler, M. L. Use of image registration and fusion algorithms and techniques in radiotherapy: Report of the

AAPM Radiation Therapy Committee Task Group No. 132: Report. *Med. Phys.* **44**, e43–e76 (2017).

15. Kirby, N. *et al.* The need for application-based adaptation of deformable image registration The need for application-based adaptation of deformable image registration. **011702**, 1–10 (2015).
16. Thor, M. *et al.* Evaluation of an application for intensity-based deformable image registration and dose accumulation in radiotherapy. *Acta Oncol.* **53**, 1329–36 (2014).
17. Cazoulat, G. *et al.* Surface-constrained nonrigid registration for dose monitoring in prostate cancer radiotherapy. *IEEE Trans. Med. Imaging* **33**, 1464–1474 (2014).
18. Nassef, M. *et al.* Quantification of dose uncertainties in cumulated dose estimation compared to planned dose in prostate IMRT. *Radiother. Oncol.* **119**, 129–136 (2016).
19. Graves, Y. J. *et al.* A deformable head and neck phantom with in-vivo dosimetry for adaptive radiotherapy quality assurance. *Med. Phys.* **42**, 1490–1497 (2015).
20. Niu, C. J. *et al.* A novel technique to enable experimental validation of deformable dose accumulation. *Med. Phys.* **39**, 765–776 (2012).
21. Janssens, G. *et al.* Evaluation of nonrigid registration models for interfraction dose accumulation in radiotherapy. *Med. Phys.* **36**, 4268–4276 (2009).
22. Jamema, S. V. *et al.* Uncertainties of deformable image registration for dose accumulation of high-dose regions in bladder and rectum in locally advanced cervical cancer. *Brachytherapy* **14**, 953–962 (2015).
23. Kadoya, N. *et al.* Evaluation of rectum and bladder dose accumulation from external beam radiotherapy and brachytherapy for cervical cancer using two different deformable image registration techniques. *J. Radiat. Res.* **58**, 720–728 (2017).
24. van Heerden, L. E. *et al.* Structure-based deformable image registration: Added value for dose accumulation of external beam radiotherapy and brachytherapy in cervical cancer. *Radiother. Oncol.* **123**, 319–324 (2017).
25. Vestergaard, A. *et al.* Adaptive plan selection vs. re-optimisation in radiotherapy for bladder cancer: a dose accumulation comparison. *Radiother. Oncol.* **109**, 457–62 (2013).
26. Niebuhr, N. I. *et al.* The ADAM-pelvis phantom - An anthropomorphic, deformable and multimodal phantom for MRgRT. *Phys. Med. Biol.* **64**, (2019).
27. Niebuhr, N. I. *et al.* Technical Note: Radiological properties of tissue surrogates used in a multimodality deformable pelvic phantom for MR-guided radiotherapy. *Med. Phys.* **43**, 908–916 (2016).
28. Johnen, W., Niebuhr, N., Runz, A. & Echner, G. EP-1737: The ADAM-pelvis phantom: from DICOM data to a patient-like model. *Radiother. Oncol.* **127**, S930 (2018).
29. Barten, D. L. J., Hoffmans, D., Palacios, M. A., Heukelom, S. & Van Battum, L. J. Suitability of EBT3 GafChromic film for quality assurance in MR-guided

radiotherapy at 0.35 T with and without real-time MR imaging. *Phys. Med. Biol.* **63**, 0–10 (2018).

30. Pinter, C., Lasso, A., Wang, A., Jaffray, D. & Fichtinger, G. SlicerRT: radiation therapy research toolkit for 3D Slicer. *Med. Phys.* **39**, 6332–8 (2012).

31. Klein, S., Staring, M., Murphy, K., Viergever, M. A. & Pluim, J. P. W. elastix: A Toolbox for Intensity-Based Medical Image Registration. *Med. Imaging, IEEE Trans.* **29**, 196–205 (2010).

32. Marstal, K., Berendsen, F., … M. S.-P. of the I. & 2016, undefined. SimpleElastix: A user-friendly, multi-lingual library for medical image registration registration segmentation sensing unread. *Cv-Foundation.Org*

33. Bohoudi, O. *et al.* Fast and robust online adaptive planning in stereotactic MR-guided adaptive radiation therapy (SMART) for pancreatic cancer. *Radiother. Oncol.* **125**, 439–444 (2017).

34. Low, D. a., Harms, W. B., Mutic, S. & Purdy, J. a. A technique for the quantitative evaluation of dose distributions. *Med. Phys.* **25**, 656–61 (1998).

35. Dice, L. R. Measures of the Amount of Ecologic Association Between Species Author (s): Lee R . Dice Published by : Ecological Society of America Stable URL : http://www.jstor.org/stable/1932409. **26**, 297–302 (2009).

36. Dubuisson, M., Jain, A. K., Lansing, E. & B, A. B. A Modi ed Hausdor Distance for Object Matching between two point sets A = f 1 compute and does not require the solution of the cor- 1 Introduction two point sets A and B can be combined in the follow- 2 Distance Between Point Sets Research supported by a . 566–568 (1994).

37. Yeo, U. J. *et al.* Is it sensible to 'deform' dose 3D experimental validation of dose-warping. *Med. Phys.* **39**, 5065–5072 (2012).

38. Bohoudi, O. *et al.* Fast and robust online adaptive planning in stereotactic MR-guided adaptive radiation therapy (SMART) for pancreatic cancer. *Radiother. Oncol.* (2017). doi:10.1016/j.radonc.2017.07.028

39. Henke, L. *et al.* Phase I trial of stereotactic MR-guided online adaptive radiation therapy (SMART) for the treatment of oligometastatic or unresectable primary malignancies of the abdomen. *Radiother. Oncol.* **126**, 519–526 (2018).

40. Palacios, M. A. *et al.* Role of daily plan adaptation in MR-guided stereotactic ablative radiotherapy for adrenal metastases. *Int. J. Radiat. Oncol.* (2018). doi:10.1016/j.ijrobp.2018.06.002

41. Bohoudi, O. *et al.* Identification of patients with locally advanced pancreatic cancer benefitting from plan adaptation in MR-guided radiation therapy. *Radiother. Oncol.* **132**, 16–22 (2019).

42. Fischer-Valuck, B. W. *et al.* Two-and-a-half-year clinical experience with the world's first magnetic resonance image guided radiation therapy system. *Adv. Radiat. Oncol.* **2**, 485–493 (2017).

43. Werensteijn-Honingh, A. M. *et al.* Feasibility of stereotactic radiotherapy using a 1.5

T MR-linac: Multi-fraction treatment of pelvic lymph node oligometastases. *Radiother. Oncol.* **134**, 50–54 (2019).

Supplementary materials

Treatment planning constraints

The planning objectives and constraints used were: D95% ≥95% and D2% ≤110% for PTVprostate, D100% ≤ 1cc and D90% ≤ 10 cc for rectum and D100% ≤ 1 cc and D90% ≤ 15 cc for the bladder. All online adapted plans obtained for the six simulated patient treatments, $TX_{PAT1–6}$ met all these constraints.

Correcting for the contribution simulation CT dose

For each treatment simulation a CT-scan was acquired at baseline to obtain an electron density map for dose calculation. EBT3 films were used to determine the dose per CT scan and to develop a correction method. A separate dose response calibration curve was devised by irradiating two sets of EBT3 films simultaneously. The first set of filmstrips was used as a control set. The second set of films was additionally exposed to a simulation CT scan following the irradiation. Both sets were analyzed and the mean dose difference over all pixels between both sets was calculated to obtain a correction factor for the dose delivered with a CT scan. A mean dose contribution of **4.4 cGy** by the CT scan was obtained and added to the ROIs extracted from the treatment plans.

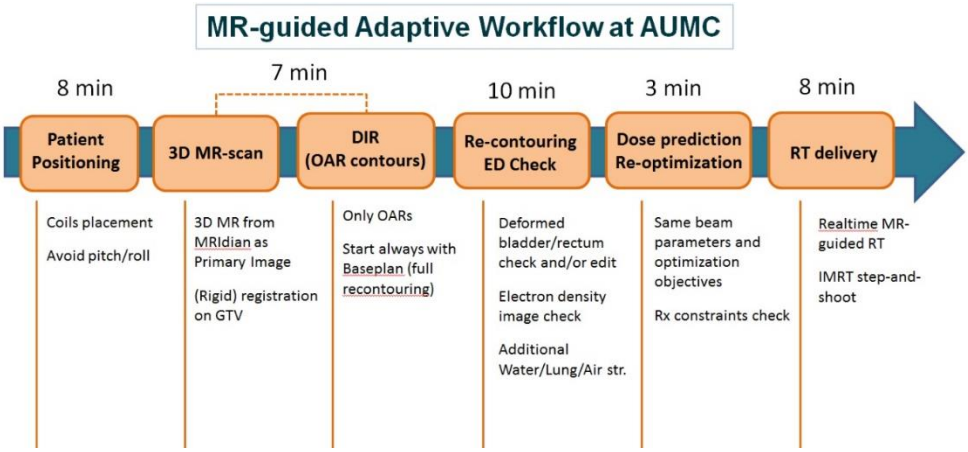

Supplementary Figure 1. *MRgRT workflow including the simulation, planning and delivery steps followed in this study.*

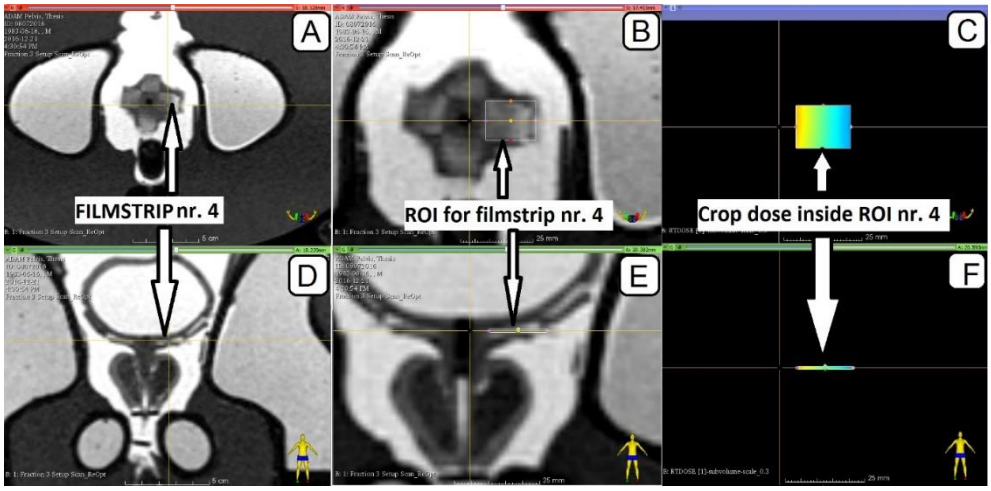

Supplementary Figure 2. *Extraction of the DIR-based accumulated dose distribution from ROI at the exact EBT3 film location on* MR_{REF}*. Axial reconstruction of the phantom shown in panels A and B. Coronal reconstruction is shown in panels D and E. Extracted dose distribution according to the film position in pocket is displayed in panels C and F.*

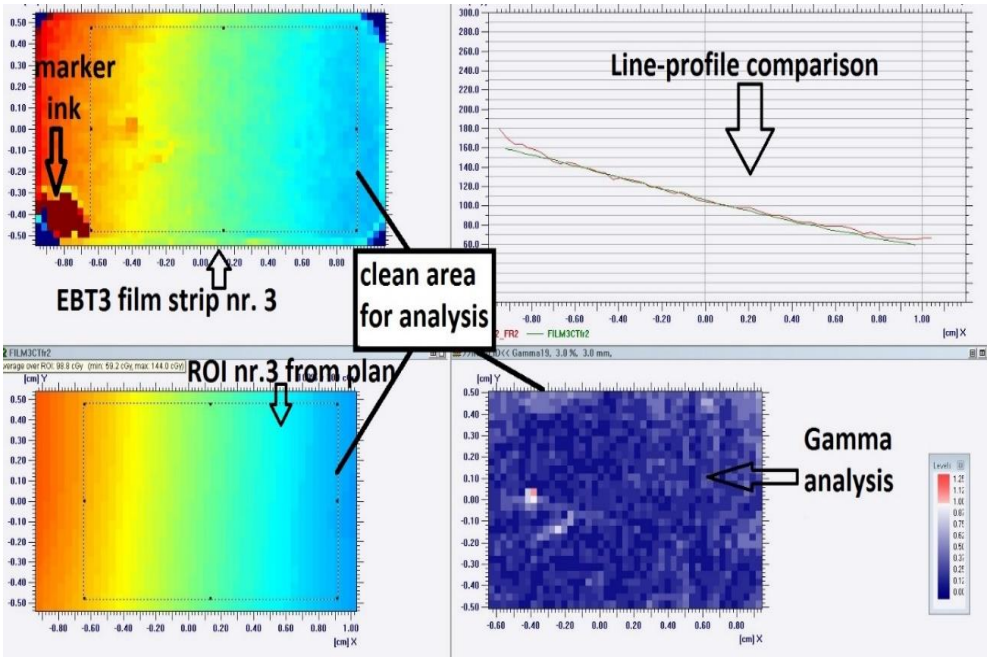

Supplementary Figure 3: *2D pixel-by-pixel analysis of the calibrated filmstrips and the extracted ROI dose distribution (OmniPo-I'mRT). A dose profile comparison of measurement and accumulated dose, together with a gamma analysis are shown on the right side.*

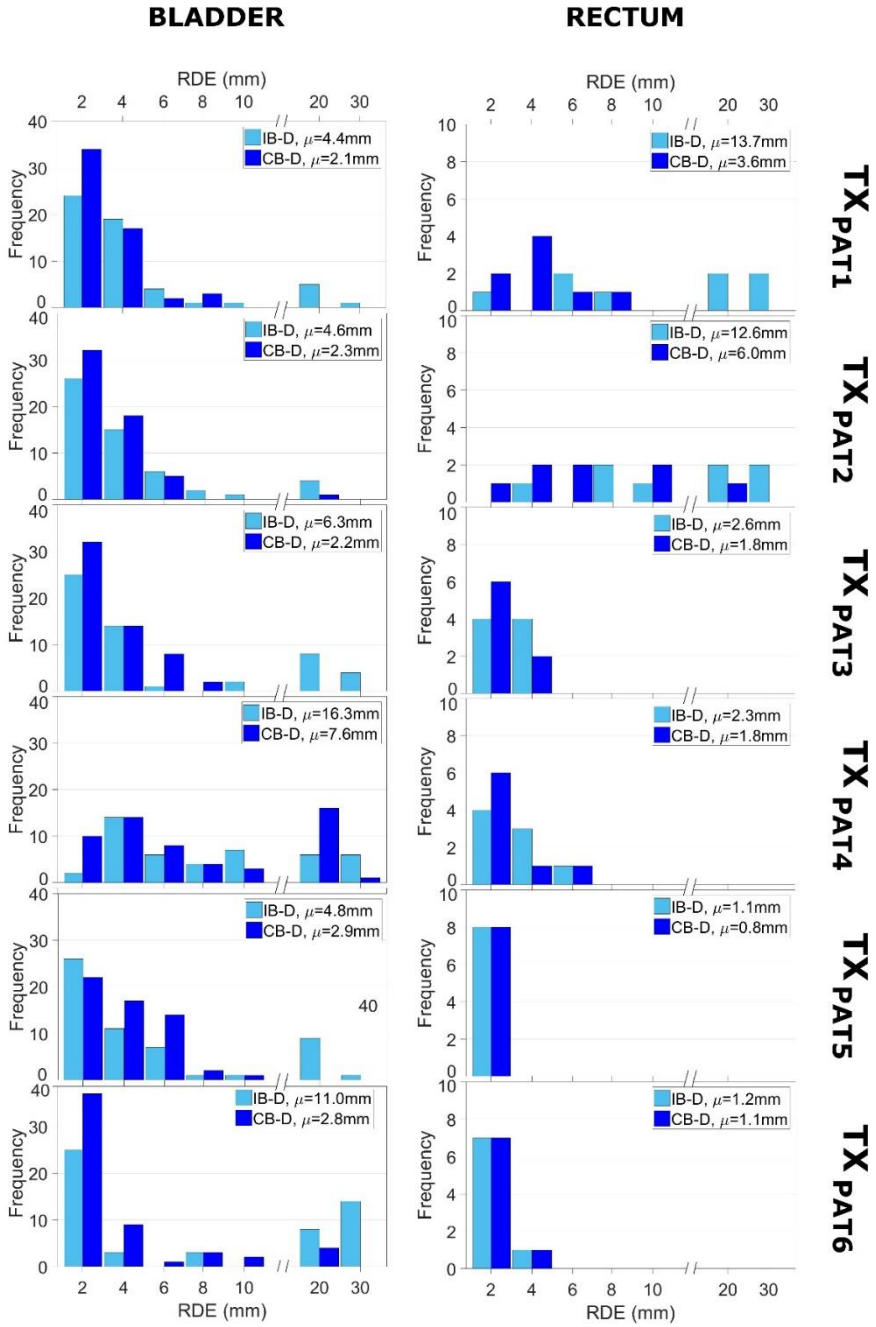

Supplementary Figure 4: *Frequency distribution of the 3D error for each simulated patient (TX_{PAT1-6}) and all fractions for both image registration methods, IB-D and CB-D. Average error for each patient for IB-D and CB-D is shown in the figure legend.*

Chapter 9

Dose accumulation for personalized stereotactic MR-guided adaptive radiation therapy in prostate cancer

Omar Bohoudi
Anna M.E Bruynzeel
Shyama Tetar
Ben J. Slotman
Miguel A. Palacios
Frank J. Lagerwaard

Radiotherapy and Oncology. 2021; 157:197-202

Abstract

Background and purpose: Adaptive MR-guided radiotherapy (MRgRT) is an innovative approach for delivering stereotactic body radiotherapy (SBRT) in prostate cancer (PC). Despite the increased clinical use of SBRT for PC, there is limited data on the relation between the actual delivered dose and toxicity. We aimed to identify dose parameters based on the total accumulated delivered bladder dose ($DOSE_{ACC}^{TX}$). Furthermore, for future personalization, we studied whether prospective accumulation of the first 3 of 5 fractions ($DOSE_{ACC}^{3FR}$) could be used as a representative of $DOSE_{ACC}^{TX}$.

Materials and methods: We deployed a recently validated deformable image registration-based dose accumulation strategy to reconstruct $DOSE_{ACC}^{TX}$ and $DOSE_{ACC}^{3FR}$ in 101 PC patients treated with stereotactic MRgRT. IPSS scores at baseline, end of MRgRT, at 6 and 12 weeks after treatment were analyzed to identify a clinically relevant increase of acute urinary symptoms. A receiver operator characteristic curve analysis was used to investigate the correlation of an increase in IPSS and bladder $DOSE_{ACC}^{TX}$ (range V_5–$V_{36.25\ Gy}$, D_{1cc}, D_{5cc}) and $DOSE_{ACC}^{3FR}$ (range V_6–$V_{21.8\ Gy}$, D_{1cc}, D_{5cc}) parameters.

Results: A clinically relevant increase in IPSS in the three months following MRgRT was observed in 25 patients. The $V_{20Gy\text{-}32Gy}$ from $DOSE_{ACC}^{TX}$ and $V_{15Gy\text{-}18Gy}$ from $DOSE_{ACC}^{3FR}$ showed good correlation with IPSS increase with area under the curve (AUC) values ranging from 0.71 to 0.75. In contrast, baseline dosimetry showed a poor correlation with AUC values between 0.53 and 0.62.

Conclusion: $DOSE_{ACC}^{TX}$ was superior to baseline dosimetry in predicting acute urinary symptoms. Because $DOSE_{ACC}^{3FR}$ also showed good correlation, this can potentially be used to optimize MRgRT for the remaining fractions.

Introduction

Stereotactic body radiation therapy (SBRT) is an increasingly used treatment option for localized prostate cancer (PC), allowing precise delivery of up to five fractions of high biological radiation doses while sparing the surrounding bladder and rectum[1,2]. Several studies have shown an equal efficiency and tolerance for SBRT and conventionally fractionated treatments for PC, particularly for low and intermediate risk PC[3–5]. Despite the increased clinical use of SBRT for PC, there is limited data on the relation between dosimetric parameters and toxicity or quality of life (QoL). The available data is either based on moderately hypofractionated treatments[6], or toxicity was correlated to static baseline dosimetry [7] rather than the total accumulated delivered dose ($DOSE_{ACC}^{TX}$) which is recommended to facilitate a more precise dose-toxicity modeling[8,9]. The latter becomes particularly relevant with the option for daily plan re-optimization.

Magnetic resonance guided radiation therapy (MRgRT) is a most recent clinically implemented technological advancement, inter alia, for SBRT delivery in PC[10,11]. The superior soft tissue imaging capability of MRgRT improves the visualization of the prostate, the base of seminal vesicles and surrounding organs at risk (OARs), allowing precise soft tissue setup, real-time planar imaging and gated delivery with minimal safety margins. An additional advantage is the ability to perform online plan adaptation to address the adverse dosimetric effects in target and OARs due to inter-fractional changes[12]. Beyond the use of MRI for setup, adaptation and gating, the availability of MRI imaging before and during each fraction in combination with a validated deformable image registration (DIR) strategy can provide a unique opportunity to measure the $DOSE_{ACC}^{TX}$ in OARs[13].

Recently, our group completed a prospective phase II study using stereotactic MRgRT with daily plan adaptation in patients with localized PC to evaluate the clinical benefit with regard to early toxicity and QoL[14]. In addition to a very low incidence (5.0%) of early grade ≥ 2 gastro-intestinal (GI) toxicity, early grade ≥ 2 genito-urinary (GU) toxicity was observed in 23.8% of patients. These moderate GU toxicity rates should, however, not detract our pursuit of a more personalized treatment and to minimize the chance of acute bladder toxicity. In an attempt to better understand the relationship between the incidence of early bladder toxicity and $DOSE_{ACC}^{TX}$ of the bladder, we analyzed the dosimetric data and the International Prostate Symptoms Score (IPSS) from patients treated in this phase II MRgRT study. In the current paper, we aim to identify bladder $DOSE_{ACC}^{TX}$ parameters associated with acute treatment-related urinary symptom flare. Furthermore, for future personalization of the MRgRT treatment, we studied whether pretreatment baseline dosimetry or prospective accumulation of delivered doses throughout the treatment could be used as a representative of $DOSE_{ACC}^{TX}$.

Materials and Methods

Patient characteristics and adaptive MRgRT details

Data of 101 patients with clinical stage T1-3b PC who underwent MRgRT on the MRIdian system (ViewRay Inc., Mountain View, USA) between August 2016 and March 2018, were collected within a prospective institutional review board approved database (IRB approval 2018.3216). The study population includes 4 low-risk patients, 60 high-risk patients and 37 intermediate-risk patients (AUA/ASTRO/SUO 2017). All patients received adaptive MRgRT in 5 fractions of 7.25 Gy on alternate days within 14 days overall treatment time. The dose was

normalized such that the 95% isodose covered 95% of the PTV, both in baseline and adaptive planning. A detailed description of our entire MRgRT workflow including simulation, adaptive planning and gated IMRT delivery for PC, was presented in a previous publication[10] and is provided in the supplementary materials. A full description of literature-based planning objectives and constraints used during baseline and adaptive planning are listed in supplementary Table 1.

Dose accumulation and dosimetric parameters

We deployed our recently evaluated DIR-based dose accumulation strategy to ensure an accurate reconstruction of $DOSE_{ACC}^{TX}$ [13]. Briefly, this strategy uses a contour-based DIR to obtain an OAR-specific accumulated dose. Available MR scans, contours and dose distributions of each patient were imported into the open-source software 3DSlicer (v4.10.0) [15]. We used the SlicerElastix extension (intensity-based DIR toolkit) for voxel-to-voxel mapping between the reference image (MRI fraction 1; MR_{REF}) and subsequent images (MR_{FR2}-MR_{FR5}). Noteworthy, MR_{REF} and MR_{FR2}-MR_{FR5} were subject to a rigid CTV registration during the online adaptive workflow. DIR algorithm parameters were a normalized mutual information similarity metric with a B-spline parametrized transformation. This algorithm uses a three leveled multi-resolution registration scheme, where at each level the image resolution and grid spacing were down-sampled by a factor of 2 (final B-spline grid spacing: 10 mm). The optimization parameter was a Gradient Descent with up to 500 iterations at each multi-resolution level[16]. A bladder-specific voxel-to-voxel mapping was established between MR_{REF} and MR_{FR2}-MR_{FR5} by constraining the DIR to areas encompassed by the bladder contours, resulting in four bladder-specific deformation vector fields (DVF_{FR2-5}) for each patient. The average dice similarity coefficient (DSC_{mean})[17] was calculated to evaluate the similarity of the deformed (DVF_{FR2-5}) and reference bladder contour for each patient. Furthermore, the DVF_{FR2-5}

were applied to dose distributions of corresponding fractions to map the dose distributions at each fraction to the dose distribution of fraction 1 (reference image, MR_{REF}). The resulting warped dose distributions were summed to acquire the $DOSE_{ACC}^{TX}$. In addition, we accumulated the delivered dose of only fraction 1, 2 and 3 ($DOSE_{ACC}^{3FR}$) as a representative of $DOSE_{ACC}^{TX}$. Three patient-specific bladder dose volume histograms (DVH) were generated from 1) the pre-treatment plan based on the simulator scan ($DOSE_{BASELINE}$), 2) $DOSE_{ACC}^{TX}$ and 3) $DOSE_{ACC}^{3FR}$. For this analysis, we derived the following absolute DVH parameters from $DOSE_{ACC}^{TX}$ and $DOSE_{BASELINE}$; V_{10Gy}, V_{15Gy}, V_{20Gy}, V_{25Gy}, V_{30Gy}, $V_{32.6Gy}$, $V_{36.25Gy}$, D_{1cc}, and D_{5cc}. Dose levels for the $DOSE_{ACC}^{FR3}$ DVH parameters were scaled back to 3 fractions (60%), i.e. ; V_{6Gy}, V_{9Gy}, V_{12Gy}, V_{15Gy}, V_{18Gy}, $V_{19.6Gy}$, $V_{21.8Gy}$, D_{1cc}, and D_{5cc}.

Patient follow-up and PROMs

Within the clinical phase II study, both clinician- and patient-scored GI and GU toxicity were evaluated during the first year[14,18]. However, in the current study we only focus on the early GU toxicity, considering the very low incidence of late GU and both early and late GI toxicity. For the most objective scoring early GU toxicity, we have used the patient-scored International Prostate Symptom Scoring questionnaire (IPSS), collected at baseline, at the end of MRgRT, at 6 and 12 weeks after treatment. The IPSS questionnaire evaluates urological symptoms based on seven questions (incomplete emptying, frequency, weak stream, intermittency, urgency, straining, and nocturia) measured on a 0 to 5 scale, representing a range from “not at all” to “almost always”. Total scores are transformed to a 0–35 point scale with a high urinary score on a symptom scale represents a high level of symptoms. An increase in IPSS of 10 points or more from baseline in the first three months following MRgRT was considered a clinically relevant increase in urinary symptoms, as previously described and used by other authors[19,20].

Statistical analysis

Standard descriptive statistic for baseline patient and tumor characteristics were recorded. Statistical analysis used for plan comparisons was performed using the Wilcoxon Signed-Rank test (p-value <0.05; statistically significant). We performed a Receiver Operator Characteristic (ROC) curves analysis to investigate the correlation of $DOSE_{ACC}^{TX}$ and $DOSE_{BASELINE}$ dose-volume parameters and a clinically relevant increase in IPSS. For each ROC curve, we calculated the average area under the curve (AUC) and corresponding 95% confidence intervals (CIs) as a measure of correlation. Cut-off values for the relevant parameters were selected by minimizing the Euclidean distance ($Ed = \sqrt{(1 - Sn.)^2 + (1 - Sp.)^2}$) between the ROC curve and the ($Sn.$ = 1, 1–$Sp.$ = 0) point [21]. A secondary analysis was performed to evaluate the correlation of prospective dose accumulation of the first 3 fractions ($DOSE_{ACC}^{3FR}$) and a clinically relevant increase in IPSS, and hence can be used as a representation of $DOSE_{ACC}^{TX}$. The same ROC analysis and cut-off point determination was repeated only this time for dose-parameters derived from $DOSE_{ACC}^{3FR}$. All statistical analyses were performed using SPSS version 26 (IBM® SPSS Statistics, Armonk, NY, USA).

Results

Baseline patient and tumor characteristics of 101 patients included in this study are shown in Table 1. Planning objectives for PTV coverage (median $D_{99\%}$: 33.7Gy) and the high-dose OAR constraints were met for all patients in baseline planning. As a consequence of manual CTV adjustments (due to possible rotations or deformations) during adaptive MRgRT, the PTV coverage was comprised in 59% of non-re-optimized fractions. In 495 out of 505 fractions (98.0%) online re-optimized plans have been delivered. Plan re-optimization increased the percentage of fractions that

complied with institutional PTV constraints from 41% to 98.8% and at the same time decreased the percentage of fractions that exceeded the intermediate and high dose bladder constraints from 7.9% to 1.2%. During real-time MR-guided radiation delivery, 2D table shifts (max. 3 mm) were performed in 102 out of 505 fractions (20.2%). Larger intra-fraction prostate shifts or OAR deformations necessitating repeat 3D imaging were observed in 6.0% of the delivered fractions.

Table 1: *Baseline patient and tumor characteristics (n = 101).*

	mean	**range**
Age (y)	72	55 – 88
PTV (cc)	108.6	25.0 – 204.5
Mean Bladder volume (cc)	228.0	78.2 – 624.4
Risk classification		
Low	4	4.0
Intermediate	37	36.6
High	60	59.4
Hormonal treatment	83	82.2
Prior TUR prostate	14	13.9
Prior tamsulosin	15	14.4

The resulting DIRs (MR_{FR2}-MR_{FR5} to MR_{REF}) for all patients were visually inspected, and deformed bladder volumes showed a good correspondence with the bladder on MR_{REF}. Overall, the average (IQR) value for DSC_{mean} was 0.93 (0.89–0.95). Seven patients with large bladder volume change (>65%) between MR_{REF} and MR_{FR2}-MR_{FR5}, had small cranially located discrepancies in more than 2 fractions after DIR (DSC_{mean} range = 0.84 - 0.90).

With the exception of a single missing follow-up data at 6 weeks, trial data on IPSS scoring were complete for the first three months. Most relevant acute GU symptoms were an increased urge and urinary frequency, incontinence was uncommon and reported by 4% of patients at the end of MRgRT and decreasing at 3 months. IPSS scores showed a peak at the end of MRgRT (mean IPSS = 13.0) and decreased to a similar average as baseline scores (mean IPSS = 7.4) at 3-month follow-up (mean IPSS = 7.6). Figure 1 displays a box-and-whisker plot of IPSS scores at baseline, end of MRgRT, 6 weeks and 12 weeks, respectively. An increase in IPSS of 10 points or more from baseline in the first three months following MRgRT was observed in 25 patients (24.8%).

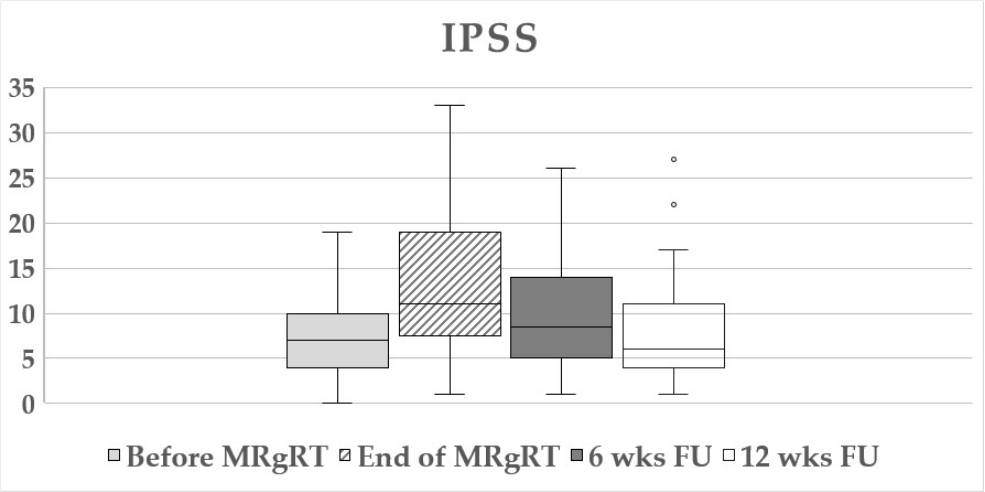

Figure 1. *Box and whisker plots showing IPSS scores at baseline, end of MRgRT, 6 weeks, and 12 weeks.*

Table 2 presents the ROC statistics (AUC, 95% CI, *p*-value) for the bladder specific $DOSE_{BASELINE}$ and $DOSE_{ACC}^{TX}$ dose-volume parameters for a clinically relevant increase in IPSS. $DOSE_{BASELINE}$ parameters showed a relatively poor correlation, with AUC values ranging from 0.532 to 0.617. In contrast, parameters from $DOSE_{ACC}^{TX}$ showed a good correlation for the mid- to high dose levels in the range of $V_{20 - 32.6Gy}$, with the V_{25Gy} having highest AUC value (0.754).

Table 2: *ROC analysis for the correlation of the bladder specific DOSE$_{ACC}^{TX}$ and DOSE$_{BASELINE}$ dose-volume parameters and a clinically relevant increase in IPSS score.*

DOSE$_{BASELINE}$ parameters					**DOSE$_{ACC}^{TX}$ parameters**				
	AUC	95% CI				AUC	95% CI		
	Mean	Lower	Upper	*p*-Value		Mean	Lower	Upper	*p*-Value
V10Gy	0.600	0.474	0.727	0.151	V10Gy	0.535	0.400	0.669	0.622
V15Gy	0.617	0.489	0.744	0.096	V15Gy	0.651	0.523	0.779	0.031
V20Gy	0.603	0.471	0.736	0.140	**V20Gy**	**0.731**	**0.612**	**0.849**	**0.001**
V25Gy	0.592	0.459	0.725	0.188	***V25Gy**	**0.754**	**0.640**	**0.868**	**0.000**
V30Gy	0.560	0.427	0.693	0.390	**V30Gy**	**0.747**	**0.626**	**0.868**	**0.000**
V32.6Gy	0.528	0.395	0.662	0.687	**V32.6Gy**	**0.709**	**0.577**	**0.841**	**0.003**
V36.25Gy	0.532	0.392	0.671	0.651	V36.25Gy	0.619	0.485	0.753	0.089
D1cc	0.551	0.408	0.694	0.453	D1cc	0.608	0.471	0.745	0.122
D5cc	0.571	0.439	0.704	0.315	D5cc	0.619	0.490	0.748	0.089

Good correlations (AUC > 0.7) has been presented in bold. *Dose-volume parameter with highest AUC score.

Table 3 lists the AUC values for the DOSE$_{ACC}^{3FR}$ parameters. These results exhibit the same trend as DOSE$_{ACC}^{TX}$ were the mid- to high dose levels in the range of $V_{15\text{ - }18Gy}$ have the highest AUC values of 0.713 and 0.727, respectively. Figure 2 points the minimum Euclidean distance between the ROC curves and the (Sn. = 1, 1–Sp. = 0) point for DOSE$_{ACC}^{TX}$ and DOSE$_{ACC}^{3FR}$ parameters, illustrating the cut-off values or constraints for these parameters. The constraints for relevant parameters derived from DOSE$_{ACC}^{TX}$ and their 3 fraction representative (DOSE$_{ACC}^{3FR}$) show large similarities; the bladder V_{25Gy} (5fx) and V_{15Gy} (3fx) constraints were 39.9 and 41.2 cc, and the V_{30Gy} (5fx) and V_{18Gy} (3fx) 17.6 and 18.9, respectively.

Table 3: *Results from ROC analysis for the correlation of prospective bladder dose accumulation of the first 3 fractions ($DOSE_{ACC}^{3FR}$) and a clinically relevant increase in IPSS score.*

Mid-treatment dose parameters for predicting a significant increase IPSS symptom score					
		AUC	95% CI		
$DOSE_{ACC}^{3FR}$ parameter	*$DOSE_{ACC}^{TX}$ equivalent*	Mean	Lower	Upper	*p*-Value
V6Gy	*V10Gy*	0.517	0.380	0.654	0.805
V9Gy	*V15Gy*	0.628	0.500	0.756	0.067
V12Gy	*V20Gy*	0.687	0.563	0.811	0.007
V15Gy	*V25Gy*	**0.713**	**0.592**	**0.834**	**0.002**
***V18Gy**	*V30Gy*	**0.727**	**0.607**	**0.840**	**0.001**
V19.6Gy	*V32.6Gy*	0.690	0.564	0.815	0.007
V21.8Gy	*V36.25Gy*	0.617	0.484	0.750	0.095
D1cc	*D1cc*	0.626	0.495	0.757	0.072
D5cc	*D5cc*	0.632	0.504	0.760	0.058

Good correlations (AUC > 0.7) has been presented in bold. *Dose-volume parameter with highest AUC score.

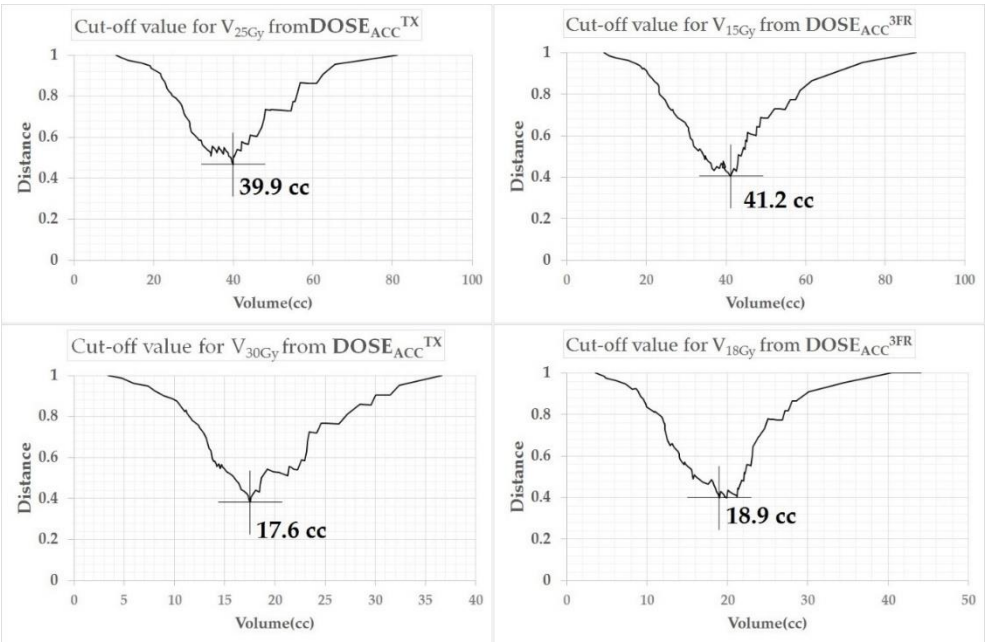

Figure 2. *The Euclidean distance between the ROC curves and the (Sn. = 1, 1–Sp. = 0) point as a function of volume for the $DOSE_{ACC}^{TX}$ and $DOSE_{ACC}^{3FR}$ derived parameters. The smallest d value defines the cut-off point (volume constraint) for the relevant dose parameter.*

Discussion

MRgRT with daily online plan adaptation is an innovative approach for delivering SBRT in PC. In our first feasibility and clinical study, we reported the safety and the minimal incidence of radiation induced rectal toxicity[10,14,18]. This is likely the result from benefits of MRgRT, in particular the small CTV to PTV margin (3 mm), facilitated by daily plan adaptation and online CTV monitoring. Although, plan adaptation ensured compliance with institutional bladder constraints (Supplementary Table 1) in the vast majority of patients, early GU toxicity was still observed in 23.8% of patients. However, it is a possibility that stricter bladder constraints can reduce the incidence of GU toxicity because the constraints used were mainly focused on the high doses that were previously associated with grade ≥ 3 urinary toxicity[4].

The correlation between base plan dose parameters and treatment related side-effects in this study was poor, as described previously[9]. This lack of correlation seen within our data may be because the average baseline bladder volume (338.5cc) was significantly larger ($p < 0.0001$) compared to the mean bladder volume at fraction 1 to fraction 5 (273.4, 240.4, 221.7, 210.1 and 194.6cc). However, using DIR we could identify accumulated, i.e. actually delivered bladder parameters (V_{20Gy} - $V_{32.6Gy}$) and cut-off points associated with a relevant risk of acute treatment-related urinary symptom flare (Table 4). In contrast to previous publications, we could not find correlations with the high dose bladder parameters (>$V_{32.6Gy}$). This is probably due to the fact that plan adaptation in combination with the 3mm CTV to PTV margin, reduced the very high doses to the bladder volume significantly. Supplementary Table 4 compares the very high dose (≥V_{35Gy}) volumes in our study with values from four phase II trials combined in a pooled cohort for a dose-toxicity study in prostate

SBRT[7]. Notably, in our study no patient received 38 Gy or more to the bladder (prescribed dose: 5 x 7,25 Gy) while the average V_{38Gy} was 6.1cc in the pooled cohort (prescribed dose: 5 x 7 Gy).

Table 4: *Example of proposed bladder constraints to guide the adaptive MRgRT treatment after delivering three fractions.*

Structure	Constraints
Bladder	$D_{102\%}$ (22.2 Gy) ≤ 0.1 cc $D_{100\%}$ (21.75 Gy) ≤ 1 cc $D_{90\%}$ (19.6 Gy) ≤ 9 cc $D_{83\%}$ (18 Gy) ≤ 17 cc $D_{70\%}$ (15 Gy) ≤ 40 cc

MRgRT with daily plan adaptation also opens the door for more personalized approaches using prospective dose accumulation. In a simulation of this approach, we found that the cumulative delivered bladder dose in the first three fractions showed large similarities in correlation (and constraints) for acute increase of urinary symptoms with those of the total delivered dose. This suggests that prospective dose accumulation using the first delivered fractions guided by interim bladder constraints may be used to adapt remaining fractions with the goal to minimize urinary toxicity. An example of such interim constraints after three fractions is illustrated in Table 4. When prospective accumulation of the first fractions show significantly violated bladder constraints, it may be feasible to: 1) increase bladder sparing during plan adaptation in the remaining fractions[22]; 2) increase the interval in between the remaining fractions[23,24]; or 3) prophylactically prescribe e.g. alpha1-blocking medication such as tamsulosin[25]. To ascertain the feasibility of increasing bladder sparing in the remaining fractions, we performed offline re-planning in 19 patients of our patient cohort for whom the $DOSE_{ACC}^{3FR}$ constraint was violated at the third fraction. Thereafter, dose accumulation was carried out again for those 19 patients with the new plans generated for fractions 4 and 5, in which a higher priority for bladder sparing was given. A significant

(average) decrease in the accumulated bladder V_{25Gy} (8 cc) and V_{30Gy} (6 cc) was achieved at the cost of a slightly (average) increase of 2 cc for the V_{20Gy} of rectum and of the inhomogeneity in the target. It is worth mentioning that these gains will also be dependent on the specific departmental procedures and planning techniques, but they show the feasibility of increased bladder sparing in MRgRT based on the evaluation of $DOSE_{ACC}^{3FR}$ constraints at mid-treatment.

Our study has potential limitations as we focused primarily on dosimetric parameters, however non-dosimetric variables, such as prior transurethral resection, baseline IPSS, age may also be associated with the development of acute urinary toxicity. Although our study was mainly based on the IPSS score, it is generally recognized that patient-reported outcome measures (PROMs) such as the IPSS and QLQ-PR25 questionnaires, can be more sensitive for detecting treatment-related toxicity compared to generic clinician-scored toxicity scales such as CTCAE or RTOG[26,27]. We also acknowledge that a statistically significant dose constraint does not automatically mean the constraint is clinically significant. Therefore, it is important to validate our findings in a new cohort of PC patients to see whether acute GU toxicity can be better controlled using this personalized treatment approach using prospective dose accumulation and inter-fractional plan adaptation.

Conclusions

In conclusion, total accumulated delivered bladder dose was superior to baseline dosimetry in predicting acute treatment related increase in urinary symptoms. Prospective dose accumulation using the first delivered fractions also showed good correlation, which can potentially be used to optimize MRgRT for the remaining fractions to reduce the risk of acute urinary toxicity.

References

1. Baker, B. R., Basak, R., Mohiuddin, J. J. & Chen, R. C. Use of stereotactic body radiotherapy for prostate cancer in the United States from 2004 through 2012. *Cancer* **122**, 2234–2241 (2016).
2. Malouff, T. D. *et al.* Current use of stereotactic body radiation therapy for low and intermediate risk prostate cancer: A National Cancer Database Analysis. *Prostate Cancer Prostatic Dis.* **23**, 349–355 (2019).
3. Datta, N. R., Stutz, E., Rogers, S. & Bodis, S. Conventional Versus Hypofractionated Radiation Therapy for Localized or Locally Advanced Prostate Cancer: A Systematic Review and Meta-analysis along with Therapeutic Implications. *International Journal of Radiation Oncology Biology Physics* vol. 99 573–589 (2017).
4. Hannan, R. *et al.* Stereotactic body radiation therapy for low and intermediate risk prostate cancer-Results from a multi-institutional clinical trial. *Eur. J. Cancer* **59**, 142–151 (2016).
5. King, C. R. *et al.* Stereotactic body radiotherapy for localized prostate cancer: Pooled analysis from a multi-institutional consortium of prospective phase II trials. *Radiother. Oncol.* **109**, 217–221 (2013).
6. Wilkins, A. *et al.* Derivation of Dose/Volume Constraints for the Anorectum from Clinician- and Patient-Reported Outcomes in the CHHiP Trial of Radiation Therapy Fractionation. *Int. J. Radiat. Oncol. Biol. Phys.* **106**, 928–938 (2020).
7. Alayed, Y. *et al.* Dosimetric predictors of toxicity and quality of life following prostate stereotactic ablative radiotherapy. *Radiother. Oncol.* **144**, 135–140 (2020).
8. Jaffray, D. A., Lindsay, P. E., Brock, K. K., Deasy, J. O. & Tomé, W. A. Accurate Accumulation of Dose for Improved Understanding of Radiation Effects in Normal Tissue. *Int. J. Radiat. Oncol. Biol. Phys.* **76**, 135–139 (2010).
9. Shelley, L. E. A. *et al.* Delivered dose can be a better predictor of rectal toxicity than planned dose in prostate radiotherapy. *Radiother. Oncol.* **123**, 466–471 (2017).
10. Tetar, S. U. *et al.* Clinical implementation of magnetic resonance imaging guided adaptive radiotherapy for localized prostate cancer. *Phys. Imaging Radiat. Oncol.* **9**, 69–76 (2019).
11. Dunlop, A. *et al.* Daily adaptive radiotherapy for patients with prostate cancer using a high field MR-linac: Initial clinical experiences and assessment of delivered doses compared to a C-arm linac. *Clin. Transl. Radiat. Oncol.* **23**, 35–42 (2020).
12. McVicar, N., Popescu, I. A. & Heath, E. Techniques for adaptive prostate radiotherapy. *Physica Medica* vol. 32 492–498 (2016).
13. Bohoudi, O. *et al.* End-to-end empirical validation of dose accumulation in MRI-guided adaptive radiotherapy for prostate cancer using an anthropomorphic deformable pelvis phantom. *Radiother. Oncol.* (2019) doi:10.1016/j.radonc.2019.09.014.
14. Bruynzeel, A. M. E. *et al.* A Prospective Single-Arm Phase 2 Study of Stereotactic Magnetic Resonance Guided Adaptive Radiation Therapy for Prostate Cancer: Early Toxicity Results. *Int. J. Radiat. Oncol. Biol. Phys.* **105**, 1086–1094 (2019).
15. Pinter, C., Lasso, A., Wang, A., Jaffray, D. & Fichtinger, G. SlicerRT: radiation therapy research toolkit for 3D Slicer. *Med. Phys.* **39**, 6332–8 (2012).

16. Klein, S., Staring, M., Murphy, K., Viergever, M. A. & Pluim, J. P. W. elastix: A Toolbox for Intensity-Based Medical Image Registration. *Med. Imaging, IEEE Trans.* **29**, 196–205 (2010).
17. Dice, L. R. Measures of the Amount of Ecologic Association Between Species Author (s): Lee R . Dice Published by : Ecological Society of America Stable URL : http://www.jstor.org/stable/1932409. **26**, 297–302 (2009).
18. Tetar, S. U. *et al.* Magnetic Resonance-guided Stereotactic Radiotherapy for Localized Prostate Cancer: Final Results on Patient-reported Outcomes of a Prospective Phase 2 Study. *Eur. Urol. Oncol.* 1–7 (2020) doi:10.1016/j.euo.2020.05.007.
19. Henderson, D. R. *et al.* An Investigation of Dosimetric Correlates of Acute Toxicity in Prostate Stereotactic Body Radiotherapy: Dose to Urinary Trigone is Associated with Acute Urinary Toxicity. *Clin. Oncol.* **30**, 539–547 (2018).
20. Ghadjar, P. *et al.* Impact of dose to the bladder trigone on long-term urinary function after high-dose intensity modulated radiation therapy for localized prostate cancer. *Int. J. Radiat. Oncol. Biol. Phys.* **88**, 339–344 (2014).
21. Perkins, N. J. & Schisterman, E. F. The Inconsistency of " Optimal " Cut-points Using Two ROC Based Criteria. *Am J Epidemiol* **163**, 670–675 (2006).
22. Tol, J. P., Dahele, M., Doornaert, P., Slotman, B. J. & Verbakel, W. F. A. R. Toward optimal organ at risk sparing in complex volumetric modulated arc therapy: An exponential trade-off with target volume dose homogeneity. *Med. Phys.* **41**, 1–10 (2014).
23. Alayed, Y. *et al.* Accelerating prostate stereotactic ablative body radiotherapy: Efficacy and toxicity of a randomized phase II study of 11 versus 29 days overall treatment time (PATRIOT). *Radiother. Oncol.* **149**, 8–13 (2020).
24. Quon, H. C. *et al.* Once-weekly versus every-other-day stereotactic body radiotherapy in patients with prostate cancer (PATRIOT): A phase 2 randomized trial. *Radiother. Oncol.* **127**, 206–212 (2018).
25. Prosnitz, R. G. *et al.* Tamsulosin palliates radiation-induced urethritis in patients with prostate cancer: Results of a pilot study. *Int. J. Radiat. Oncol. Biol. Phys.* **45**, 563–566 (1999).
26. Morton, G. C. *et al.* Health-related quality of life after single-fraction high-dose-rate brachytherapy and hypofractionated external beam radiotherapy for prostate cancer. *Int. J. Radiat. Oncol. Biol. Phys.* **80**, 1299–1305 (2011).
27. Litwin, M. S., Lubeck, D. P., Henning, J. M. & Carroll, P. R. Differences in urologist and patient assessments of health related quality of life in men with prostate cancer: Results of the capsure database. *J. Urol.* **159**, 1988–1992 (1998).
28. Kawrakow, I. & Fippel, M. Investigation of variance reduction techniques for Monte Carlo photon dose calculation using XVMC. *Phys. Med. Biol.* **45**, 2163–2183 (2000).
29. Kawrakow, I. Accurate condensed history Monte Carlo simulation of electron transport. I. EGSnrc, the new EGS4 version. *Med. Phys.* **27**, 485–498 (2000).

Supplementary material:

Adaptive MRgRT workflow and details

All patients underwent a simulation CT scan with a slice thickness of 2mm for dose calculation purposes, followed by a high-resolution MR scan (TR/TE: 3.37 ms/1.45 ms, FA: 60°, resolution: 1.5mm×1.5mm×1.5mm) based on a balanced steady-state free precession technique (True FISP) acquired at the MRIdian. The simulation (CT+MR) and treatment were both performed with the patient in a supine position, where flexible (dummy) coils were placed around the patient's pelvic region. All patients received instructions to empty their bladder, followed by an intake of 500 ml of water 2 hours before the simulation and each treatment fraction. The CTV (low-risk: prostate gland, intermediate/high-risk: prostate gland + base of the vesicles) and relevant OAR, i.e. the bladder, rectum, urethra, and femora were delineated on the simulation MR. An isotropic margin of 3 mm around the CTV was used to generate the planning target volume (PTV). Step-and-shoot IMRT was used to construct baseline treatment plans ($PLAN_{BASELINE}$) including ±15 equidistant beams (±45 segments) that provide enough degrees of freedom and flexibility to adapt $PLAN_{BASELINE}$ in account for daily anatomical changes. Dose calculation was executed using a VMC and EGSnrc code based Monte-Carlo algorithm implemented in the MRIdian system. This algorithm can complete an IMRT plan calculation subject to a magnetic field and a dose grid resolution of 0.2 cm × 0.2 cm × 0.2 cm (statistical uncertainty of 1%) within 2 min. The prescribed dose of 36.25 Gy was normalized such that the 95% isodose covered 95% of the PTV, both in baseline and adaptive planning. All patients received Adaptive MRgRT in 5 fractions of 7.25 Gy on alternate days within 14 days. At each fraction, daily plan re-optimization was achieved using an in-house developed strategy which can be executed within several minutes and only requires checking and (where necessary) manually

adjusting the CTV and relevant OAR contours within the first 3 cm of the PTV. Briefly, this strategy comprises the following steps: (1) A new MR scan at each fraction, followed by rigid 3D alignment of the baseline and the new MR-scan based on the CTV; (2) A rigid propagation of the CTV contour (manually adjusted by the attending radiation oncologist), followed by automatic deformation of OAR contours (only corrected within the first 3 cm outside the PTV); (3) Recalculation of $PLAN_{BASELINE}$ on the current anatomy, using the electron density map subject to the same deformation applied to the OAR contours ($PLAN_{PREDICT}$); (4) Re-optimization of the $PLAN_{PREDICT}$ to derive a $PLAN_{REOPTIMIZED}$ using the same beam numbers, beam directions and optimization objectives as was used in $PLAN_{BASELINE}$; (5) Patient-specific QA using an independent Monte-Carlo dose calculation algorithm and gamma analysis prior to each treatment delivery; (6) A gated IMRT delivery during MR-planar acquisition for intra-fraction monitoring using a 3mm gating boundary around the CTV. Two-dimensional table shifts (max. 3 mm) were performed, in occurrence of intra-fractional CTV position shift (e.g. due to increasing bladder filling or air in the rectum). Larger prostate shifts or OAR deformations required repeat 3D imaging. The average duration of all steps in adaptive MRgRT for prostate is ±45 min.

Supplementary Table 1: *Planning objectives and dose constraints for OARs used in the phase II adaptive MRgRT for PC study.*

Structure	Objectives/constraints
PTV (36.25 Gy / 5 fractions)	$D_{95\%}$ ≥95% prescribed dose
	$D_{2\%}$ ≤110% prescribed dose
Rectum	$D_{105\%}$ (38.1 Gy) ≤ 0.1 cc
	$D_{100\%}$ (36.25 Gy) ≤ 1cc
	$D_{95\%}$ (34.4 Gy) ≤ 5cc
	$D_{90\%}$ (32.6 Gy) ≤ 10 cc
Bladder	$D_{102\%}$ (37.0 Gy) ≤ 0.1 cc
	$D_{100\%}$ (36.25 Gy) ≤ 1 cc
	$D_{90\%}$ (32.62 Gy) ≤ 15 cc

Supplementary Table 2: *Comparison of the very high dose volumes in our study with volumes from four phase II trials combined in a pooled cohort dose-toxicity study for prostate SBRT.*

	Current study *n* = 101	**Y. Alayed et al.** [7] *n* = 258
	Mean ± SD	Mean ± SD
V35Gy (cc)	1.8 ± 2.4	11.7 ±7.7
V38Gy (cc)	0.0 ± 0.0	6.1 ± 5.6
V40Gy (cc)	0.0 ± 0.0	1.7 ± 2.3
D5Gy (cc)	33.3 ± 1.2	37.5 ± 2.4
D1cc (Gy)	34.9 ± 0.9	**38.8** ± 2.2

Chapter 10

General discussion and future directions

The physicist Harold Johns stated; 'If you can't see it, you can't hit it, and if you can't hit it, you can't cure it'[1]. If we consider the dynamics of changes in shape and position of the tumor and surrounding organs at risk within our body, this also means that 'if you can't see it, you can't *adapt* to such anatomical changes to hit it'. Historically, large margins for uncertainty have been used around tumors to ensure 'hitting' the target even in a changing anatomy. However, a consequence of using large margins is the exposure of the surrounding healthy tissue to high doses of radiation, and thereby, increasing the risk of both acute and late side effects. Various image-guided radiation therapy (IGRT) techniques have been developed to *verify* the target volume (or a surrogate thereof) and guide the treatment setup process. The implementation of IGRT approaches allow for the use of smaller margins for uncertainty, resulting in a subsequent reduction in integral dose to the surrounding tissue. The latter is even more important when delivering ablative radiation doses, such as in stereotactic ablative radiotherapy (SABR) or stereotactic body radiation therapy (SBRT). IGRT techniques have been widely adopted in clinical practice. In addition, adaptive radiation therapy (ART) techniques have emerged with the aim of *adapting* treatment plans in response to anatomical or functional changes in either target volumes or organs-at risk (OARs). Such changes can occur at different time scales, ranging from seconds (i.e. intrafractional) to days or weeks (i.e. interfractional)[2].

Offline ART refers to the adaptation of a radiotherapy plan based on images acquired during the course of treatment, for delivery during a subsequent treatment session. Offline ART has been used to address large systematic changes such as patient weight loss, tumor shrinkage or volume increase after delivery of several treatment fractions. This approach has been shown in prospective clinical studies for head and neck-, prostate- and lung cancer to yield improved target coverage and/or

OAR sparing[3–5]. However, many anatomical changes are random and occur within a shorter time frame, making offline ART inadequate. A more suitable method to account for interfractional changes is to adapt treatment plans based on a patient's anatomy-of-the-day while in the pre-treatment position (online ART). The dosimetric benefits of online ART vary between patients and depend on treatment delivery strategies, but it often improves target coverage or OAR sparing, or a combination of the two.

Despite the potential advantages of online ART, clinical adoption was not widespread until recently due to its time- and resource-intensive nature, but mainly due to the poor soft tissue contrast available using on-treatment couch CT based imaging. The clinical availability of MR-linacs represents a revolution in radiation therapy as MR-imaging permits high-resolution soft tissue-based setup, a more accurate definition of OAR's, and it can also allow continuous planar imaging of the target during delivery[6,7] (Figure 1). IGRT capabilities on MR-linacs have now led to a growing confidence among clinicians in the delivery of high radiation doses, with even smaller confidence margins at sites where anatomy is continuously changing. This development in online ART using the so-called adaptive MR-guided radiation therapy (MRgRT) approach, has been facilitated by availability of hardware platforms and computational advances that allow for fast adaptation of contours with deformable image registration (DIR) and Monte Carlo dose recalculations, incorporating the effect of magnetic fields, to be performed within minutes[8,9].

The MRgRT treatment process broadly consists of pre-treatment high-resolution imaging, image co-registration, re-contouring of target and OAR's, treatment plan re-optimization and QA, followed by treatment delivery under image guidance, all performed while the patient is in treatment position (Figure 2).

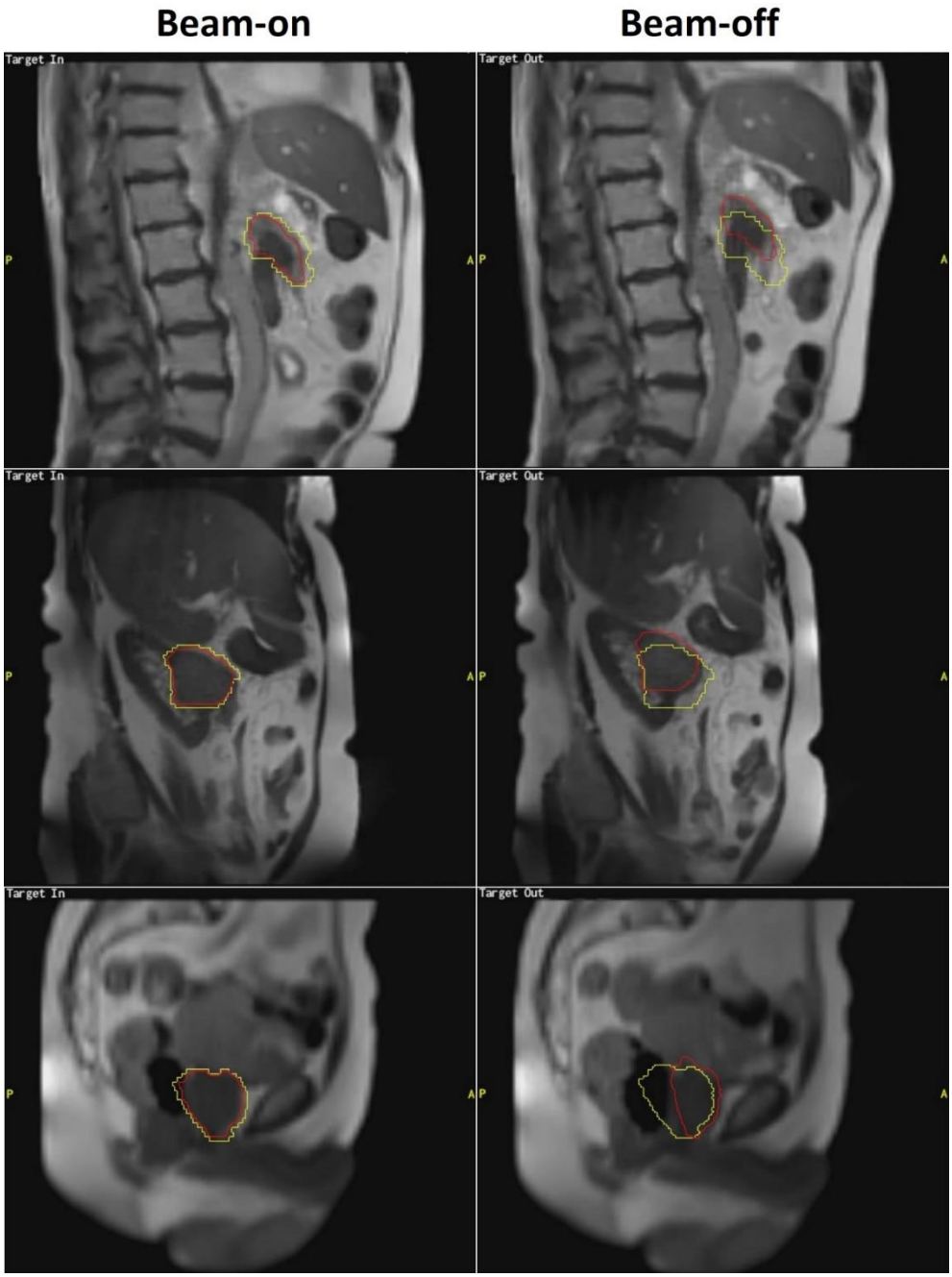

Figure 1: *Sagittal planes for tumor tracking during radiation delivery, in pancreas (upper panel), kidney (middle panel) and prostate (lower panel) patients. The gating target (GTV or CTV; green contour) and the gating boundary (red contour) are visualized on-screen. The geometric coverage ("Target in" or" Target out") is continuously displayed in the left upper corner.*

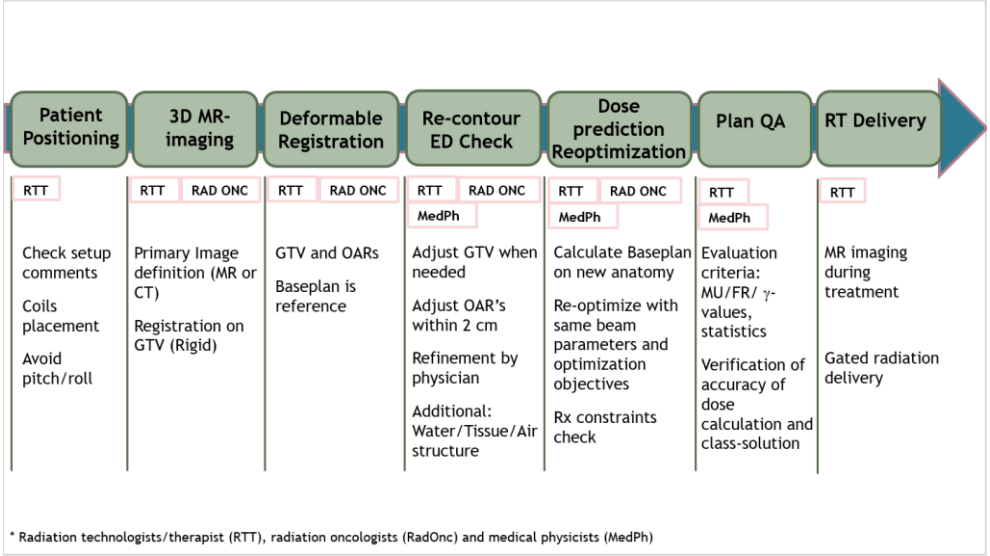

Figure 2: *The online adaptive MRgRT workflow used in clinical practice. Abbreviations: RTT = Radiation technologist/therapist, RadOnc = radiation oncologist, MedPh = medical physicists, MR = magnetic resonance, CT = computerized tomography, GTV = gross tumor volume, OARs = organs at risk, MU = monitor unit, γ values = values from gamma (pass-fail) analysis.*

The steps in Figure 2 represent logistical challenges that are time sensitive. Different strategies have been clinically adopted for performing adaptive MRgRT. In order to decide if there is a need for plan adaptation for a particular fraction, some departments have used a visual review by the radiation oncologist and/or physicist of the daily MR images[10], and also dosimetry of the superimposed baseline plan[11]. As the available deformable contour propagation methods are imperfect, manual contour adjustment is needed before detailed re-assessment of dosimetry is complete. Consequently, the editing of contours remains a major bottleneck in online ART.

When the Amsterdam UMC became one of the early adopters of MRgRT in early 2016, our strategy was to treat patients using only SABR, and to aim for daily online plan adaptation as the default procedure. This led to the development of in-house approaches for each step in the MRgRT process in order to ensure a practical and

feasible workflow. For the latter purpose, we defined workflows and planning strategies to streamline our online ART process by; 1) standardizing workflow for each tumor site; 2) routinely generating and using a re-optimized plan for each fraction, unless the latter was clearly inferior to the baseline plan; 3) performing only limited OAR recontouring by physicians, and not full organ contouring; 4) creating robust treatment plans at baseline which can lead to a new re-optimized plan online with one single optimization.

The strategy which had the greatest role in facilitating implementation of daily adaptive MRgRT at the Amsterdam UMC was our decision to account for only high dose regions in OARs as being relevant for MRgRT. This approach is justified by the fact that high dose regions in OAR's correlate well with the risk of serious complications and toxicity. Consequently, we restricted the review and any re-contouring of contours of adjacent OARs only when these were located within 2-3 cm of the PTV, an area where approximately ≥35% of the prescribed fraction dose is distributed. For treatments on the ^{60}Co version of the MRIdian machine, this corresponded to an area of 3 cm. Given the steeper dose gradient for the ViewRay MR-Linac, this region for OAR contouring is reduced to 2 cm. The procedure developed for our approach has been described in detail in Chapter 2, and it relies on partitioning and combining OAR contours located at 6, 12 and 20 mm from the PTV in order to allow for spatial control of the dose distribution. A baseline treatment plan is generated using planning objectives that ensure PTV coverage, and for avoiding the partitioned OAR structures, where the steepest dose gradients are placed. For online plan adaptation, all plan parameters and optimization objectives are kept unchanged, but the structures used in the optimization are modified according to the anatomy of that particular day. This approach allows for the

steepest dose gradients to be re-directed to the current OAR positions with a single re-optimization.

The Amsterdam UMC has had experience with use of volumetric modulated arc therapy (VMAT)- based SABR for various tumor sites. When preparing the workflow for our MRIdian Co^{60} MRgRT protocol, we succeeded in generating IMRT SABR treatment plans of similar quality to our routine VMAT based SABR plans[12], a finding attributed among others to the double focused MLC system that is designed to sharpen ^{60}Co beams. Some differences observed between plans derived using both techniques included minor increases in PTV heterogeneity and slight increase in low-dose volumes in the MRgRT plans[13]. We also demonstrated that our OAR partitioning method generates similar quality baseline plans compared to the traditional planning approach using fully contoured OAR's (Chapter 2). During online re-optimization using only a single optimization step, our approach almost always fulfilled institutional constraints, and resulted in lower doses to OARs than plans where full OARs contouring had been performed. This described approach has been performed in our center for more than 1200 patients and 6000 fractions in tumor sites such as the prostate, pancreas, high-risk lung cancer, renal- and adrenal lesions, and liver metastases (Figure 3). The vast majority of fractions (≥ 93%) have been delivered using the re-optimized plan. An obvious advantage of our OAR partitioning method is the relatively fast workflow, with plan adaptation, including re-contouring, re-optimization and independent QA of the generated plan, adding approximately 15 minutes to the total workflow. Our approach for online adaptive MRgRT has now been clinically implemented by many institutions worldwide[14–16]. Depending on the clinical indication for online ART, similar findings on the time required for adaptive planning have been reported in the recent MRgRT literature[10,17–19].

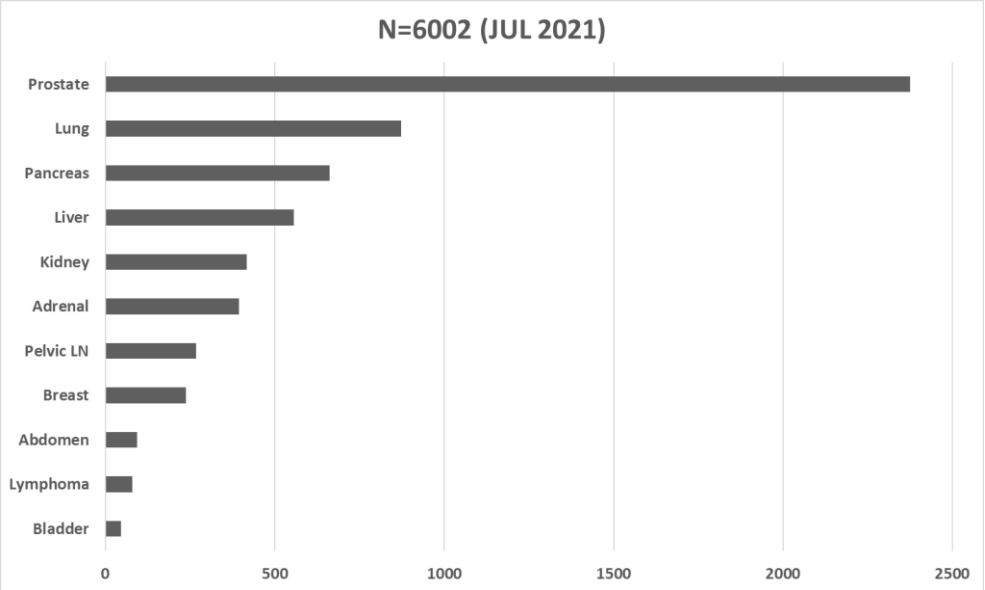

Figure 3. *Clinical indications and number of fractions clinically treated using MRgRT at Amsterdam UMC.*

Figure 4 shows the typical time required for each step in our current online adaptive MRgRT workflow, and the re-contouring phase of the OAR's and small adjustments to the GTV, remaining the most time consuming phase in MRgRT.

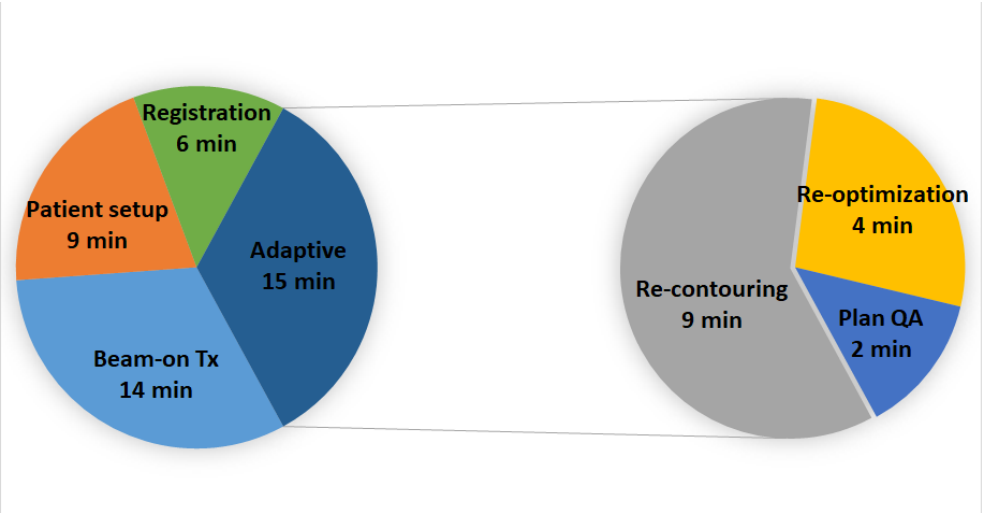

Figure 4: *The average time required for steps in the adaptive MRgRT process (N=150 fx in different target groups).*

Substantial improvement in software for deformable contour propagation are required in order to improve the workflow. Proposed solutions to reduce contouring times are automated contouring using artificial intelligence and deep learning[20,21]. The latter is an already active area of research, but features for online adaptive MRgRT that could improve the accuracy of autocontouring are the specific weighting of the patient's own baseline anatomy for subsequent fractions rather than using a pooled database. In addition, a focus on the OAR areas around the PTV could speed up the process. A drawback of our limited OAR approach is the inability to evaluate regions of low radiation dose exposure, and for comparisons with existing relative volume constraints for the entire OAR. In addition, the OAR partitioning approach requires an extra plan QA step to check on plan robustness, which refers to a process to determine whether the plan, contours and constraints also work in a virtually changed anatomy.

The clinical implementation of daily adapted MRgRT constitutes a major logistic challenge for departments also because the need for the physician and/or physicist to be present at the treatment console for re-contouring, plan review and approval. In addition, daily adapted MRgRT requires time slots of 45 to 60 minutes for SABR delivery, thereby limiting both the number of patients that can be treated per day and restricting daily adaptation to hypofractionated treatments. Until such time that treatment times can be reduced substantially, it is essential to quantify the dosimetric and clinical benefits, and to identify patients groups that are most likely to benefit from this approach. Table 1 summarizes the overall dosimetric benefit of online ART at the Amsterdam UMC with regards to target coverage and compliance with OAR objectives for various tumor sites. It is evident that plan adaptation succeeds in improving both OAR sparing and target coverage for all tumor sites.

Table 1. *Overall benefit of plan adaptation for different tumor sites at Amsterdam UMC. Figures represent the percentage of fractions not fulfilling the defined plan constraints.*

	Non-adaptive		Adaptive	
	Target volume (GTV)	OARs	Target volume (GTV)	OARs
Prostate	33%	8%	3%	2%
Pancreas	32%	29%	15%	1%
Adrenal	37%	27%	23%	4%
Kidney	3%	14%	0%	1%

Of note is the relatively poorer target coverage in pancreatic (5 x 8 Gy) and adrenal tumor locations (5 x 10 Gy) as a result of the proximity of OAR's with fixed high-dose constraints. In addition, our studies described in Chapters 4-6 revealed that not all patients at any particular tumor site benefit to the same extent. Subgroups not requiring daily plan adaptation could be identified for all abdominal tumor sites, thereby allowing for clustering of such patients in order to permit a more efficient planning of patients and resources on the MR linac.

Currently, intrafraction changes due to breathing motion are accounted for with DIR-based target tracking and gating. It is also possible to visualize the position of OARs in a 2D MR cine in the sagittal plane with the MRIdian system. In addition, this system allows for 2D corrections (cranial-caudal or anterior-posterior) for smaller intrafractional variations that are visualized on a sagittal plane during treatment delivery. During the relatively long duration of SABR delivery, 2D shifts are performed during approximately 10-20% of treatment fractions. Current workflows for performing both 2D and 3D corrections are time consuming, and faster software solutions are needed to improve setup corrections. For larger displacements, or when a lateral movement is suspected, a volumetric MR scan is

acquired in order to perform a 3D correction. Future developments should allow intrafractional tracking or gating in multiple planes in order to detect displacements in all directions, particularly as intrafraction motion of GI organs can be significant and should be taken into account during the adaptive MRgRT[22,23]. To account for large intrafractional changes where there is for instance, a systematic shift in the position of OARs, intrafractional plan adaptation would be required.

Another shortcoming of the current MRgRT workflow is the absence of robust real-time (intrafractional) dose accumulation and contouring capabilities. In Chapter 7 of this thesis, we simulated intrafractional adaptation partitioning of all fractions, each with half the original fraction dose. Between successive deliveries, the patient remained in the treatment position and all steps of the initial plan adaptation were repeated. Thus, this second re-optimization served as an intrafractional plan adaptation at 50% of the total delivery. In this case study, interfractional changes in adjacent OARs were larger than intrafractional changes. However, the 'intrafractional' re-optimization appeared to be equally important to correct inappropriately high doses to the adjacent duodenum as a result of OAR displacement during delivery. Although steps required for repeated re-optimization prolonged treatment duration to 90 minutes, this simplified approach may be useful in selected cases where high doses to adjacent OARs are regarded as critical. Solutions to increase the speed of intrafractional re-optimization would be of great benefit.

Current tumor control and normal tissue complication probability such as the QUANTEC data are derived using dosimetry based on 'snapshot' images of patient anatomy projected on a single pre-treatment planning CT scan[24]. Interfractional anatomical changes can introduce an inherent uncertainty in dose-toxicity modelling[25]. To improve the accuracy of the tumor control and normal tissue

complication probability models, the availability of volumetric MR imaging before each fraction, used with in combination with our validated DIR strategy (Chapter 8) can provide an unique opportunity to realistically measure the total accumulated delivered dose. This DIR strategy has successfully been applied to data from one hundred patients treated for prostate cancer, deriving accumulated (delivered) bladder dose parameters (V_{20Gy}-$V_{32.6Gy}$). The accumulated bladder dose parameters were superior for predicting acute treatment-related urinary toxicity, as opposed to the same baseline constraints. This finding opens the door for personalized approaches using prospective dose accumulation for each subsequent fraction. Such a personalized approach would allow for changes to adaptation priorities for subsequent fractions in response to accumulated doses of OARs and/or the target volume, potentially allowing for safer Isotoxic dose-escalation, and ultimately for refining dose-toxicity parameters based on real dosimetry.

In conclusion, daily adaptive MRgRT has been implemented into clinical practice by developing a novel practical workflow using among others partitioned OAR volumes rather than full contouring. Plan adaptation has been shown to be beneficial for the majority of tumor sites, although better definition of patients actually having a dosimetric benefit is still warranted. Future practical developments that would enable increased utilization are summarized in Table 2.

Table 2: *Developments that can improve delivery of adaptive MRgRT*

- Artificial intelligence/deep learning for improved autocontouring
- Multiplanar gating/tumor contour tracking during delivery
- Higher dose rate delivery
- Improved methods for intrafraction dose re-optimization
- Dose accumulation in tumor and organs at risk during each fraction
- Additional MR sequences for use in target definition and response monitoring

References

1. Njeh, C. F. Tumor delineation: The weakest link in the search for accuracy in radiotherapy. *Journal of Medical Physics* vol. 33 136–140 (2008).
2. Sheng, Y., Li, T., Lee, W. R., Yin, F. F. & Wu, Q. J. Exploring the Margin Recipe for Online Adaptive Radiation Therapy for Intermediate-Risk Prostate Cancer: An Intrafractional Seminal Vesicles Motion Analysis. *Int. J. Radiat. Oncol. Biol. Phys.* **98**, 473–480 (2017).
3. Schwartz, D. L. *et al.* Adaptive radiotherapy for head and neck cancer - Dosimetric results from a prospective clinical trial. *Radiother. Oncol.* **106**, 80–84 (2013).
4. Ahunbay, E. E. *et al.* Online adaptive replanning method for prostate radiotherapy. *Int. J. Radiat. Oncol. Biol. Phys.* **77**, 1561–1572 (2010).
5. Spoelstra, F. O. B., Pantarotto, J. R., van Sörnsen de Koste, J. R., Slotman, B. J. & Senan, S. Role of Adaptive Radiotherapy During Concomitant Chemoradiotherapy for Lung Cancer: Analysis of Data From a Prospective Clinical Trial. *Int. J. Radiat. Oncol. Biol. Phys.* **75**, 1092–1097 (2009).
6. Mutic, S. & Dempsey, J. F. The ViewRay System: Magnetic Resonance-Guided and Controlled Radiotherapy. *Seminars in Radiation Oncology* vol. 24 196–199 (2014).
7. Lagendijk, J. J. W., Raaymakers, B. W. & van Vulpen, M. The Magnetic Resonance Imaging-Linac System. *Semin. Radiat. Oncol.* **24**, 207–209 (2014).
8. Kawrakow, I. Accurate condensed history Monte Carlo simulation of electron transport. I. EGSnrc, the new EGS4 version. *Med. Phys.* **27**, 485–498 (2000).
9. Ziegenhein, P., Kozin, I. N., Kamerling, C. P. & Oelfke, U. Towards real-time photon Monte Carlo dose calculation in the cloud. *Phys. Med. Biol.* **62**, 4375–4389 (2017).
10. Tyran, M. *et al.* Retrospective evaluation of decision-making for pancreatic stereotactic MR-guided adaptive radiotherapy. *Radiother. Oncol.* (2018) doi:10.1016/j.radonc.2018.08.009.
11. Acharya, S. *et al.* Online Magnetic Resonance Image Guided Adaptive Radiation Therapy: First Clinical Applications. *Int. J. Radiat. Oncol.* **94**, 394–403 (2016).
12. Bohoudi, O. *et al.* OC-0519: Radiotherapy plan quality using a double focused, double stacked multi-leaf collimator. *Radiother. Oncol.* **127**, S273 (2018).
13. Wooten, H. O. *et al.* Quality of Intensity Modulated Radiation Therapy Treatment Plans Using a (60)Co Magnetic Resonance Image Guidance Radiation Therapy System. *Int. J. Radiat. Oncol. Biol. Phys.* **92**, 771–8 (2015).
14. Olberg, S. *et al.* Optimization of treatment planning workflow and tumor coverage during daily adaptive magnetic resonance image guided radiation therapy (MR-IGRT) of pancreatic cancer. *Radiat. Oncol.* **13**, (2018).
15. Werensteijn-Honingh, A. M. *et al.* Feasibility of stereotactic radiotherapy using a

1.5 T MR-linac: Multi-fraction treatment of pelvic lymph node oligometastases. *Radiother. Oncol.* **134**, 50–54 (2019).

16. Boldrini, L. *et al.* MR-Guided Radiotherapy for Liver Malignancies. *Front. Oncol.* **11**, 1–13 (2021).
17. Henke, L. *et al.* Phase I trial of stereotactic MR-guided online adaptive radiation therapy (SMART) for the treatment of oligometastatic or unresectable primary malignancies of the abdomen. *Radiother. Oncol.* **126**, 519–526 (2018).
18. Henke, L. E. *et al.* Online Adaptive MR Guided Stereotactic Body Radiation Therapy for the Treatment of Oligometastatic Disease of the Abdomen and Central Thorax: Characterization of Potential Advantages. *Int. J. Radiat. Oncol.* **93**, S20–S21 (2015).
19. Güngör, G. *et al.* Time Analysis of Online Adaptive Magnetic Resonance–Guided Radiation Therapy Workflow According to Anatomical Sites. *Pract. Radiat. Oncol.* **11**, e11–e21 (2021).
20. Chen, Y. *et al.* Fully automated multiorgan segmentation in abdominal magnetic resonance imaging with deep neural networks. *Med. Phys.* **47**, 4971–4982 (2020).
21. Fu, Y. *et al.* A novel MRI segmentation method using CNN-based correction network for MRI-guided adaptive radiotherapy. *Med. Phys.* **45**, 5129–5137 (2018).
22. Liu, L. *et al.* Modeling intra-fractional abdominal configuration changes using breathing motion-corrected radial MRI. *Phys. Med. Biol.* **66**, 85002 (2021).
23. van Sörnsen de Koste, J. R. *et al.* Changes in gastric anatomy after delivery of breath-hold MR-guided SABR for adrenal metastases. *Radiother. Oncol.* **152**, 26–29 (2020).
24. Jaffray, D. A., Lindsay, P. E., Brock, K. K., Deasy, J. O. & Tomé, W. A. Accurate Accumulation of Dose for Improved Understanding of Radiation Effects in Normal Tissue. *Int. J. Radiat. Oncol. Biol. Phys.* **76**, 135–139 (2010).
25. Shelley, L. E. A. *et al.* Delivered dose can be a better predictor of rectal toxicity than planned dose in prostate radiotherapy. *Radiother. Oncol.* **123**, 466–471 (2017).

Summary

Summary

Summary

MR-guided radiation therapy (MRgRT) has become a clinical reality in recent years in several centers worldwide and has been available at the Amsterdam UMC since May 2016, with the introduction of the MRIdian system (ViewRay Inc., Mountain View, USA). MRgRT involves high-resolution MR-imaging, daily re-optimization (i.e. adaptation) of the baseline treatment plans to correct for changes in daily anatomy and real-time cine MRI for intra-fraction motion management. This thesis describes aspects of developing a novel method for adaptive planning, as well as evaluating the benefit of plan adaptation in different patient groups.

In **Chapter 2,** an in-house developed strategy is described for robust and fast online adaptation that is in clinical use at our institution. This strategy relies on robust prediction of optimization objectives obtained by building an artificial neural network (ANN), deformable image registration (DIR) and physician's review of (organs at risk) OARs within the first few cm's from the planning target volume (PTV). For (adaptive) treatment planning, OAR contours are partitioned in separate portions to allow for spatial control of the dose distribution. In this chapter, we showed that this method generates similar quality baseline plans compared to the traditional planning approach using fully contoured OARs. During online re-optimization using only a single optimization step, our approach almost always fulfilled institutional constraints, and resulted in lower doses to OARs while requiring only limited online (re-) contouring from clinicians.

In prostate cancer radiotherapy, the superior soft tissue imaging capability of MRgRT improves the visualization of the prostate, the base of seminal vesicles and surrounding organs at risk, allowing precise soft tissue setup, real-time planar

imaging and gated delivery with minimal safety margins. In **chapter 3** we describe our clinical experience of such daily online adaptive MRgRT workflow for SBRT in prostate cancer. In this chapter, we reported on the extended time slots needed for the clinical MRgRT workflow and the frequency of online corrections because of intra-fractional variations in the prostate position. Patient reported outcomes and results from patient-specific QA showed that adaptive MRgRT was well tolerated, a modest proportion of patients reported light complaints of noise.

MRgRT with daily plan adaptation is a time- and resource-intensive treatment. It is therefore essential to quantify the dosimetric and clinical benefits, and to identify patient groups that are most likely to gain from this approach. In **chapter 4,** we analyzed the benefit in target coverage and OAR sparing of daily plan adaptation in 36 consecutive locally advanced pancreatic cancer patients treated with MRgRT to 40Gy in 5 fractions. The percentage of plans fulfilling institutional constraints increased from 43.9% (non-adapted plans) to 83.3% after online plan adaptation, with significant improvements in GTV coverage and lower V_{33Gy} OAR doses. Daily plan adaptation was overall beneficial in 52.8% of fractions and appeared less important in cases where there was ≥3 mm distance between the tumor and relevant OARs. This information can be used for pretreatment selection of LAPC patients in the logistical challenges associated with adaptive MRgRT, including daily re-contouring, plan review and approval.

Chapter 5 describes an analysis of inter-fractional changes in GTV and OARs and the role of online plan re-optimization in ensuring both adequate target coverage and OAR sparing for adrenal gland metastases. Significant inter-fractional changes in OAR positions were observed despite breath-hold radiation delivery under MR-guidance. Maximum volume changes for the stomach, bowel and duodenum within 3 cm of PTV were 23.8, 20.5, and 20.9 cm^3, respectively. Center of mass displacements

of 17, 27 and 36 mm were observed for stomach, bowel and duodenum, respectively. Baseline plans recalculated on anatomy-of-the-day revealed a suboptimal target coverage and undue exposure of the OARs to high doses of radiation, leading to a failure to meet institutional constraints in a third of all fractions. Online re-optimization improved target coverage in 63% of fractions and reduced the number of fractions not meeting the $V_{95\%}$ objective. Furthermore, plan re-optimization ensured that the high-dose OAR constraints were met in nearly all fractions.

In chapter 6, we evaluated the clinical impact of stereotactic MRgRT and routine plan re-optimization for 36 patients with large primary renal cell carcinoma. Our evaluation showed good oncological results with minimal side-effects. In this patient group daily plan re-optimization was required for only 14.1% of fractions mainly because of exceeding OAR constraints. In 83.9% of fractions the predicted plans (without re-optimization) met all institutional target and OAR constraints and was of similar quality as the re-optimized plans. Thus, daily plan re-optimization was required for only a minority patients, who could be identified by a higher volume (0.5cc) of normal organs receiving 25 Gy in baseline plans. Clustering of subgroups not requiring daily plan adaptation can permit a more efficient planning of patients and resources on the treatment console.

Interfractional plan adaptation has been routinely performed for almost each patient and each fraction at our center. However, the extent of intra-fractional changes in relevant OARs during radiation delivery and the need for intra-fractional plan adaptation is unknown. In **chapter 7,** we described in a case report our first attempt to quantify the relative importance of inter- and intra-fractional plan adaptation. Fixed fraction partitioning was used to perform intra-fractional plan adaptation, in this case, at 50% of total fraction delivery. In between successive deliveries, the patient remained in the treatment position and all steps of the initial plan adaptation

were repeated. The second re-optimization served as an intra-fractional plan adaptation at 50% of the total delivery. We evaluated the practical feasibility of this approach in a patient treated with MRgRT for locally advanced pancreatic cancer. Inter-fractional changes in surrounding OARs were larger than intra-fractional changes. However, the 'intra-fractional' re-optimization appeared to be equally important to correct inappropriately high doses to the adjacent duodenum because of OAR displacement during delivery. Although steps required for repeated re-optimization prolonged treatment duration to 90 minutes, this simplified approach may be useful in selected cases where high doses to adjacent OARs are critical.

Parallel with recent technological advancements for in room image guidance, there has been a growing interest in DIR-based dose accumulation for adaptive radiation therapy. **Chapter 8** provides an evaluation of our DIR-based dose accumulation strategy to ensure an accurate reconstruction of the total delivered dose. An anthropomorphic phantom of the human pelvic region was used to simulate a SBRT prostate cancer treatment course. Empirical validation of dose accumulation using our strategy in MR-guided SBRT for prostate cancer obtained a good agreement with reference film measurements, with an average deviation of -0.6% and 0.3% for bladder and rectal surfaces, respectively, when using a contour-based DIR approach.

Despite the increased clinical use of SABR for PC, there is limited data on the relation between the actual delivered dose and toxicity. In **Chapter 9,** we aimed to identify dose parameters correlated with acute urinary toxicity based on the total accumulated delivered bladder dose. For this purpose, we deployed our DIR-based dose accumulation strategy described in **Chapter 8** to reconstruct the actual delivered dose in 101 prostate cancer patients treated within a prospective phase 2 toxicity study with stereotactic adaptive MRgRT. The $V_{20Gy-32Gy}$ from the total accumulated delivered bladder dose was superior in predicting acute treatment

related increase in urinary symptoms, with area under the curve (AUC) values ranging from 0.71 to 0.75. In contrast, baseline dosimetry showed a poor correlation with AUC values between 0.53 and 0.62. For future personalization, we also studied whether prospective bladder dose accumulation (approximately halfway during treatment) could be used as an early predictor of urinary toxicity, in which case this could be used to further optimize MRgRT for the remaining fractions. Prospective dose accumulation using the first delivered fractions showed large similarities in correlation (and constraints) for acute increase of urinary symptoms with those of the total delivered dose. This suggests that prospective dose accumulation using the first delivered fractions guided by interim bladder constraints may be used to adapt remaining fractions with the goal to reduce the risk of acute urinary toxicity.

Samenvatting

Samenvatting

Magnetic resonance imaging (MRI) gestuurde radiotherapie (MRgRT) is de afgelopen jaren een klinische realiteit geworden in verschillende centra wereldwijd. Met de introductie van het MRIdian systeem (ViewRay Inc., Mountain View, USA) is MRgRT sinds mei 2016 beschikbaar in het Amsterdam UMC. Deze techniek omvat hoge-resolutie MR-beeldvorming, dagelijkse re-optimalisatie van de *baseline* behandelplannen om te corrigeren voor veranderingen in de dagelijkse anatomie en intra-fractie veranderingen middels real-time cine MRI. Dit proefschrift beschrijft aspecten van het ontwikkelen van een nieuwe methode voor adaptieve planning, alsmede het evalueren van het voordeel van planaanpassing bij verschillende patiëntengroepen.

In **hoofdstuk 2** wordt een zelf ontwikkelde strategie beschreven voor robuuste en snelle online plan adaptatie die in onze kliniek wordt gebruikt. Deze strategie berust op een voorspelling van robuuste optimalisatie parameters verkregen door het bouwen van een *artificial neural network* (ANN), *deformable image registration* (DIR) en beoordelen en contouren van de *organs at risk* (OARs) door de arts binnen een afstand van 3 cm vanaf het *planning target volume* (PTV). Voor het (adaptive) treatment planning proces worden deze OAR-contouren opgedeeld in afzonderlijke delen om ruimtelijke controle van de dosisverdeling mogelijk te maken. Dit hoofdstuk laat onder andere zien dat deze methode een *baseline* behandelplan genereert van vergelijkbare kwaliteit als de traditionele planningsbenadering met volledig ingetekende OARs. Tijdens het online re-optimalisatie proces voldeed onze aanpak bijna altijd aan de institutionele voorschriften na slechts een enkele optimalisatie poging, resulterend in lagere doses voor OARs terwijl beperkte online (re-) contouring/aanpassing van clinici nodig was.

Bij MR-gestuurde radiotherapie van de prostaat zorgt het superieure beeldvormingsvermogen van de weke delen van de MR voor een verbetering van

de visualisatie en plaatsbepaling van de prostaat, de basis van de zaadblaasjes en andere omliggende OARs. Tevens maakt MRgRT *real-time* beeldvorming en *gated* bestraling met beperkte veiligheidsmarges mogelijk. In **hoofdstuk 3** wordt onze klinische ervaring met de dagelijkse online adaptieve MRgRT workflow voor SBRT bij patiënten met prostaatkanker beschreven. In dit hoofdstuk rapporteren we over de langere behandeltijd die nodig is voor deze workflow en de frequentie van online correcties vanwege intra fractionele variaties in de prostaatpositie. Uit prospectief verzamelde vragenlijsten, gericht op het verdragen en het comfort van de patiënt tijdens MRgRT blijkt dat adaptieve MRgRT goed werd verdragen, waarbij een beperkt deel van deze patiënten lichte klachten meldde van geluidsoverlast.

Adaptieve MRgRT is een behandeling die veel tijd en middelen kost. Het is daarom van essentieel belang om de dosimetrische en klinische voordelen te kwantificeren en om patiëntengroepen te identificeren die het meeste baat lijken te hebben bij deze benadering. In **hoofdstuk 4** wordt het voordeel van dagelijkse aanpassing van het behandelplan geanalyseerd bij 36 opeenvolgende patiënten met *locally advanced pancreascarcinoom* (LAPC), die werden behandeld middels MRgRT tot 40 Gy in 5 fracties. Het percentage plannen dat voldeed aan de voorgeschreven voorwaarden steeg van 43,9% (niet-aangepaste plannen) tot 83,3% van de fracties na online planaanpassing, met aanzienlijke verbeteringen in GTV dekking en lagere V_{33Gy} in OARs. Dagelijkse planaanpassing was over het algemeen gunstig in 52,8% van de fracties en bleek minder belangrijk in gevallen waar er ≥3 mm afstand was tussen de tumor en nabije OARs, zoals het duodenum en de maag. Deze informatie kan worden gebruikt voor de triage van LAPC-patiënten, waarbij gedacht kan worden aan eventuele aanpassingen van de logistieke uitdagingen die gepaard gaan met adaptieve MRgRT, zoals bijvoorbeeld dagelijkse re-contouring, planbeoordeling en goedkeuring.

Hoofdstuk 5 beschrijft een analyse van inter-fractionele veranderingen in GTV en OAR's en de rol van online plan re-optimalisatie bij het waarborgen van zowel adequate dekking van het doelgebied als het sparen van OARs bij bijniermetastasen. Bij *breath-hold* bestraling onder MR-geleiding werden significante inter-fractionele veranderingen in OAR-posities waargenomen. Maximale volumeveranderingen voor maag, darm en duodenum binnen 3 cm van de PTV waren respectievelijk 23.8, 20.5 en 20.9 cm3. Verschuivingen van 17, 27 en 36 mm van het *center of mass* (COM) werden waargenomen voor respectievelijk maag, darm en duodenum. Herberekende *baseline* plannen op basis van de anatomie van de dag toonden een suboptimale dekking van het doelgebied en een overmatige blootstelling van de OAR's aan hoge stralingsdoses, waardoor een derde van de fracties niet aan de voorgeschreven voorwaarden voldeed. Online re-optimalisatie verbeterde de dekking van het doelgebied in 63% van de fracties waardoor het aantal fracties dat niet aan de V95% voorschriften voldeed afnam. Bovendien zorgde de re-optimalisatie van het plan ervoor dat in bijna alle fracties de hoge dosis voorwaarden van de OARs werden gehaald.

Hoofdstuk 6 bevat een evaluatie van de klinische impact van stereotactische MRgRT en routine plan re-optimalisatie voor 36 patiënten met een primair niercelcarcinoom. Onze evaluatie toonde goede oncologische resultaten, waarbij sprake is van een hoge lokale controle van de ziekte met minimale bijwerkingen tijdens en door de behandeling. In deze patiëntengroep was dagelijkse plan re-optimalisatie nodig voor slechts 14,1% van de fracties, voornamelijk wegens overschrijding van de OAR *constraints*. In 83,9% van de fracties voldeden de niet aangepaste plannen (zonder re-optimalisatie) aan alle voorgeschreven voorwaarden voor wat betreft dekking van het doelgebied en sparing van de OARs en was de kwaliteit vergelijkbaar met de opnieuw geoptimaliseerde plannen. In een minderheid van de patiënten was

dagelijkse re-optimalisatie van het plan nodig. Deze groep kon geïdentificeerd worden doordat in het baselineplan meer dan 0.5cc van een van de OARs 25 Gy of meer kreeg. Het klusteren van subgroepen die geen dagelijkse planaanpassing vereisen, kan een efficiëntere planning van patiënten en middelen op het bestralingstoestel mogelijk maken.

Interfractionele planaanpassing wordt in ons centrum routinematig uitgevoerd voor bijna elke patiënt en elke fractie. De mate van intra fractionele veranderingen in relevante OARs tijdens bestraling en de noodzaak voor intra fractionele planaanpassing is echter nog onbekend. In **hoofdstuk 7** beschrijven wij in een case report onze eerste poging om het relatieve belang van inter- en intra fractionele planaanpassing te kwantificeren. In deze casus werd er gebruik gemaakt van een vaste fractieverdeling om intra fractionele planaanpassing uit te voeren, in dit geval bij 50% van de totale afgegeven fractie dosis. Tussen de opeenvolgende toedieningen bleef de patiënt in de behandelpositie en werden alle stappen van de initiële planaanpassing herhaald. De tweede re-optimalisatie diende als een intra-fractionele planaanpassing bij 50% van de totale toegediende dosis. De praktische uitvoerbaarheid van deze aanpak werd geëvalueerd bij een patiënt die met MRgRT werd behandeld voor LAPC. Interfractionele veranderingen in omliggende OARs waren groter dan intra fractionele veranderingen. De intra fractionele re-optimalisatie bleek echter even belangrijk voor correctie van onacceptabele hoge doses aan het aangrenzende duodenum tijdens de behandeling. Hoewel de vereiste stappen voor herhaalde re-optimalisatie de behandelingsduur verlengde tot 90 minuten, kan deze vereenvoudigde aanpak nuttig zijn in geselecteerde gevallen waarin hoge doses voor aangrenzende OAR's zeer kritisch zijn, bijvoorbeeld in het geval van herbestraling.

Parallel aan de recente technologische vooruitgang op het gebied van beeldgeleide radiotherapie, is er een groeiende belangstelling voor op DIR gebaseerde dosisaccumulatie voor adaptieve radiotherapie. **Hoofdstuk 8** geeft een evaluatie van onze DIR gebaseerde dosisaccumulatiestrategie om een nauwkeurige reconstructie van de totale afgegeven dosis te verzorgen. Een antropomorfe fantoom van het menselijk bekkengebied werd gebruikt om een stereotactische MRgRT prostaatkanker behandeling te simuleren. Empirische validatie van dosisaccumulatie met behulp van onze strategie bij MR-geleide SBRT voor prostaatcarcinoom leverde een goede overeenkomst op met referentie filmmetingen, met een gemiddelde afwijking van -0,6% en 0,3% voor respectievelijk blaas- en rectale oppervlakken, bij gebruik van een contour-gebaseerde DIR benadering.

Ondanks het toegenomen klinische gebruik van stereotaxie bij patiënten met een prostaatcarcinoom zijn er beperkte gegevens over de relatie tussen de werkelijk toegediende dosis en de toxiciteit. In **Hoofdstuk 9** hebben wij ons gericht op het identificeren van dosisparameters die gecorreleerd zijn aan acute urinaire toxiciteit, gebaseerd op de totale geaccumuleerde afgegeven blaasdosis. Voor dit doel hebben wij onze DIR-gebaseerde dosisaccumulatiestrategie, zoals beschreven in hoofdstuk 8, gebruikt om de werkelijk toegediende dosis te reconstrueren bij 101 prostaatkankerpatiënten die werden behandeld binnen een prospectieve fase 2 toxiciteitsstudie met stereotactische adaptieve MRgRT. De $V_{20Gy-32Gy}$ van de totale geaccumuleerde afgegeven blaasdosis was superieur in het voorspellen van acute behandeling gerelateerde toename van urineweg symptomen, met *area under the curve* (AUC) waarden variërend van 0,71 tot 0,75. In tegenstelling tot de baseline dosimetrie, waarbij een slechte correlatie met AUC waarden tussen 0,53 en 0,62 werd gezien. Met het oog op toekomstige patiënt specifieke behandeling (*"personalized treatment"*) hebben wij ook bekeken of prospectieve accumulatie van de blaasdosis

(ongeveer halverwege de behandeling) kan worden gebruikt als een vroege voorspeller van urinaire toxiciteit, zodat dit kan worden gebruikt om de resterende fracties aan te passen. Prospectieve dosisaccumulatie gebruikmakend van de eerste toegediende fracties vertoonde een duidelijke overeenkomst met die van de totale toegediende dosis voor wat betreft toename van acute urinaire symptomen. Dit suggereert dat prospectieve dosisaccumulatie gebruikmakend van de eerst toegediende fracties op basis van tussentijdse nieuwe blaas *"constraints"* kan worden gebruikt om de resterende fracties aan te passen, met als doel het risico op acute urinaire toxiciteit te verminderen.

Curriculum Vitae

Curriculum Vitae

Curriculum Vitae

Omar Bohoudi was born on June 17th 1983 in Meknes, Morocco. He moved to Amsterdam at an early age and finished his secondary education at the Berlage Lyceum in Amsterdam in 2002. From youth, he developed an interest for science in healthcare and obtained a Bachelor's degree in 2008 from Inholland University (Haarlem) in medical imaging and radiation therapy techniques. He has worked from 2009 to 2016 as radiation therapy technologist at the Haagland Medical Center in The Hague and in the Amsterdam UMC. During those years, he specialized in treatment planning and was among others involved in the development of a predictive model for radiosurgery planning and plan QA, which was published in 2016. He continued his education during that period and obtained in 2017 a master's degree in medical physics at the University of Heidelberg in collaboration with the German Cancer Research Center (DKFZ). This master gave him a solid theoretical grounding in advanced cancer treatment techniques (IMRT, IGRT and proton and heavy ion therapy) and gained more in-depth knowledge during his practical training at the Heidelberg University Hospital and the Heidelberg Ion-Beam Therapy Center (HIT). Thereafter, he started his PhD at the Vrije University of Amsterdam for the implementation of MR-guided online adaptive radiotherapy at the Radiation Oncology Department of the Amsterdam UMC. During his PhD, he has presented his work several times in international conferences and has contributed to several publications in this field. His main work has been presented in this thesis, with the title: "Adaptive MR-guided Radiotherapy: from concept to routine practice".

List of publications

List of publications

This thesis

Bohoudi, O., Bruynzeel, A. M. E., Senan, S., Cuijpers, J. P., Slotman, B. J., Lagerwaard, F. J., Palacios, M. A. Fast and robust online adaptive planning in stereotactic MR-guided adaptive radiation therapy (SMART) for pancreatic cancer. Radiotherapy and Oncology. 2017; 125: 439–44.

Tetar, S. U., Bruynzeel, A. M. E., Lagerwaard, F. J., Slotman, B. J., **Bohoudi, O**., Palacios, M. A. Clinical implementation of magnetic resonance imaging guided adaptive radiotherapy for localized prostate cancer. Physics and Imaging in Radiation Oncology. 2019; 9: 69-76.

Bohoudi, O., Bruynzeel, A. M. E., Meijerink, M. R., Senan, S., Slotman, B. J., Palacios, M. A., Lagerwaard, F. J. Identification of patients with locally advanced pancreatic cancer benefitting from plan adaptation in MR-guided radiation therapy. Radiotherapy and Oncology. 2017; 125: 439–44.

Palacios, M. A., **Bohoudi, O.**, Bruynzeel, A. M. E., van Sörsen de Koste, J. R., Cobussen, P., Slotman, B. J., Lagerwaard, F. J., Senan, S. Role of Daily Plan Adaptation in MR-Guided Stereotactic Ablative Radiation Therapy for Adrenal Metastases. International Journal of Radiation Oncology, Biology, Physics. 2018; 102: 426–433.

Tetar, S. U. & **Bohoudi, O.**, Senan, S., Palacios, M. A., Oei, S. S., van der Wel, A. M., Slotman, B. J., van Moorselaar, R. J. A., Lagerwaard, F. J., Bruynzeel, A. M. E. The role of daily adaptive stereotactic mr-guided radiotherapy for renal cell cancer. Cancers (Basel). 2020; 12(10), 2763

Lagerwaard, F., **Bohoudi, O**., Tetar, S., Admiraal, M. A., Rosario, T. S., & Bruynzeel, A. Combined Inter- and Intrafractional Plan Adaptation Using Fraction Partitioning in Magnetic Resonance-guided Radiotherapy Delivery. Cureus. 2018; 10: 1–11

Bohoudi, O., Lagerwaard, F. J., Bruynzeel, A. M. E., Niebuhr, N. I., Johnen, W., Senan, S., Slotman, B. J., Pfaffenberger, A., & Palacios, M. A. End-to-end empirical validation of dose accumulation in MRI-guided adaptive radiotherapy for prostate cancer using an anthropomorphic deformable pelvis phantom. Radiotherapy and Oncology. 2019; 141: 200-207.

Bohoudi, O., Bruynzeel, A. M. E., Tetar, S., Slotman, B. J., Palacios, M. A., Lagerwaard, F. J. Dose accumulation for personalized stereotactic MR-guided adaptive radiation therapy in prostate cancer. Radiotherapy and Oncology. 2021; 157:197-202

Other publications

Chen, H., Schneiders, F. L., M. E. Bruynzeel, A., Lagerwaard, F. J., van Sornsen de Koste, J. R., Cobussen, P., **Bohoudi, O.,** Slotman, B. J., Louie, A. V., & Senan, S. (2021). Impact of Daily Plan Adaptation on Organ-At-Risk Normal Tissue Complication Probability for Adrenal Lesions undergoing Stereotactic Ablative Radiation Therapy. Radiotherapy and Oncology. 2021; *in press*.

Corradini, S., Alongi, F., Andratschke, N., Azria, D., **Bohoudi, O.**, Boldrini, L., Bruynzeel, A., Hörner-Rieber, J., Jürgenliemk-Schulz, I., Lagerwaard, F., McNair, H., Raaymakers, B., Schytte, T., Tree, A., Valentini, V., Wilke, L., Zips, D., Belka, C. ESTRO-ACROP recommendations on the clinical implementation of hybrid MR-linac systems in radiation oncology. Radiotherapy and Oncology. 2021; 159: 146–154.

Hoffmans, D., Niebuhr, N., **Bohoudi, O.**, Pfaffenberger, A., Palacios, M. An end-to-end test for MR-guided online adaptive radiotherapy. Physics in Medicine and Biology. 2020; 65(12): 125012

Bohoudi, O., Bruynzeel, A. M., Senan, S., Cuijpers, J. P., Slotman, B. J., Lagerwaard, F. J., Palacios, M. A. SBRT for pancreatic cancer: In regard of Bohoudi et al. Radiotherapy and Oncology. 2018; 127(3): 511–512.

Bohoudi, O., Bruynzeel, A. M. E., Lagerwaard, F. J., Cuijpers, J. P., Slotman, B. J., & Palacios, M. A. Isotoxic radiosurgery planning for brain metastases. Radiotherapy and Oncology. 2016; 120(2): 253–257.

Doornaert, P., Dahele, M., Verbakel, W. F. A. R., **Bohoudi, O.**, Slotman, B. J., Langendijk, J. A. The effect of induction chemotherapy on tumor volume and organ-at-risk doses in patients with locally advanced oropharyngeal cancer. Radiotherapy and Oncology. 2013; 109(2): 269–274.

Acknowledgements

Acknowledgements / Dankwoord

Acknowledgements / Dankwoord

Verschillende mensen hebben bijgedragen aan het verwezenlijken van dit proefschrift. Al deze mensen wil ik enorm bedanken voor hun inzet. Een aantal van hen wil ik graag in het bijzonder noemen in dit dankwoord.

Mijn dank en gebeden gaan allereerst uit naar mijn wijlen broer "*mijn gharbous*" **Salah** (**رحمك الله يا أخي**), die mij jarenlang heeft bijgestaan, gemotiveerd en geïnspireerd om het beste uit mijzelf te halen en nooit op te geven ondanks tegenslagen. Een prachtige genie met een stralende glimlach die zijn leven heeft toegewijd om anderen te helpen, mijn maatje, mijn grote voorbeeld. Hij zal dit proefschrift helaas niet meer te lezen krijgen omdat hij kort geleden plotseling is komen te overlijden. Ik draag dit boekje aan hem op. Wat je kort voor je overlijden tegen me hebt gezegd is wat me op de been houdt. Ik zal nooit vergeten wat je voor mij hebt gedaan en hebt betekend **رحمك الله يا أخي**.

Dr. Anna Bruynzeel, beste Anna, mijn mentor. Ik wil je enorm bedanken voor je onschatbare tijd, advies en steun zowel privé als werk gerelateerd. Je hebt ontelbare weekenden opgeofferd om mij te helpen tijdens mijn promotie traject. Bij geboorte, verjaardag en of begrafenis; je bent altijd de eerste die feliciteert en of steunt, dit zegt enorm veel over de persoon die jij bent, dit zal ik niet vergeten. Je gedrevenheid en de manier waarop jij je bezighoudt met de wetenschap en klinische zaken zijn echt inspirerend; je bent de hoeksteen voor de MRidian en ook mijn promotie project.

Dr. Frank Lagerwaard, beste Frank, Maestro! Zonder jou was dit nooit mogelijk geweest. In de periode die ik jou ken ben je mijn supervisor, copromotor en familie geweest. Je constante steun zowel privé als werk gerelateerd, zullen mij altijd bij blijven. Jouw visie, leiding en betrokkenheid zijn de sleutel tot succes in alle projecten die we gedaan hebben en enorm belangrijk in elk onderdeel van mijn

proefschrift. Mijn interesse en motivatie voor onderzoek is ongetwijfeld door jou geïnspireerd en ik voel me bevoorrecht om onder jouw supervisie te mogen werken, ik ben jou enorm dankbaar.

Dr. Miguel Palacios, beste Miguel. Bedankt voor jouw begeleiding, advies, expertise en je enorme bijdrage in alle fysica-gerelateerde zaken bij het MRIdian-project en rond mijn promotie en dank dat je mijn copromotor wilde zijn. Ik ben ontzettend onder de indruk geraakt van onder andere jouw MRI kennis en planning skills; ik heb veel van jou geleerd. Je was bereid om na je werkdag in de avonden samen heel kritisch naar alle data te kijken en je was altijd beschikbaar om te sparren of voor een goed gesprek, *gracias!*.

Professor. dr. S. Senan, beste Suresh. Bedankt voor het vertrouwen dat je in mij hebt gesteld. Ik voel me bevoorrecht dat jij mijn promotor wilde zijn. In het weekend of in de avond, je bent altijd bereid om jouw enorme kennis te delen, recente literatuur te sturen of feedback te geven. Jouw deur staat altijd voor mij open, dank dat je ondanks je drukke werkschema altijd tijd voor mij hebt gemaakt.

Professor. dr. B.J. Slotman, beste Ben. Ik wil je enorm bedanken voor alle steun en de mogelijkheid die je me hebt gegeven om onderzoek te doen op een afdeling waar innovatie wordt omarmd wordt. De fijne samenwerking en je snelle feedback op onze artikelen heb ik altijd enorm gewaardeerd.

Prof.dr. M.R. Meijerink, prof.dr. U.A. van der Heide, prof.dr. M.S. Hoogeman, prof.dr. Enis Özyar, dr. Linda G.W. Kerkmeijer and **dr. Davide Cusumano**. Thank you very much for your willingness to serve as a member of my doctorate committee and reviewing my thesis.

Alle **co-auteurs** in dit proefschrift wil ik van harte bedanken voor hun bijdrage en individuele feedback.

Dear **co-authors from the Heidelberg Institute for Radiation Oncology and German Cancer Research Center (DKFZ)**, thank you all very much for your help and critical review of our work. I would like to express my gratitude to **Dr. Asja Pfaffenberger** for her precious advice and support. Warmest thanks to **Nina Niebuhr, Wibke Johnen and Katharina Spindeldreier** for their support with the phantom.

Mijn paranimfen, **Marloes en Paul,** wat een enorme eer dat jullie straks aan mijn zijde staan! Ik wil jullie enorm bedanken voor jullie steun en alle hilarische tijden die we de afgelopen 12 jaar hebben meegemaakt. We waren nog jonkies en nu hebben we allemaal kinderen, wat is de tijd toch snel gegaan. De ongekende en hilarische concurrentie om het beste plan te maken (vaak tot diep in de nacht) heeft ons vele mooie momenten gebracht, zal die mooie tijden altijd koesteren. Dank jullie wel; ik heb het meest van jullie geleerd jongens!

Shyama, Merle en Hilâl, dank jullie wel voor alle tips and tricks en jullie adviezen bij mijn inschrijving en tijdens mijn promotie traject, ik heb er veel aan gehad.

Alle fantoom metingen waren niet mogelijk geweest zonder de hulp van onze dosimetrie experts, met dank **aan Leo van Battum, Daan Hoffmans** en **Stan Heukelom**.

Annette en Olga, dank voor al jullie hulp, de afdeling mag blij zijn met jullie als secretaresses.

En tot slot mijn **familie.** In alles wat ik bereikt heb is de bijdrage van mijn familie van onschatbare waarde geweest. Lieve ouders, door jullie onvoorwaardelijke liefde, steun, mogelijkheden en opofferingen heb ik alles bereikt.

اللهم بارك لأبي وأمي في أعمارهم ، وبارك اللهم في أعمالهم ويسر اللهم لهم سبل الفلاح والطاع.

Ik hoop dat dit een beetje verlichting geeft en jullie trots maakt. Mijn lieve broers en zussen, mijn maatjes waar ik blindelings op kan vertrouwen. Jullie zijn er altijd voor me geweest in goede en slechte tijden. Zonder jullie had ik dit absoluut niet kunnen bereiken. Ik ben jullie voor eeuwig dankbaar. Aan mijn lieve, lieve Ilyas, Inssaf, Yassin en Yousra, ik had geen beter gezin kunnen wensen, bedankt voor jullie onvoorwaardelijke liefde en vreugde die jullie in mijn leven brengen. Mijn laatst woorden zijn voor mijn vrouw Hafida, jouw steun, begrip en geduld zijn echt grenzeloos, getuige alle keren dat ik 's avonds en weekend achter de computer verdween, dank je wel voor alles. Ik kijk uit naar de komende periode… maar eerst onze lange vakantie.

Alhamdoulillah